JAERI-M
83-103

ASSESSMENT OF CORE THERMO-HYDRODYNAMIC MODELS OF REFLA-1D WITH CCTF DATA

July 1983

Tsutomu OKUBO and Yoshio MURAO

日本原子力研究所
Japan Atomic Energy Research Institute

JAERI-M レポートは，日本原子力研究所が不定期に公刊している研究報告書です。

入手の問合わせは，日本原子力研究所技術情報部情報資料課（〒319-11茨城県那珂郡東海村）あて，お申しこしください。なお，このほかに財団法人原子力弘済会資料センター（〒319-11 茨城県那珂郡東海村日本原子力研究所内）で複写による実費頒布をおこなっております。

JAERI-M reports are issued irregularly.

Inquiries about availability of the reports should be addressed to Information Section, Division of Technical Information, Japan Atomic Energy Research Institute, Tokai-mura, Naka-gun, Ibaraki-ken 319-11, Japan.

編集兼発行　日本原子力研究所
印　　刷　いばらき印刷㈱

Assessment of Core Thermo-hydrodynamic Models of REFLA-1D with CCTF Data

Tsutomu OKUBO and Yoshio MURAO

Department of Nuclear Safety Research,
Tokai Research Establishment, JAERI

(Received June 9, 1983)

In order to assess the core thermo-hydrodynamic models of REFLA-1D/MODE3, which is the latest version of REFLA-1D, several calculations of the core thermo-hydrodynamics have been performed for the CCTF Core-I series tests. The measured initial and boundary conditions were used for these calculations. The calculational results showed that the water accumulation model of Case 2 could predict the CCTF results fairly well as it could for the JAERI small scale facility. The calculated results for the base case and the EM tests were in good agreement with the CCTF data. The parameter effects, such as system pressure, initial clad temperature, Acc injection rate, LPCI injection rate and initial downcomer wall temperature, were predicted correctly, except for the high system pressure and the high LPCI injection rate tests.

Keywords : REFLA-1D/MODE3, CCTF, Assessment Calculation, PWR, LOCA, Reflood Phase, Thermo-hydrodynamic

CCTF データによる REFLA－1D 炉心熱水力モデルの検証

日本原子力研究所東海研究所安全工学部
大久保　努・村尾　良夫

（1983 年 6 月 9 日受理）

REFLA－1Dの最新版であるREFLA－1D／MODE 3の炉心熱水力モデルを検証するため，CCTF第1次炉心試験に対する炉心計算を行った。計算には，初期および境界条件として実測された値を用いた。計算結果から，炉心蓄水モデルのうちケース2のモデルが原研の小型再冠水実験の場合と同様にCCTFの結果を良く予測することが分った。

基準試験およびEM試験に対する計算値は，CCTFのデータと良い一致を示した。系圧力，初期被覆管温度，Acc流量，LPCI流量および初期ダウンカマ壁温のパラメータ効果は，高系圧力および高LPCI流量試験の場合を除いて正しく予測された。

Contents

目　　次

List of Tables

List of Figures

1. Introduction

REFLA-1D[1] is a computer code being developed at the Japan Atomic Energy Research Institute (JAERI) for the analysis of the thermo-hydrodynamic behavior in a pressurized water reactor (PWR) during the reflood phase of a loss-of-coolant accident (LOCA). This code belongs under the category of the best-estimate (BE) code.

The latest version of the code is REFLA-1D/MODE3[2]. This version includes some new improvements[3] in the core thermo-hydrodynamic models, which were developed using the experimental data of the small scale reflood facilities, such as, the JAERI small scale reflood test facility[4] and the FLECHT facilities[5]. The scaling ratios of the core flow area of these facilities to a 1000 MWe class PWR are 1/2500 and 1/370 for the JAERI and the FLECHT facilities, respectively. The results of the assessment calculations for the small scale facilities were fairly in good agreement with the experimental data, as presented in reference 3.

The JAERI's Cylindrical Core Test Facility (CCTF)[6] is a large scale reflood test facility and the scaling ratio of the core flow area to a 1000 MWe class PWR is 1/21.44. Furthermore, the CCTF simulates an actual reactor as closely as possible, and hence, is expected to give the realistic data of the thermo-hydrodynamic behavior in an actual PWR.

The possible differences related with the facility scaling are the multi-dimensionality of the thermo-hydrodynamics and the wall effect. Although the wall effect is important in small scale facilities, it becomes negligible in larger facilities. The characteristics and the degree of the multi-dimensional effect has not clarified, and hence, the JAERI's experimental project using the CCTF and the Slab Core Test Facility (SCTF)[6] is intended to investigate the effect.

In this report the results of REFLA-1D/MODE3 core calculations, *i.e.* calculations of the thermo-hydrodynamics in the core, for the CCTF Core-I series tests are presented and discussed in order to assess the core thermo-hydrodynamic models, which were developed using the data of the small scale facilities, with the data of the large scale facility CCTF.

2. Core Thermo-hydrodynamic Models in REFLA-1D/MODE3

The thermo-hydrodynamic correlations used in REFLA-1D/MODE3 are tabulated in Table 2.1. The correlations improved since REFLA-1D/MODE1[1] are the correlation for slip velocity in the saturated two-phase flow and transition flow regions and the hydrodynamic and heat transfer correlations in the dispersed flow region. The quench velocity correlation was also improved.[3]

For the estimation of the slip velocity in the saturated two-phase flow and the transition flow, the modified Lockhart-Martinelli's correlation[7] is introduced in addition to the modified Yeh's correlation.[7] In the dispersed flow region, two types of hydrodynamic models, *i.e.* Case 1 and Case 2, are introduced.[3] In both cases, the liquid accumulation regions are assumed to exist above the quench front. The length of this region is now set to 0.3 m. Above the liquid accumulation region, there exists the normal dispersed flow region in Case 1, whereas the other liquid accumulation region in Case 2. In this region, the void fraction has a value between the values corresponding to the transition flow and the dispersed flow due to the integration of dispersed droplets. The heat transfer coefficient in the dispersed flow region for Case 2 is calculated as,

$$h = h_t \cdot \frac{\alpha_d - \alpha}{\alpha_d - \alpha_t} + h_d \cdot \frac{\alpha - \alpha_t}{\alpha_d - \alpha_t}$$

where, the void fraction and heat transfer coefficient for the transition flow are expressed by α_t and h_t, respectively, and for the dispersed flow α_d and h_d, respectively. The void fraction α_t is calculated using the slip velocity, which is obtained with the modified Yeh's correlation or the Lockhart-Martinelli's correlation, whereas α_d is calculated based on the slip velocity corresponding to the critical Weber number Wec.

The drag coefficient for the liquid droplet was also changed as,

$$C_D = \begin{cases} 24/Re & (Re < 2) \\ 17.54 \cdot Re^{-0.5473} & (2 \le Re < 1000) \\ 0.4 & (1000 \le Re) \end{cases}$$

The quench velocity correlation was improved in order to extend the applicability of the correlation to the lower quench temperature than the maximum liquid superheat temperature and to the lower and higher system pressures than 0.4 MPa. This improvement is described in detail in reference 3.

Table 2.1 Correlations used in REFLA-1D/MODE3 (From Reference 3)

Flow region	Hydrodynamic correlations	Heat transfer correlations
(1) Single liquid phase flow/Subcooled nucleate boiling region	$V_\ell + V_g = F \cdot (1/2) \cdot (\rho_\ell/De) \cdot u_\ell^2$ $F = 0.3166 Re^{-0.25}$ $(Re \geq 2400)$ $F = 64/Re$ $(Re < 2400)$ $Re = Deu_\ell/\nu_\ell$ $\alpha = 0$	$Q_\ell = L/S \cdot \phi_B$ $\phi_B = 0.2434 \Delta T^4 \exp(0.6447 \times 10^{-6} P)$ (Jens & Lottes) $Q_g = 0$
(2) Saturated two-phase flow region	$V_\ell + V_g = 0$ Δu: Eq.(4-4) $\equiv \Delta u_s$ α_{Yeh}: Eqs.(2-35) ∿ (2-37) α_{LM} : Eq.(4-3), K=3 α : Eq.(2-34) $\equiv \alpha_s$	$Q = L/S \cdot \phi_B$ $Q_g = 0$ $T = T_g = T_{sat}$
(3) Subcooled film boiling region	$V_\ell + V_g = 0$ $\alpha = 0$	$Q_\ell = L/S \cdot h \cdot (T_w - T_{sat})$ $h = h_{sub} + h_R$: Eqs.(3-10) and (3-6)
(4) Transition flow region		$Q_\ell = L/S \cdot h \cdot (T_w - T_{sat})$ h : Eq. (3-13)
(5) Dispersed flow region (if $\Delta u \leq \Delta u_c$) $Re = D_e u_g/\nu_g$ $R_{ed} = D_d \Delta u/\nu_g$ (if $\Delta u_c < \Delta u < \Delta u_s$) Value = Value of (4)$\cdot \frac{\alpha_d - \alpha}{\alpha_d - \alpha_s}$ + Value of (5)$\cdot \frac{\alpha - \alpha_s}{\alpha_d - \alpha_s}$, where Δu_s: Δu of (2).	$V_\ell + V_g = (F \text{ of } (6)) \cdot (\rho_g/D_e) \cdot (1/2) \cdot u_g^2$ Δu : Eq.(2-39) + α C_D : Eq.(2-49) Δu_c: Eqs.(2-47), (2-49) and (2-45) α : Eq.(4-6) + $\tau_c = 15.8s$ α_d : Eq.(2-34) + Δu_c $\frac{n}{u_\ell} = (1-\alpha)/\{\frac{4}{3}\pi(\frac{D_d}{2})^3\}$ α_{max}: Eq.(2-34) + 0.01 Δu_c $(\frac{d(1-\alpha)}{dt})_{max}$: Eq.(2-56) C_1 : 2.0 m^{-1} C_2 : 0.3 m^{-1}	$Q_\ell = Q_{VD} + Q_{WD}$ $Q_{VD} = (n/u_\ell)\lambda_g \pi D_d N_{UVD} \cdot (T_g - T_{sat})$ $N_{UVD} = 2 + 0.34 R_e^{0.566} Pr^{1/3}$ $(R_{ed} \geq 1800)$ $N_{UVD} = 2 + 0.55 R_e^{0.5} Pr^{1/3}$ $(R_{ed} < 1800)$ $Q_{WD} = (L/S) h_{RWD} \cdot (T_w - T_{sat})$ $h_{RWD} = E \cdot F_s \cdot \varepsilon (T_w^4 - T_{sat}^4) / (T_w - T_{sat})$ $F_s = \min(Sn/u_\ell \cdot \pi D_d^2/L, 1)$ $Q_g = Q$ of (6) $T_\ell = T_{sat}$
(6) Superheated steam flow region $Re = D_e u_g/\nu_g$	$V_\ell + V_g = F \cdot (1/2)(\rho_g/D_e) \cdot u_g^2$ $F = 0.3166 R_e^{-0.25}$ $(R_e \geq 2400)$ $F = 64/R_e$ $(R_e < 2400)$ $\alpha = 1$	$Q_\ell = 0$ $Q_g = L/S \cdot \lambda_g/D_e \cdot N_u (T_w - T_g)$ $N_u = 0.023 R_e^{0.8} P_r^{0.4}$ $(R_e \geq 2700)$ $N_u = \max(1.077(R_e P_r D_e/Z)^{1/3}, 3.65)$ $(R_e \leq 2100)$ $N_u = N_{u2100} + (N_{u2700} - N_{u2100}) \cdot (R_e - 2100)/600$ $(2700 > R_e > 2100)$

Note : Equation No. in this table is that in Reference 3.

3. Assessment Calculation for CCTF Core-I Tests

3.1 Calculation Conditions

The total number of the CCTF tests assessed with REFLA-1D/MODE3 and presented in this report is eleven. The main conditions of these tests are summarized in Table 3.1.

In the present calculations with the REFLA-1D/MODE3, the number of the calculational nodes was set to 90 and each node represents the region of 40.67 mm high of the CCTF core. The calculational initial and boundary conditions were determined based on the CCTF data. The core flooding rate and the liquid temperature and pressure at the core inlet were given at each calculational time through the whole transient of the calculation. They are presented in Fig. 3.1 for the base case test. The core flooding rate was obtained from the mass balance calculation. Namely,

$$\dot{m}_F = \dot{m}_c + \dot{m}_U + \sum_{i=1}^{4} \dot{m}_{L,i}$$

where, symbols $\dot{m}_F$, $\dot{m}_c$, $\dot{m}_U$ and $\dot{m}_{L,i}$ are the core flooding rate, the water accumulation rate in the core, the water accumulation rate in the upper plenum and the fluid mass flow rate in the i-th ($i = 1 \sim 4$) primary loop, respectively. Smoothing, *i.e.* averaging, of the data is performed to obtain $\dot{m}_C$ and $\dot{m}_U$.

As described in the previous section, two types of water accumulation models, *i.e.* Case 1 and Case 2, are available in the calculation. Case 2 model is adopted in the present assessment calculations, because this model can predict the phenomena observed in the CCTF tests much better than the other model (Case 1) as shown in Figs. 3.2 (a) and (b). The calculated results with both models are compared with the CCTF data for the base case test in Figs. 3.2 (a) and (b). Figure 3.2 (a) is a comparison of the quench envelopes and Fig. 3.2 (b) rod surface temperatures at the midplane level. These results confirm that Case 2 predicts the phenomena in the CCTF tests better.

The input list for the base case test is given in Appendix A.

3.2 Calculational Results for Base Case Test

The calculational results for the base case test are compared with the CCTF data in Figs. 3.3 through 3.7. Figure 3.3 shows the comparison of the quench envelopes for the average power rod. The CCTF data are presented with the mean value and the standard deviation. The quench envelope of the average power rod represents the overall core cooling. Figure 3.3 shows that the calculational results are in good agreement with the CCTF data except for the top part (above 2.5 m) of the core. Therefore, it is said that the overall core cooling is predicted well by REFLA-1D/MODE3.

Figure 3.4 shows the temperature histories of the average power rod at five elevations. The corresponding heat transfer coefficients are given in Fig. 3.5. The behaviors of temperature histories in Fig. 3.4 follow those of the heat transfer coefficients in Fig. 3.5. The calculated results are generally in good agreement with the experimental data. However, in a few points, there are some differences between the calculated results and the experimental data. They are summarized in the following:

1. The cooling in the calculation is not as good as in the experiment during the period of about 100 s prior to quenching. This tendency is more significant at higher elevations.
2. The calculation tends to give the better cooling at upper elevations (2.44 m and 3.05 m) during about first 150 s.
3. The cooling in the calculation at the 1.015 m and 1.83 m elevations is not as good as in the experiment during about first 20 s.

Figure 3.6 shows the comparison of the quench temperatures of the average power rod. The calculation tends to give the higher quench temperatures.

In order to examine the hydrodynamic behavior, the core water head and sectional void fractions are compared with experimental values in Fig. 3.7. The experimental void fractions were obtained from the differential pressure data neglecting the frictional and accelerational pressure losses, because the contribution of them is evaluated to be within 2 percent of the void fraction at every section. Concerning with the water head, the calculational results are in good agreement with the experimental data. However, the predicted void fraction in each section of the core except for the lowest section (0 - 0.61 m) differs from the experimental value. The differences are summarized in the following:

1. In the initial period up to 25 s, the calculation tends to give the higher void fractions. The experimental data start to decrease from the beginning of reflooding in every section, whereas the calculational results show the delay of decrease of void fractions in the sections above 0.61 m elevation.
2. After that period, the calculation tends to give the lower void fractions in the sections below 2.44 m elevation, whereas the higher void fractions in the sections above 2.44 m elevation.

Although both the calculational and experimental values in the top section (3.05 - 3.66 m) are not presented in Fig. 3.7, they are almost identical to those in the next lower section (2.44 - 3.05 m).

The fact presented in item 2 above is the reason for the almost identical core water heads, that is, the difference in void fractions below 2.44 m elevation is almost canceled with the difference above 2.44 m elevation.

3.3 Calculational Results for Parameter Effects Tests

In this section the calculational results for the CCTF Core-I parameter effects tests are presented in order to investigate whether the calculations can predict the same parameter effects as observed in the experiments. The parameters investigated are the system pressure, initial clad temperature, accumulator system (Acc) injection rate, low pressure coolant injection system (LPCI) injection rate and initial downcomer wall temperature. The test conditions for those parameter effects tests are tabulated and compared in Table 3.1.

As the representatives of comparisons of parameter effects between in the calculations and in the experiments, the quench envelopes of the average power rod and the rod surface temperature histories of the average power rod at the midplane level (1.83 m) are compared for each parameter in the following. The other calculated results are presented in Appendix B.

Figures 3.8 and 3.9 show the comparisons for the system pressure parameter effects tests. Both figures show that the calculation can predict qualitatively the system pressure effects observed in the CCTF tests. Except for the case of 0.3 MPa, the quantitative agreement is also fairly good. In the case of 0.3 MPa the calculation underestimates the core cooling. This tendency is observed more significantly at higher elevations as shown in Fig. 3.8.

From the comparison in Fig. 3.9, it is recognized that the turn-around temperature for 0.3 MPa test is higher but lower for 0.15 MPa in the calculation. This implies that the sensitivity of REFLA-1D to the system pressure is not good enough.

Figures 3.10 and 3.11 show the comparisons for the initial clad temperature effects tests. Both figures show that the calculation can predict qualitatively the initial clad temperature effects observed in the CCTF tests. The quantitative agreement is also fairly good.

Figures 3.12 and 3.13 show the comparisons for the Acc injection rate effects tests. Both figures show that the calculation can predict qualitatively the Acc injection rate effects observed in the CCTF tests. The quantitative agreement is also fairly good.

Figures 3.14 and 3.15 show the comparisons for the LPCI injection rate effects tests. In Fig. 3.14 the calculated quench times of the high LPCI injection rate test are slightly longer than those of the base case test above the midplane level, although the CCTF data indicate the opposite tendency. Also, in Fig. 3.15, the calculated temperature histories of both tests are almost idential, whereas the CCTF data indicate the the considerable difference in the temperatures around the turnaround times. Therefore, the effect of high LPCI injection rate is not predicted well with REFLA-1D, although the quantitative difference is a little.

The effect of the low LPCI injection rate, however, is predicted well qualitatively as shown in Figs. 3.14 and 3.15. The quantitative agreement is also fairly good.

Figures 3.16 and 3.17 show the comparisons for the initial down-comer wall temperature effects tests. From Fig. 3.16 it is found that the calculated quench times for both tests are nearly identical, although the CCTF data indicate the saturated wall test gives much shorter quench times in the upper half region. The calculated temperature histories are also nearly identical in both tests, whereas the CCTF data show the better core cooling after the turnaround in the saturated wall test. These results indicate that the sensitivity of REFLA-1D to the initial downcomer temperature effects is not as good.

3.4 Calculational Results for EM Test

In the CCTF Core-I series tests, a test whose initial and boundary conditions were determined as closely as possible to those of the evaluation model (EM) analysis was conducted. This test is named the EM test[8]. The EM test was conducted in order to demonstrate the safety margin of the EM analysis experimentally and its initial clad temperature was the highest in the CCTF Core-I tests (Table 3.1). Therefore, in the following, the calculational results are compared with the CCTF data in detail.

Figure 3.18 shows the comparison of quench envelopes of the average power rod. Except for the top part (above 2.5 m), the calculational results are in good agreement with the CCTF data. This implies that the overall core cooling is predicted well with REFLA-1D/MODE3.

Figure 3.19 shows the temperature histories of the average power rod at five elevations. The corresponding heat transfer coefficients are compared in Fig. 3.20. The tendencies of temperature histories in Fig. 3.19 are consistently explained by those of heat transfer coefficients in Fig. 3.20. The calculated results are generally in good agreement with the CCTF data. In a few points, however, there are differences between the calculated results and the CCTF data. They are summarized as follows:

1. The cooling in the calculation is not as good as in the experiment during the period of about 100 s prior to quenching. This tendency is more significant at higher elevations.
2. The calculation tends to give the better core cooling at upper elevations (2.44 m and 3.05 m) during about first 150 s.
3. The cooling in the calculation at 1.015 m and 1.83 m elevations is not as good as in the experiment during about first 20 s.

These items above are the same as in the results for the base case test and seem to be the general problems in all REFLA-1D/MODE3 calculations more or less.

Figure 3.21 shows the comparison of the quench temperatures of the average power rod. The calculation tends to give the higher quench temperature. However, the differences are not significant.

In Fig. 3.22, the core water head and sectional void fractions are compared in order to examine the hydrodynamic results. The experimental void fractions were obtained from the differential pressure data neglecting the frictional and accelerational pressure lesses. Concerning with the core water head, the calculational results are in good agreement with the CCTF data. The sectional void fractions predicted, however, differ from the experimental values except for the lowest section (0 - 0.61 m). The differences are summarized as follows:

1. In the initial period, the calculation tends to give the higher void fractions. This tendency is more significant at higher elevations. The experimental value starts to decrease from the beginning of reflooding in every section, whereas the calculational results show the delay of decrease in the sections above 0.61 m elevation.
2. After that time period, the calculation tends to give the lower void fractions in the sections below 2.44 m elevation, whereas the higher void fractions in the sections above 2.44 m elevation.

Although both the calculational and experimental values in the top section (3.05 - 3.66 m) are not presented in Fig. 3.22, they are almost identical to those in the next lower section (2.44 - 3.05 m).

Table 3.1 Main conditions of CCTF tests

Item / Test name	System pressure (MPa)	Acc injection rate (m^3/s)	LPCI injection rate (m^3/s)	Initial clad temperature (°C)	Initial downcomer temperature (°C)	Test No.
Base case	0.2	78×10^{-3}	8.3×10^{-3}	600	198	C1-5
High system pressure	0.3	*	*	*	*	C1-12
Low system pressure	0.15	*	*	*	*	C1-10
High initial clad temperature	*	*	*	700	*	C1-7
High initial clad temperature	*	*	*	800	*	C1-14
Low Acc injection rate	*	67×10^{-3}	*	*	*	C1-11
High LPCI injection rate	*	*	17×10^{-3}	*	*	C1-6
Low LPCI injection rate	*	*	4.7×10^{-3}	*	*	C1-9
Superheated initial downcomer temperature	*	67×10^{-3}	*	*	*	C1-2
Saturated initial downcomer temperature	*	67×10^{-3}	*	*	120	C1-3
EM	*	90×10^{-3}	11×10^{-3}	870	*	C1-19

Note: * means the same value as in the base case test.

Average linear power density : 1.4 kW/m

ECC water temperature : 35°C

Acc injection duration : 14 s

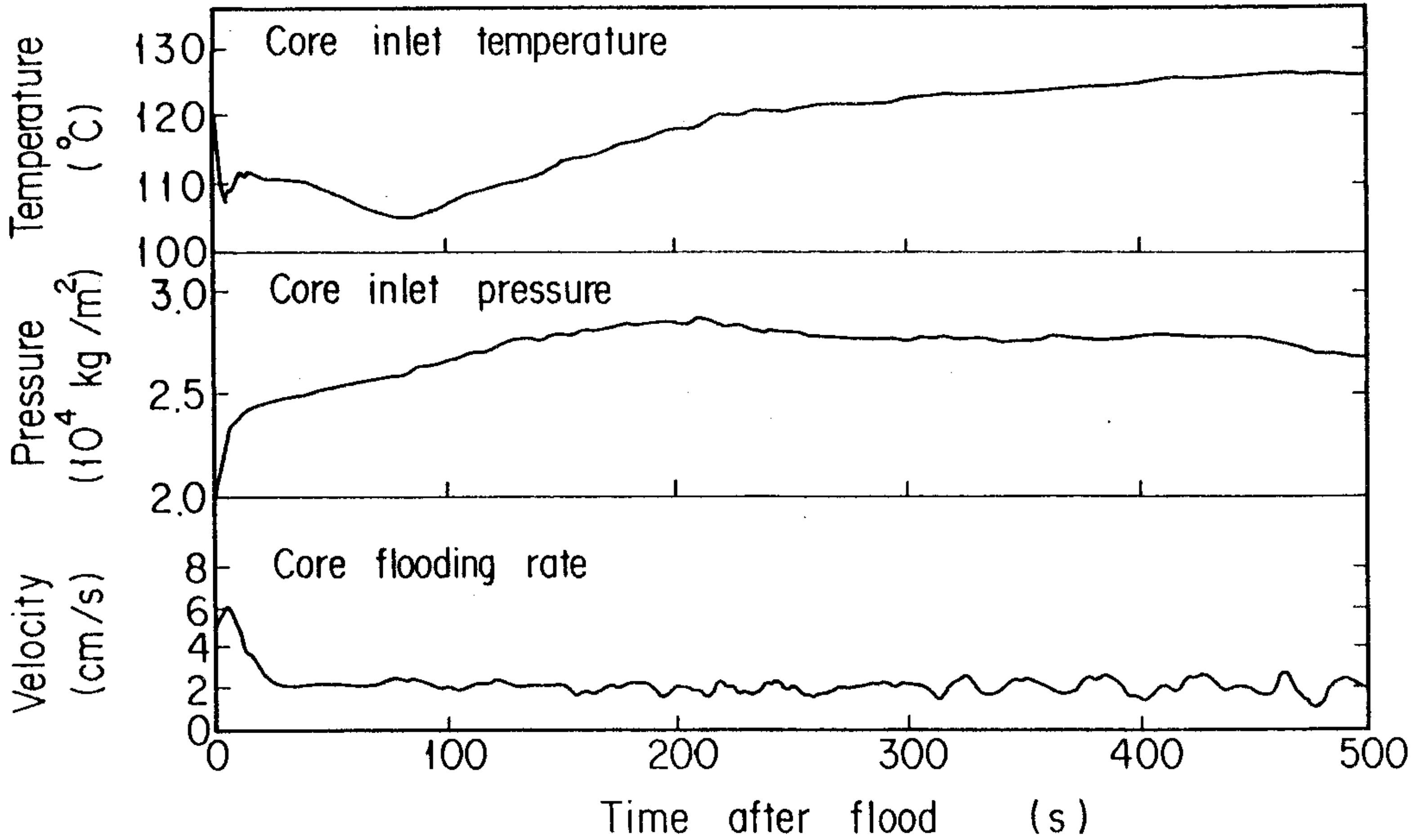

Fig. 3.1 Time-dependent boundary conditions for base case test

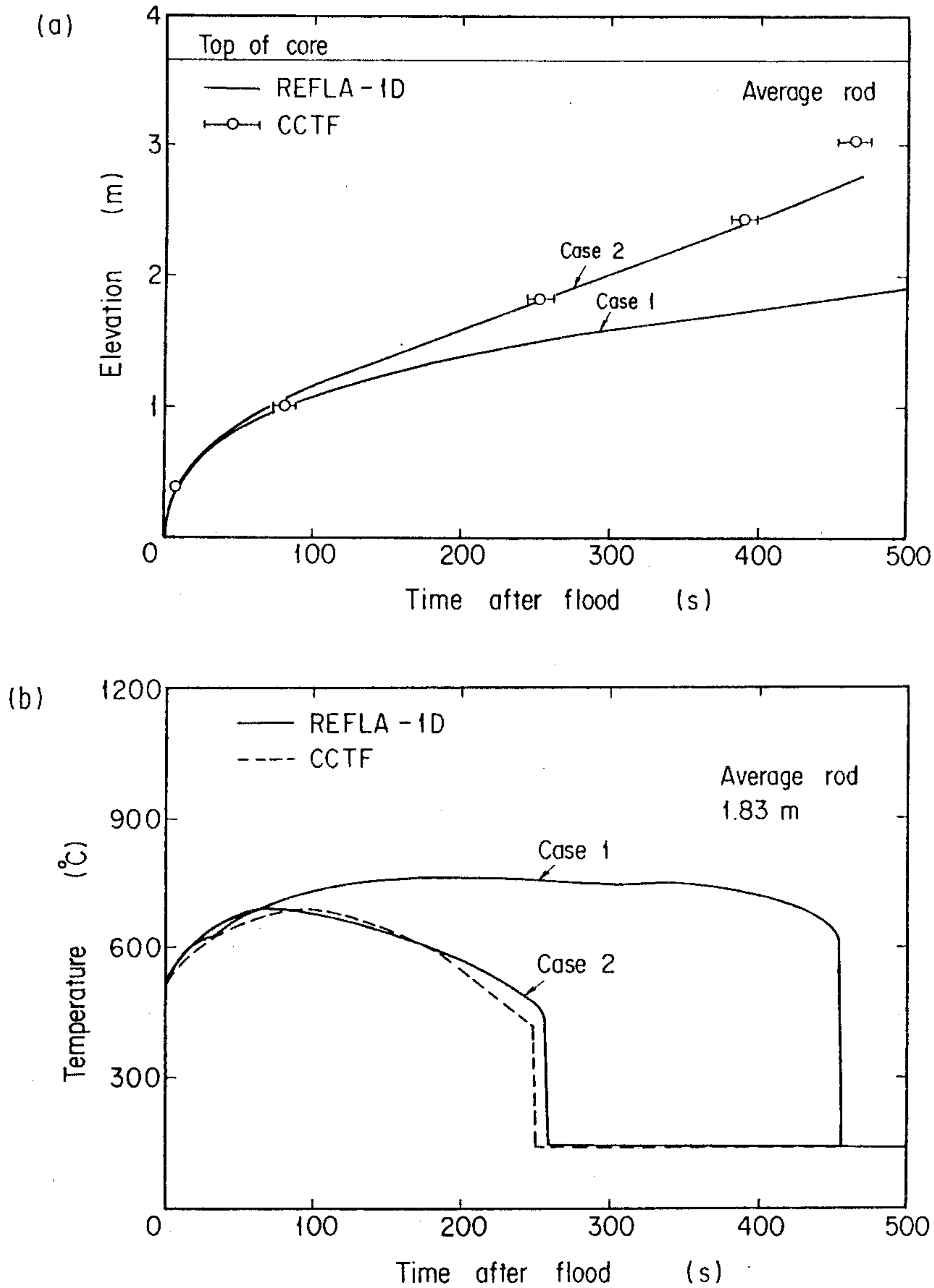

Fig. 3.2 Comparison of calculational results for Cases 1 and 2 with experimental data

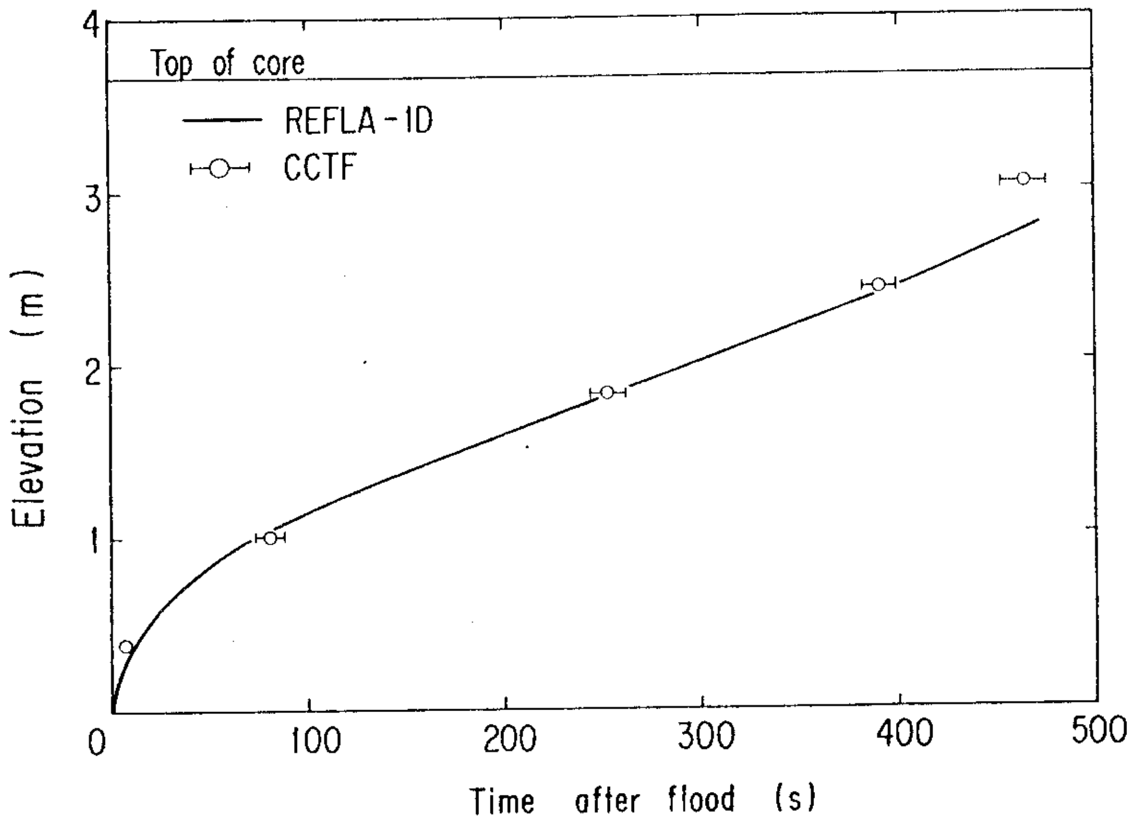

Fig. 3.3 Quench envelope for average power rod in base case test

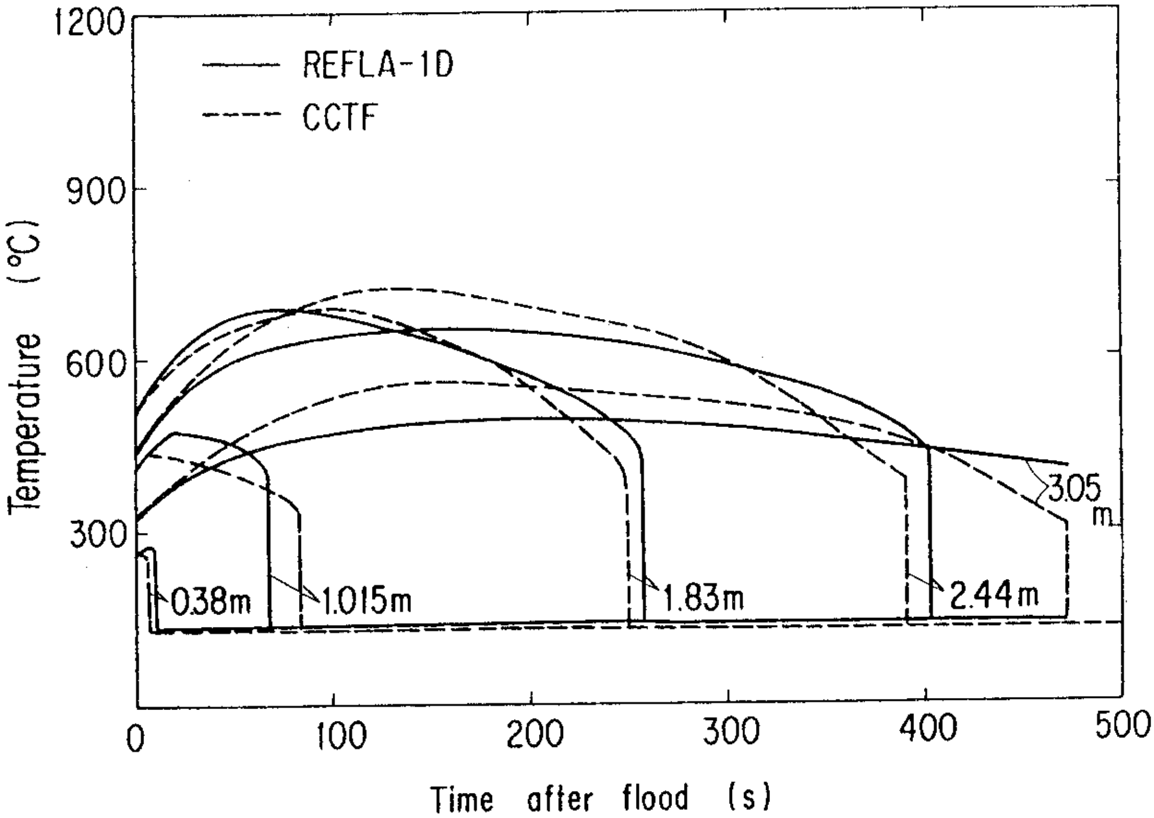

Fig. 3.4 Rod surface temperature histories for average power rod in base case test

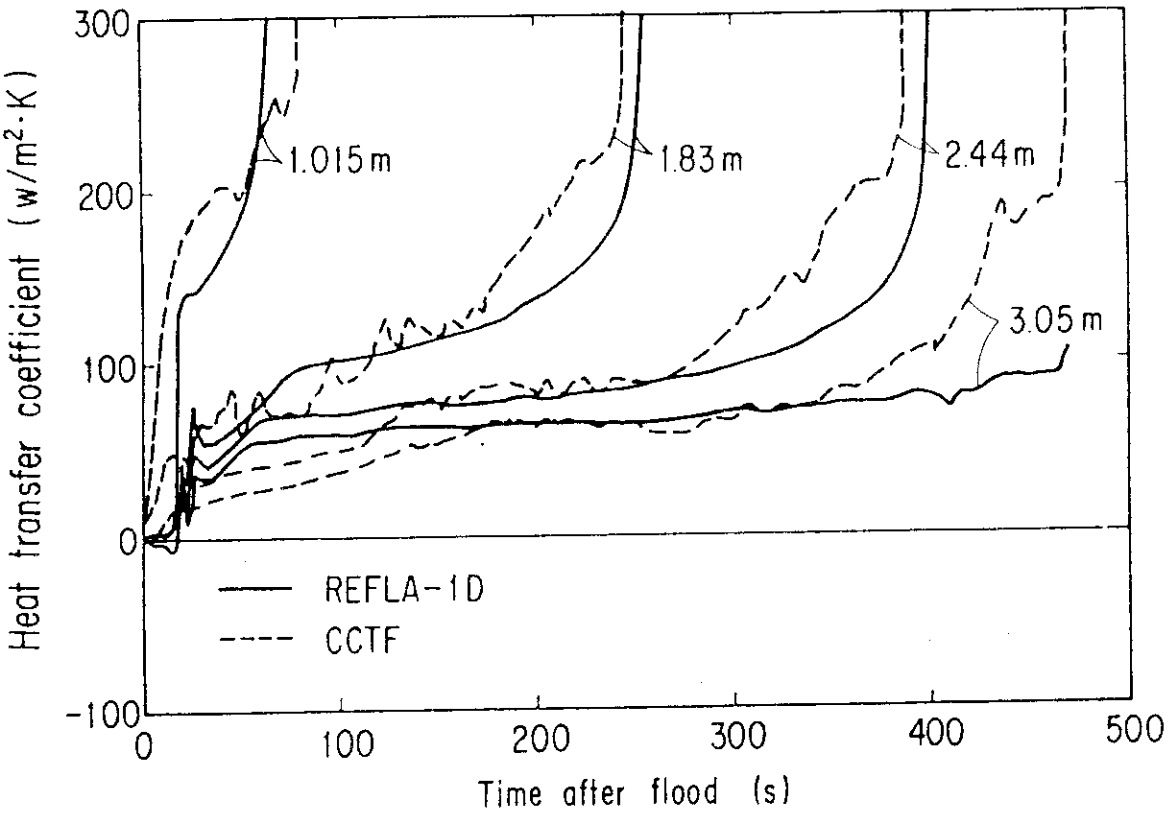

Fig. 3.5 Heat transfer coefficients for average power rod in base case test

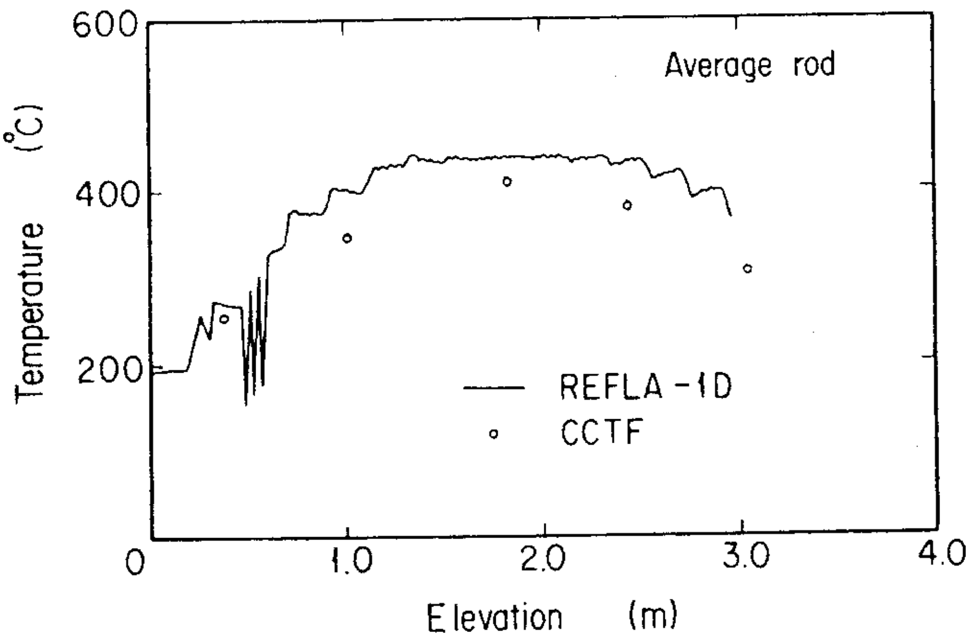

Fig. 3.6 Quench temperatures for average power rod in base case test

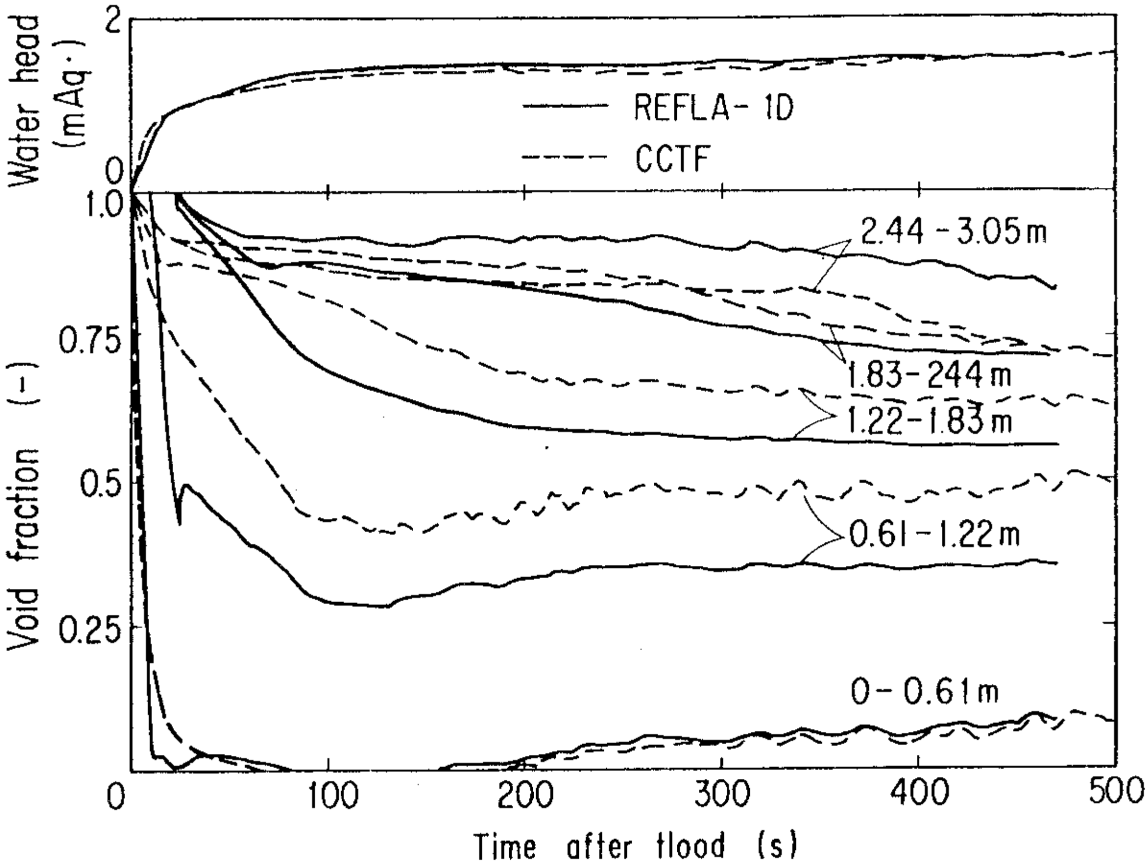

Fig. 3.7 Core water head and void fractions in base case test

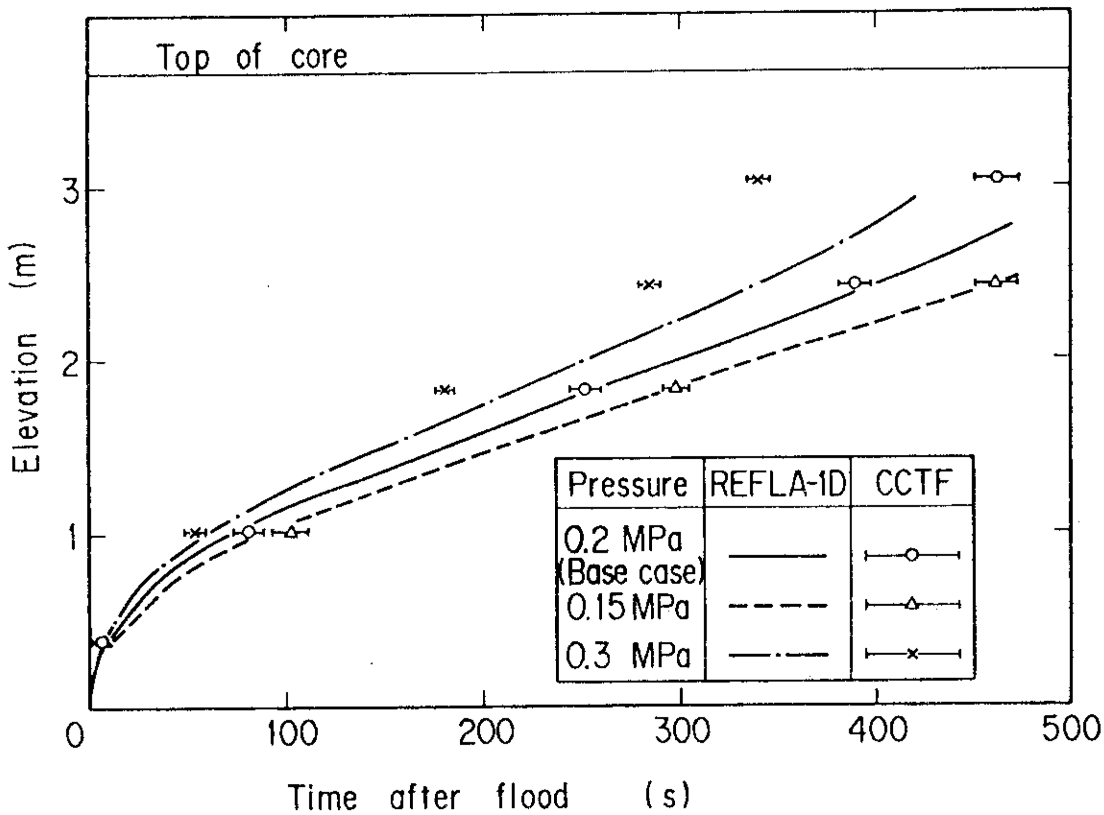

Fig. 3.8 Quench envelopes for system pressure effects tests

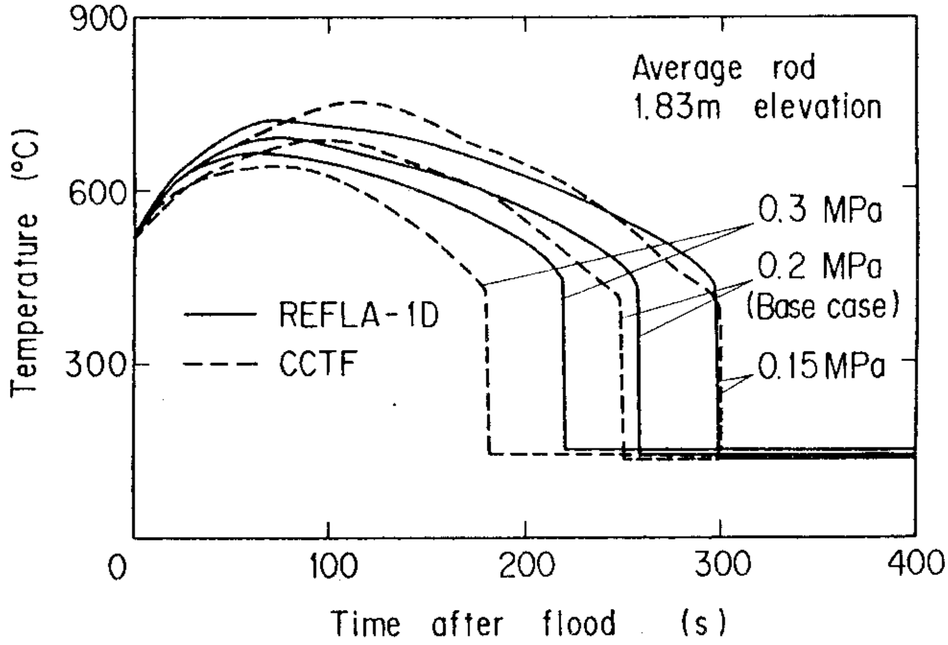

Fig. 3.9 Rod surface temperature histories for system pressure effects tests

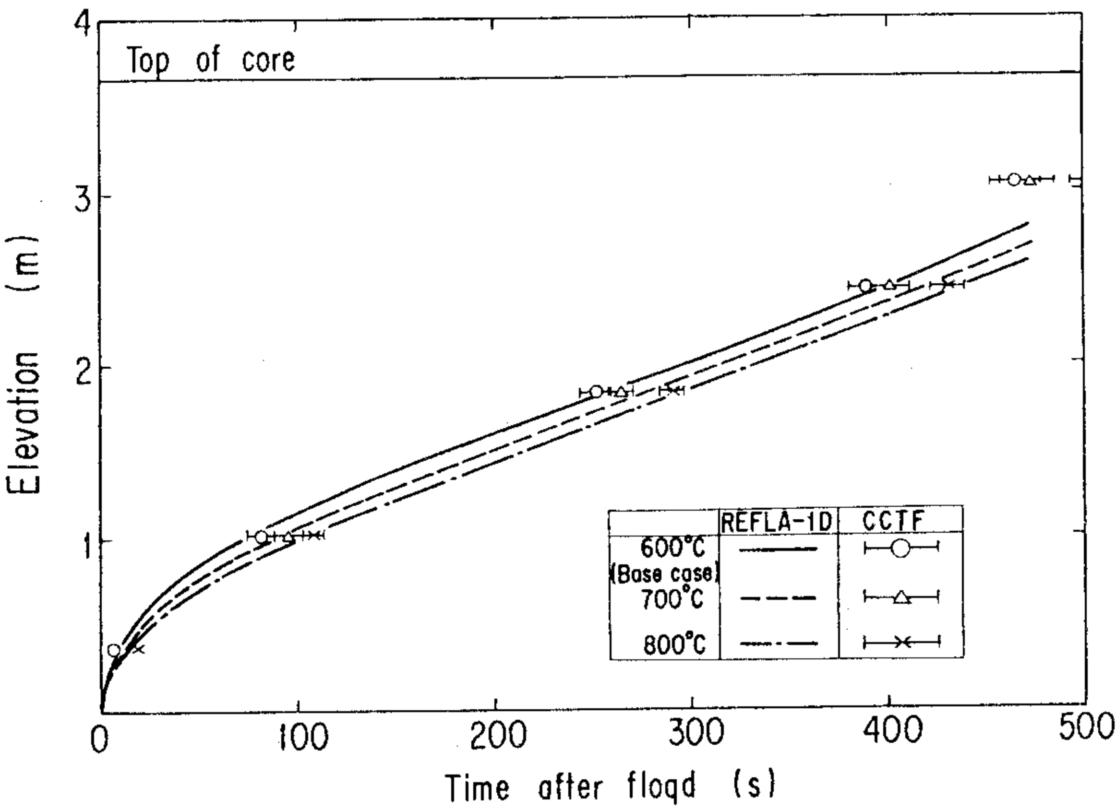

Fig. 3.10 Quench envelopes for initial clad temperature effects tests

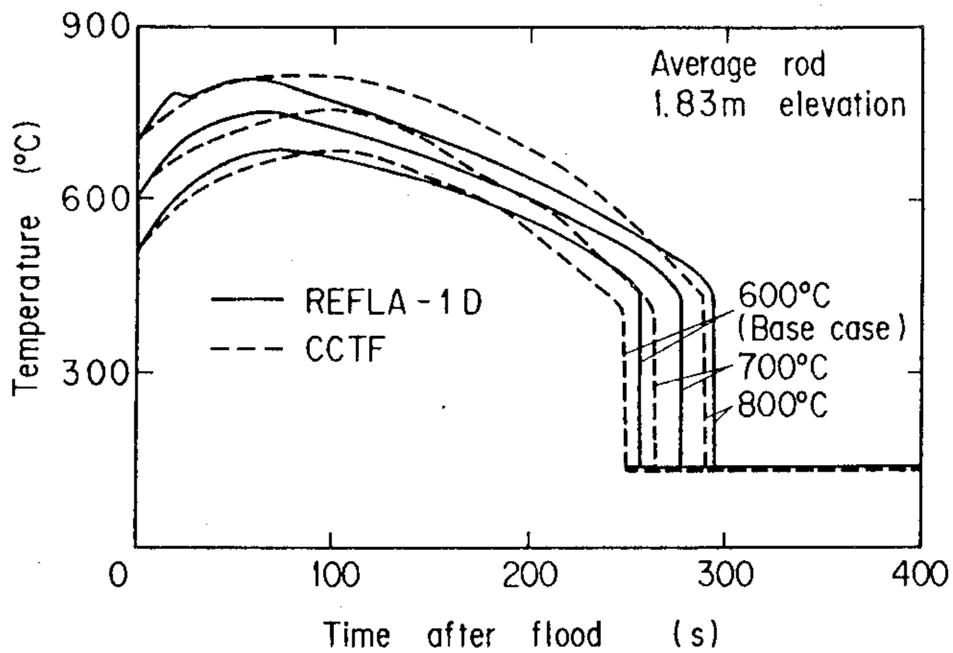

Fig. 3.11 Rod surface temperature histories for initial clad temperature effects tests

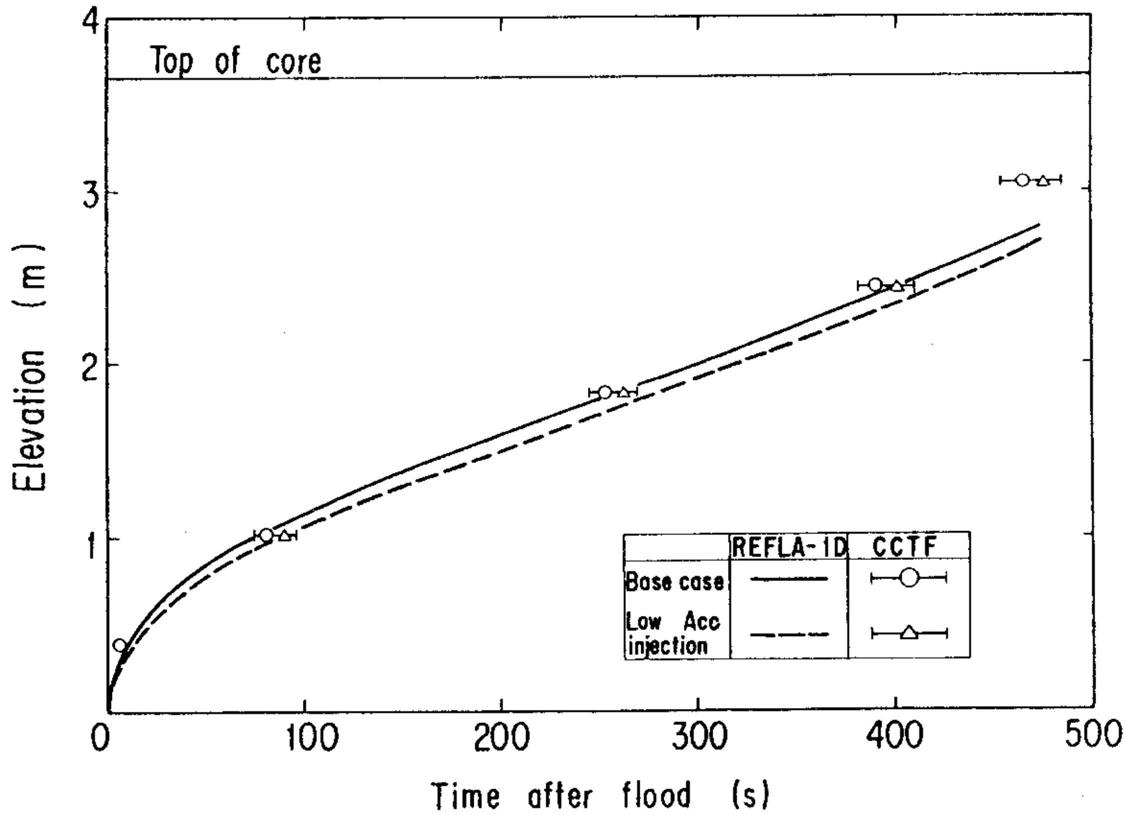

Fig. 3.12 Quench envelopes for Acc injection rate effects tests

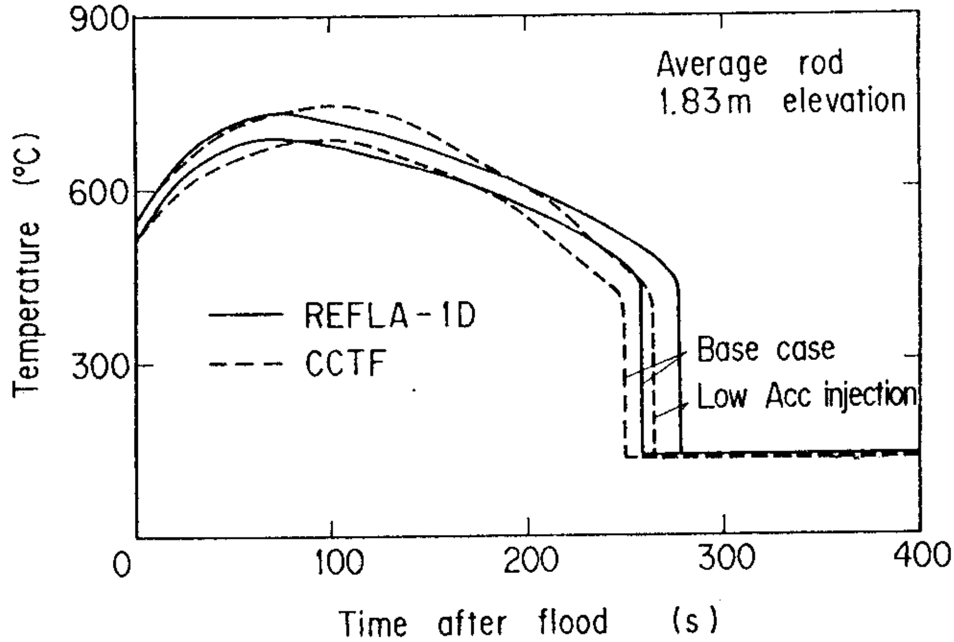

Fig. 3.13 Rod surface temperature histories for Acc injection rate effects tests

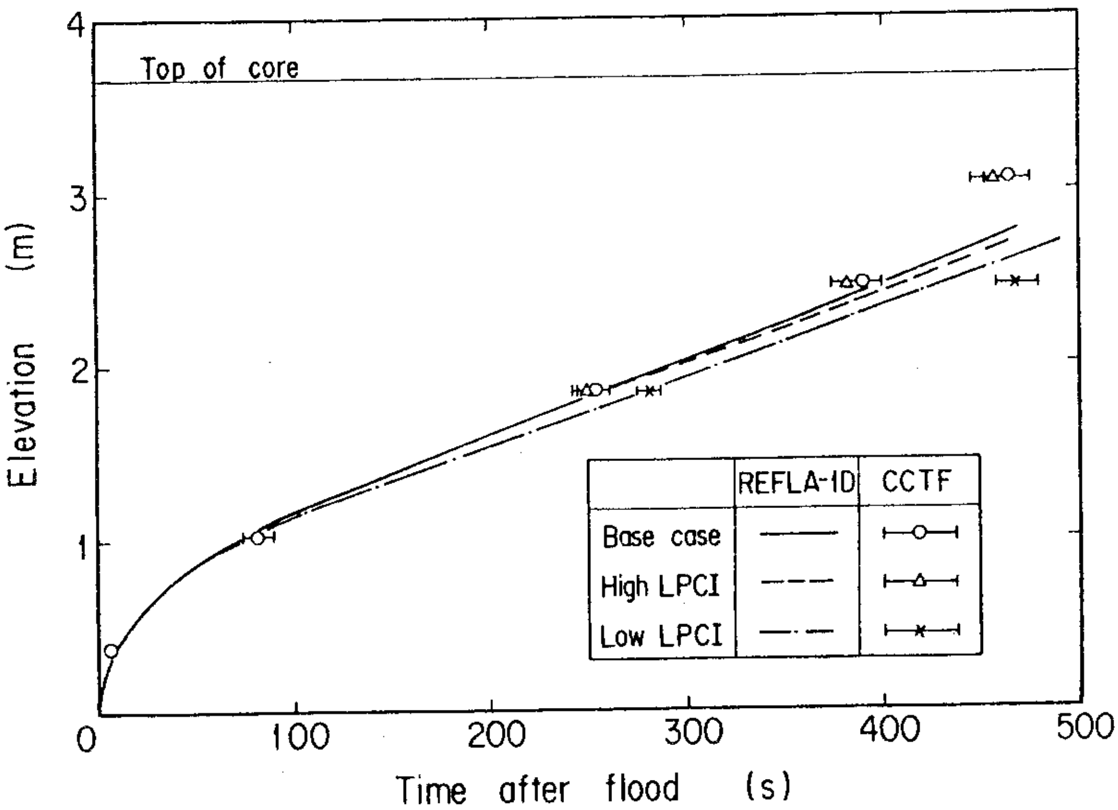

Fig. 3.14 Quench envelopes for LPCI injection rate effects tests

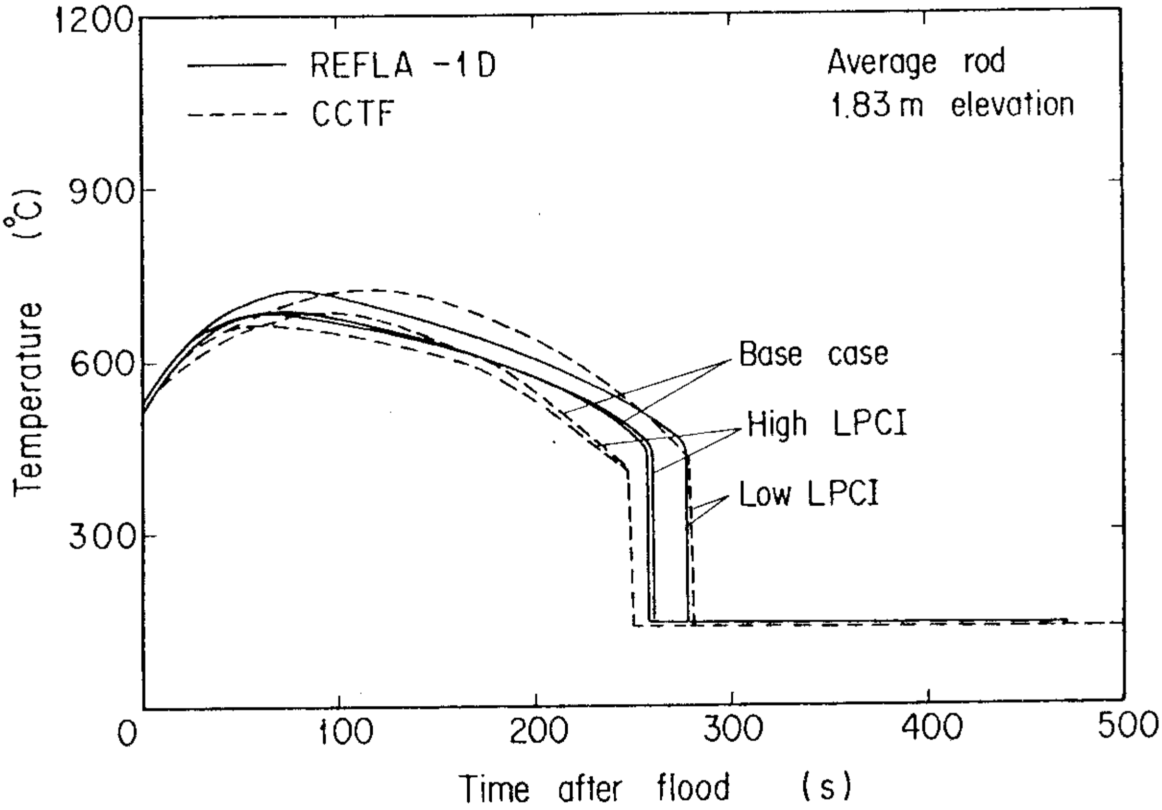

Fig. 3.15 Rod surface temperature histories for LPCI injection rate effects tests

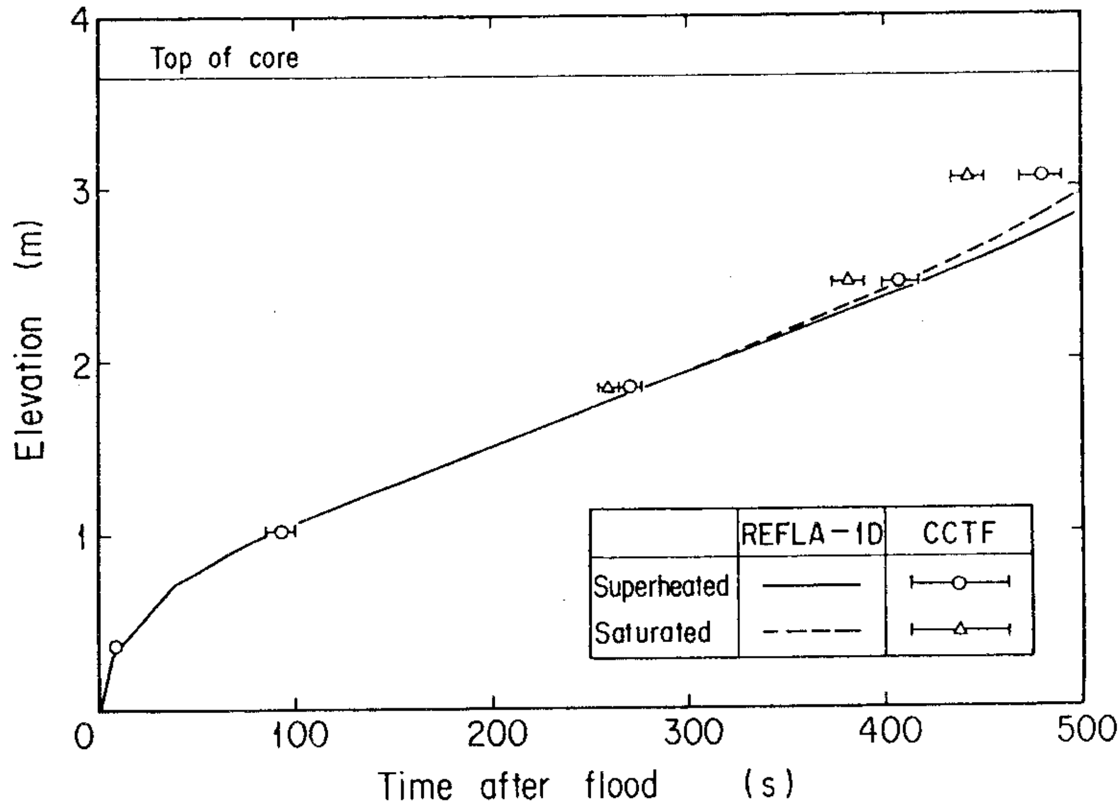

Fig. 3.16 Quench envelopes for initial downcomer wall temperature effects tests

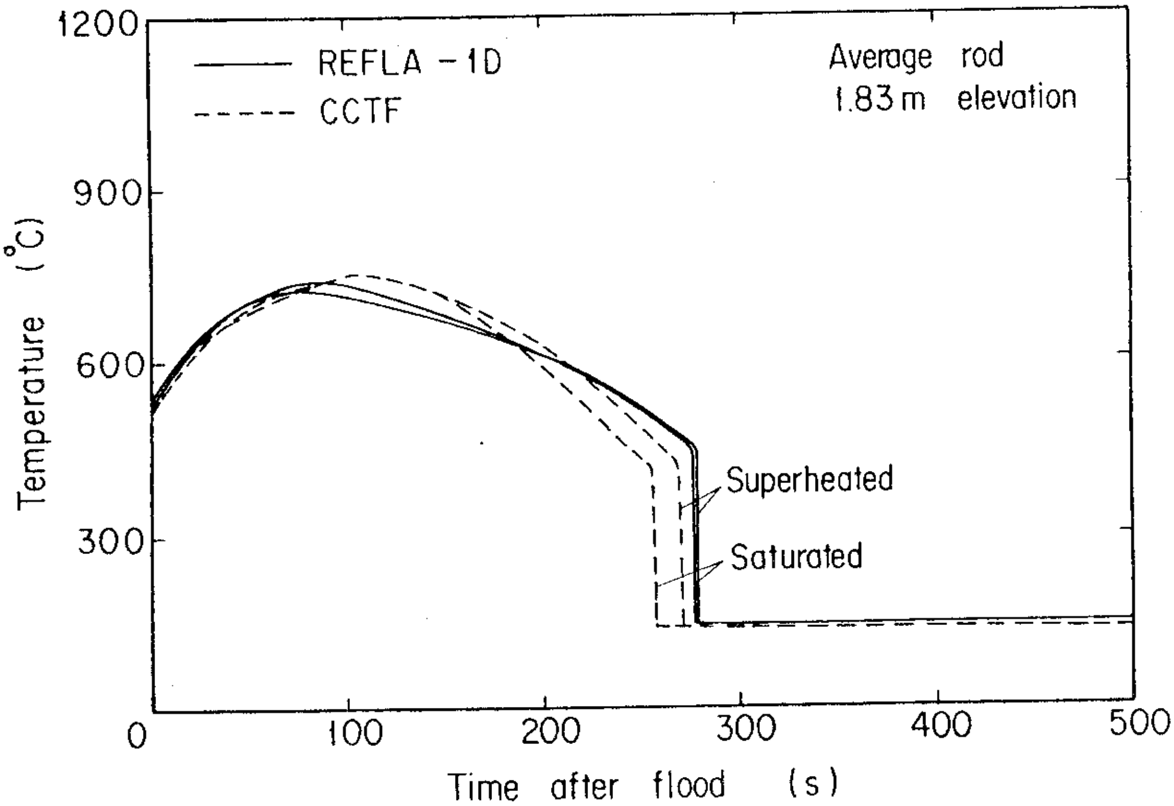

Fig. 3.17 Rod surface temperature histories for initial downcomer wall temperature effects tests

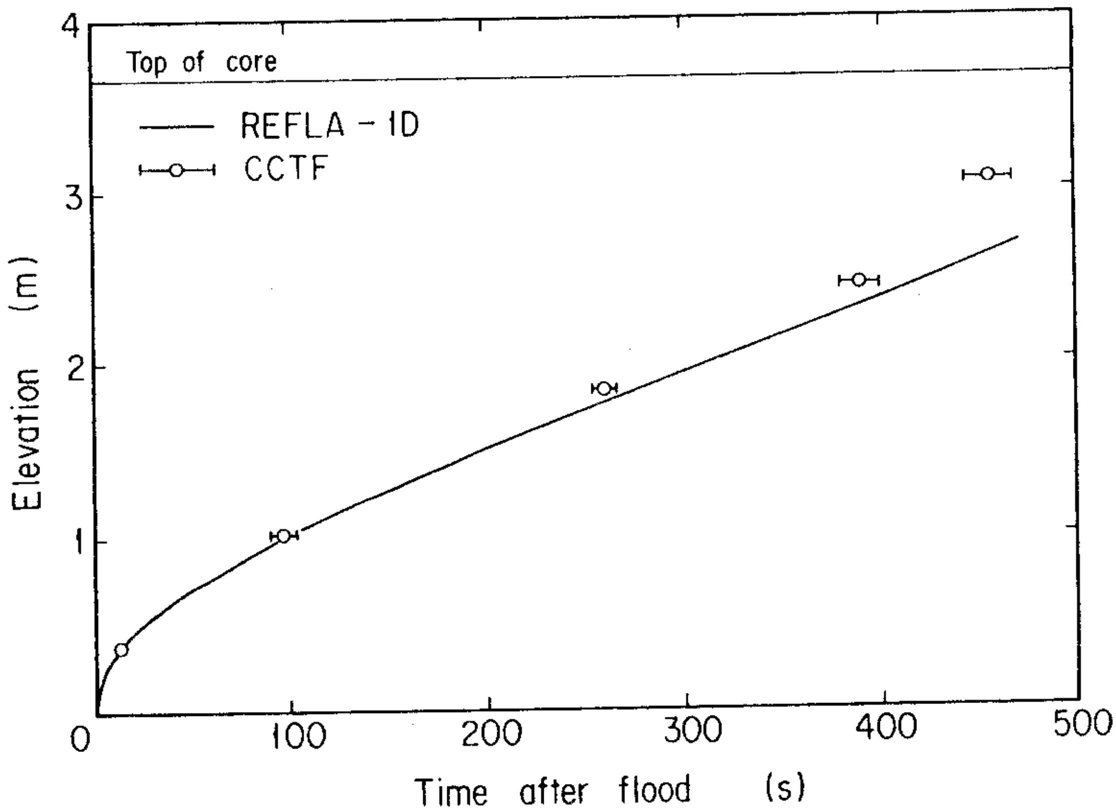

Fig. 3.18 Quench envelope for average power rod in EM test

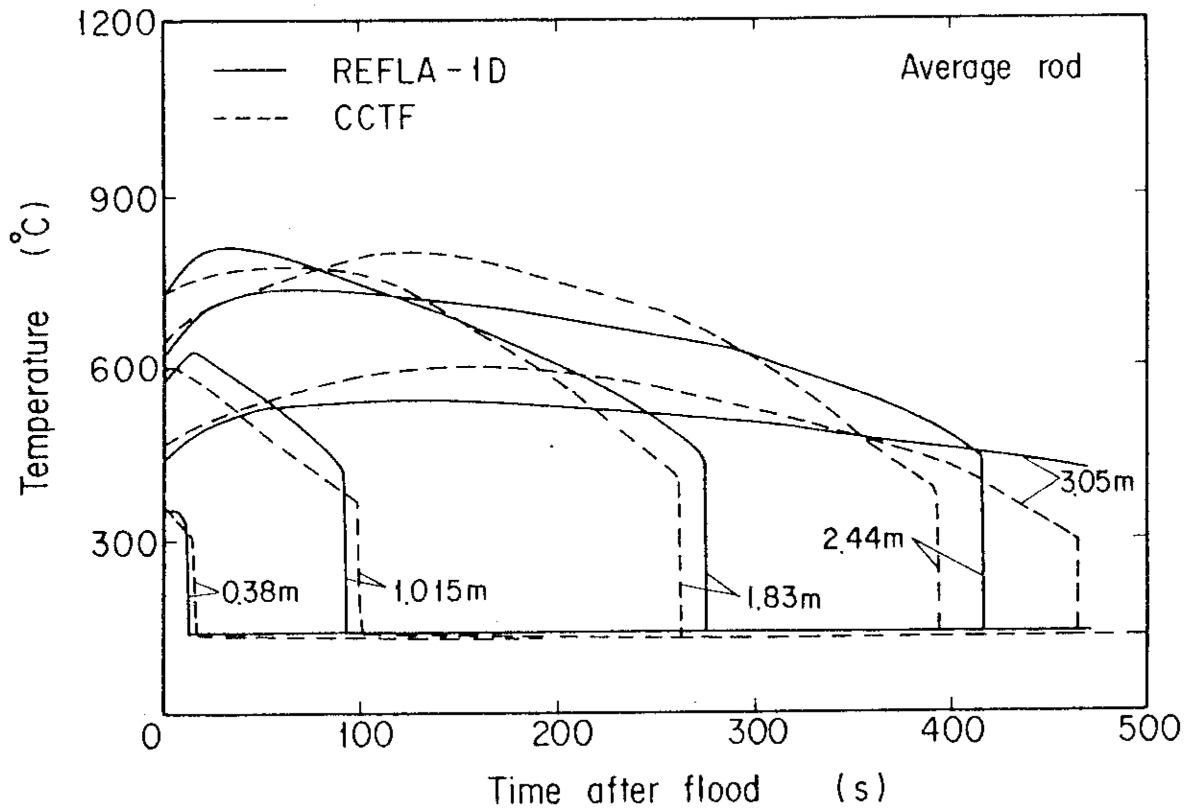

Fig. 3.19 Rod surface temperature histories for average power rod in EM test

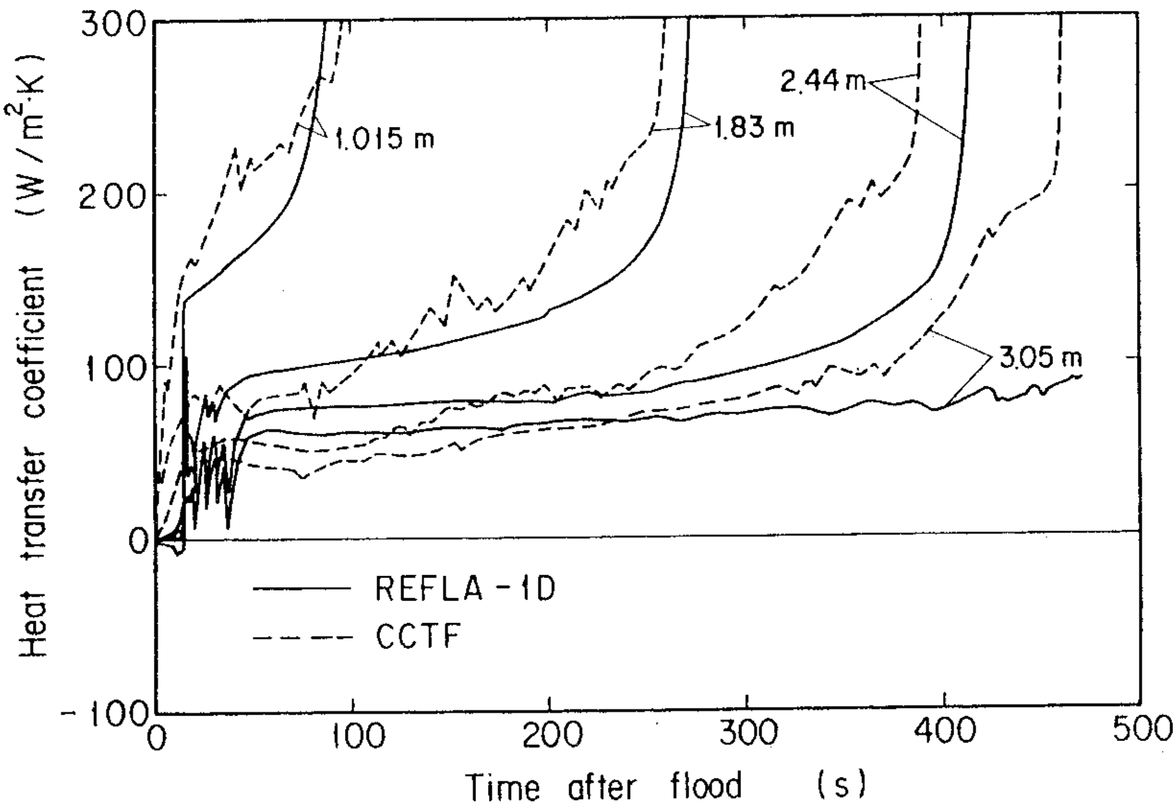

Fig. 3.20 Heat transfer coefficients for average power rod in EM test

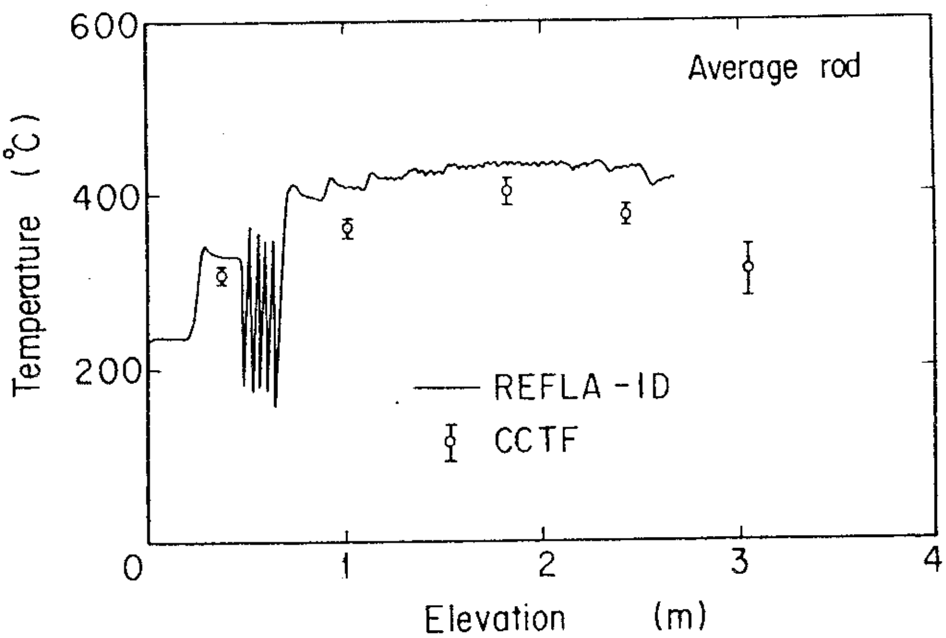

Fig. 3.21 Quench temperatures for average power rod in EM test

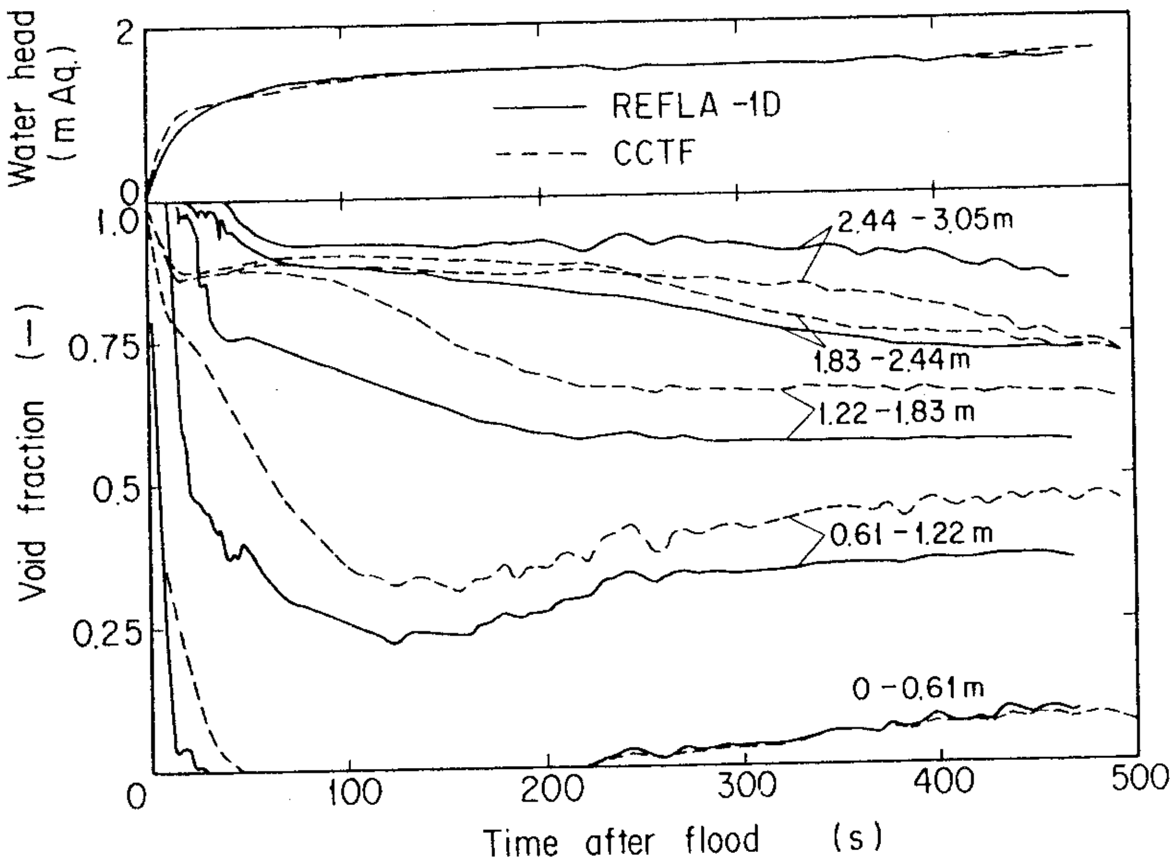

Fig. 3.22 Core water head and void fractions in EM test

4. Discussion

4.1 Characteristic of Calculational Results for CCTF Tests Comparing with Results for Small Scale Facilities' Experiments

According to the results[3] of the REFLA-1D/MODE3 calculations for the experiments using the small scale facilities, REFLA-1D/MODE3 predicts the core thermo-hydrodynamic behavior in those facilities well by selecting Case 1 or Case 2 model case by case. For the JAERI small scale facility, Case 2 predicts the experimental results well, whereas for the FLECHT low flooding facility Case 1 is generally good. As shown in Figs. 3.2 (a) and (b), Case 2 predicts the CCTF data well.

The difference like this seems to be caused by the difference in the facility design and the experimental conditions. The former means the design of flow housing and upper plenum structure including top nozzle or end box structure. The latter includes the initial temperatures of flow housing, heater rods and the core flooding rate.

Since the CCTF is a large scale facility with a wide core and its system simulates an actual PWR considerably well, the effects of flow housing is negligible and the core flooding rate is considered to be the realistic value. The upper plenum and end box regions are also simulated in the CCTF. Therefore, the core thermo-hydrodynamic behavior observed in the CCTF is inferred to be the same as that in an actual PWR. This suggests that the thermo-hydrodynamic behavior described with Case 2 model takes place in the core of an actual PWR, considering the fact that Case 2 predicts the CCTF data well.

On the other hand, Case 1 model does not describe the water accumulation above the quench front but describes the dispersed flow above the quench front which was observed generally in the family of FLECHT experiments. The reason the dispersed flow was generally observed above the quench front in those experiments seems to be the incomplete simulation of the upper plenum and end box structures. The effect of flow housing may also be important.

4.2 General Characteristics of Calculational Results for CCTF Tests

Judging from the comparisons of the calculated results with the CCTF data, such as Figs. 3.3 through 3.7 and Figs. 3.18 through 3.22, it is recognized that REFLA-1D/MODE3 can predict the core thermo-hydrodynamics in the CCTF generally well and the degree of agreement is satisfactory for the practical purpose. However, as pointed out in Sections 3.2 and 3.4, there are some differences between the prediction and the experiment. For the thermo-dynamics:

1. The cooling in the calculation is not as good as in the experiment during the period of about 100 s prior to quenching. This tendency is more significant at higher elevations.
2. The calculation tends to give the better core cooling at upper elevations (2.44 m and 3.05 m) during about first 150 s.
3. The cooling in the calculation at 1.015 m and 1.83 m elevations is not as good as in the experiment during about first 20 s.

For the hydrodynamics:

4. In the initial period, the calculation tends to give the higher void fractions. This tendency is more significant at higher elevations. The experimental value starts to decrease from the beginning of reflooding in every section, whereas the calculational results show the delay of decrease in the sections above 0.61 m elevation.
5. After that time period, the calculation tends to give the lower void fractions in the sections below 2.44 m elevation, whereas the higher void fractions in the sections above 2.44 m elevation.

Item 1 above seems to be attributed to the problem of the heat transfer coefficient model. Item 2 above is also attributed to the problem of the heat trnasfer coefficient model. Comparing the heat transfer coefficients in Fig. 3.5 with the void fractions in Fig. 3.7, it is found that the calculated heat transfer coefficients have a strong relation with the void fraction and increase rapidly following the rapid decreases of the calculated void fractions, whereas the experimental heat transfer coefficients have more weak relation with the void fractions and increase gradually during about first 150 s.

Item 3 above is mainly caused by the problem pointed out in item 4. In the present hydrodynamic model used in REFLA-1D, the liquid entrainments can not be generated and distributed to the upper portion of the core instantaneously after the reflood initiation and it takes time (about 20 s in the base case test) for void fractions in the upper portion of the core to start decreasing. By this reason the problem of item 4 occurs and this higher void fractions result in the worse core cooling in that period as pointed out in item 3.

Item 5 above is attributed to the problem in hydrodynamic model.

In the present calculation, however, the quantitative reflection to the heat transfer coefficient is not observed significantly as shown in Figs. 3.5 and 3.20.

Items 1, 2 and 5 are also observed in the calculations for the JAERI small scale tests(3). However, items 3 and 4 are not observed in these calculations. This is because the hydrodynamic characteristic is a little different between the CCTF and the JAERI small scale facility in the initial period. This difference is not easily attributed to the difference in the scaling ratio because the facility designs are not the same. For instance, the simulation of the upper plenum and end box structures are different between these facilities.

4.3 Capability of Predicting Parameter Effects

The capability and the sensitivity of REFLA-1D to predict the parameter effects are summarized in the following:

1. The parameter effects of system pressure, initial clad temperature and Acc injection rate are predicted qualitatively correctly.
2. For the LPCI injection rate effects tests, the predicted tendency in quench envelope for the high LPCI injection rate test is not the same as observed in the experiment, although the quantitative difference is a little.
3. The parameter effects of initial clad temperature and Acc injection rate are predicted also quantitatively correctly.
4. The sensitivities to the system pressure, LPCI injection rate (only for high LPCI injection rate) and initial downcomer wall temperature are not good comparing with the experimental data, although the quantitative differences are not significant.

Figure 3.14 shows the problem pointed out in item 2 above. For the low LPCI injection rate test, both the qualitative and quantitative agreement between the calculated and the experimental results are good. For the high LPCI injection rate test, however, the calculated quench times are slightly longer than those for the base case test, whereas the experimental data give slightly shorter quench times than for the base case test. The main difference between these two tests has been found in the core flooding rate which is caused by the difference in the LPCI injection rate. The core flooding rates estimated by the mass balance calculation (see Section 3.1) are compared in Fig. 4.1. The difference in the core flooding rate between them is observed during the time of 25 s through 75 s. In this period the experimental data for the high LPCI injection rate test show better core cooling as shown in Fig. 3.15 and this seems to be the reason for the slightly shorter quench times. However, in the calculation, the better core cooling in that time period is not predicted and this seems to be the reason for the slightly longer quench times.

Regarding to items 4 above, the initial downcomer wall temperature effects have been found to mainly result in the difference in the core inlet subcooling. Therefore, it can be said that the sensitivity of REFLA-1D to the core inlet subcooling is not as good. However, the quantitative difference is not significant.

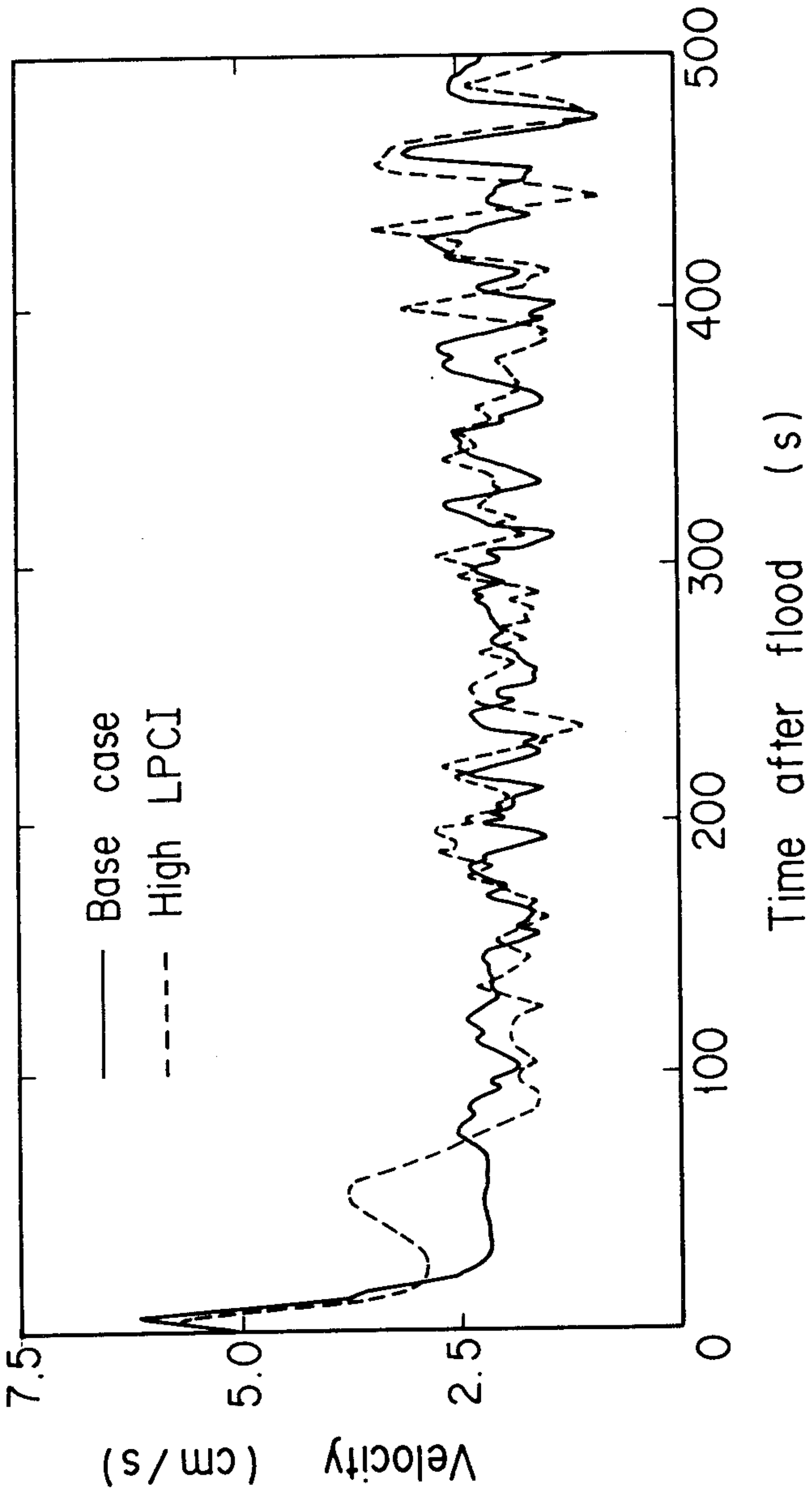

Fig. 4.1 Comparison of core flooding rate between base case and high LPCI injection rate tests

5. Conclusions

Based on the comparisons between the calculated results by REFLA-1D/MODE3 and the experimental data for eleven CCTF Core-I tests, the following conclusions are obtained.

1. The experimental results of the CCTF tests are predicted well by using the water accumulation model Case 2. The other model Case 1 can not predict the CCTF results well.
2. The calculated results are generally in good agreement with the CCTF data. However, comparing in detail, the following items 3 through 7 are pointed out as the differences.
3. The cooling in the calculation is not as good as in the experiment during the period of about 100 s prior to quenching. This tendency is more significant at higher elevations.
4. The calculation tends to give the better core cooling at upper elevations (2.44 m and 3.05 m) during about first 150 s.
5. The cooling in the calculation at 1.015 m and 1.83 m elevations is not as good as in the experiment during about first 20 s.
6. In the initial period, the calculation tends to give the higher void fractions. This tendency is more significant at higher elevations. The experimental value starts to decrease from the beginning of reflooding in every section, whereas the calculational results show the delay of decrease in the sections above 0.61 m elevation.
7. After the initial period mentioned above in item 6, the calculation tends to give the lower void fractions in the sections below 2.44 m elevation, whereas the higher void fractions in the sections above 2.44 m elevation.
8. The parameter effects of system pressure, initial clad temperature and Acc injection rate are predicted qualitatively correctly.
9. For the LPCI injection rate effects tests, the predicted tendency for the high LPCI injection rate test is not the same as observed in the experiment, although the quantitative difference is a little.
10. The parameter effects of initial clad temperature and Acc injection rate are predicted also quantitatively correctly.
11. The sensitivities to the system pressure, LPCI injection rate (only for high LPCI injection rate) and initial downcomer wall temperature are not good comparing with the experimental data, although the quantitative differences are not significant.

References

1. Murao, Y., *et al.*, "REFLA-1D/MODE1: A Computer Program for Reflood Thermo-hydrodynamic Analysis during PWR-LOCA, User's Manual", JAERI-M 9286 (1981).
2. Murao, Y., *et al.*, "REFLA-1D/MODE3: A Computer Program for Reflood Thermo-hydrodynamic Analysis during PWR-LOCA, User's Manual", (To be published).
3. Murao, Y., "Study of the Thermo-hydrodynamic Phenomena in the Nuclear Core During Reflood Phase" (in Japanese), JAERI-M 83-032 (1983).
4. For instance, Iguchi, T, *et al.*, "Data Report on Series 6 Reflood Experiment (Constant Flooding Rate Experiment Data)" (in Japanese), JAERI-M 8161 (1979).
5. For instance, Rosal E.R., *et al.*, "FLECHT Low Flooding Rate Cosine Test Series Data Report", WCAP-8651 (1975).
6. Hirano, K. and Murao, Y., "Large Scale Reflood Test" (in Japanese), J. At. Energy Soc. Japan, 22 [10], 681 (1980).
7. Murao, Y. and Iguchi, T., "Experimental Modeling of Core Hydrodynamics during Reflood Phase of LOCA", J. Nucl. Sci. Tech., 19[8] pp.613-627 (1982).
8. Murao, Y. *et al.*, "Evaluation report on CCTF Core-I reflood test C1-19 (Run 38) —— Experimental assessment of the evaluation model for the safety analysis on the reflood phase of a PWR-LOCA ——", JAERI-M 83-029 (1983).

Appendix A

Input list for the base case test.

```
** RUN 14 **  BASE CASE TEST, P=2.0 BAR, AVP=1.4KW/M
     2.086        0.25         7.0         100.0        2.000         2.000
     100.0         8.0         8.0         0.1                 4.0
         2       433.3       720.0       820.0        755.3         565.3
        90                    10.7        14.3         3.66             1
        .1                                0.25
                              10.8      2000.0      0.41318


                 510.0

    1000.0
     499.0      1500.0
120.0




 3
    2        0.1     22          2.0    211          4.0
14
TE18Z11
TE18Z12
TE18Z13
TE18Z14
TE18Z15
DPLOOP1
DPDOWN5
DPLOOP4
DPCOREA
LT07RQ5V
LT06RQ5V
LT05RQ5V
LT04RQ5V
LT03RQ5V
LT02RQ5V
ULCRI1
TACRIN
LT01RQ5
PT00RNO
TE32X13
TE29X11
TE29X12
TE29X13
TE29X14
TE29X15
TE18Y11
TE18Y12
TE18X13
TE18X14
TE18X15
```

Appendix B

Graphic output of REFLA-1D calculations.

In this Appendix, the graphic output of REFLA-1D assessment calculations is presented for each of the CCTF tests. Twelve sets of graphs are presented in the following and each set consists of twelve graphs. The classification of the sets is summarized in Table B.1.

In each set, the first through fourth figures are experimental values and the remainder is the calculated. The first, second, third and fourth figures correspond to the sixth, seventh, ninth and tenth figures, respectively. The calculated data in the fifth through the last figures are the same types of data presented in the REFLA-1D/MODE1 manual[(1)]. The correspondence of elevation (abbreviated as EL.) numbers to actual elevations for rod surface temperatures (the second and seventh figures), heat transfer coefficients (the third and ninth figures) and void fractions (the forth and tenth figures) are summarized in Table B.2.

The units for the core flooding rate in the first and sixth figures are not mAq. but cm/s and the values can be obtained with the following equation:

$$UL1 = (y - 6) \times 5 \qquad (cm/s)$$

where the core flooding rate is UL1 and the value in the figures is y.

Table B.1 Classification of sets of graphs

Set No.	Description
B.1	Test C1-5 (Base case)
B.2	Test C1-5 (Base case, Case 1 model)
B.3	Test C1-12 (High system pressure, 0.3 MPa)
B.4	Test C1-10 (Low system pressure, 0.15 MPa)
B.5	Test C1-7 (High initial clad temperature, 700 °C)
B.6	Test C1-14 (High initial clad temperature, 800 °C)
B.7	Test C1-11 (Low Acc injection rate)
B.8	Test C1-6 (High LPCI injection rate)
B.9	Test C1-9 (Low LPCI injection rate)
B.10	Test C1-2 (Superheated initial downcomer temperature)
B.11	Test C1-3 (Saturated initial downcomer temperature)
B.12	Test C1-19 (EM)

Table B.2 Correspondence of elevation numbers to elevations

Fig. No. / Elevation No. (EL.)	Figs. 2, 3, 7 and 9	Figs. 4 and 10
1	0.38	0 - 0.61
2	1.015	0.61 - 1.22
3	1.83	1.22 - 1.83
4	2.44	1.83 - 2.44
5	3.05	2.44 - 3.05
6	3.66	3.05 - 3.66

Unit : m

B.1 Test C1-5 (Base case)

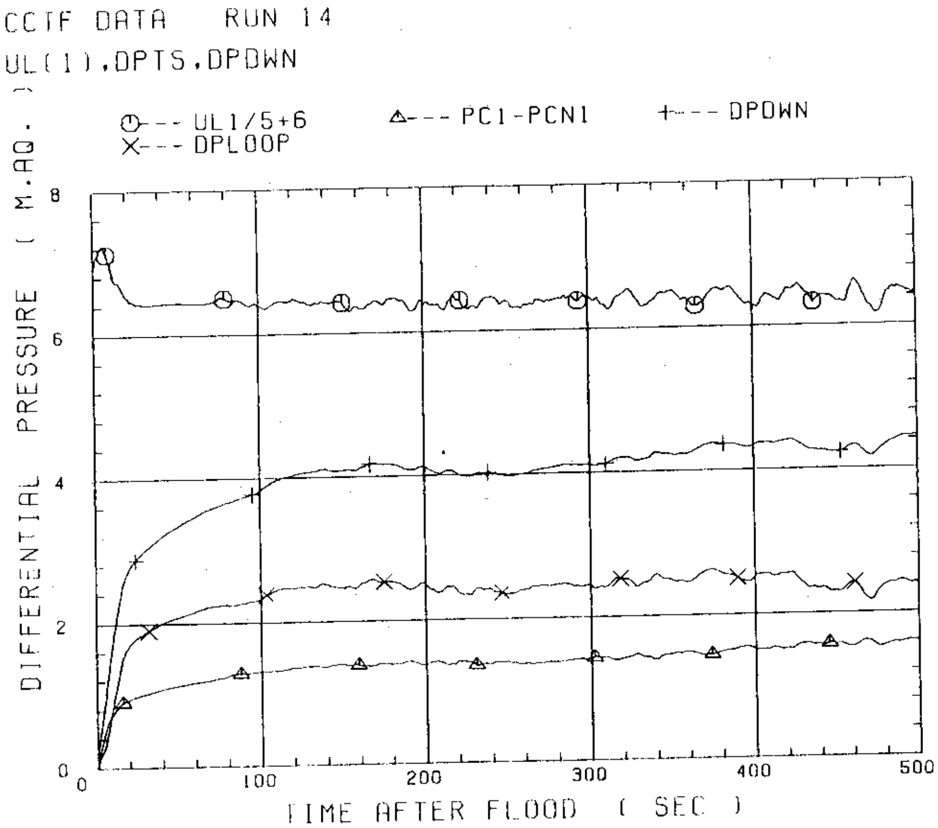

Fig. B.1.1 Core flooding rate (UL1), core differential pressure (PC1-PCN1), downcomer differential pressure (DPDWN) and loop differential pressure (DPLOOP) (Experimental value)

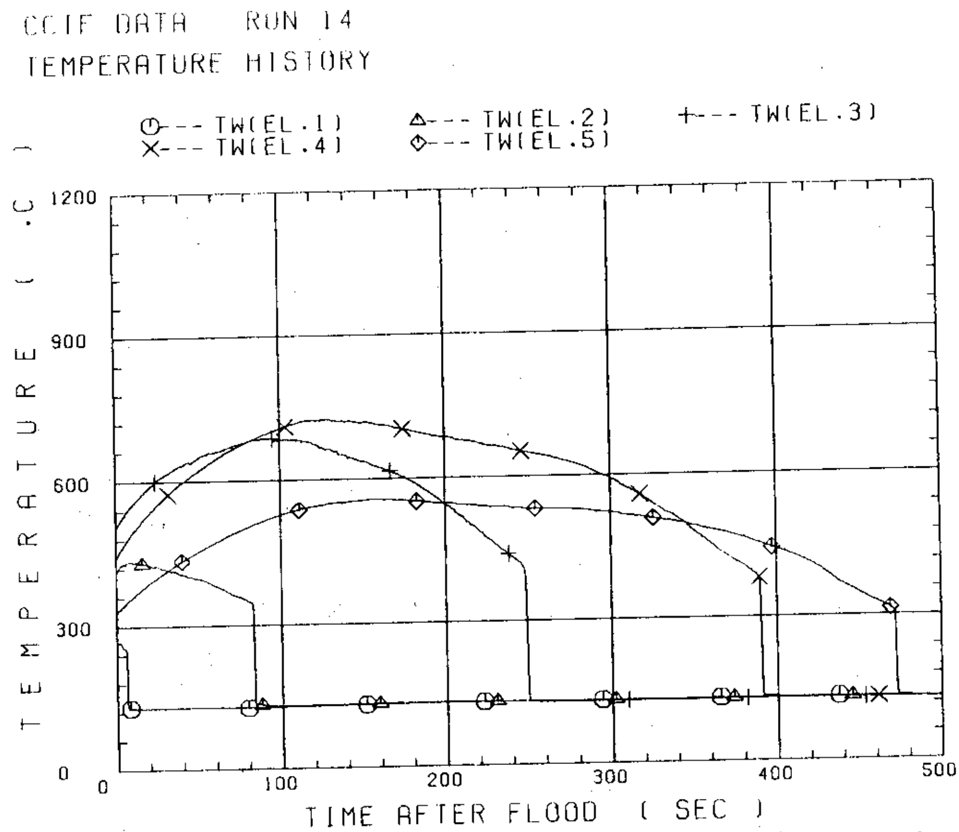

Fig. B.1.2 Rod surface temperatures (Experimental value)

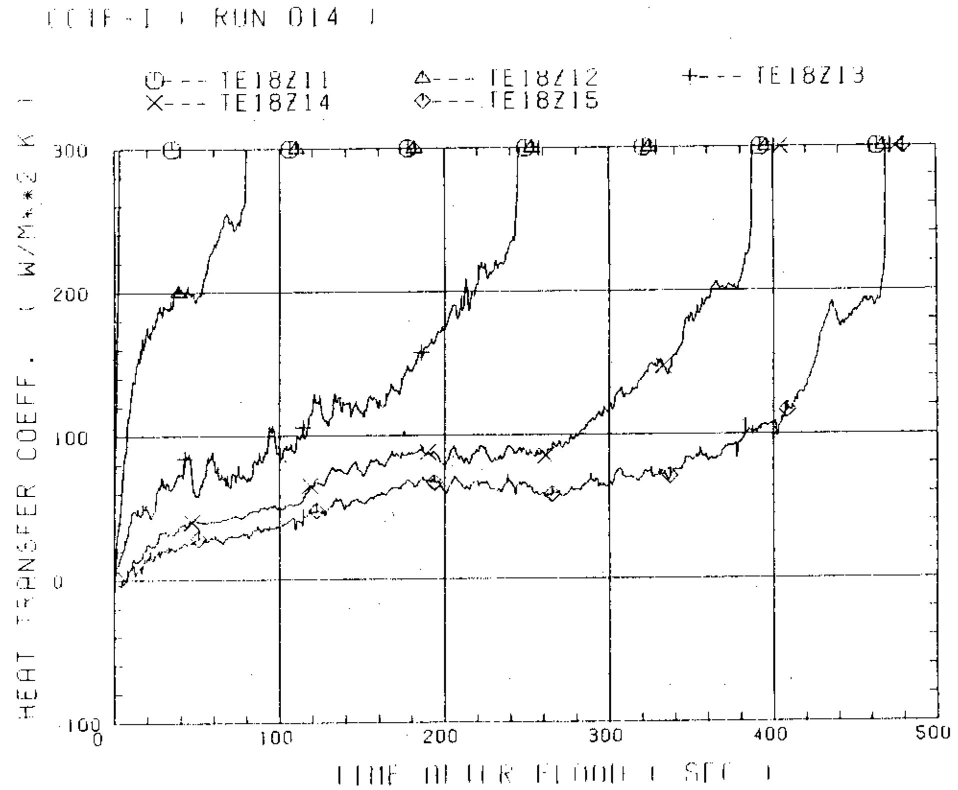

Fig. B.1.3 Heat transfer coefficients (Experimental values)

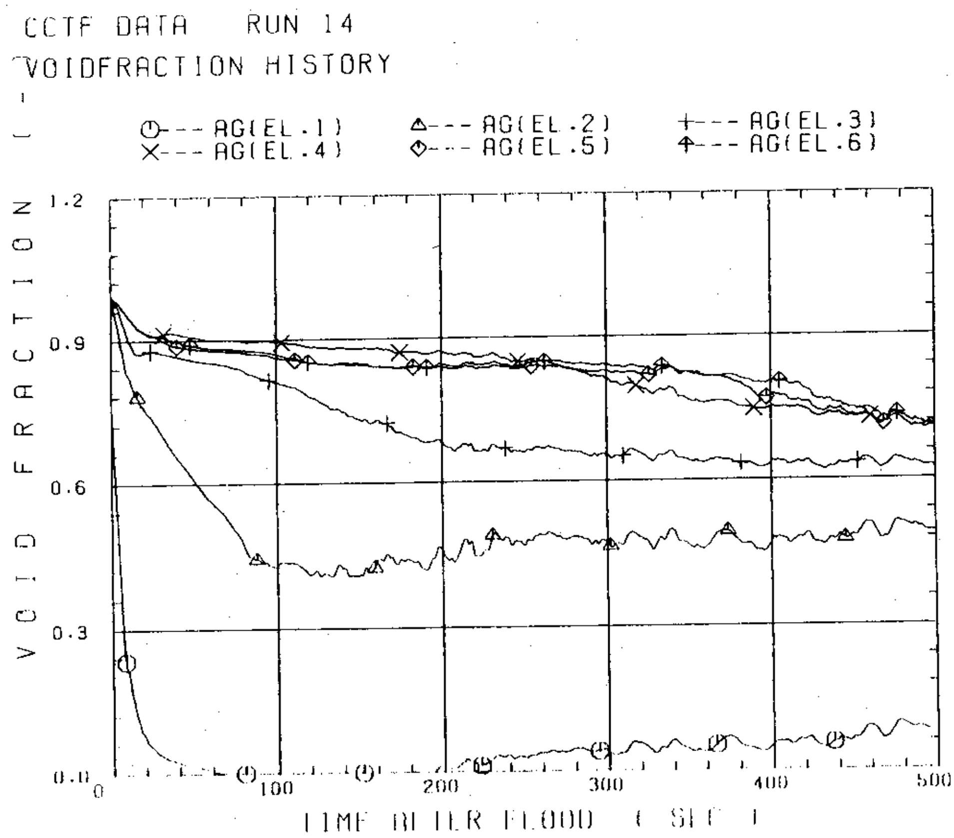

Fig. B.1.4 Void fractions (Experimental values)

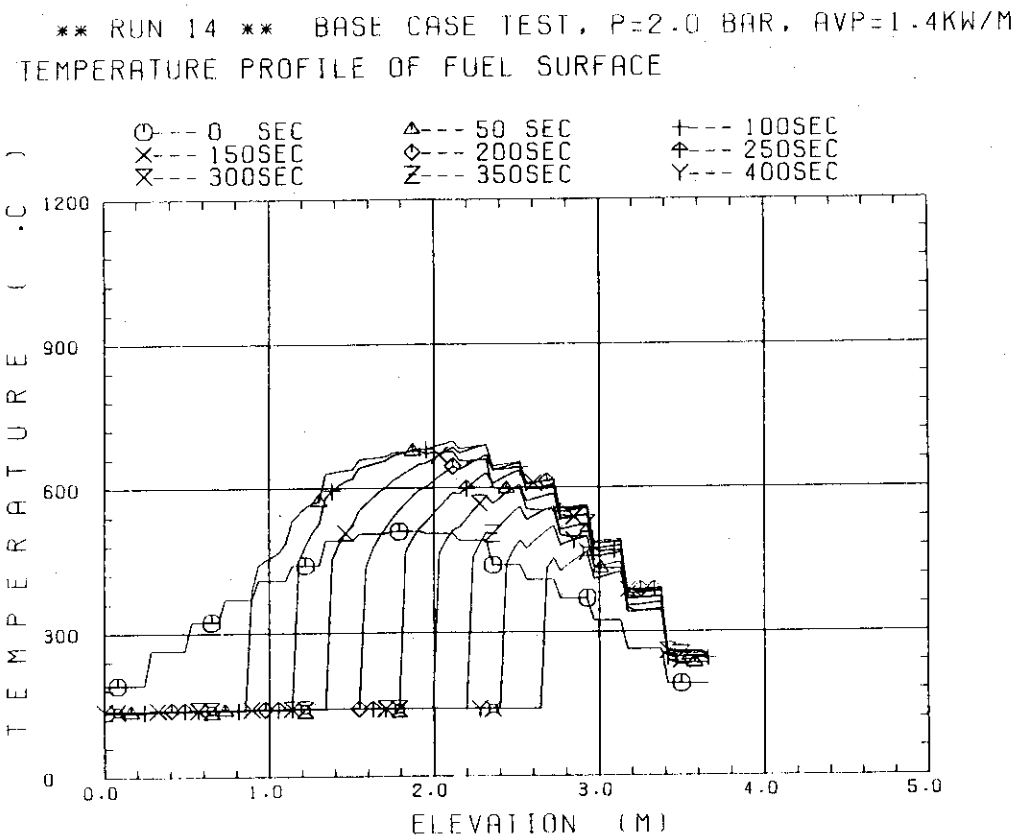

Fig. B.1.5 Rod surface temperature distributions

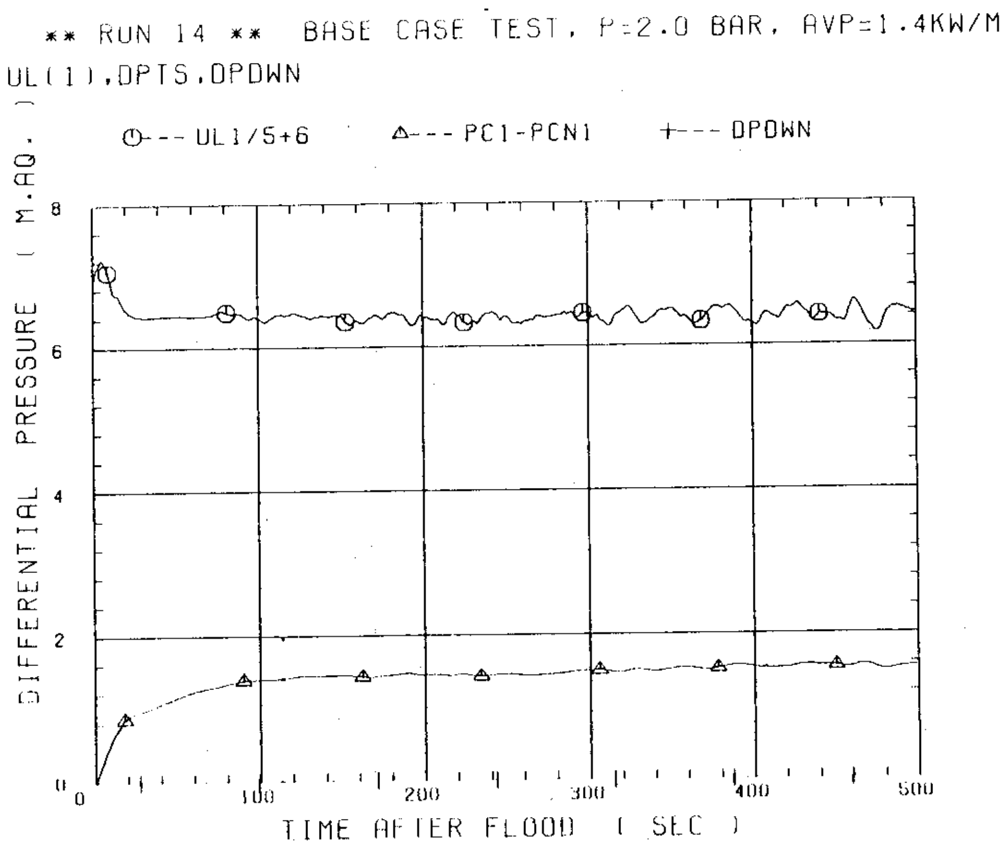

Fig. B.1.6 Core flooding rate (UL1) and core differential pressure (PC1-PCN1)

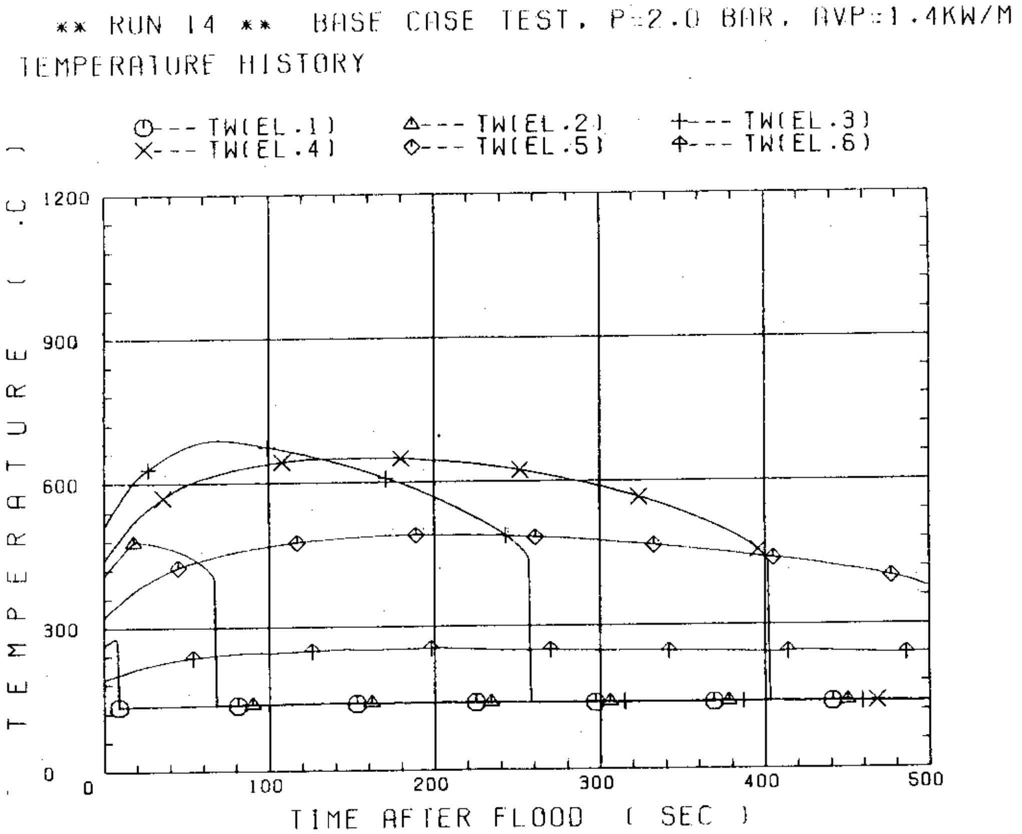

Fig. B.1.7 Rod surface temperatures

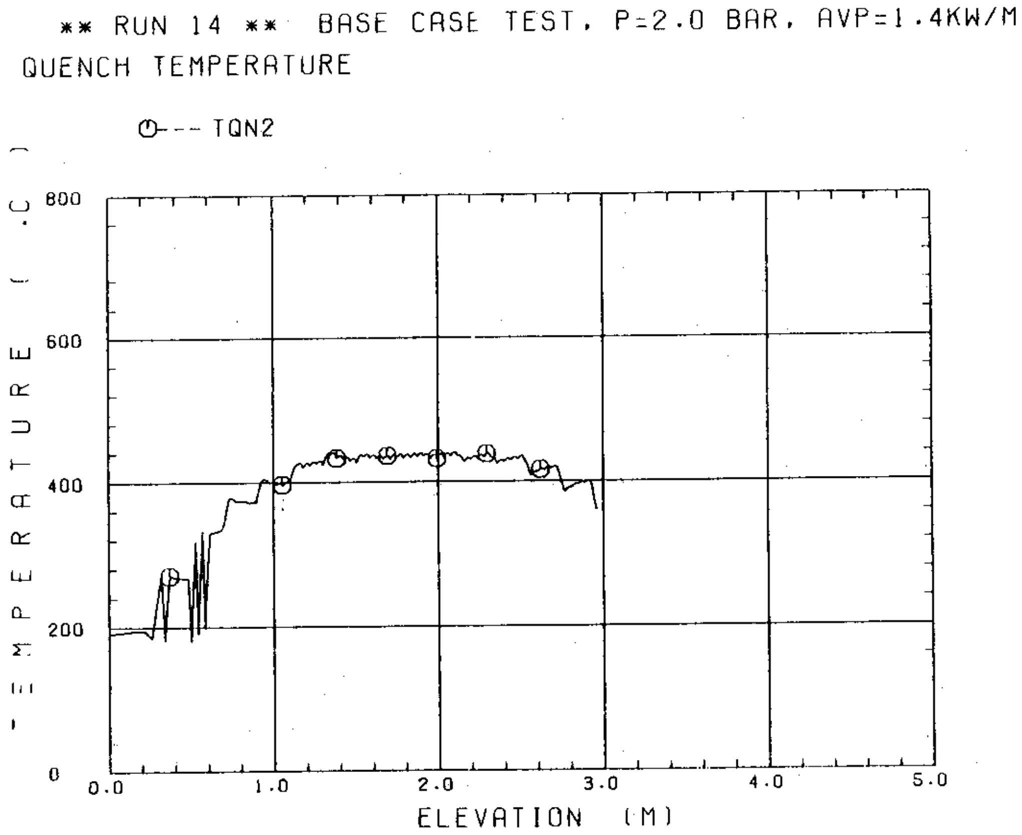

Fig. B.1.8 Quench temperatures

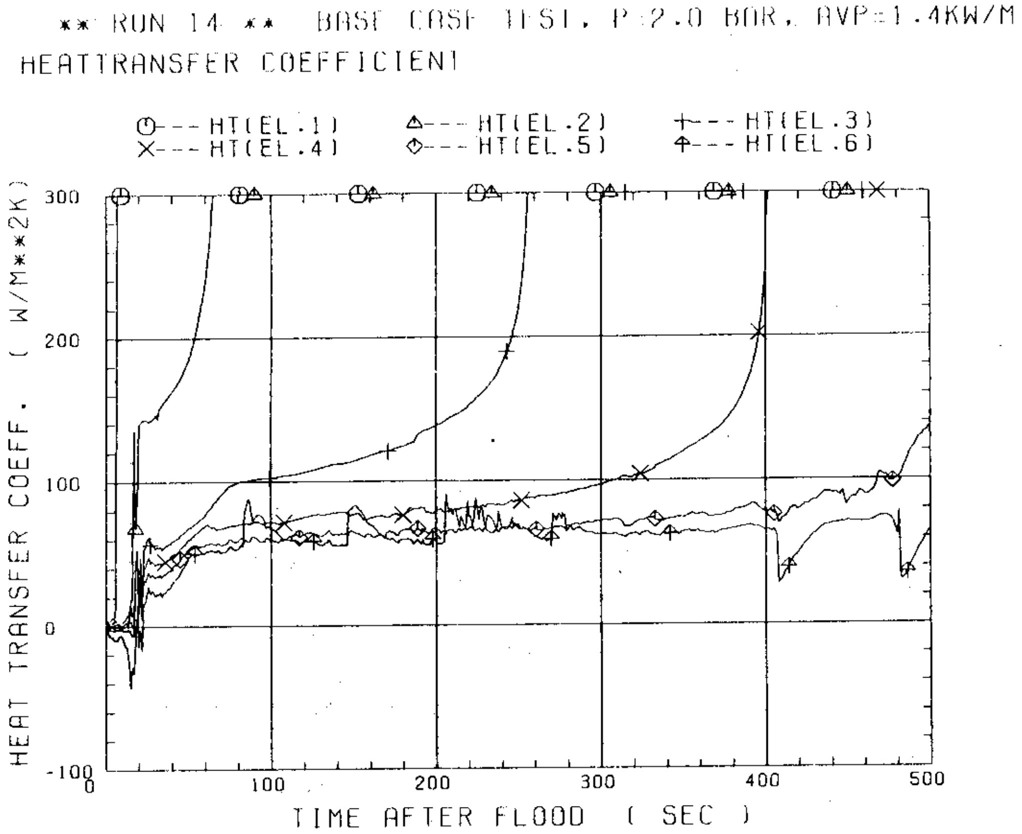

Fig. B.1.9 Heat transfer coefficients

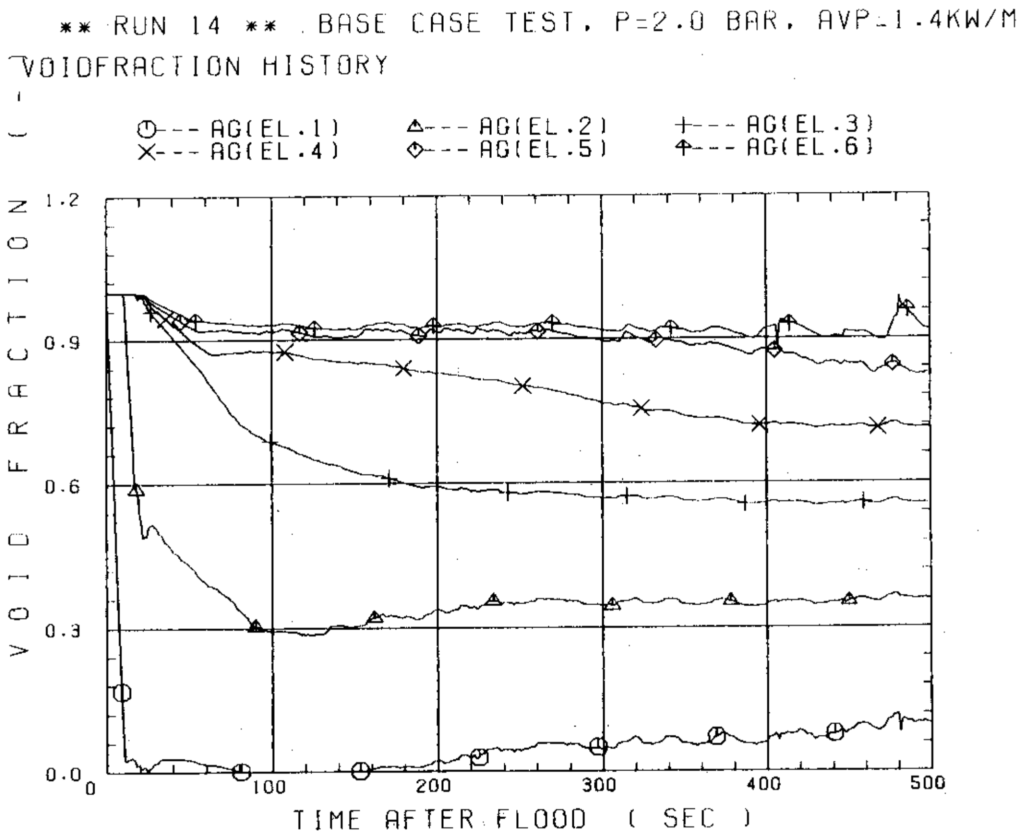

Fig. B.1.10 Void fractions

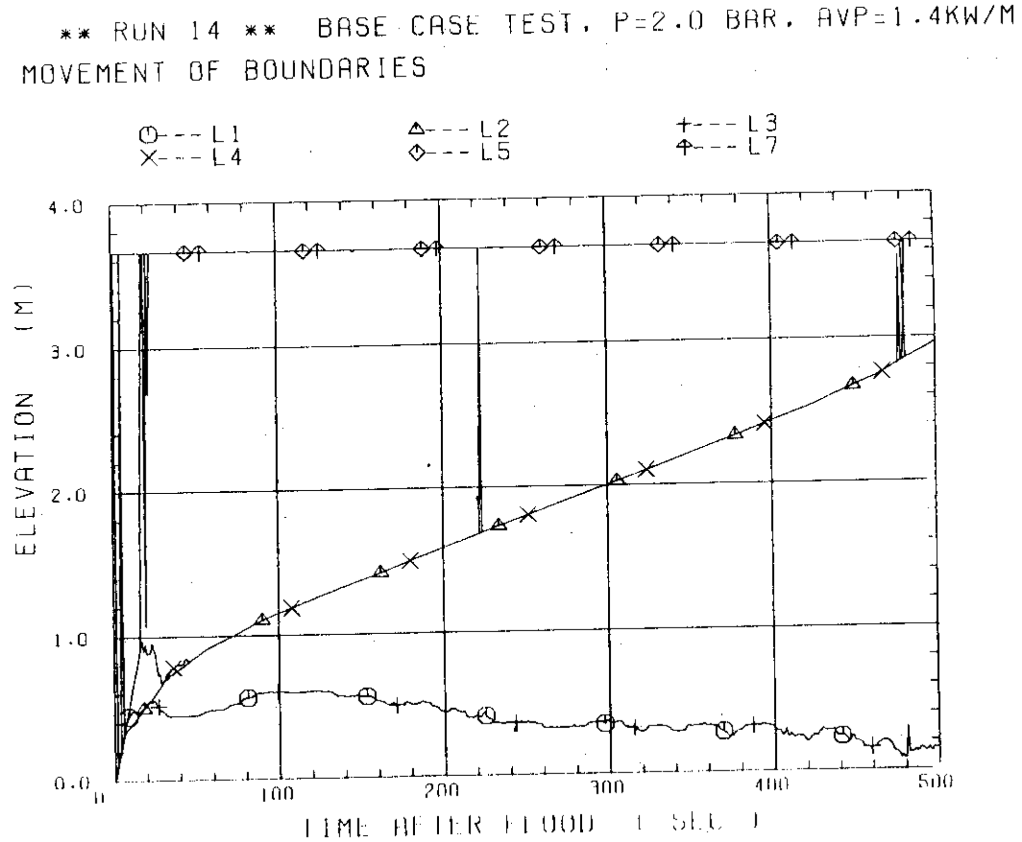

Fig. B.1.11 Movement of flow regime boundaries (L1: Boiling point, L2: Quench front)

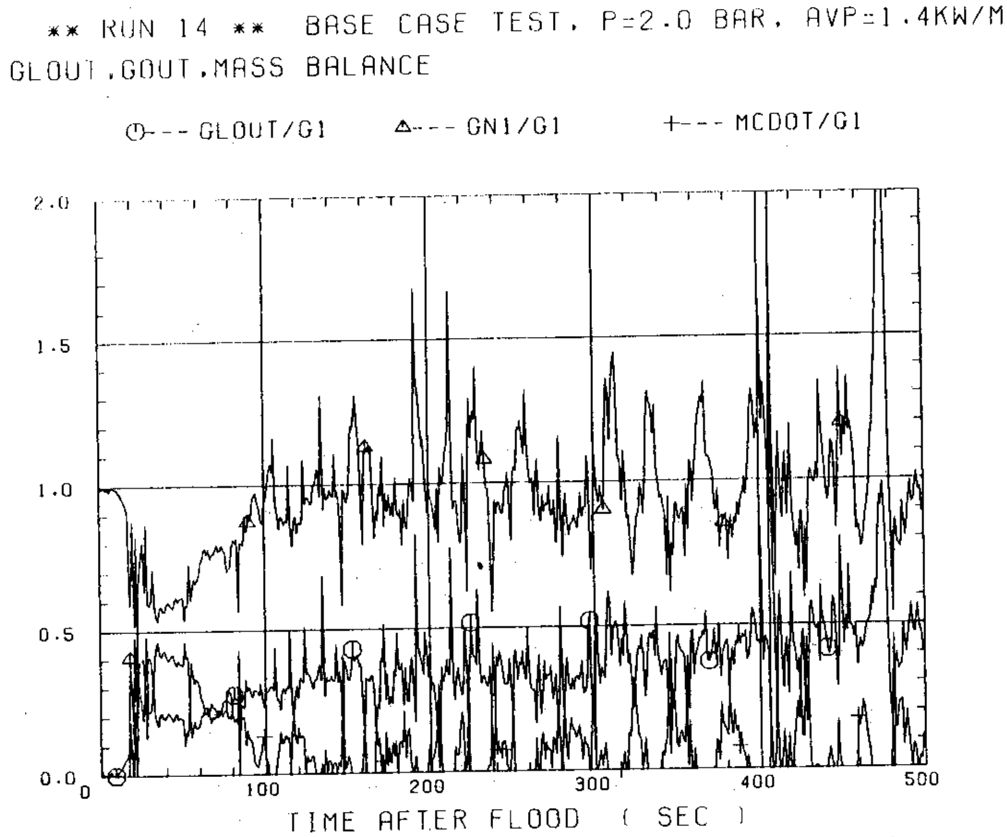

Fig. B.1.12 Liquid carryover rate fraction (GLOUT/G1), carryover rate fraction (GN1/G1) and water accumulation rate fraction (MCDOT/G1)

B.2 Test C1-5 (Base case, Case 1 model)

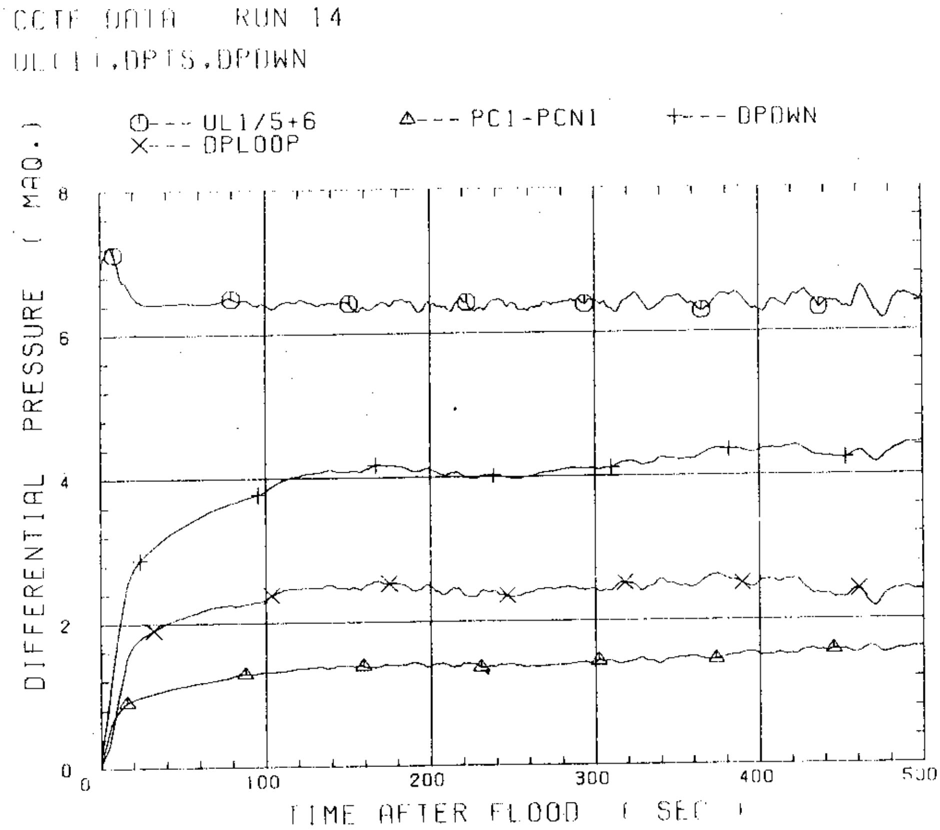

Fig. B.2.1 Core flooding rate (UL1), core differential pressure (PC1-PCN1), downcomer differential pressure (DPDWN) and loop differential pressure (DPLOOP) (Experimental value)

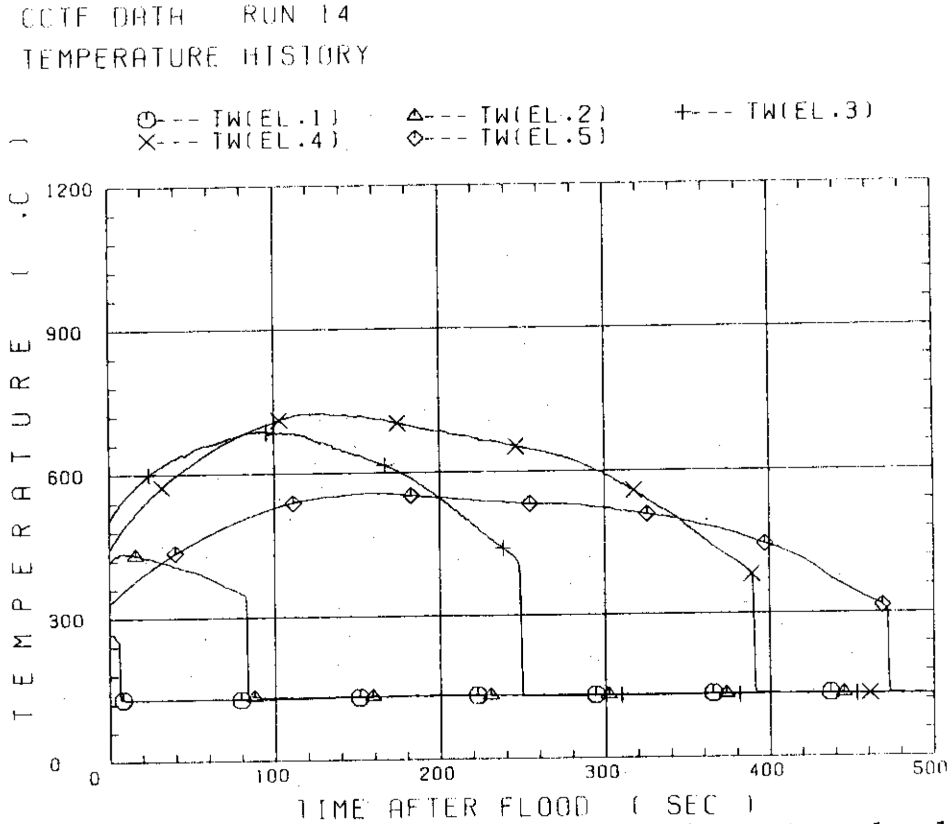

Fig. B.2.2 Rod surface temperatures (Experimental value)

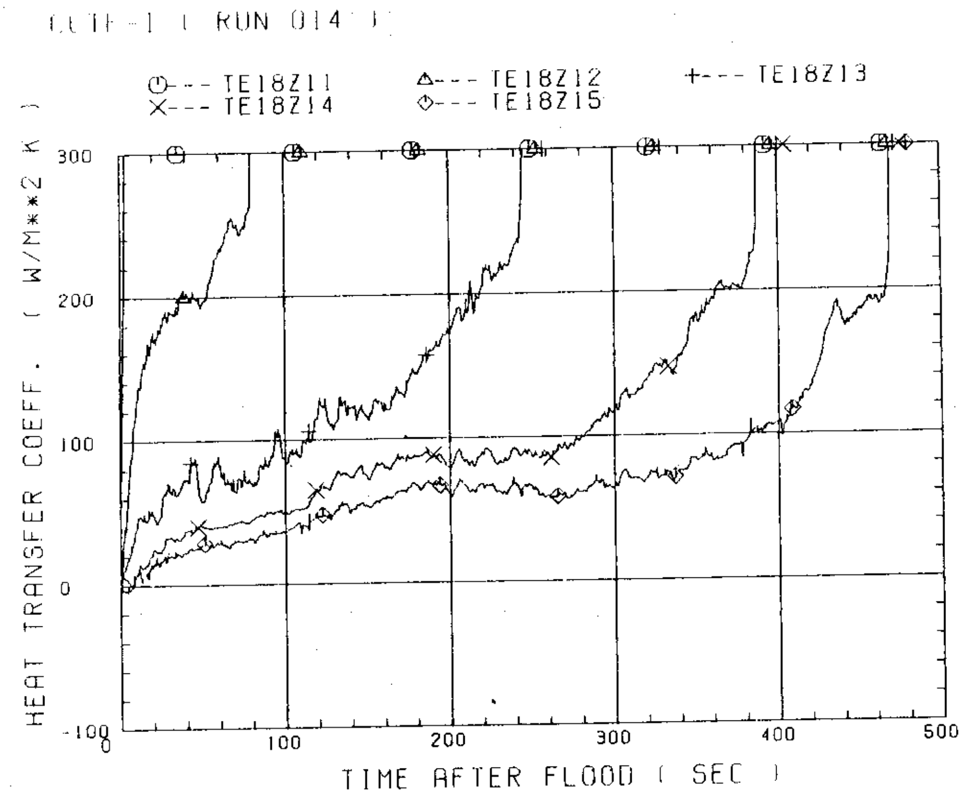

Fig. B.2.3 Heat transfer coefficients (Experimental values)

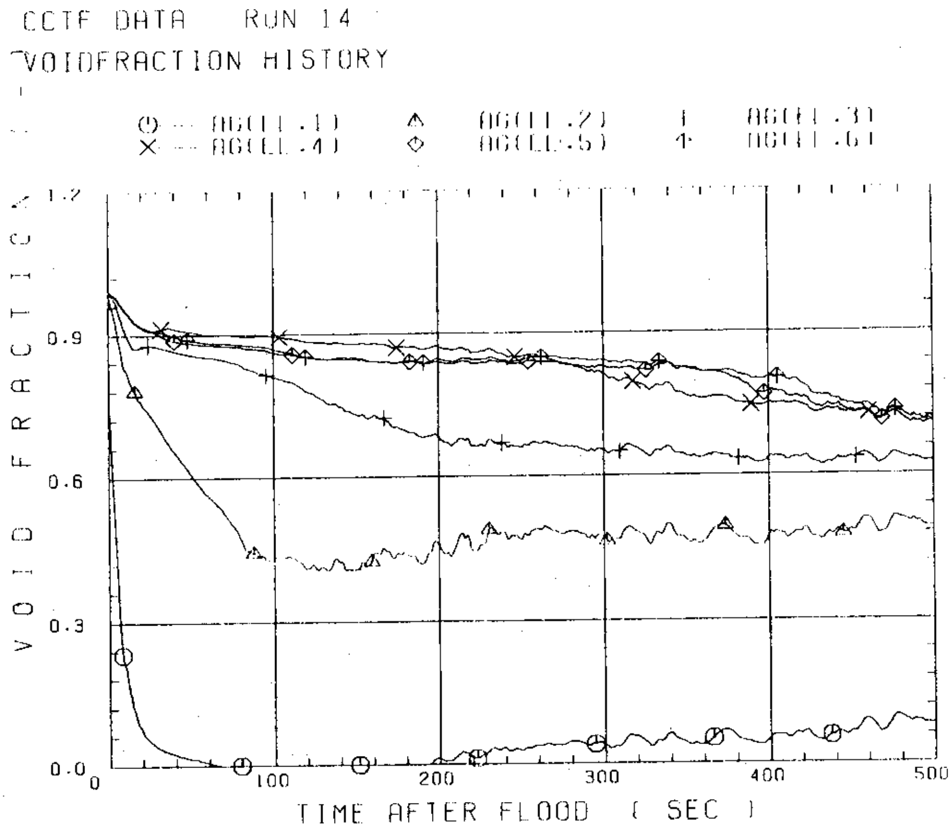

Fig. B.2.4 Void fractions (Experimental values)

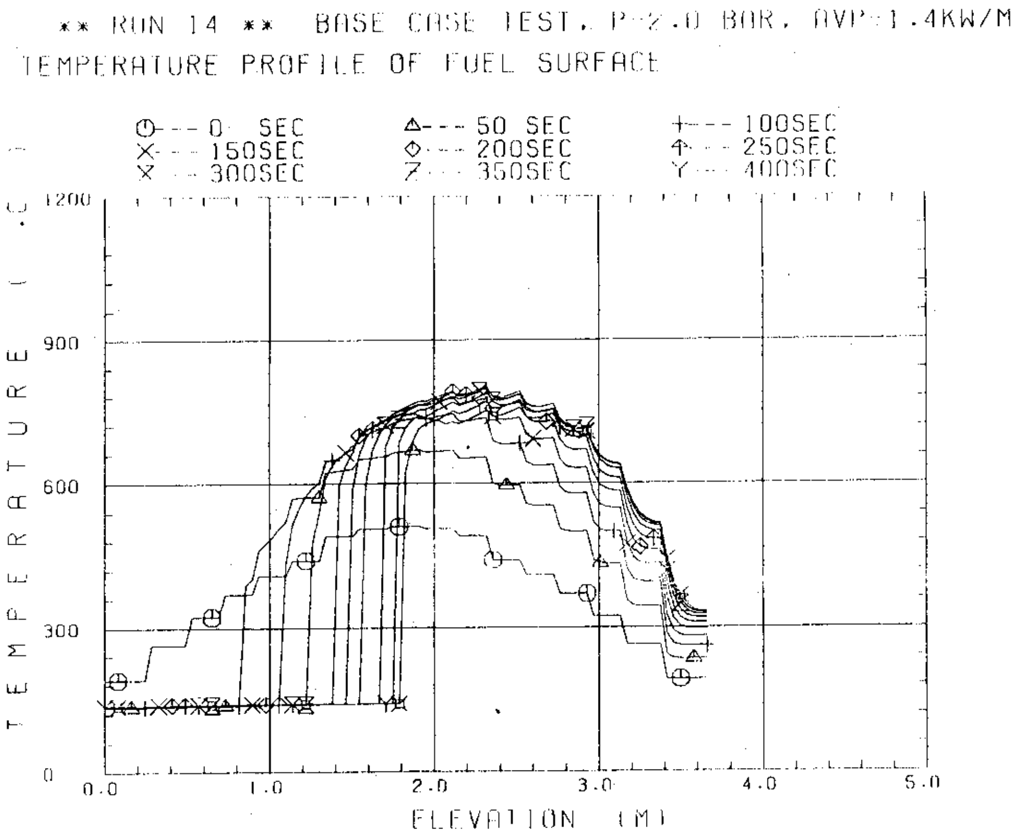

Fig. B.2.5 Rod surface temperature distributions

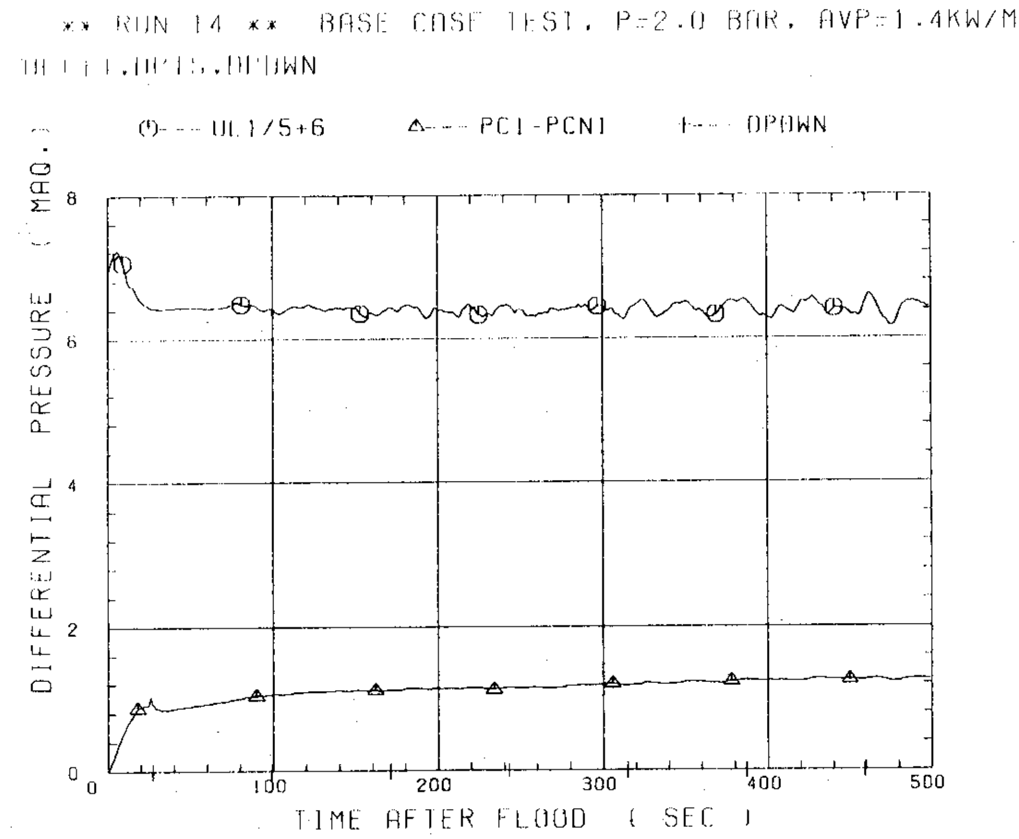

Fig. B.2.6 Core flooding rate (UL1) and core differential pressure (PC1-PCN1)

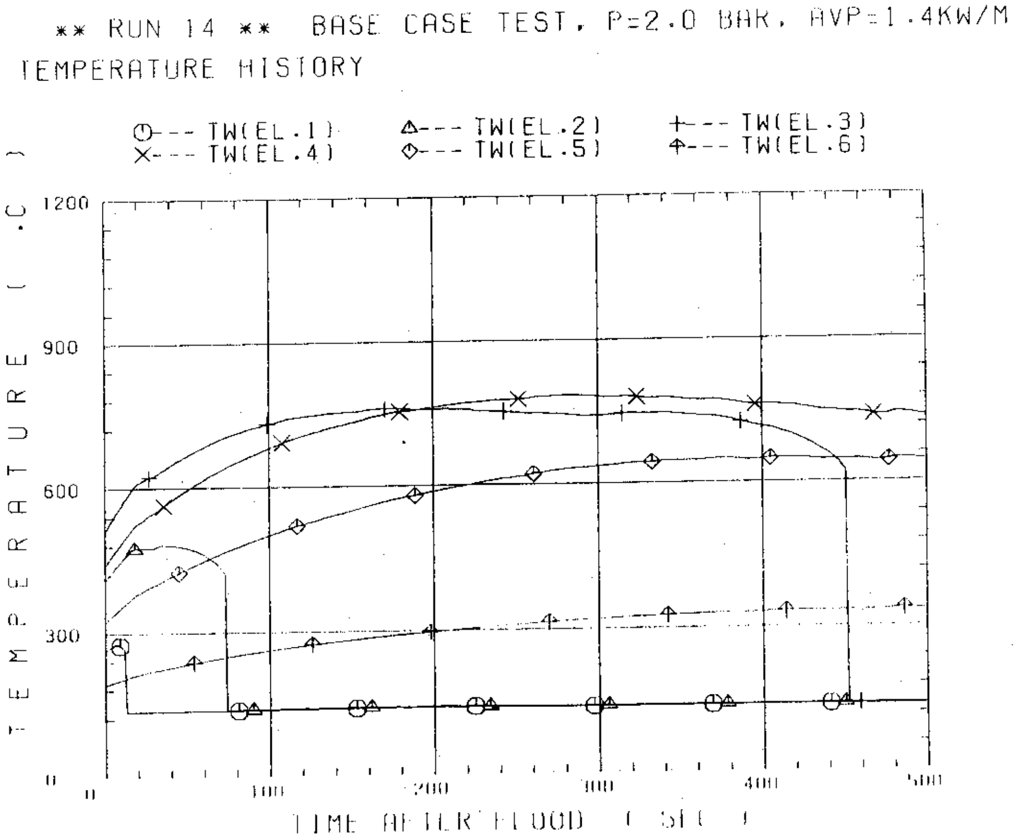

Fig. B.2.7 Rod surface temperatures

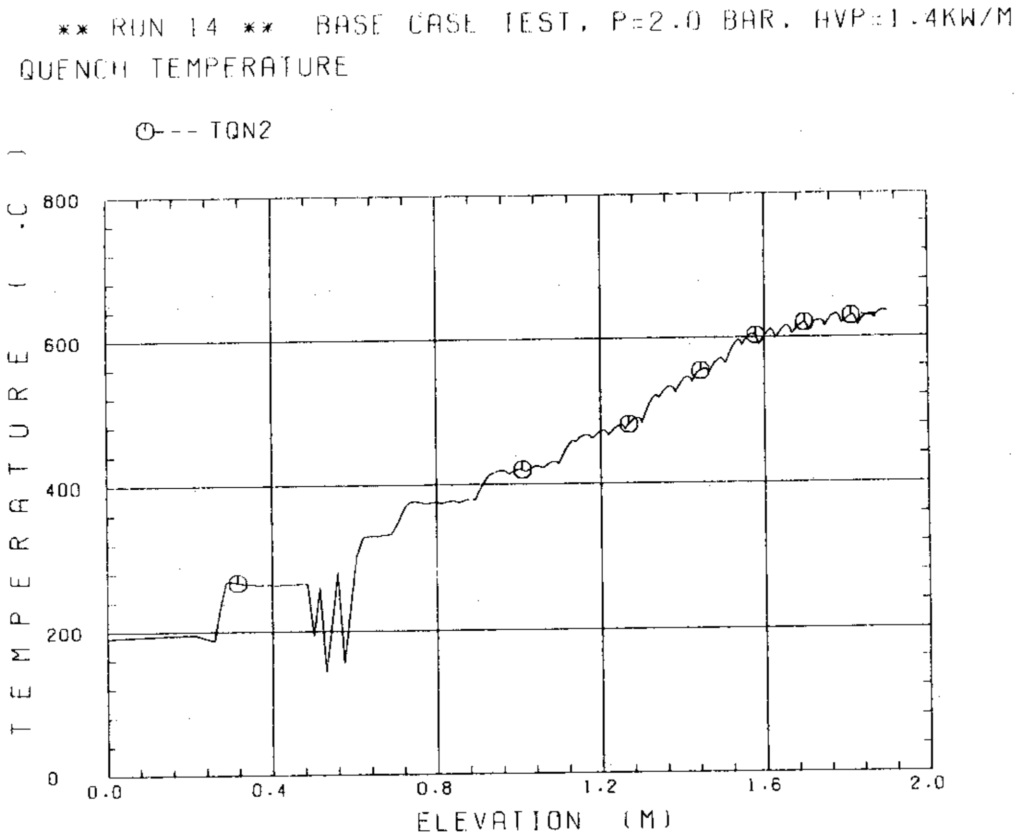

Fig. B.2.8 Quench temperatures

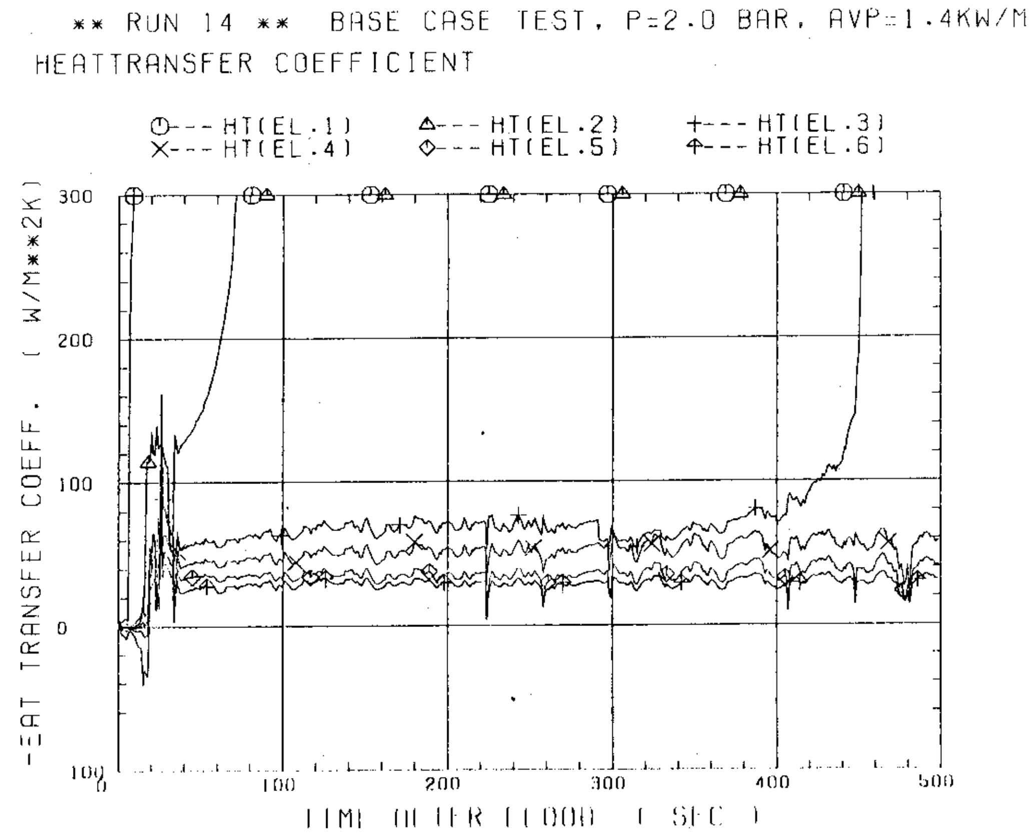

Fig. B.2.9 Heat transfer coefficients

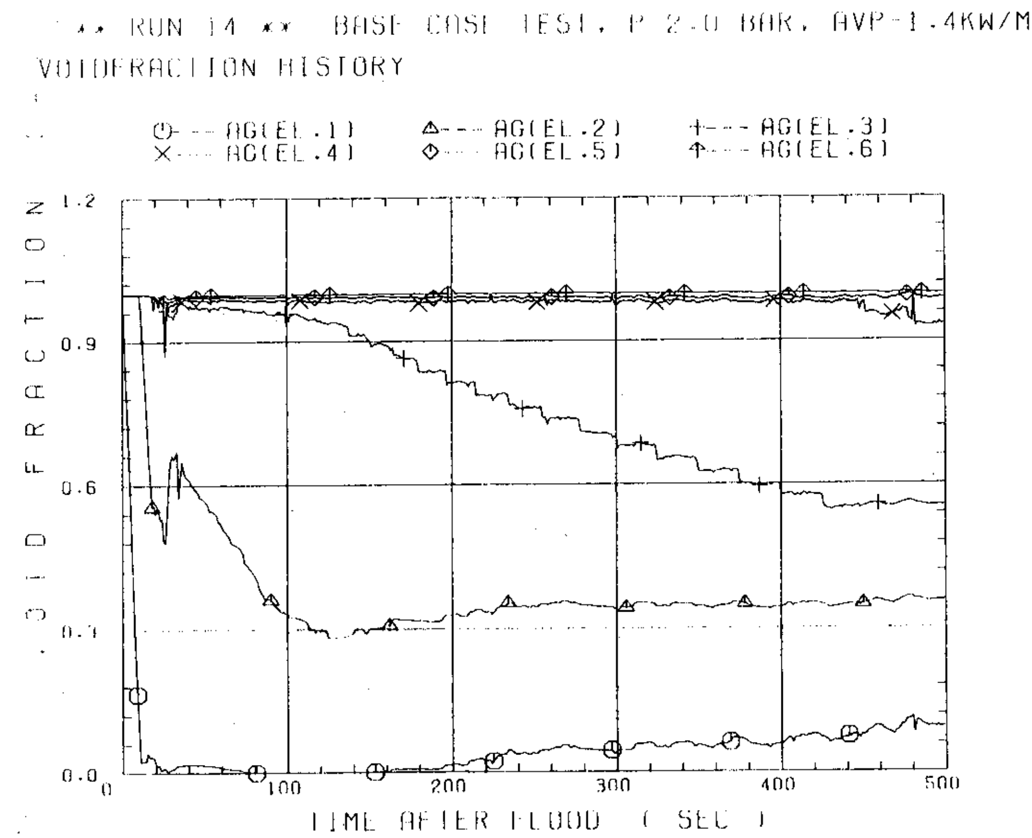

Fig. B.2.10 Void fractions

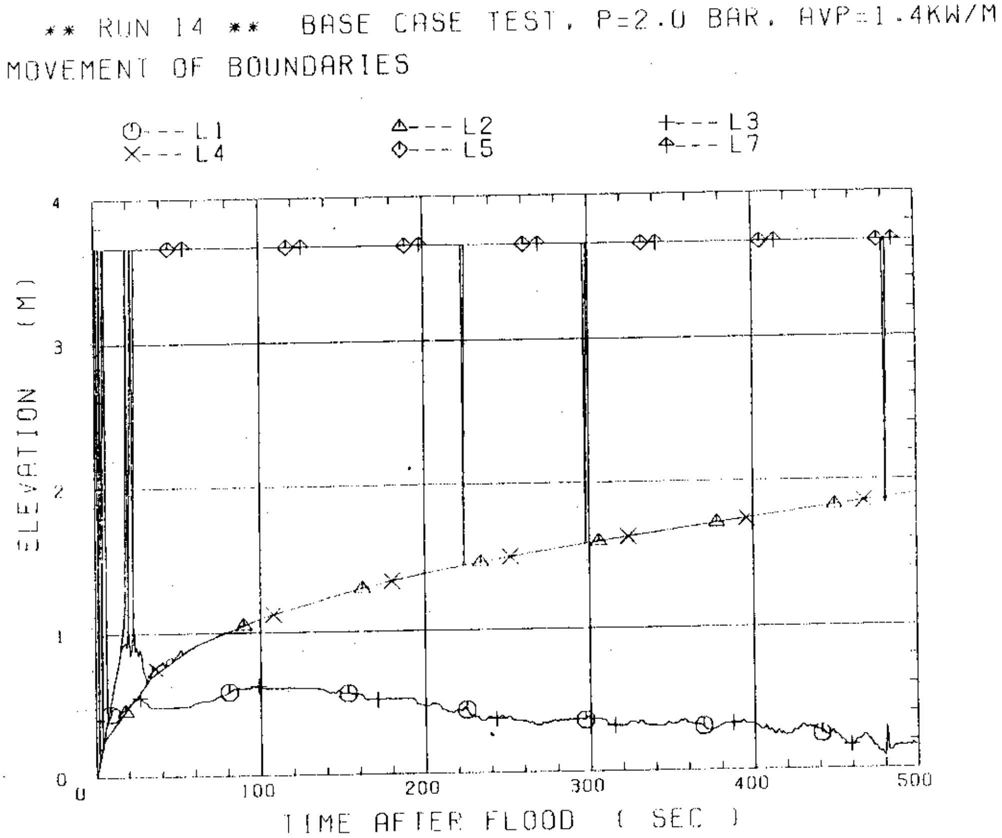

Fig. B.2.11 Movement of flow regime boundaries (L1: Boiling point, L2: Quench front)

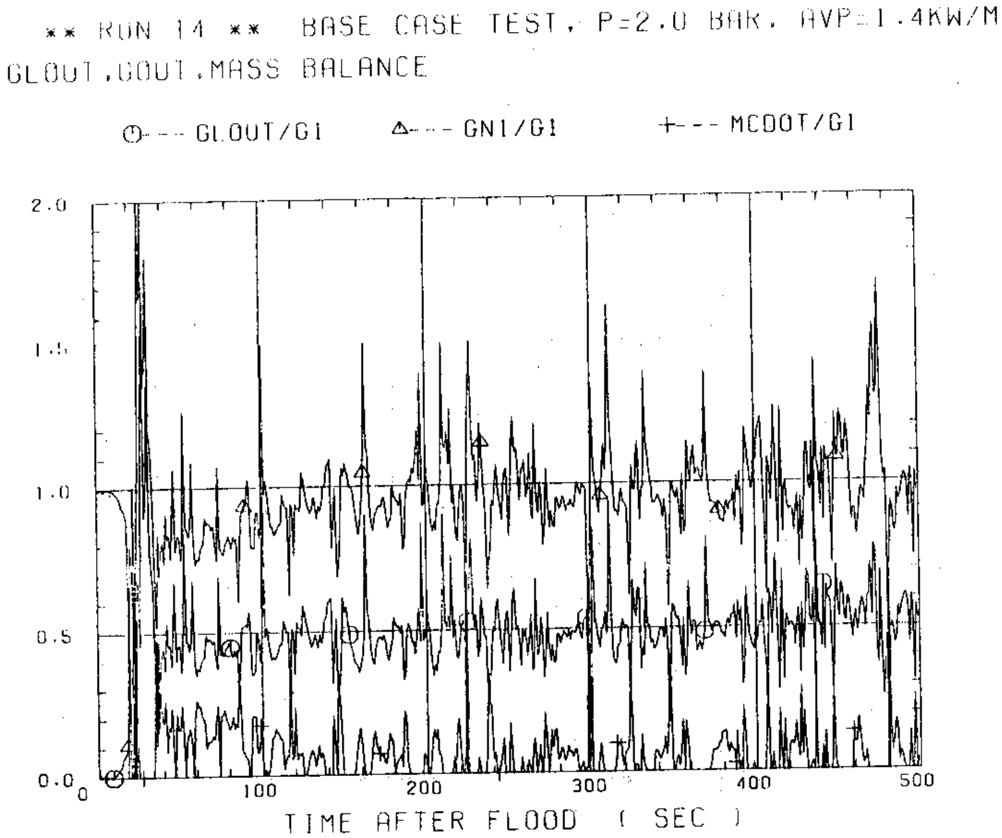

Fig. B.2.12 Liquid carryover rate fraction (GLOUT/G1), carryover rate fraction (GN1/G1) and water accumulation rate fraction (MCDOT/G1)

B.3 Test C1-12 (High system pressure, 0.3 MPa)

CCTF DATA RUN 21

UL(1),DPTS,DPDWN

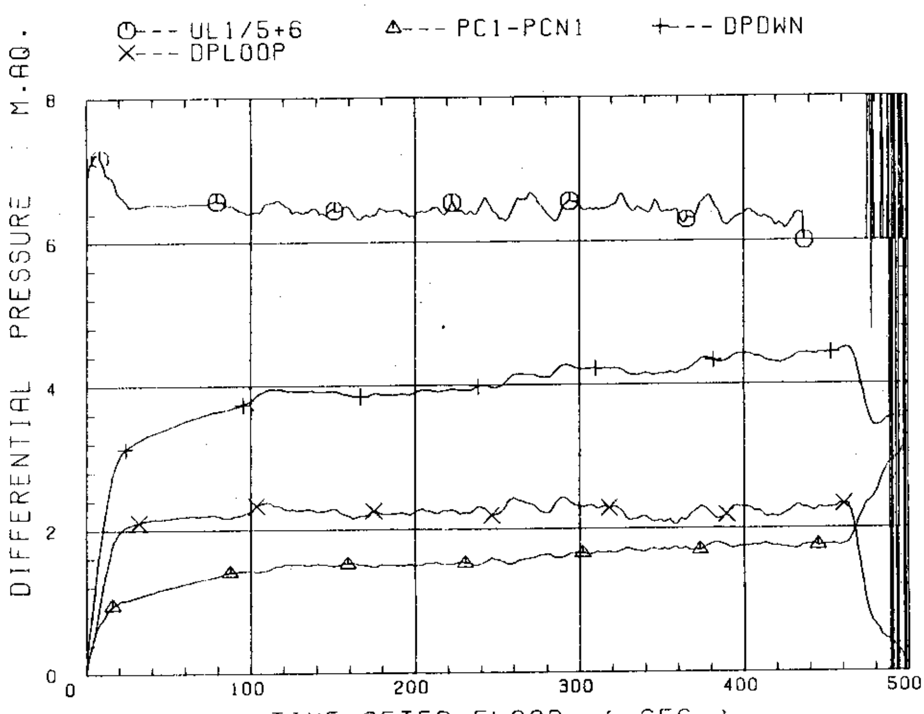

Fig. B.3.1 Core flooding rate (UL1), core differential pressure (PC1-PCN1), downcomer differential pressure (DPDWN) and loop differential pressure (DPLOOP) (Experimental value)

CCTF DATA RUN 21

TEMPERATURE HISTORY

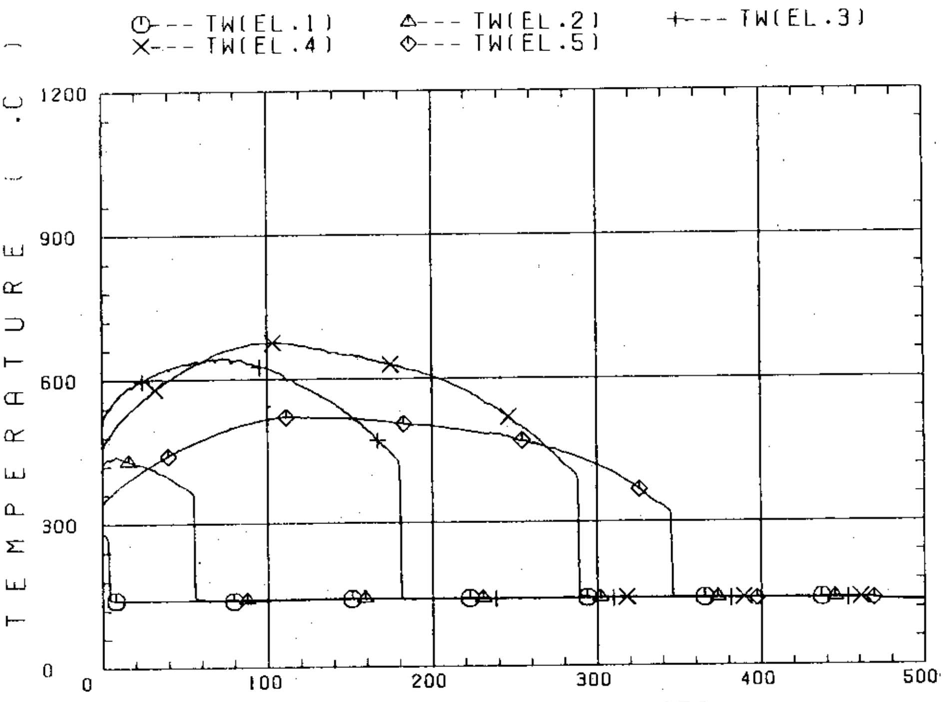

Fig. B.3.2 Rod surface temperatures (Experimental value)

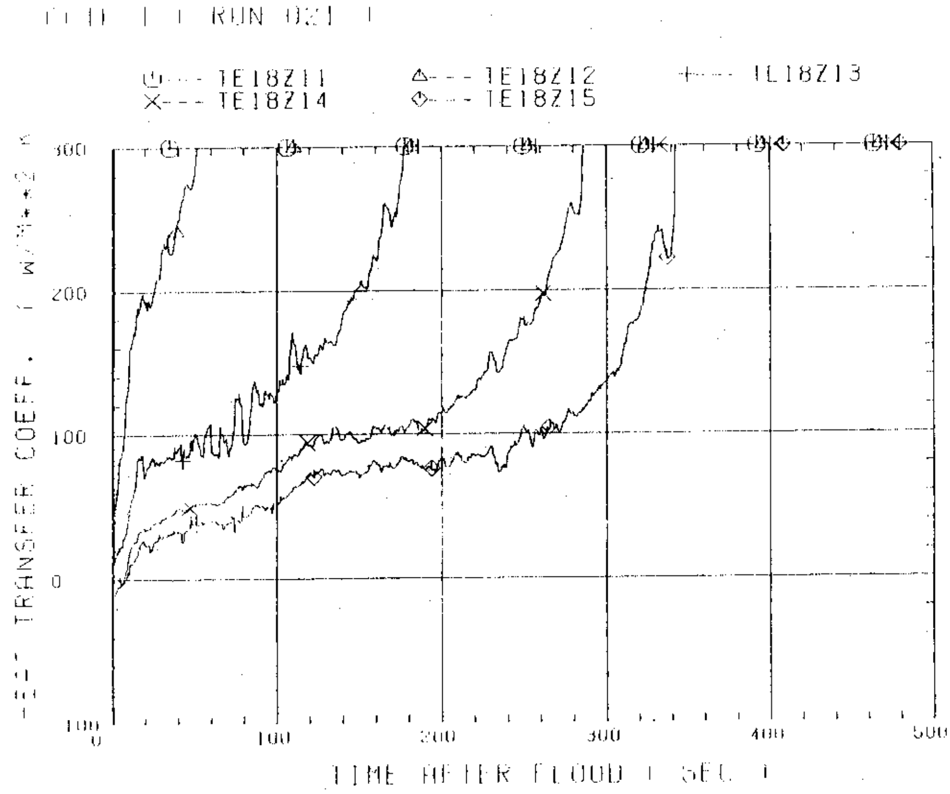

Fig. B.3.3　Heat transfer coefficients (Experimental values)

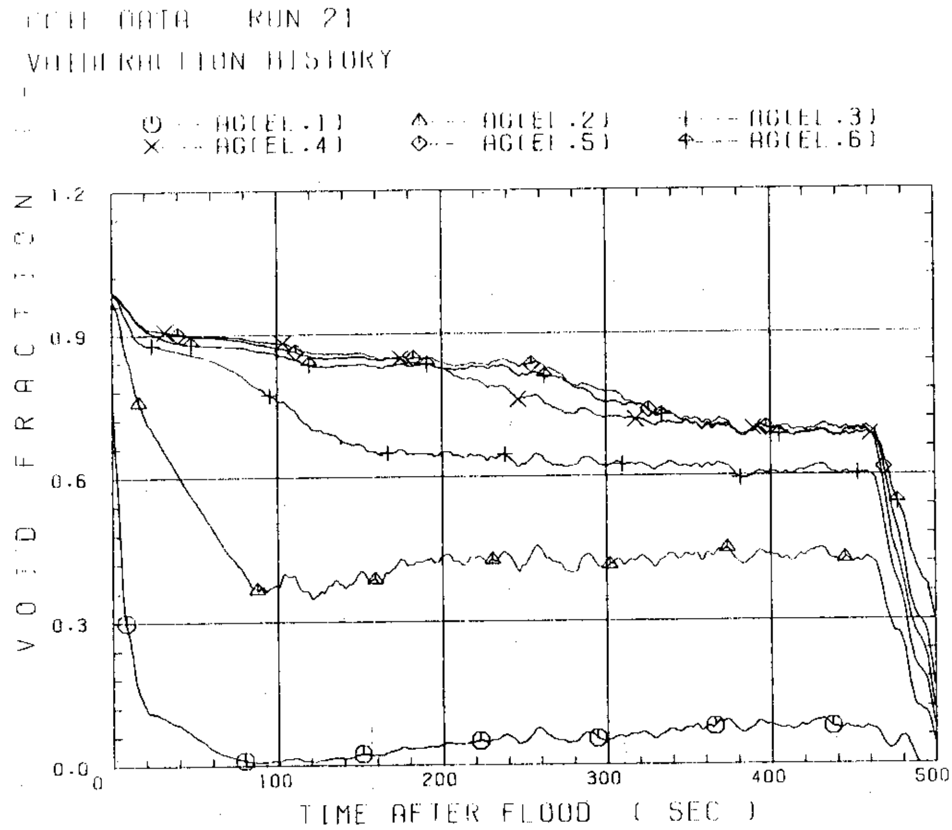

Fig. B.3.4　Void fractions (Experimental values)

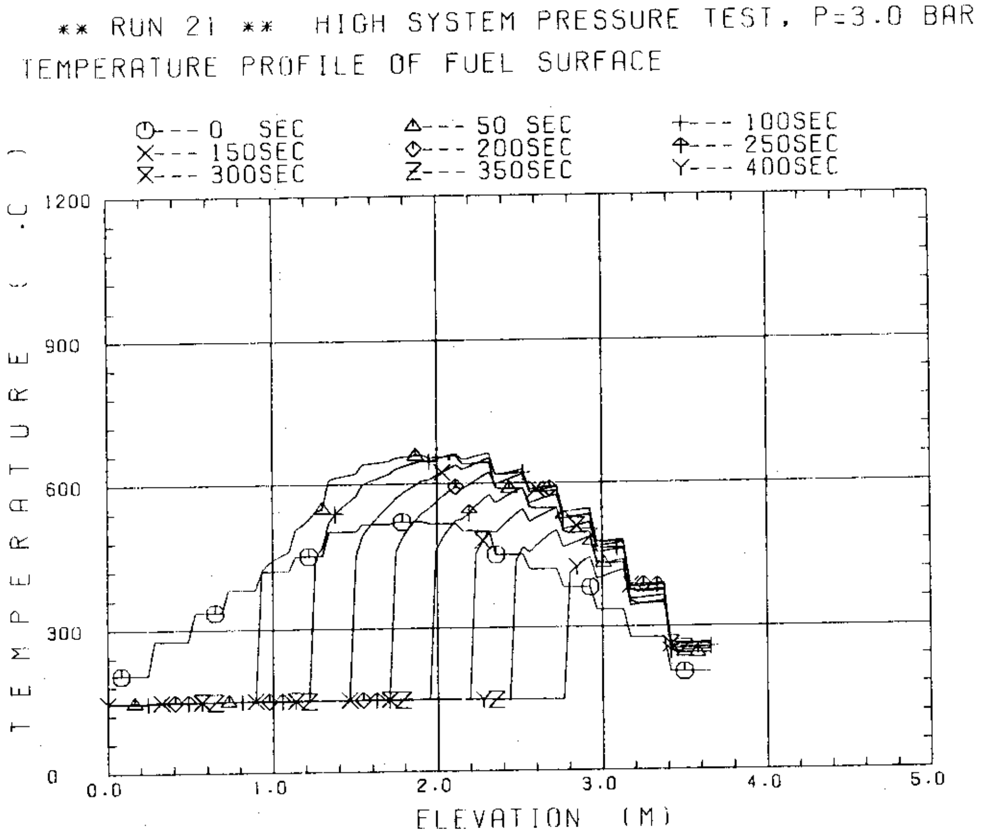

Fig. B.3.5 Rod surface temperature distributions

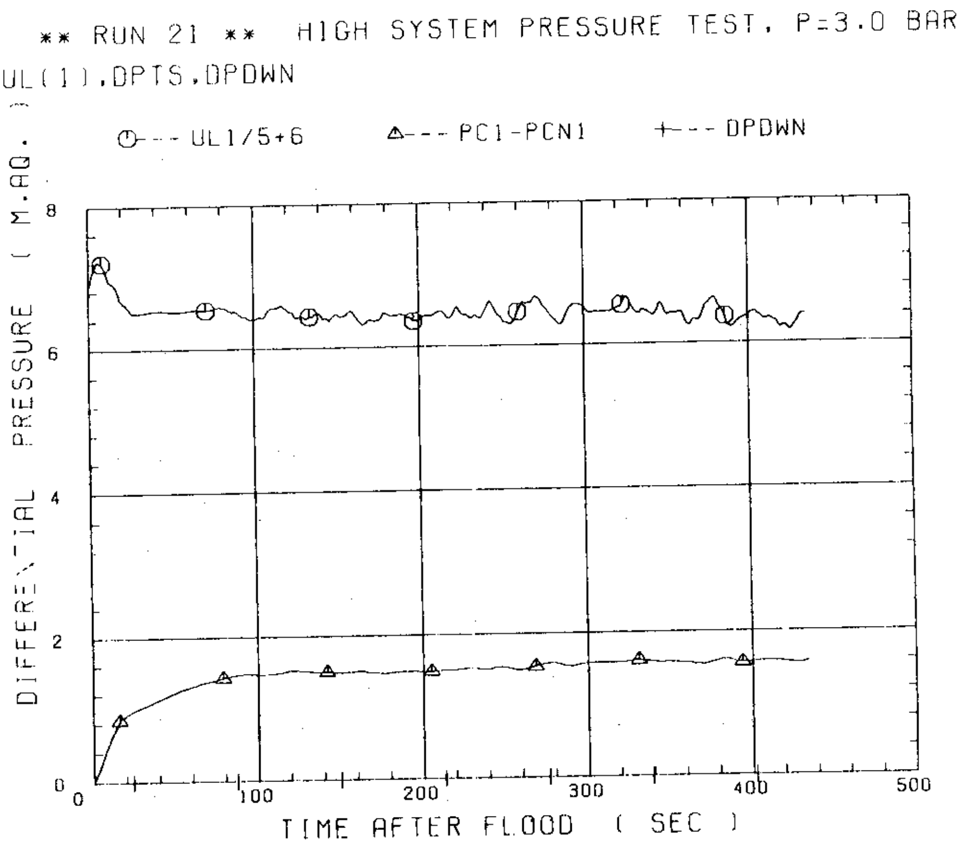

Fig. B.3.6 Core flooding rate (UL1) and core differential pressure (PC1-PCN1)

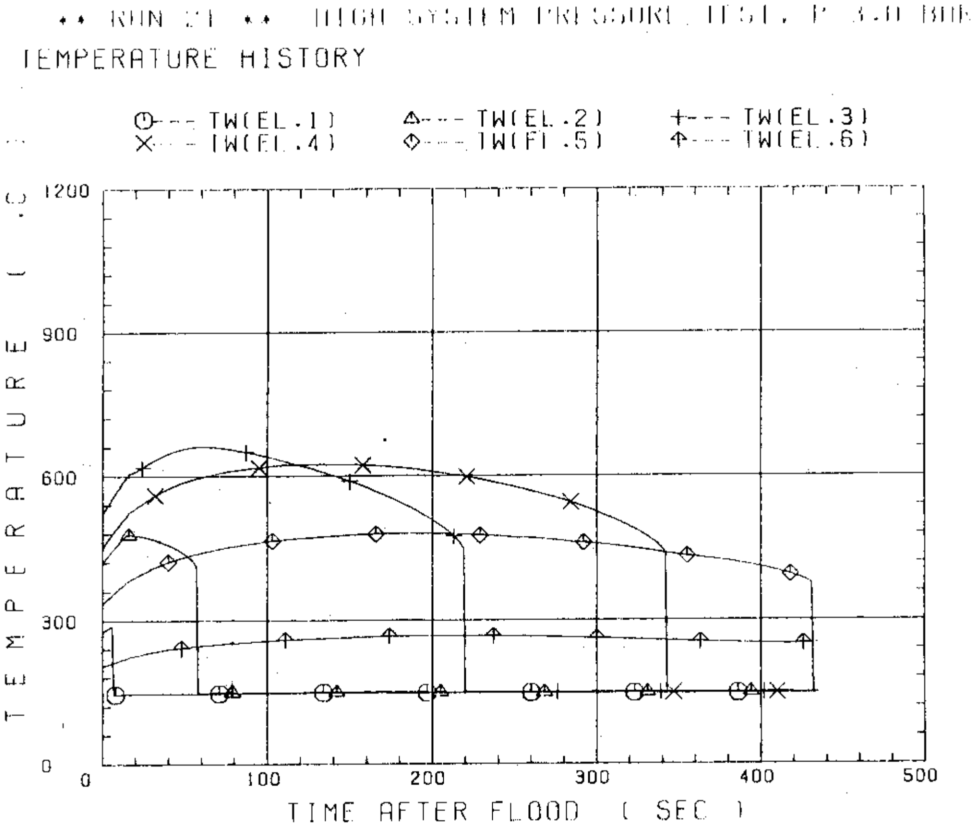

Fig. B.3.7 Rod surface temperatures

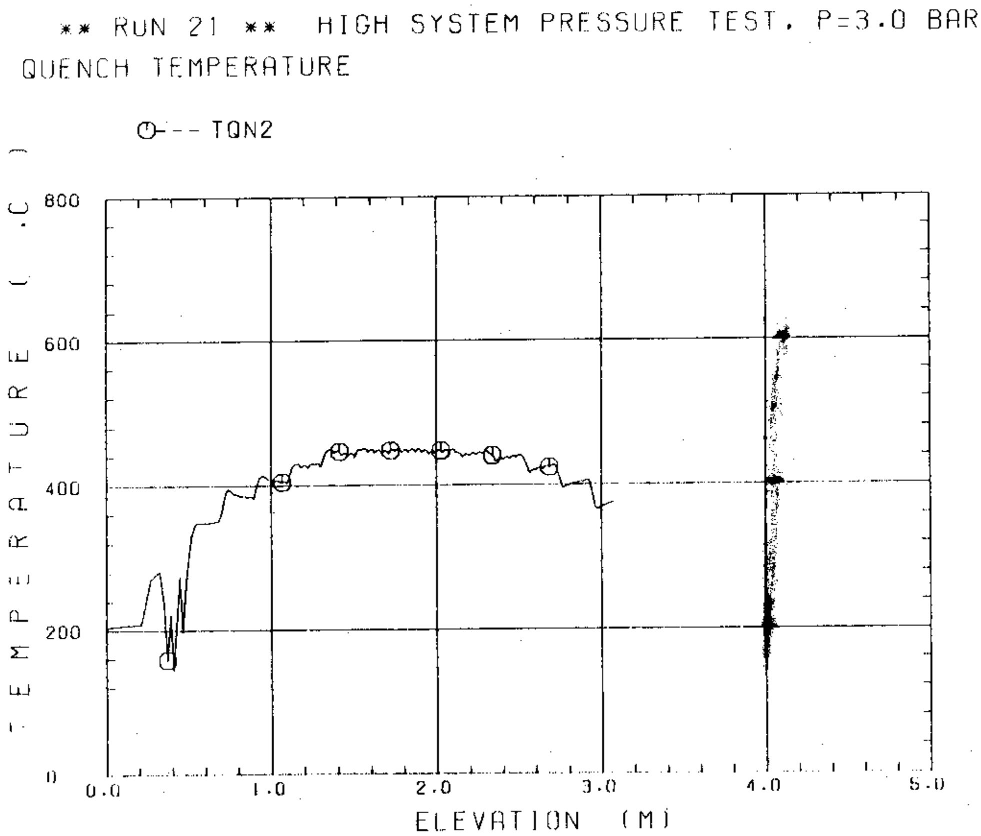

Fig. B.3.8 Quench temperatures

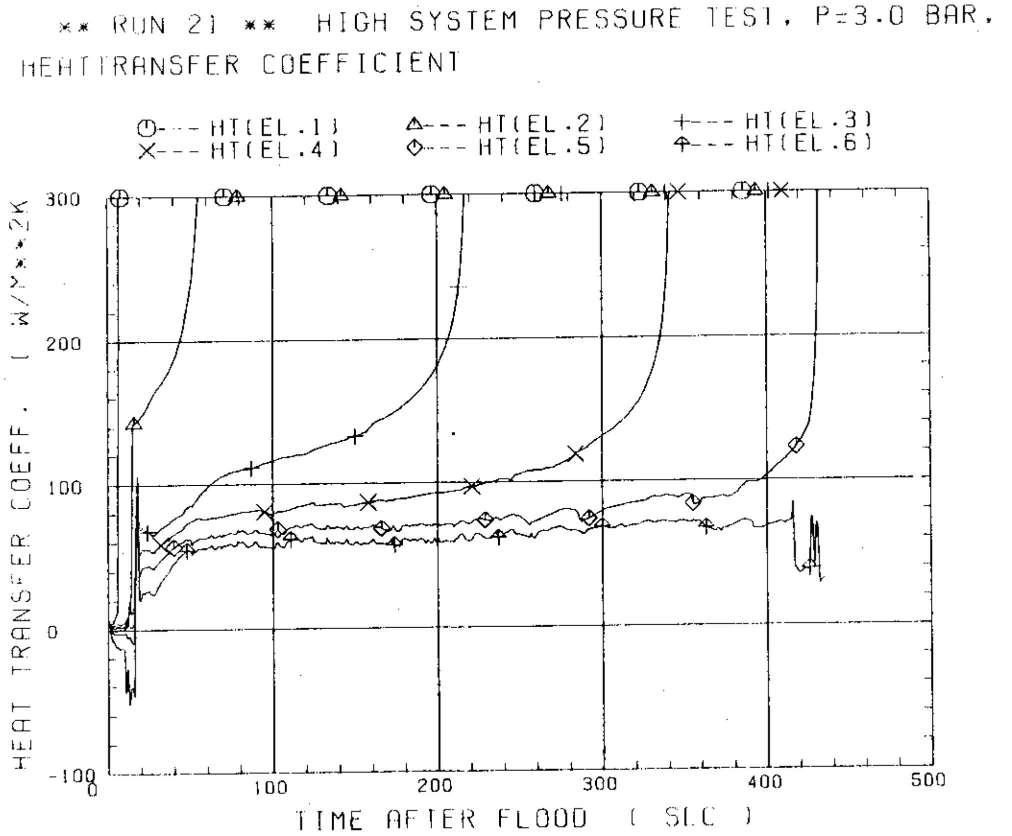

Fig. B.3.9 Heat transfer coefficients

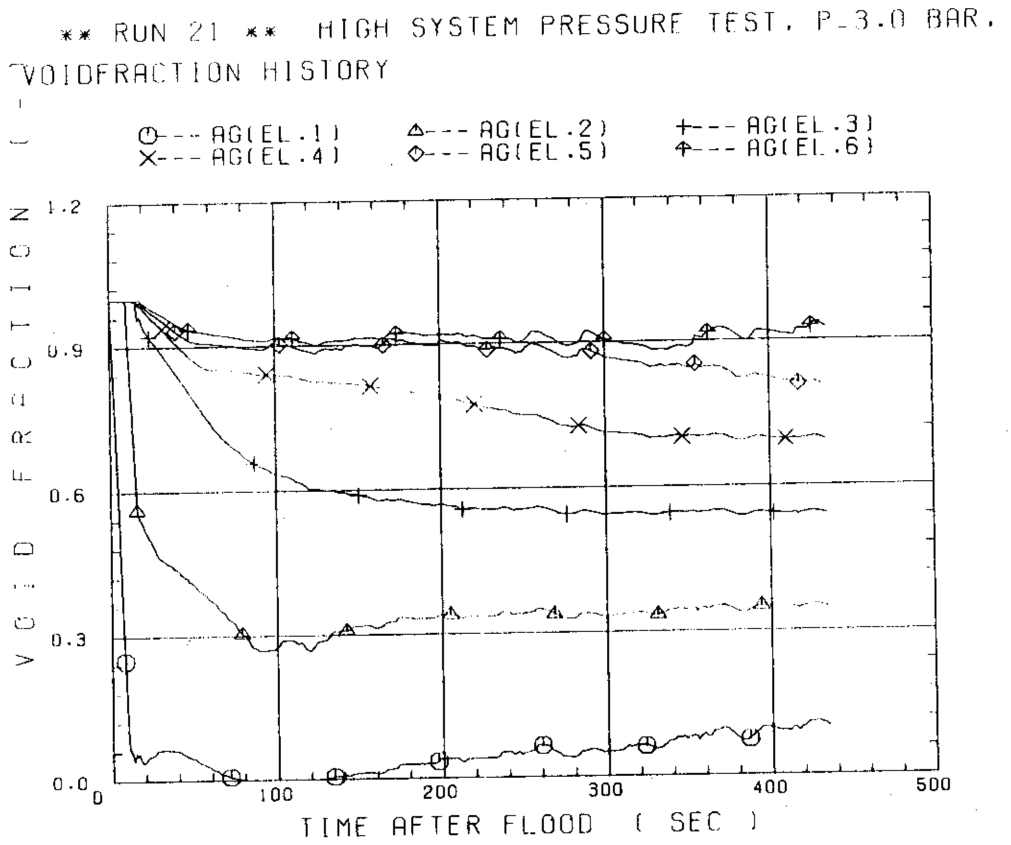

Fig. B.3.10 Void fractions

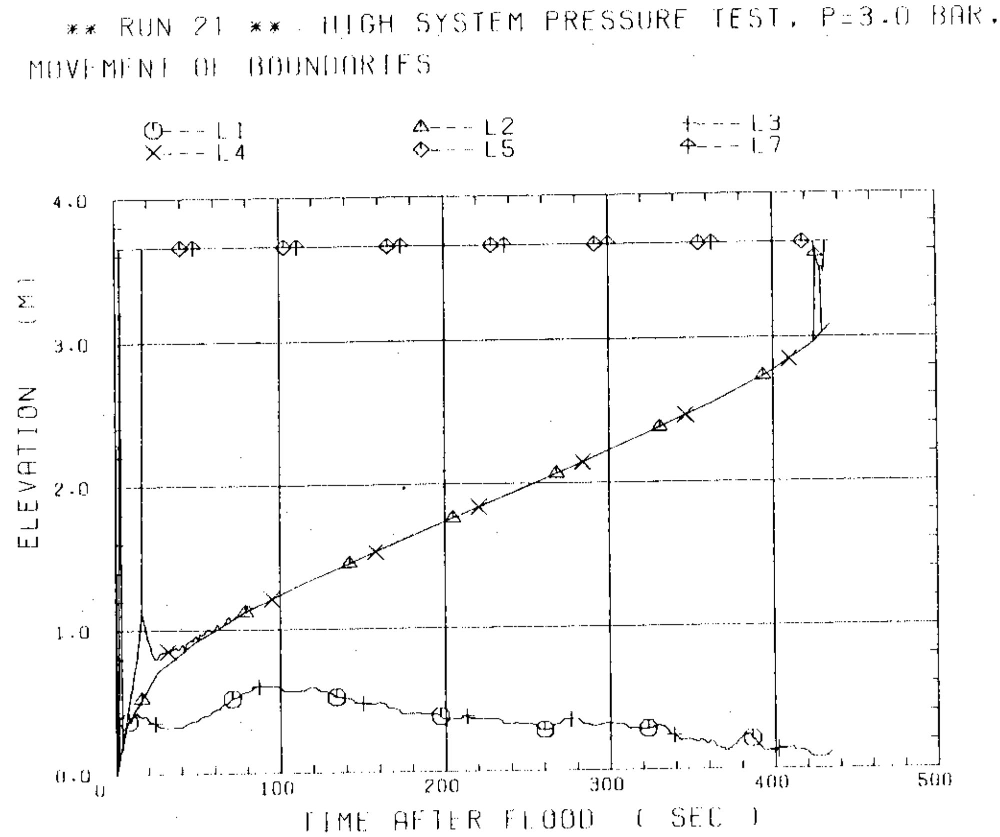

Fig. B.3.11 Movement of flow regime boundaries (L1: Boiling point, L2: Quench front)

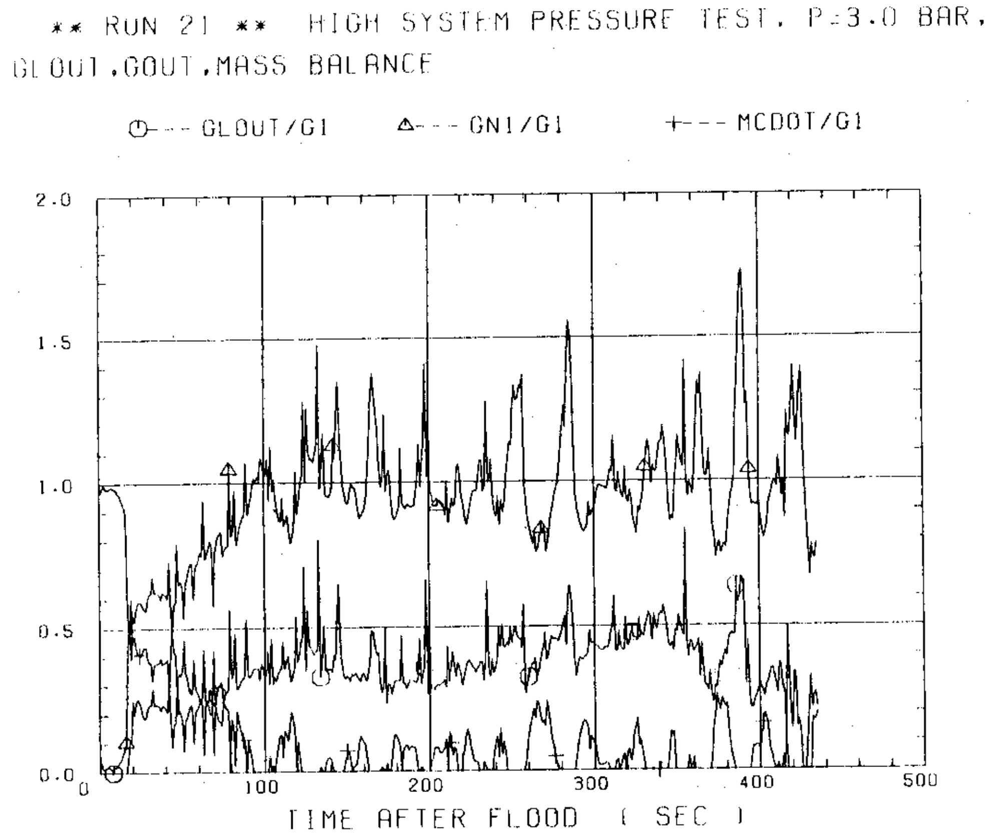

Fig. B.3.12 Liquid carryover rate fraction (GLOUT/G1), carryover rate fraction (GN1/G1) and water accumulation rate fraction (MCDOT/G1)

B.4 Test C1-10 (Low system pressure, 0.15 MPa)

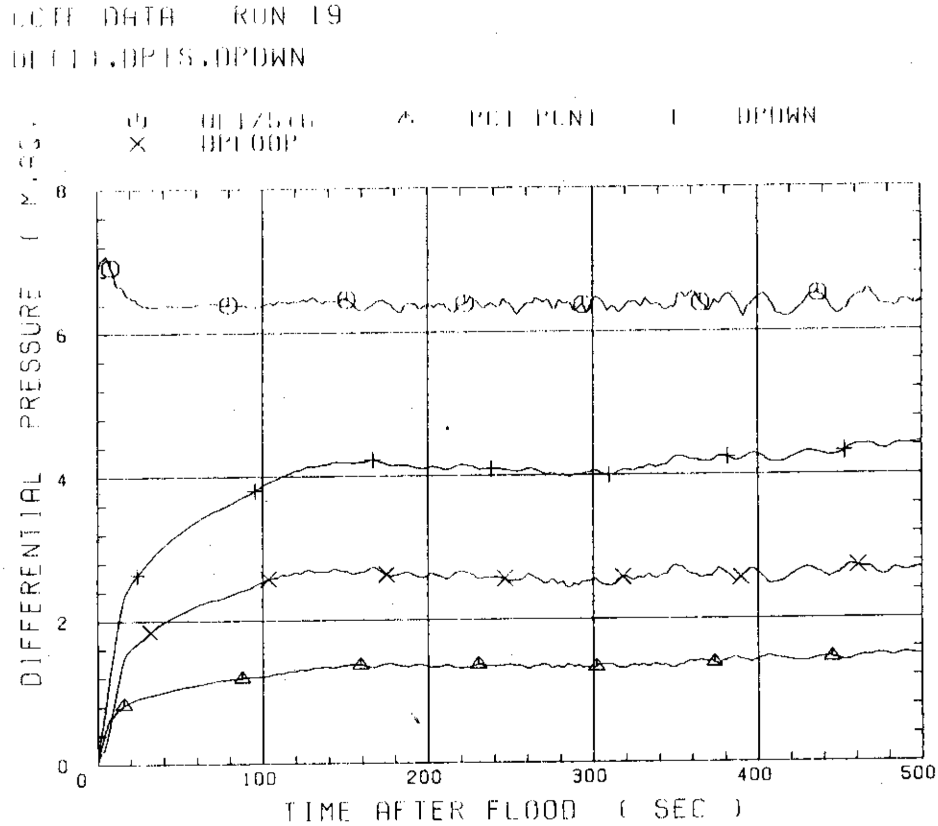

Fig. B.4.1 Core flooding rate (UL1), core differential pressure (PC1-PCN1), downcomer differential pressure (DPDWN) and loop differential pressure (DPLOOP) (Experimental value)

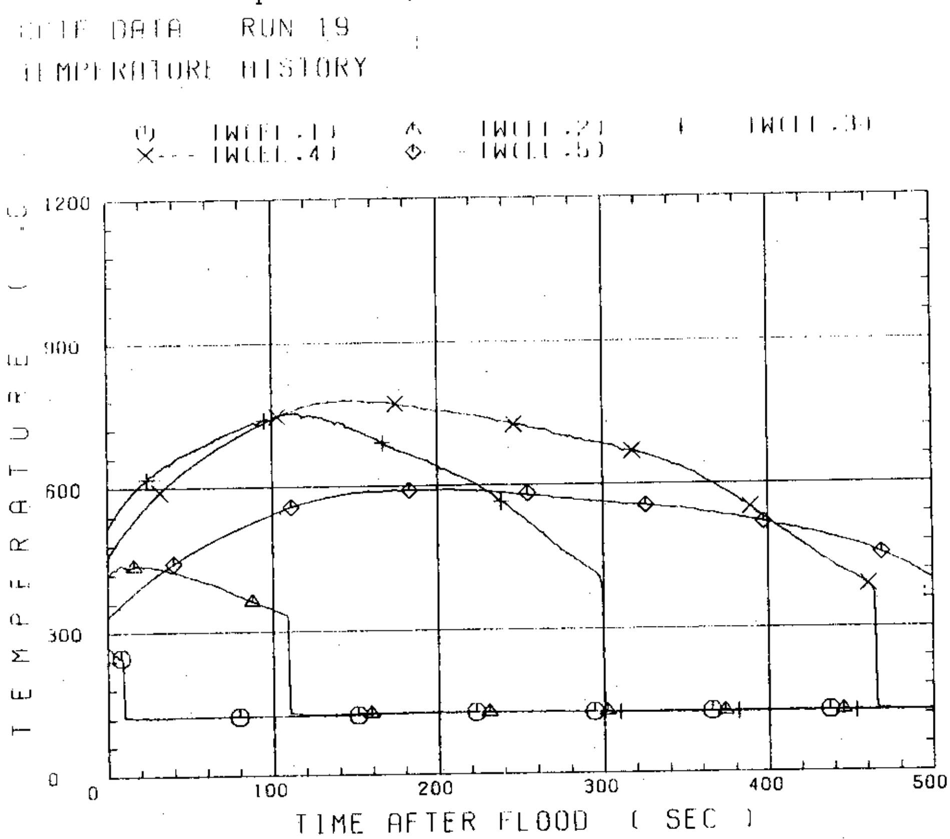

Fig. B.4.2 Rod surface temperatures (Experimental value)

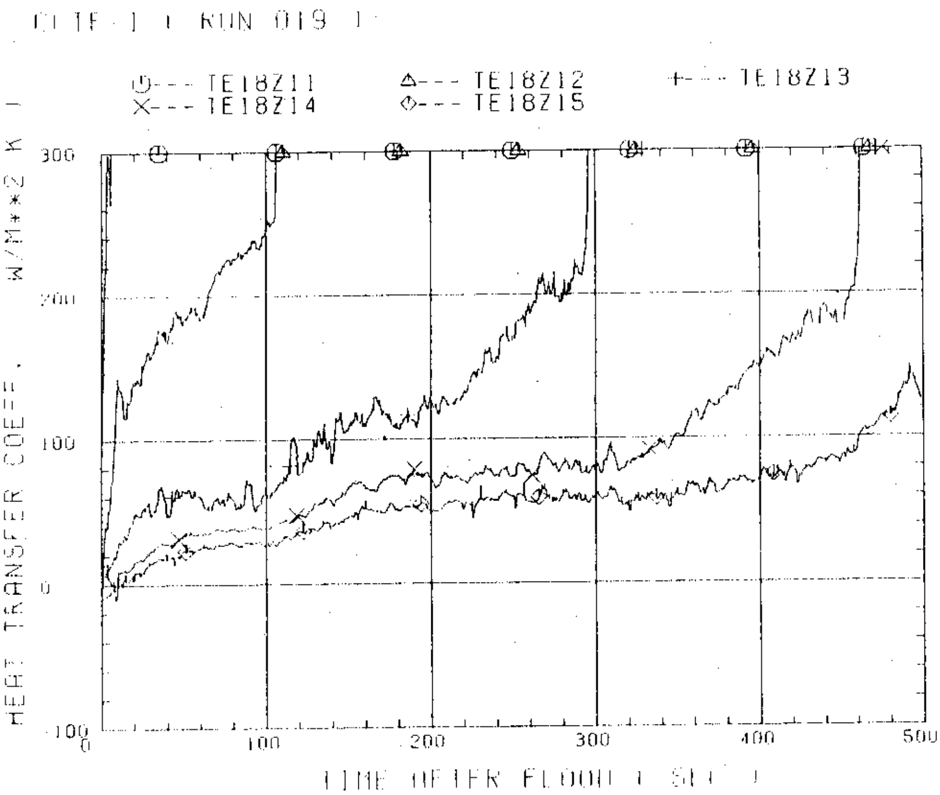

Fig. B.4.3 Heat transfer coefficients (Experimental values)

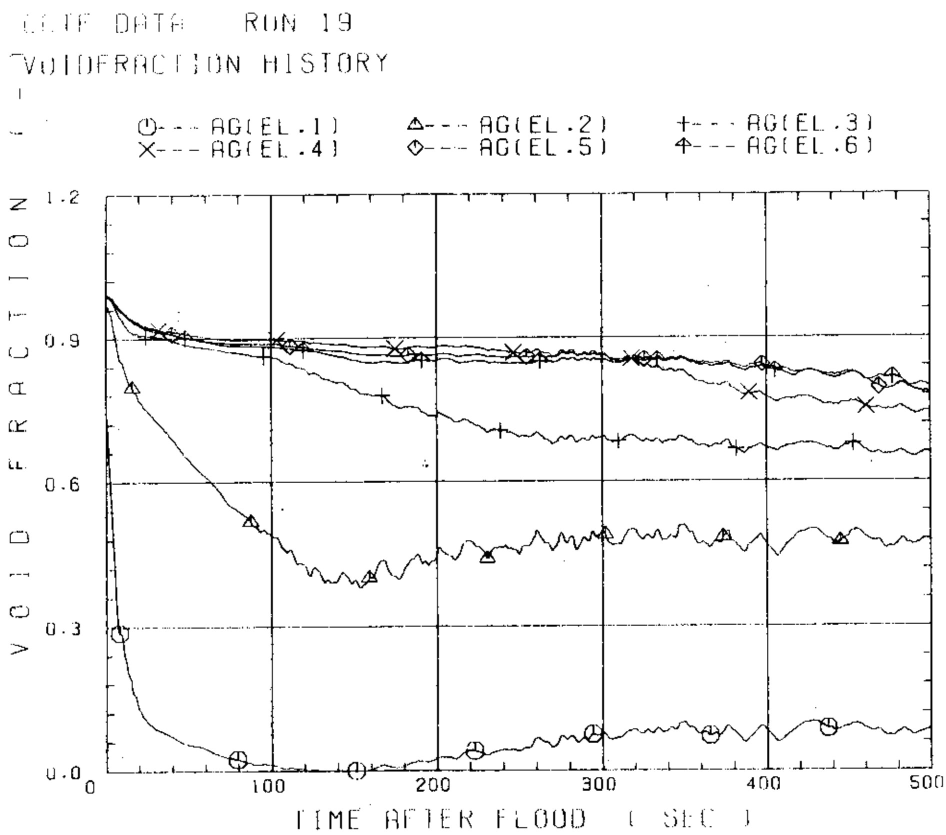

Fig. B.4.4 Void fractions (Experimental values)

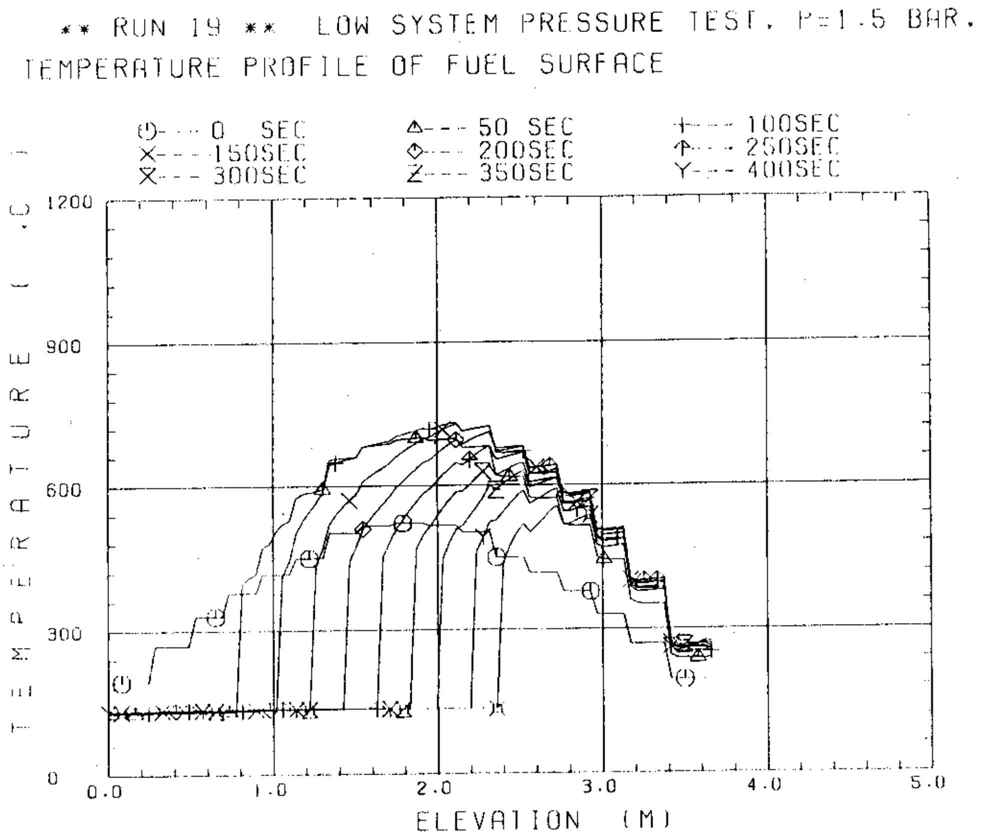

Fig. B.4.5 Rod surface temperature distributions

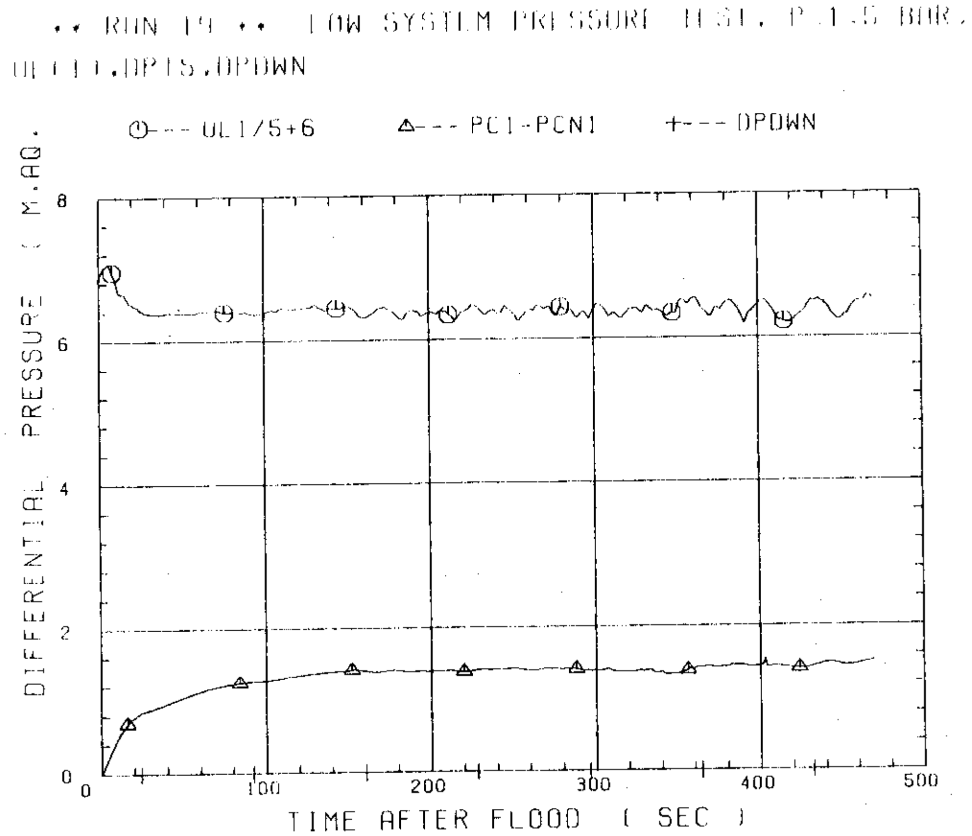

Fig. B.4.6 Core flooding rate (UL1) and core differential pressure (PC1-PCN1)

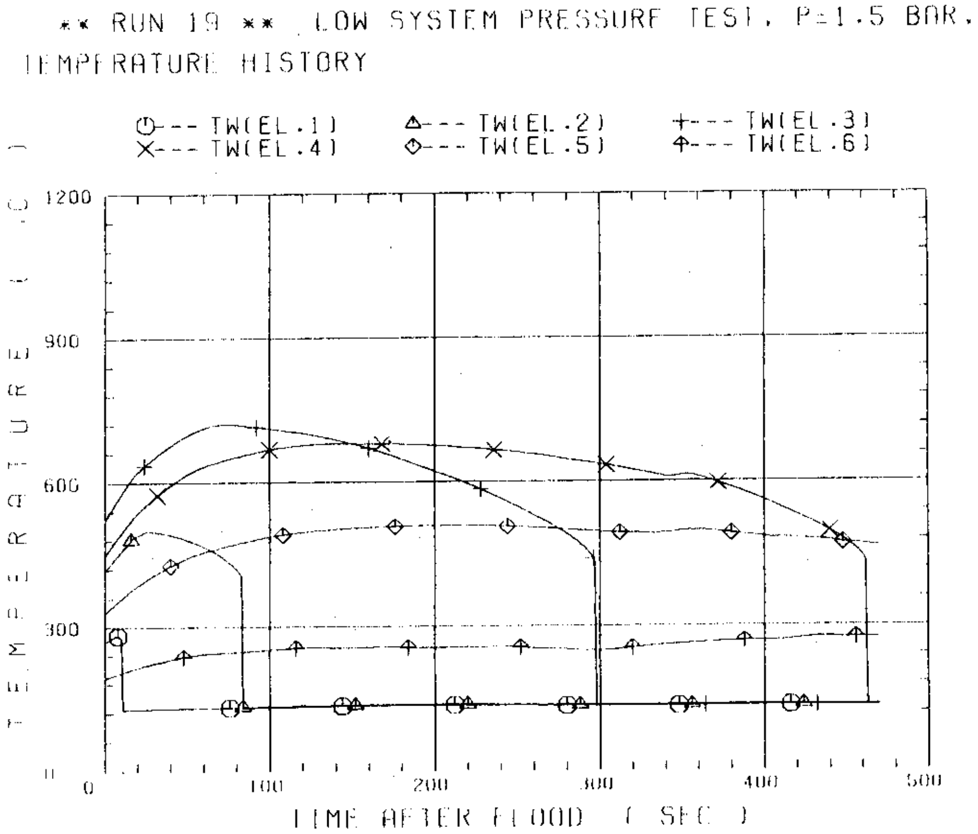

Fig. B.4.7 Rod surface temperatures

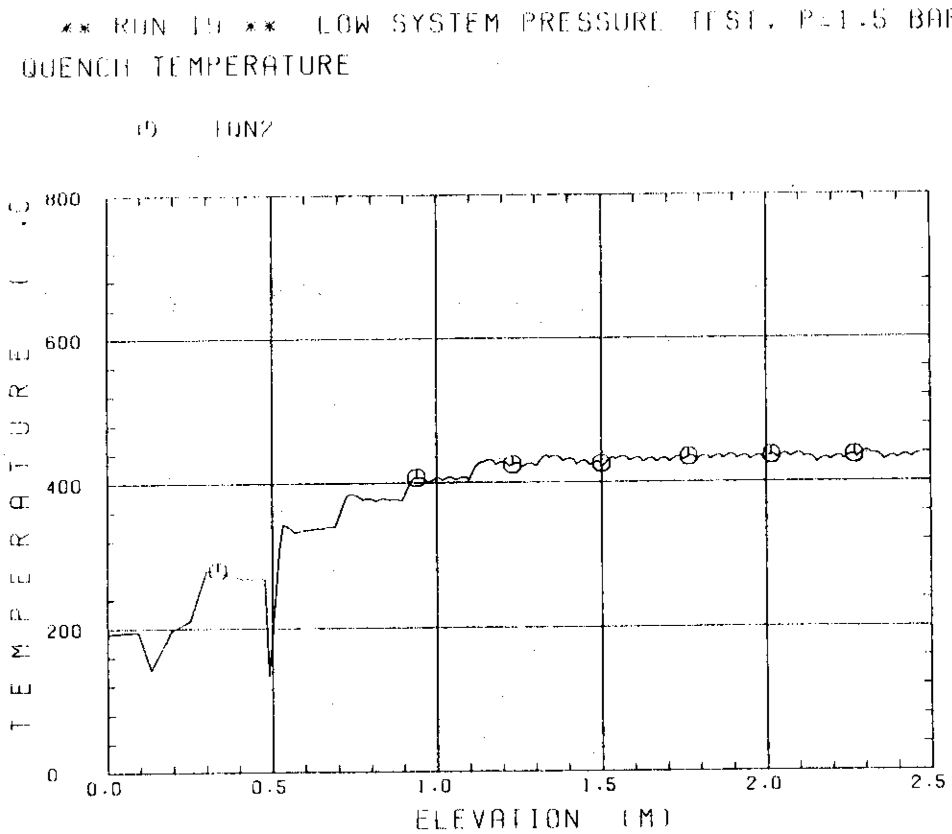

Fig. B.4.8 Quench temperatures

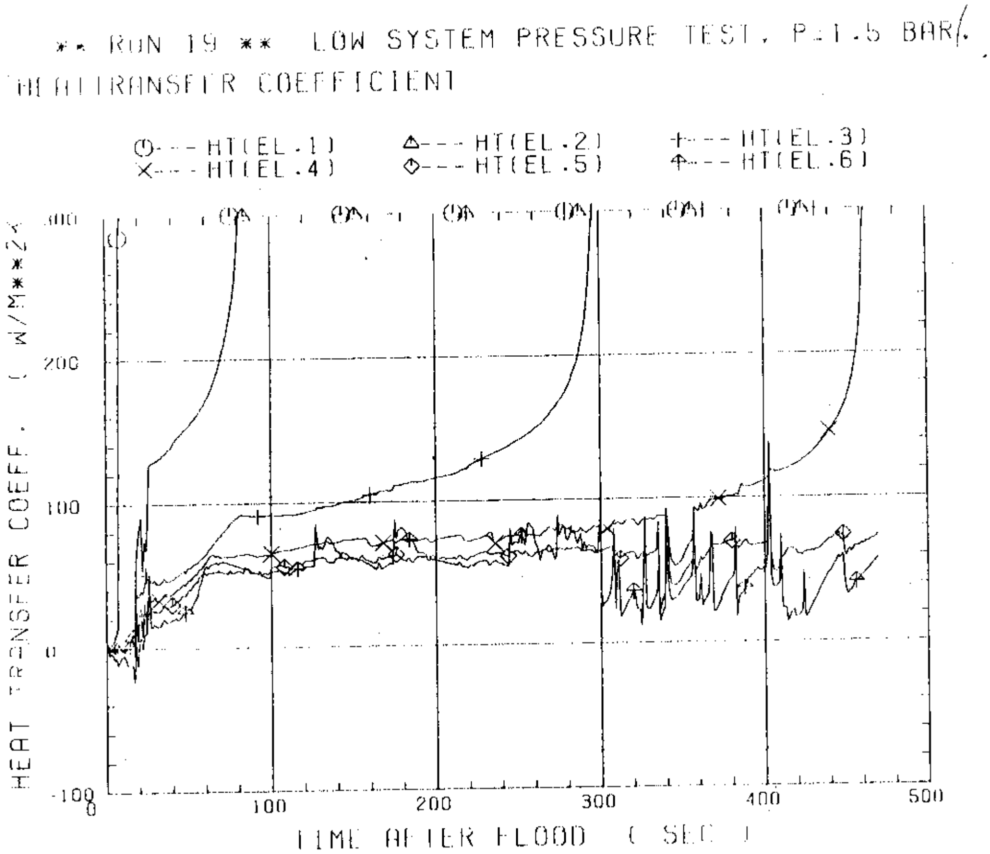

Fig. B.4.9 Heat transfer coefficients

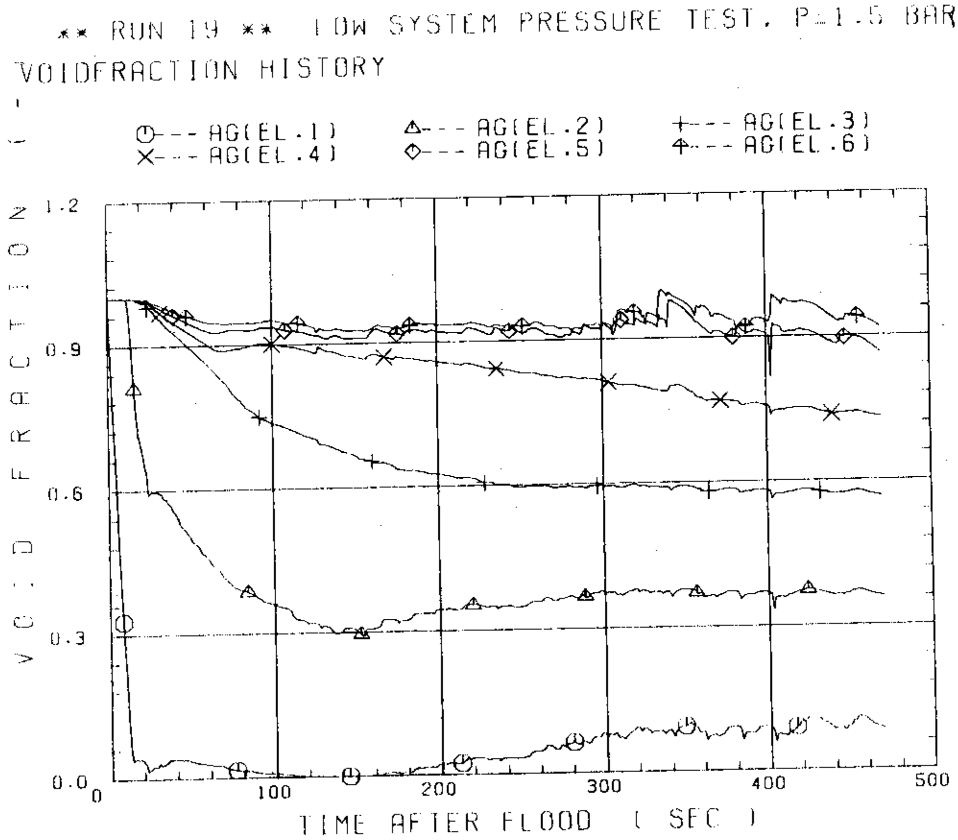

Fig. B.4.10 Void fractions

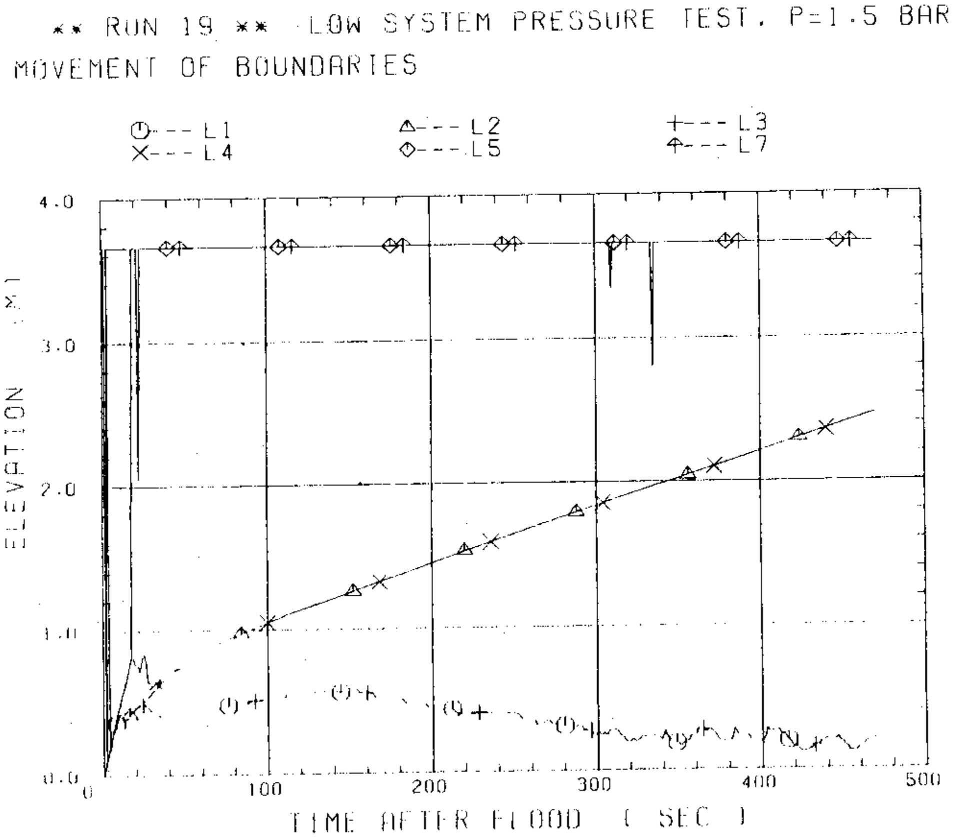

Fig. B.4.11 Movement of flow regime boundaries (L1: Boiling point, L2: Quench front)

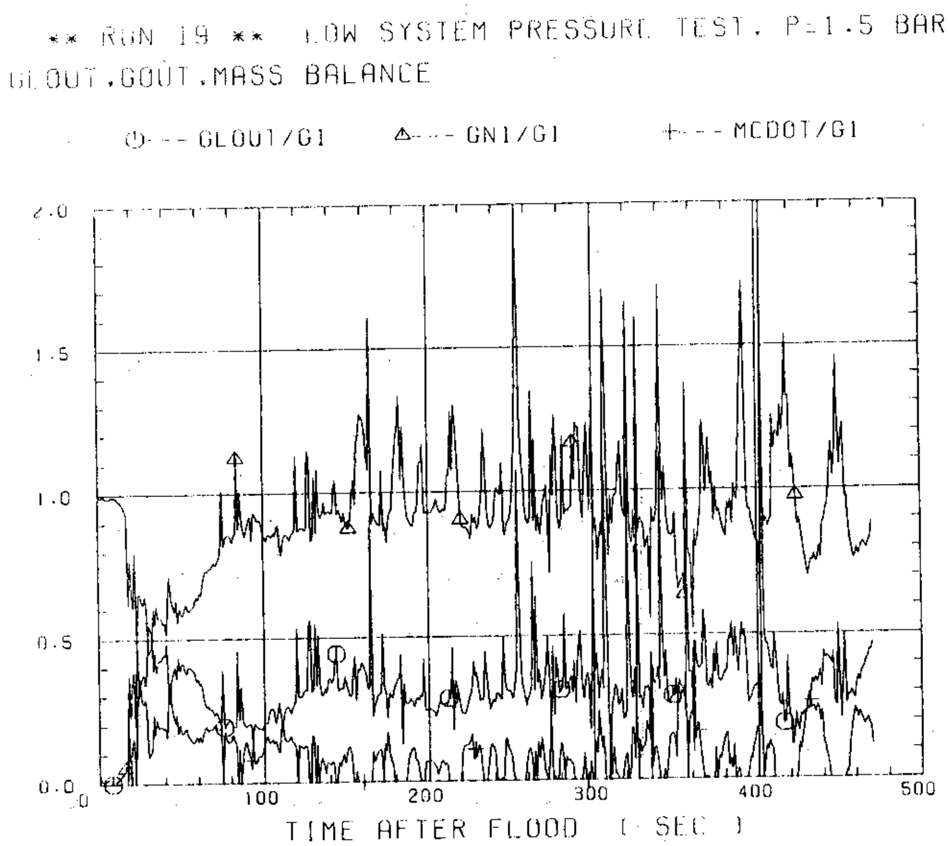

Fig. B.4.12 Liquid carryover rate fraction (GLOUT/G1), carryover rate fraction (GN1/G1) and water accumulation rate fraction (MCDOT/G1)

B.5 Test C1-7 (High initial clad temperature, 700°C)

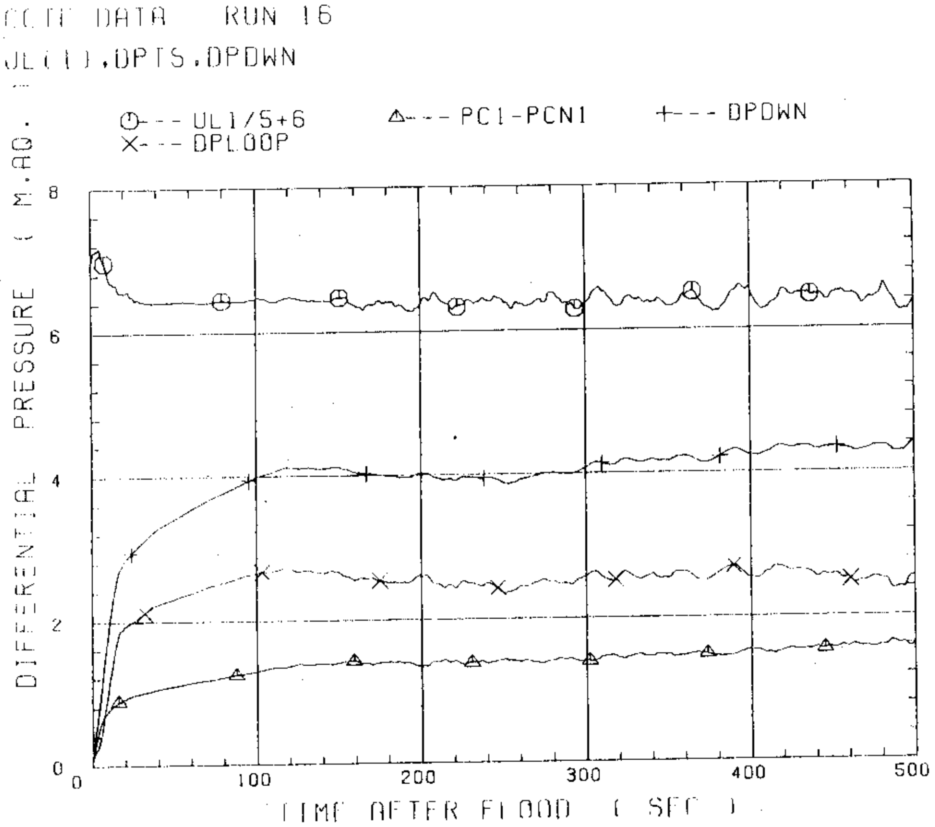

Fig. B.5.1 Core flooding rate (UL1), core differential pressure (PC1-PCN1), downcomer differential pressure (DPDWN) and loop differential pressure (DPLOOP) (Experimental value)

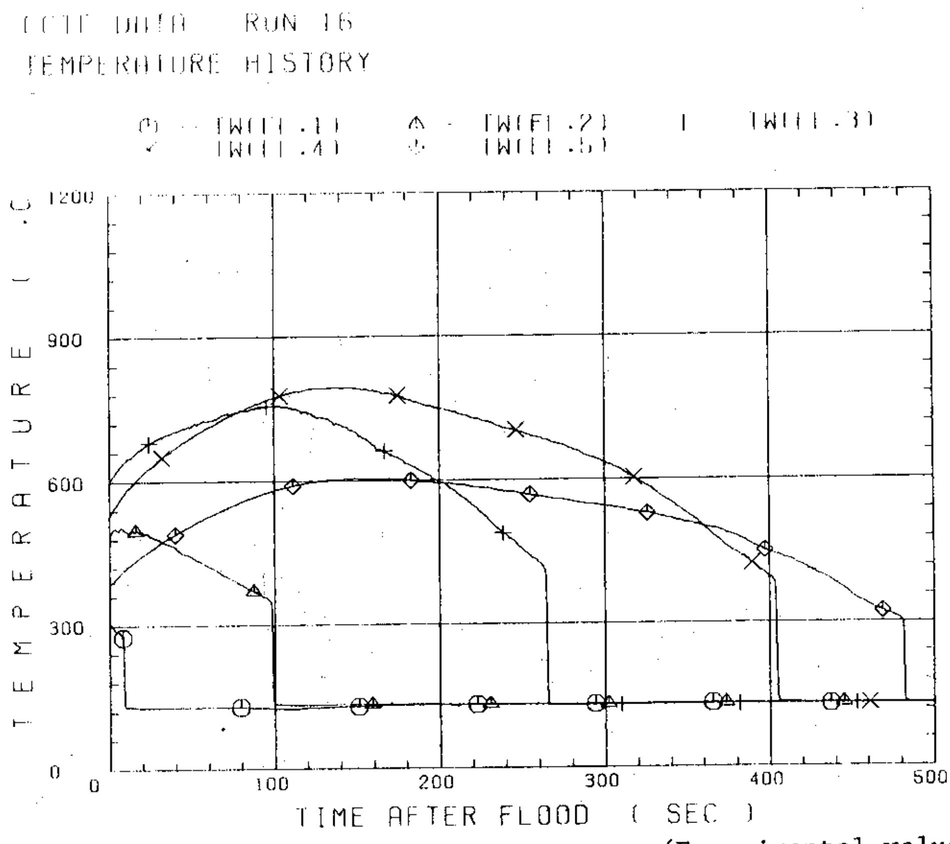

Fig. B.5.2 Rod surface temperatures (Experimental value)

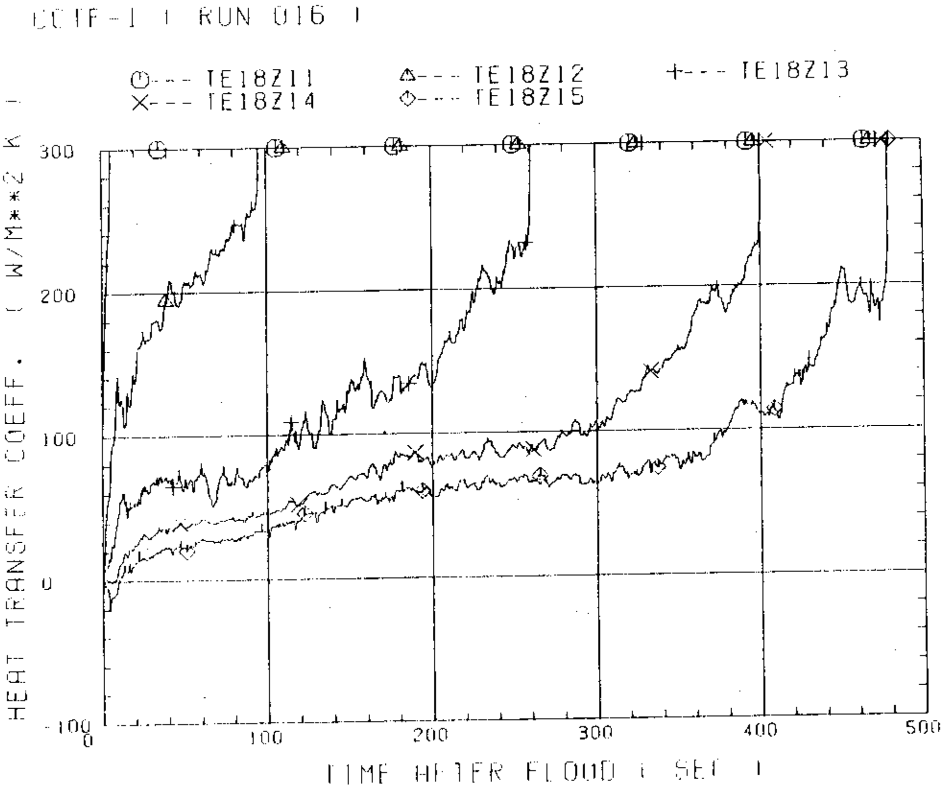

Fig. B.5.3 Heat transfer coefficients (Experimental values)

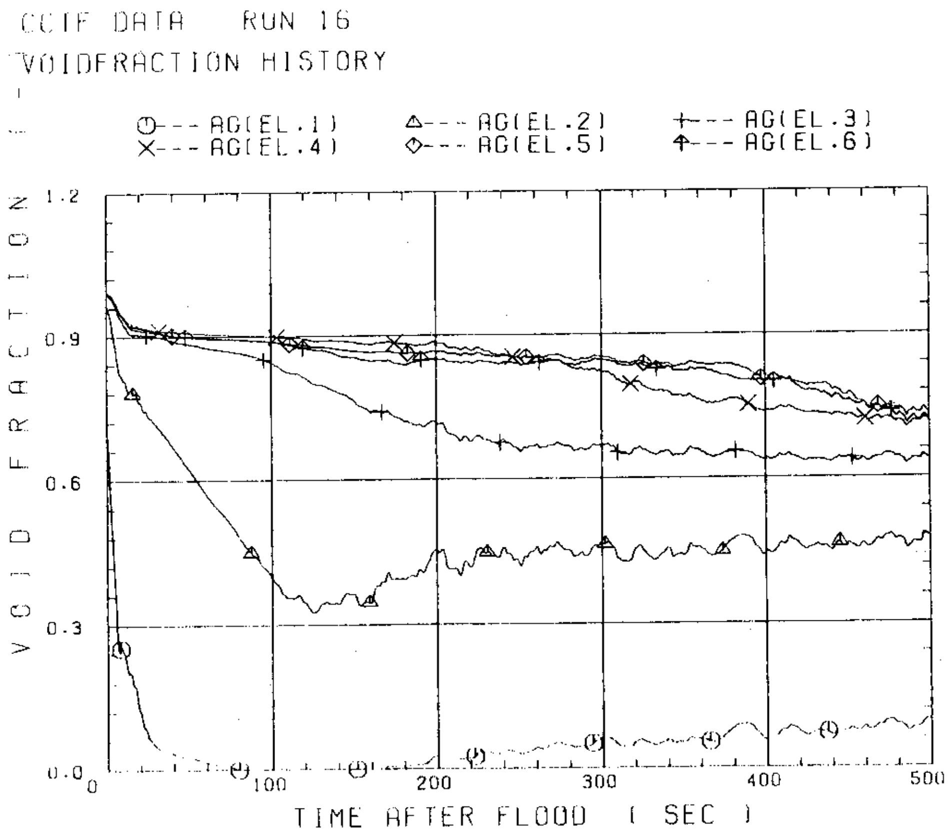

Fig. B.5.4 Void fractions (Experimental values)

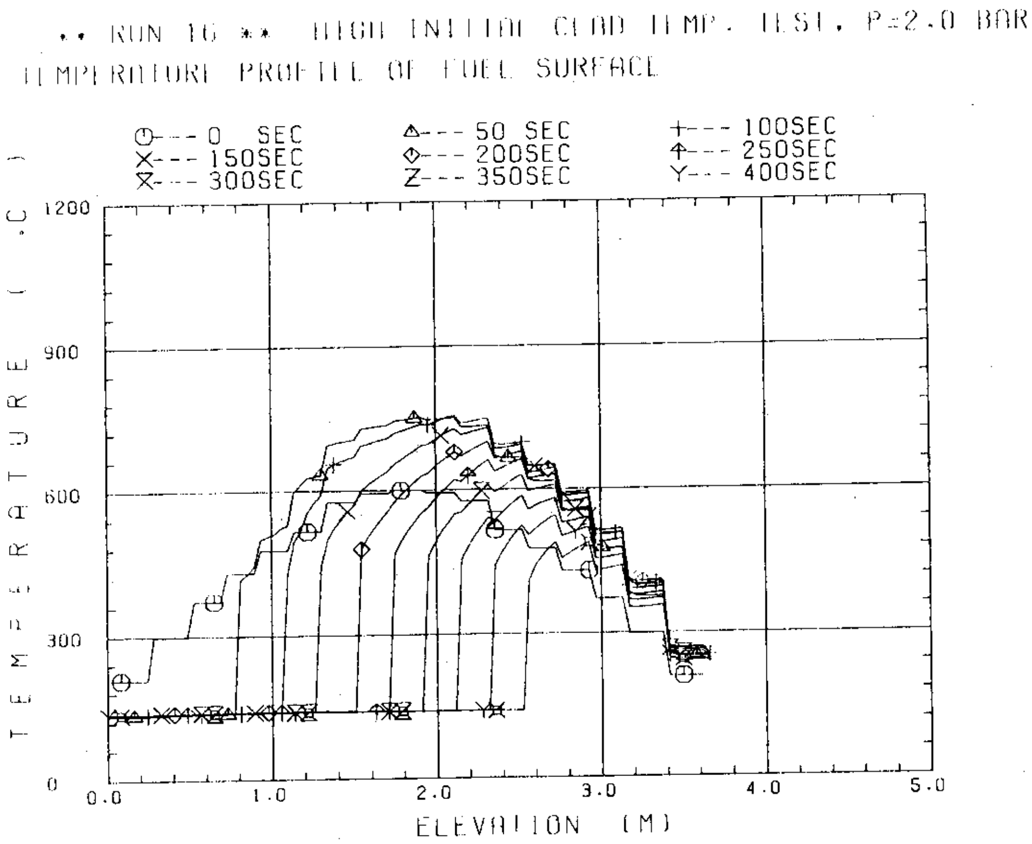

Fig. B.5.5 Rod surface temperature distributions

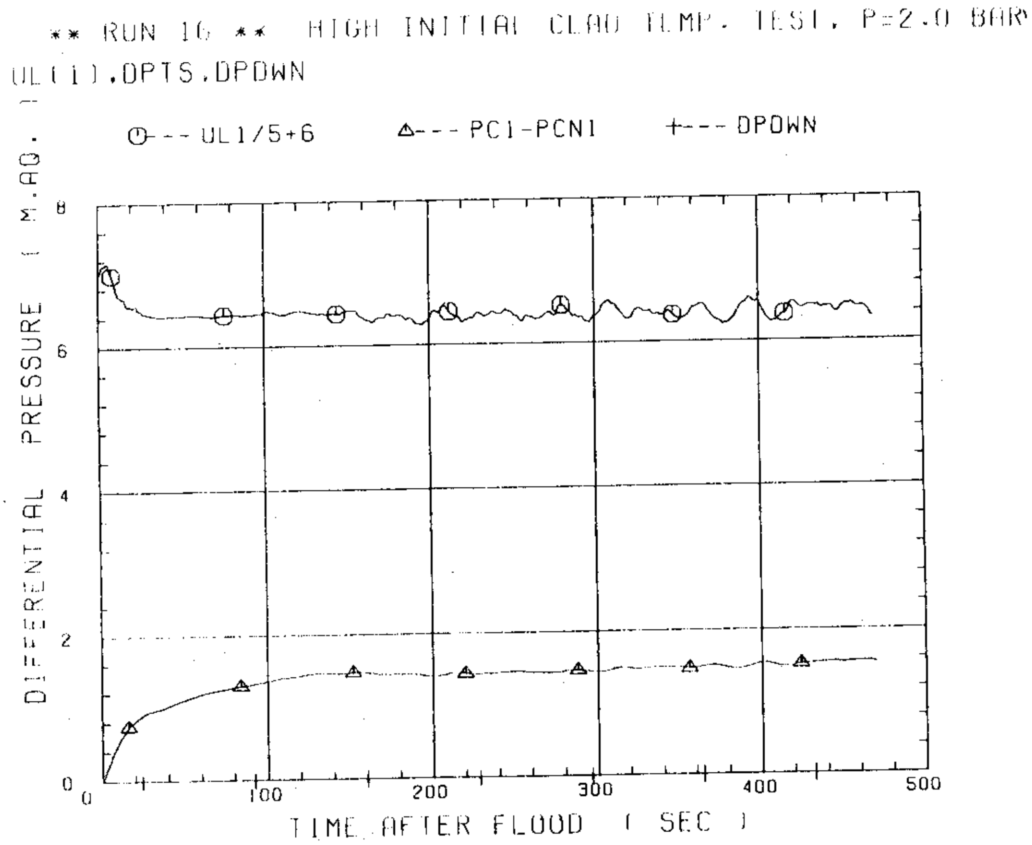

Fig. B.5.6 Core flooding rate (UL1) and core differential pressure (PC1-PCN1)

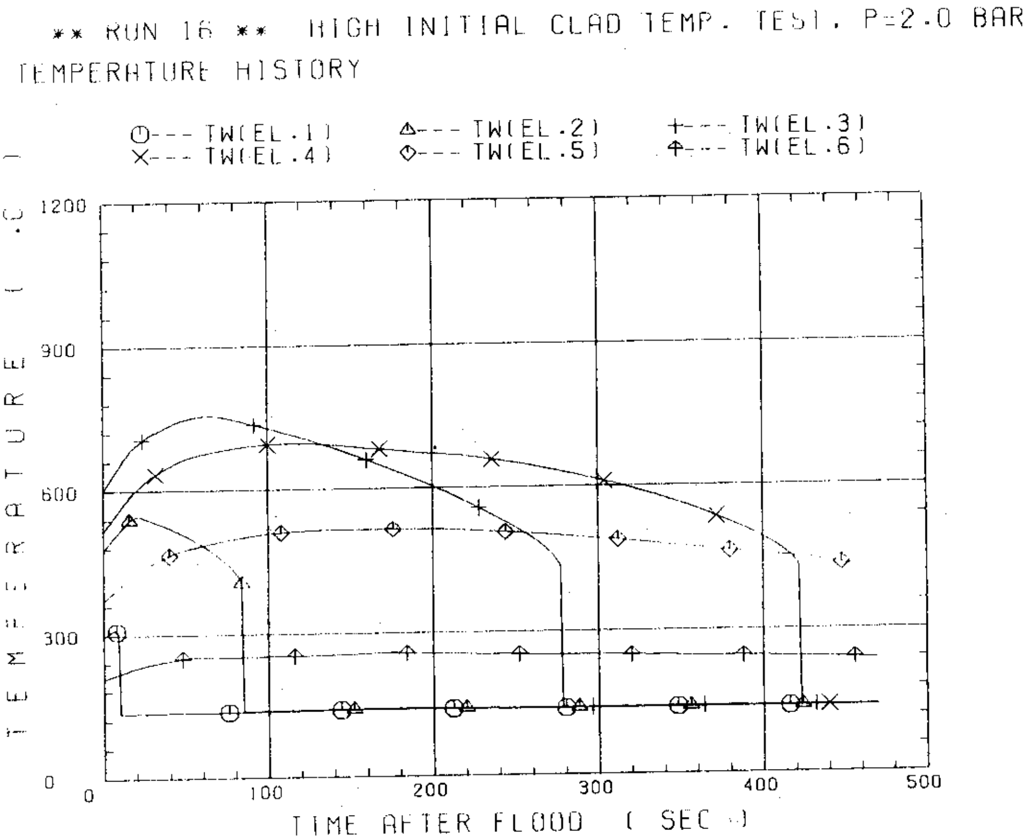

Fig. B.5.7 Rod surface temperatures

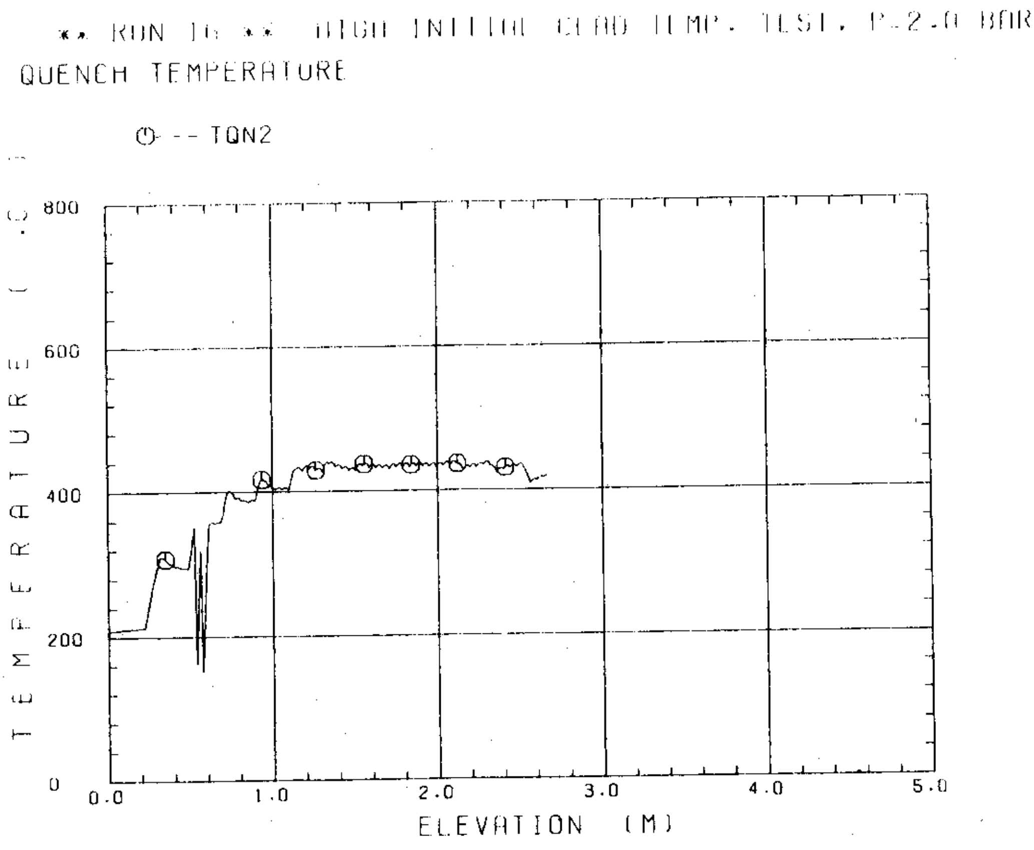

Fig. B.5.8 Quench temperatures

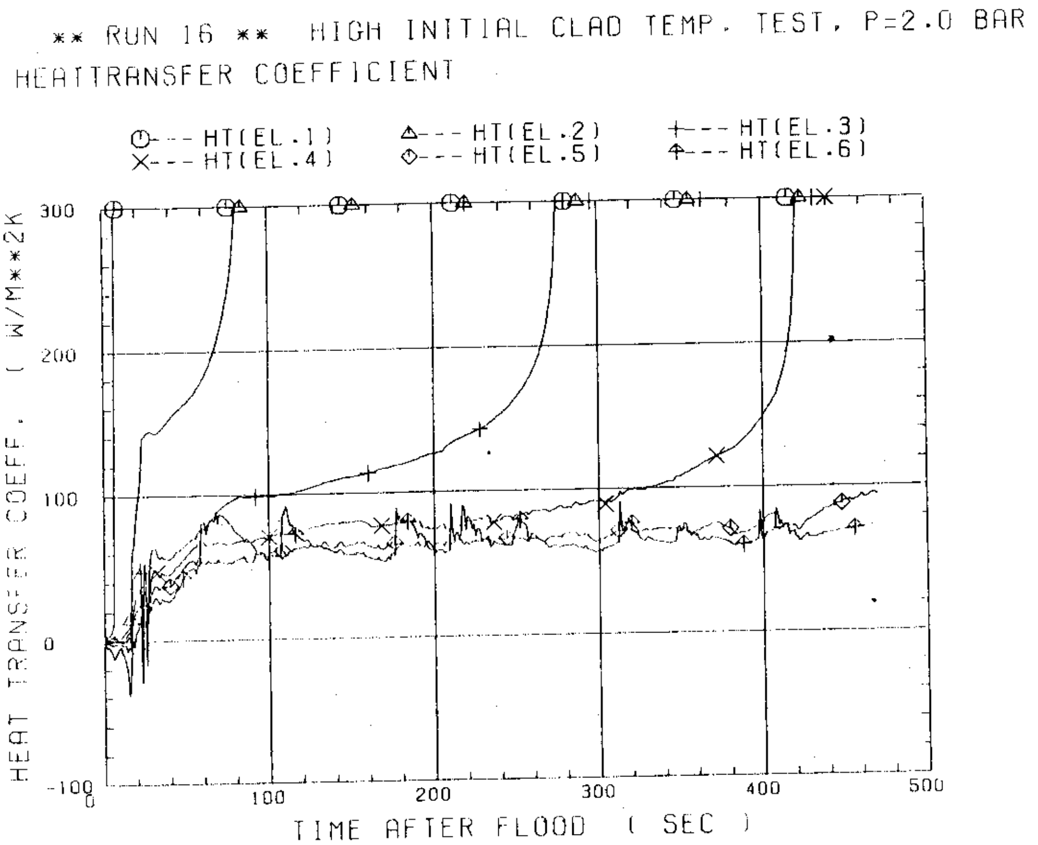

Fig. B.5.9 Heat transfer coefficients

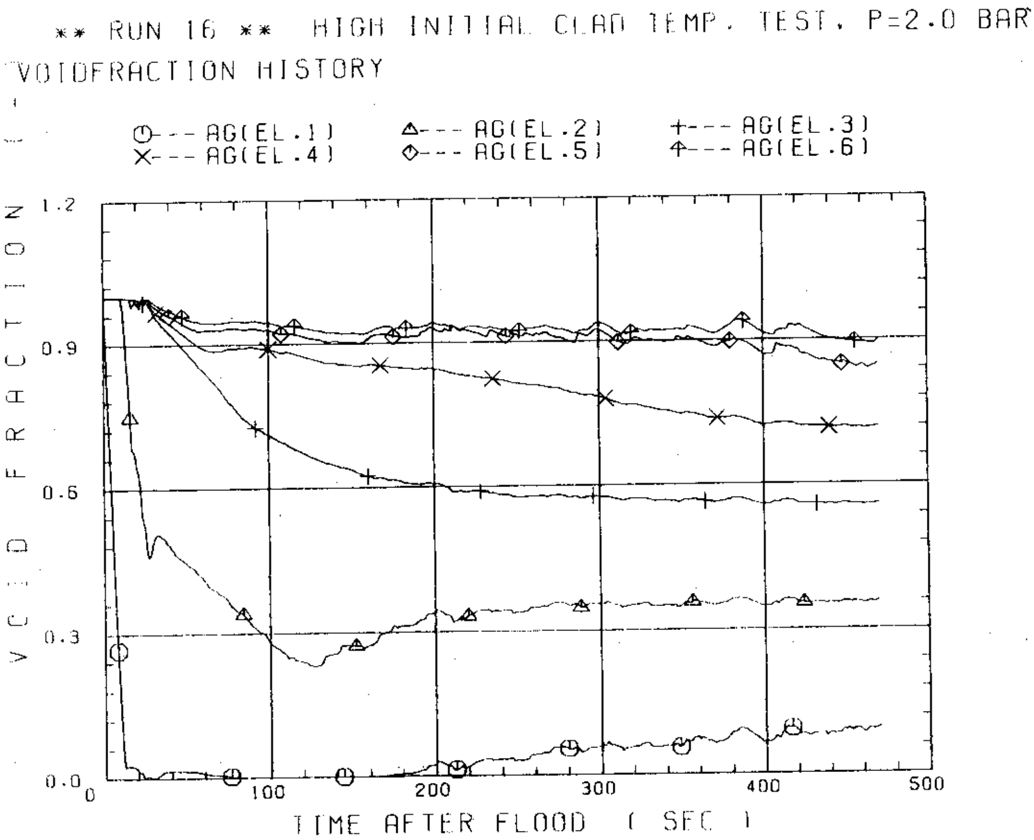

Fig. B.5.10 Void fractions

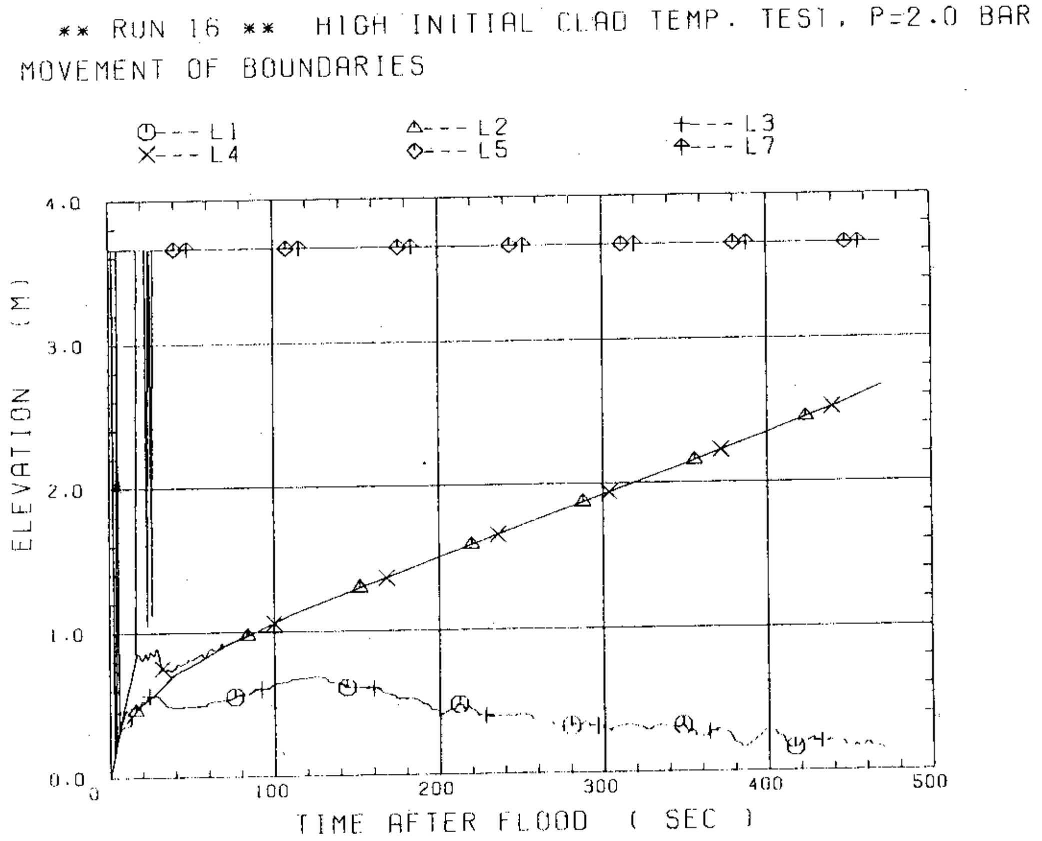

Fig. B.5.11 Movement of flow regime boundaries (L1: Boiling point, L2: Quench front)

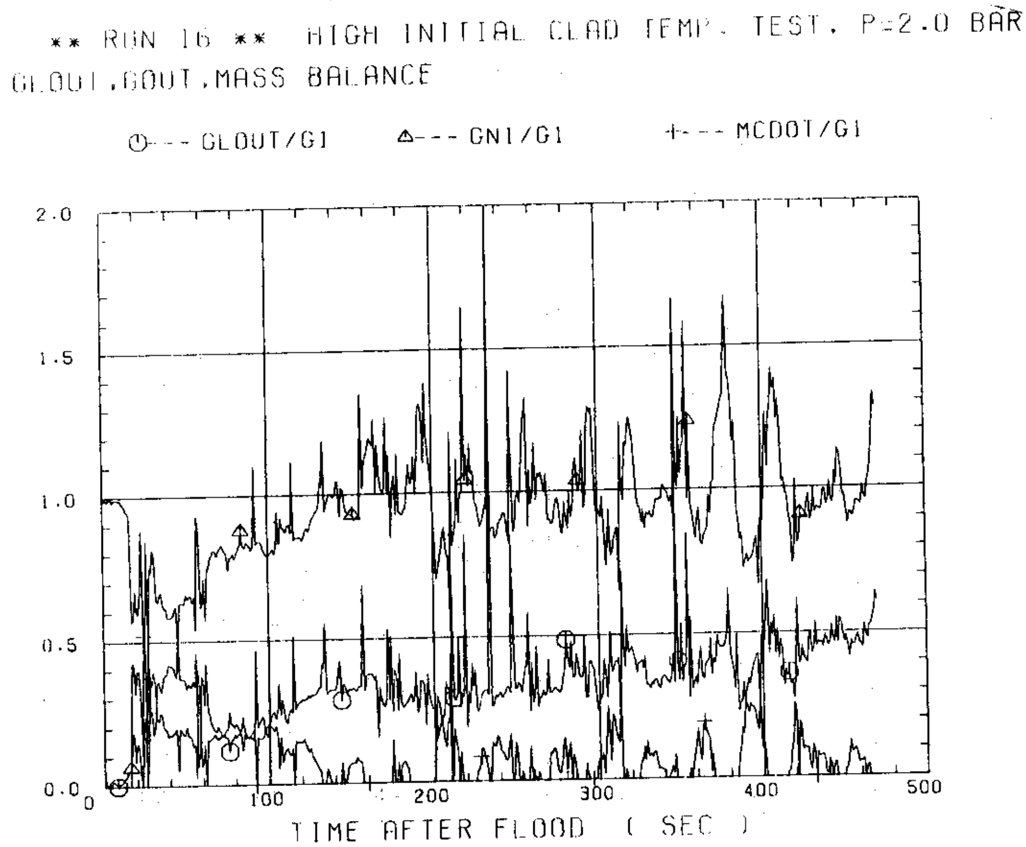

Fig. B.5.12 Liquid carryover rate fraction (GLOUT/G1), carryover rate fraction (GN1/G1) and water accumulation rate fraction (MCDOT/G1)

B.6 Test C1-14 (High initial clad temperature, 800°C)

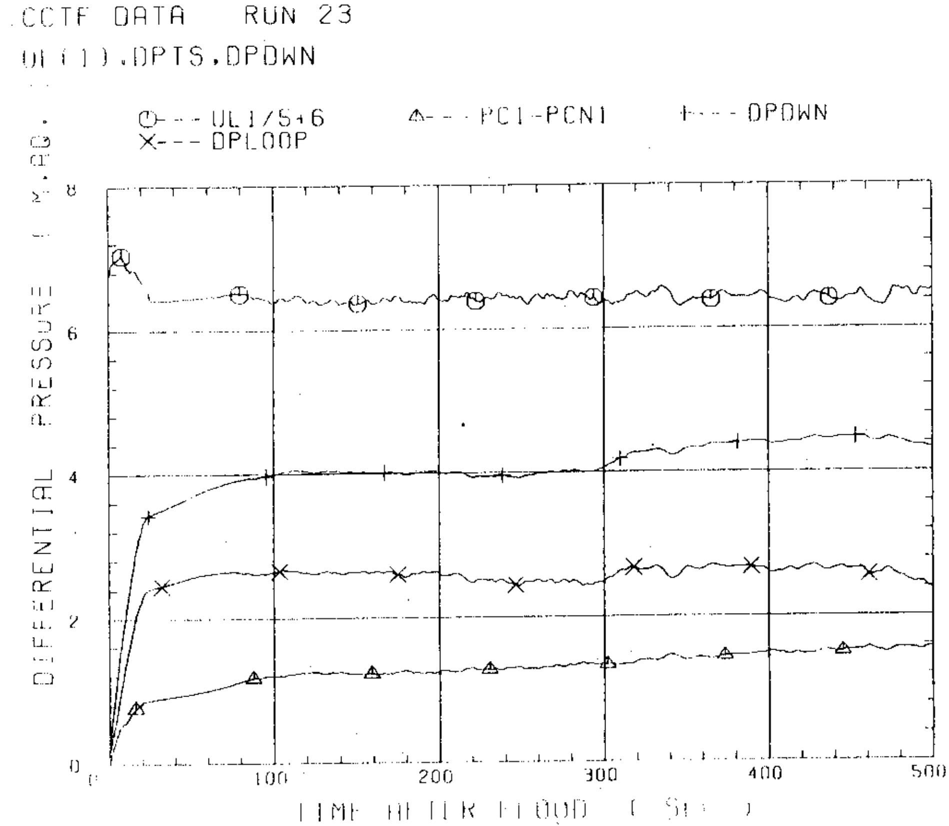

Fig. B.6.1 Core flooding rate (UL1), core differential pressure (PC1-PCN1), downcomer differential pressure (DPDWN) and loop differential pressure (DPLOOP) (Experimental value)

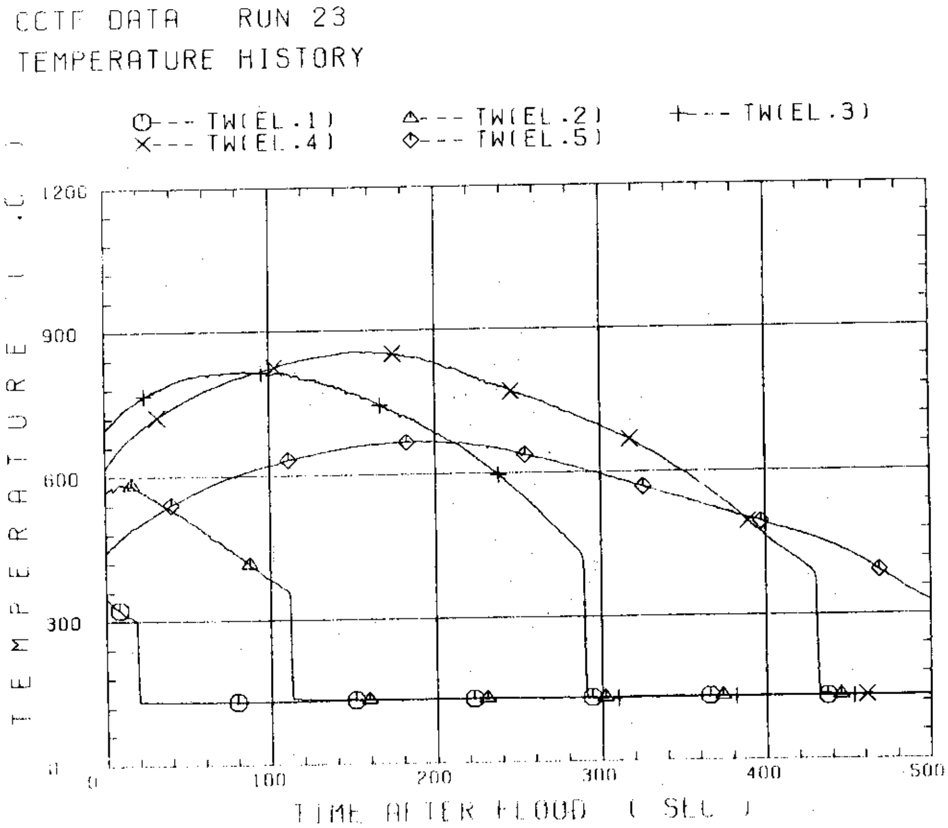

Fig. B.6.2 Rod surface temperatures (Experimental value)

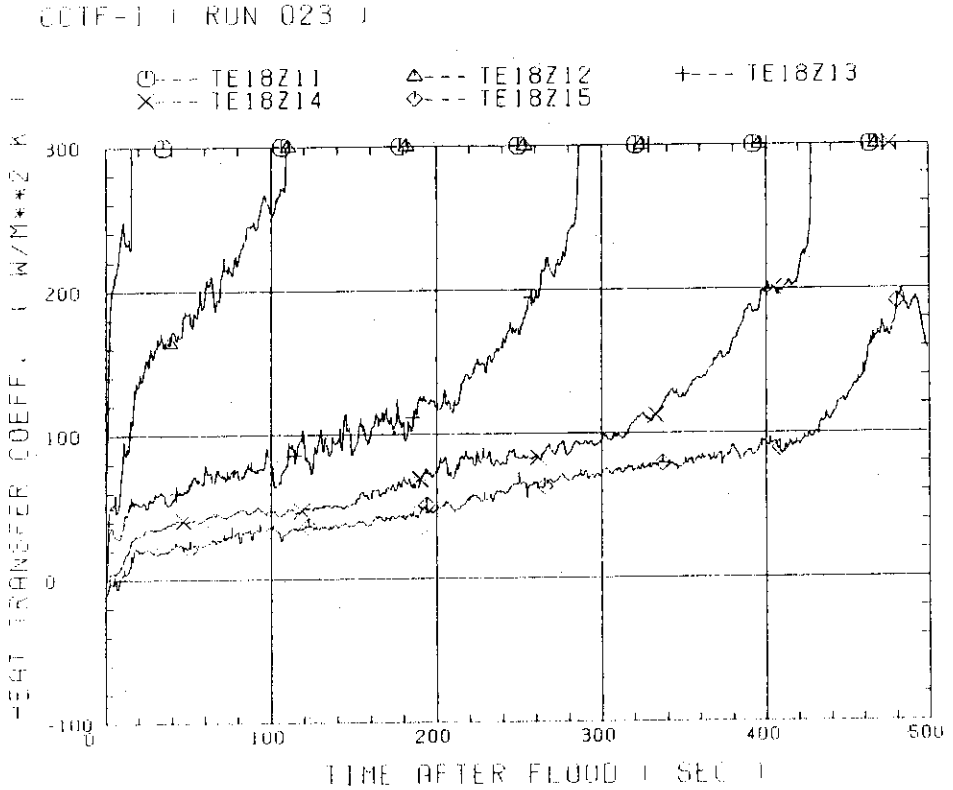

Fig. B.6.3 Heat transfer coefficients (Experimental values)

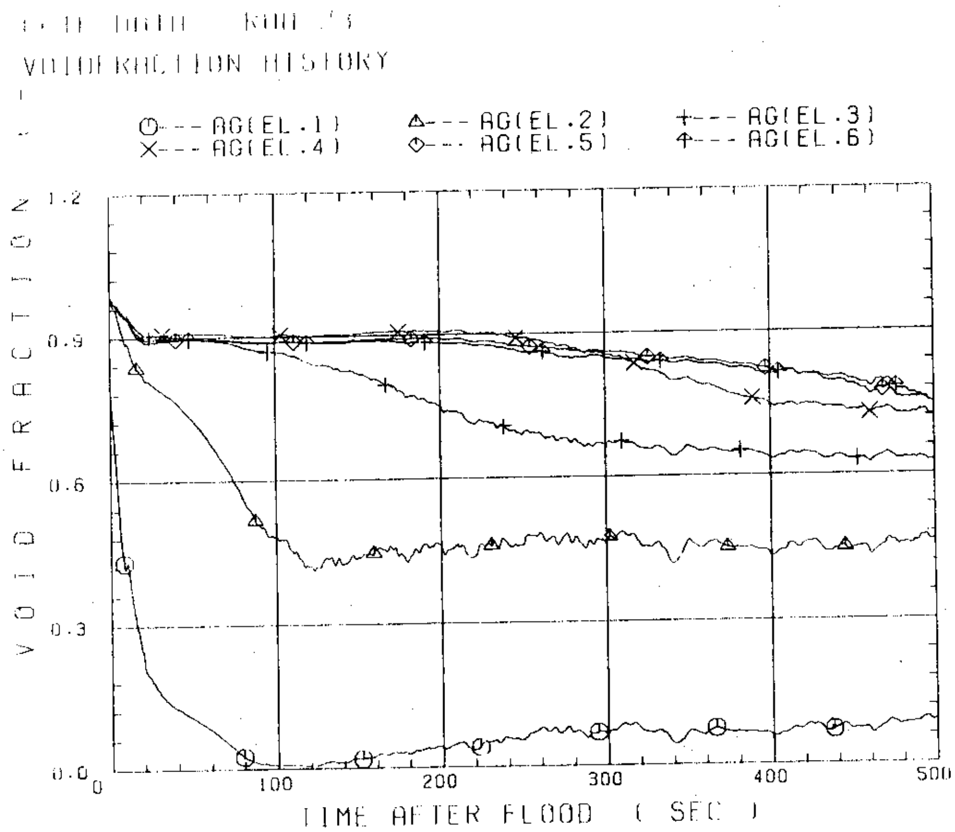

Fig. B.6.4 Void fractions (Experimental values)

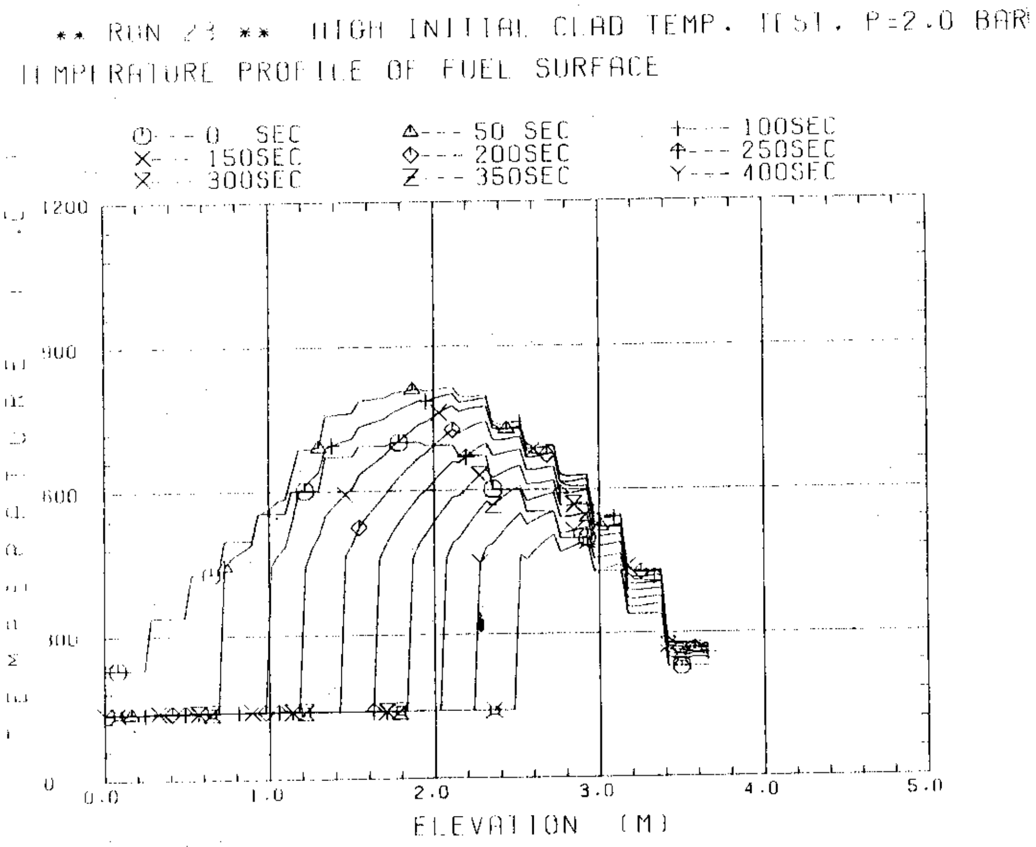

Fig. B.6.5 Rod surface temperature distributions

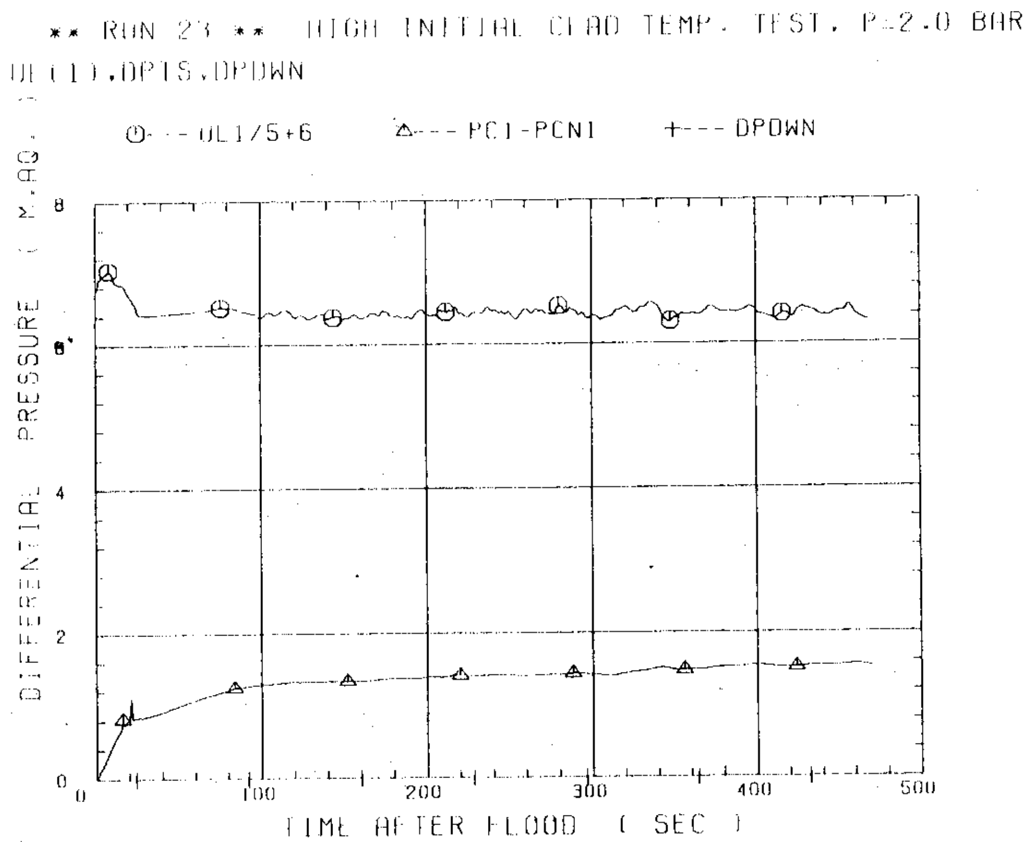

Fig. B.6.6 Core flooding rate (UL1) and core differential pressure (PC1-PCN1)

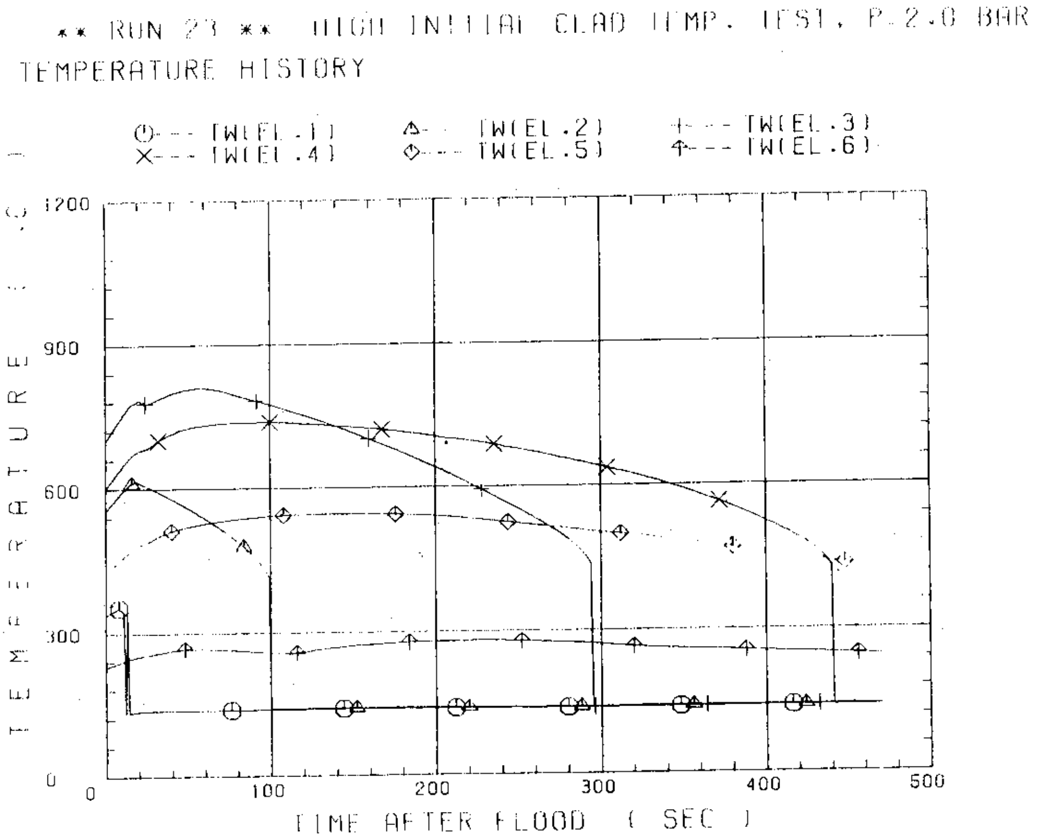

Fig. B.6.7 Rod surface temperatures

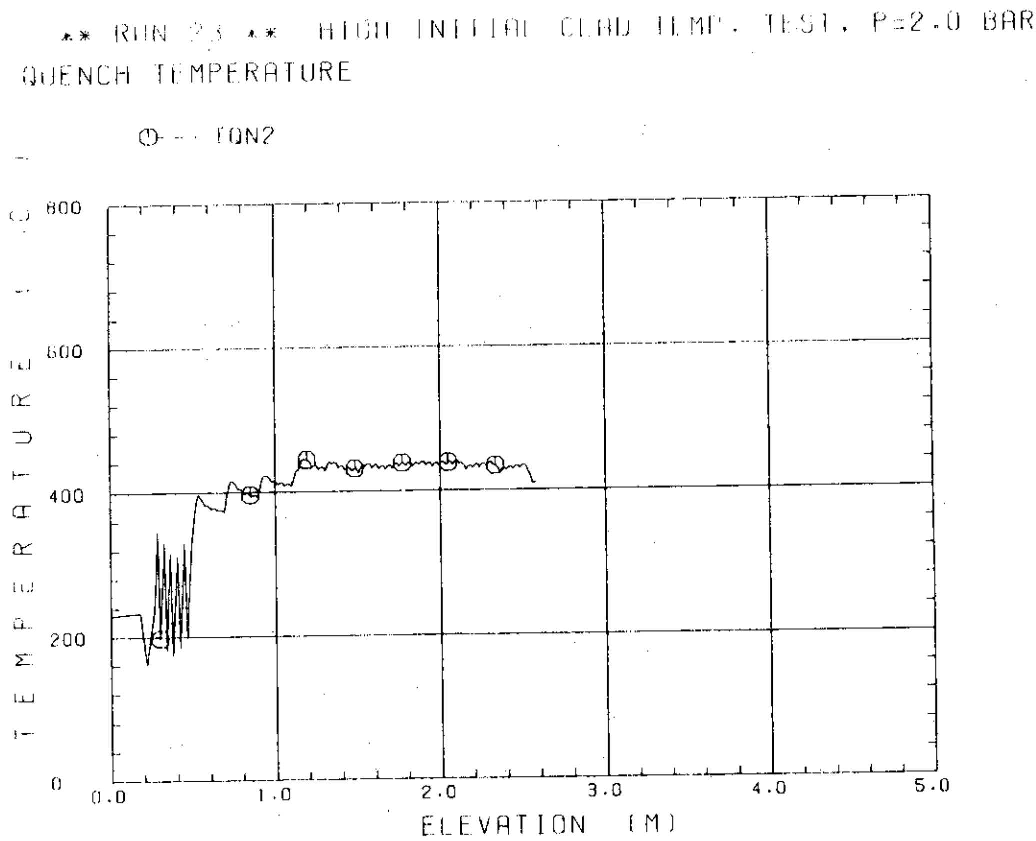

Fig. B.6.8 Quench temperatures

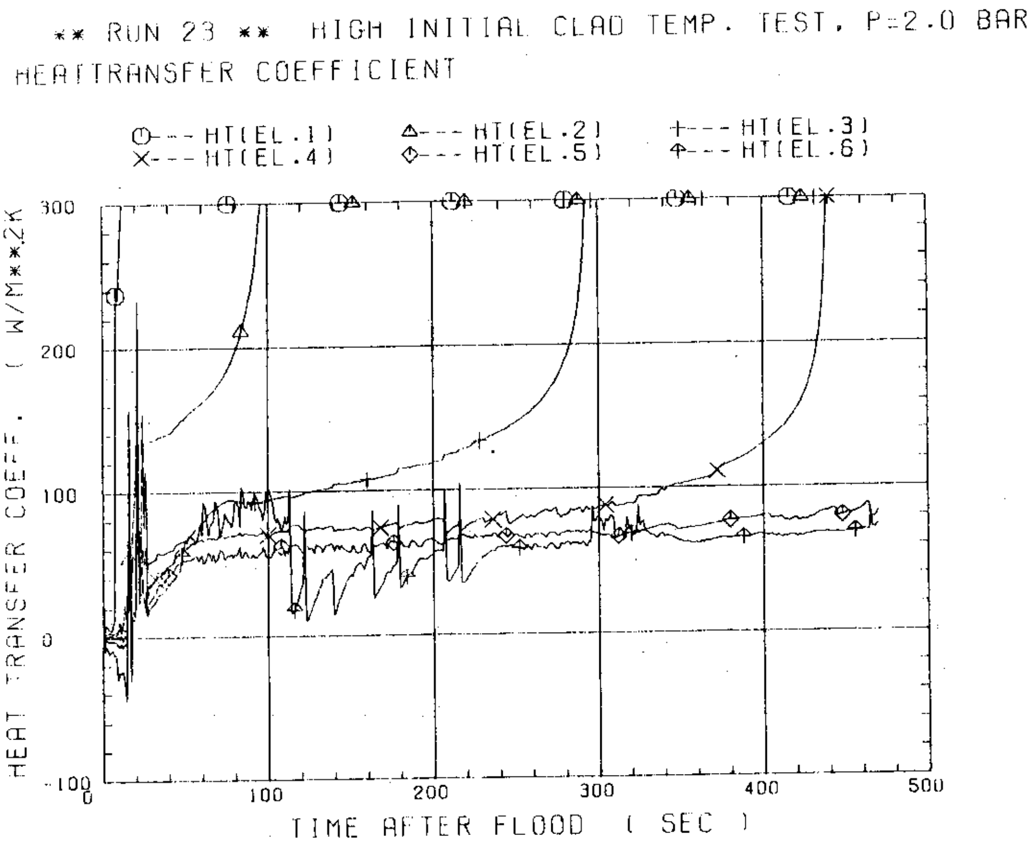

Fig. B.6.9 Heat transfer coefficients

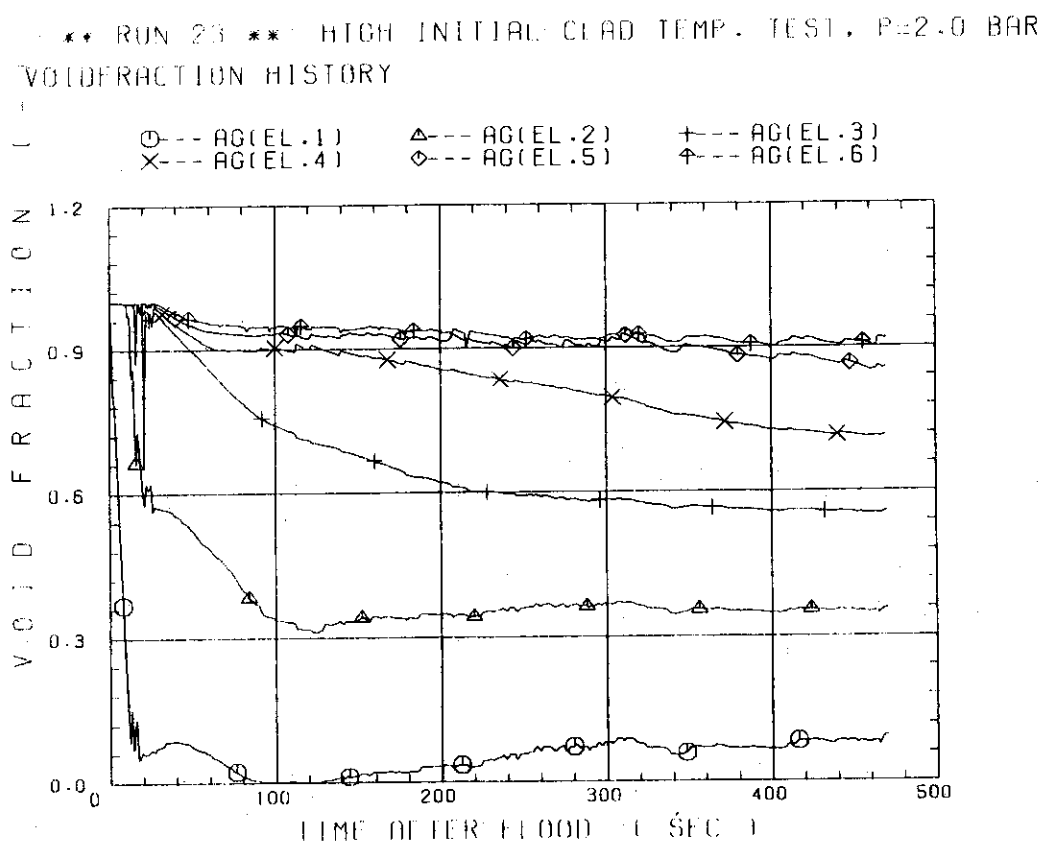

Fig. B.6.10 Void fractions

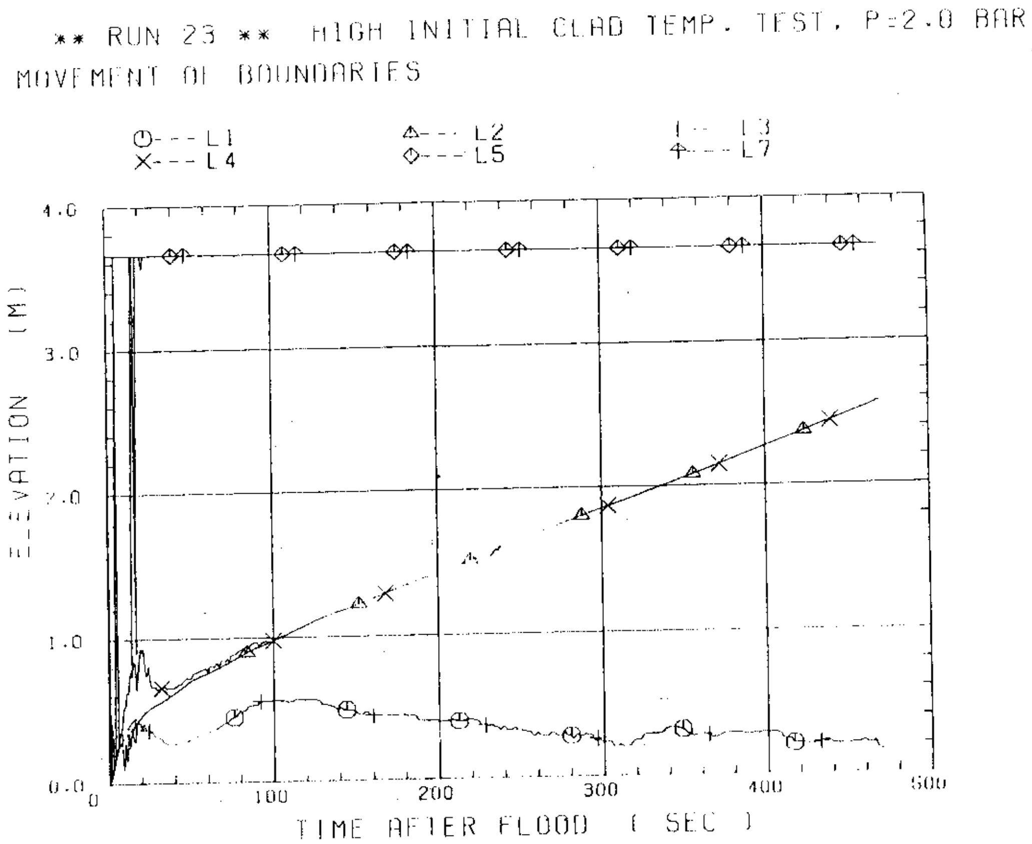

Fig. B.6.11 Movement of flow regime boundaries (L1: Boiling point, L2: Quench front)

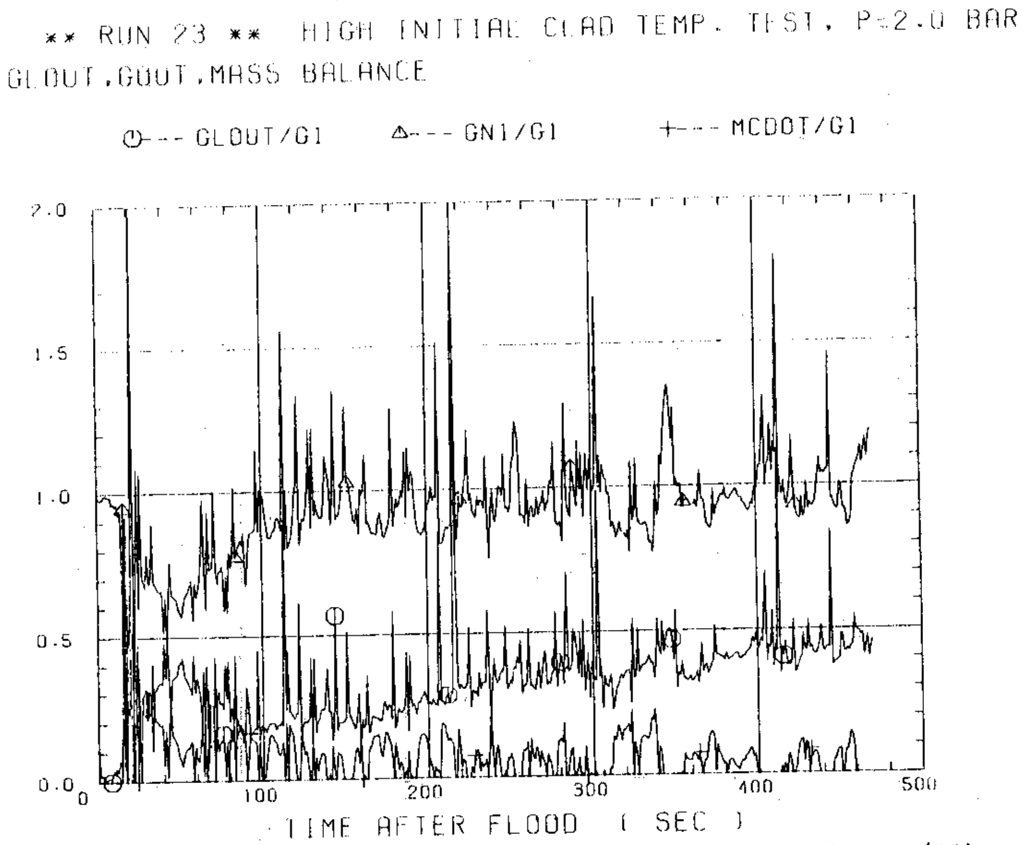

Fig. B.6.12 Liquid carryover rate fraction (GLOUT/G1), carryover rate fraction (GN1/G1) and water accumulation rate fraction (MCDOT/G1)

B.7 Test C1-11 (Low Acc injection rate)

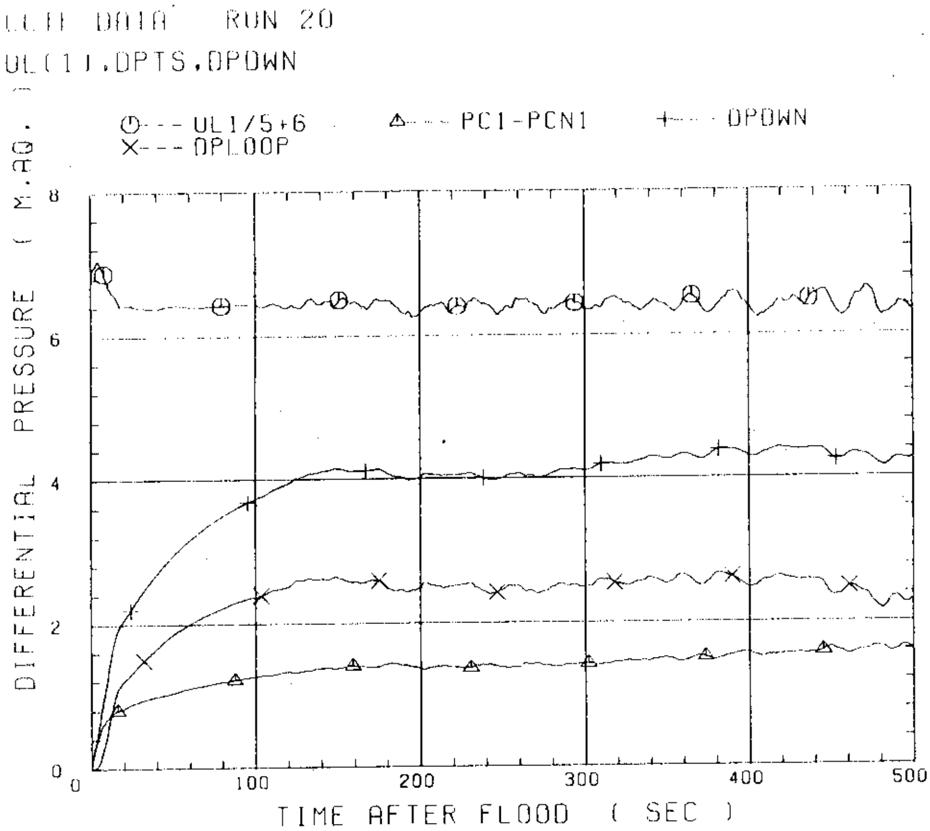

Fig. B.7.1 Core flooding rate (UL1), core differential pressure (PC1-PCN1), downcomer differential pressure (DPDWN) and loop differential pressure (DPLOOP) (Experimental value)

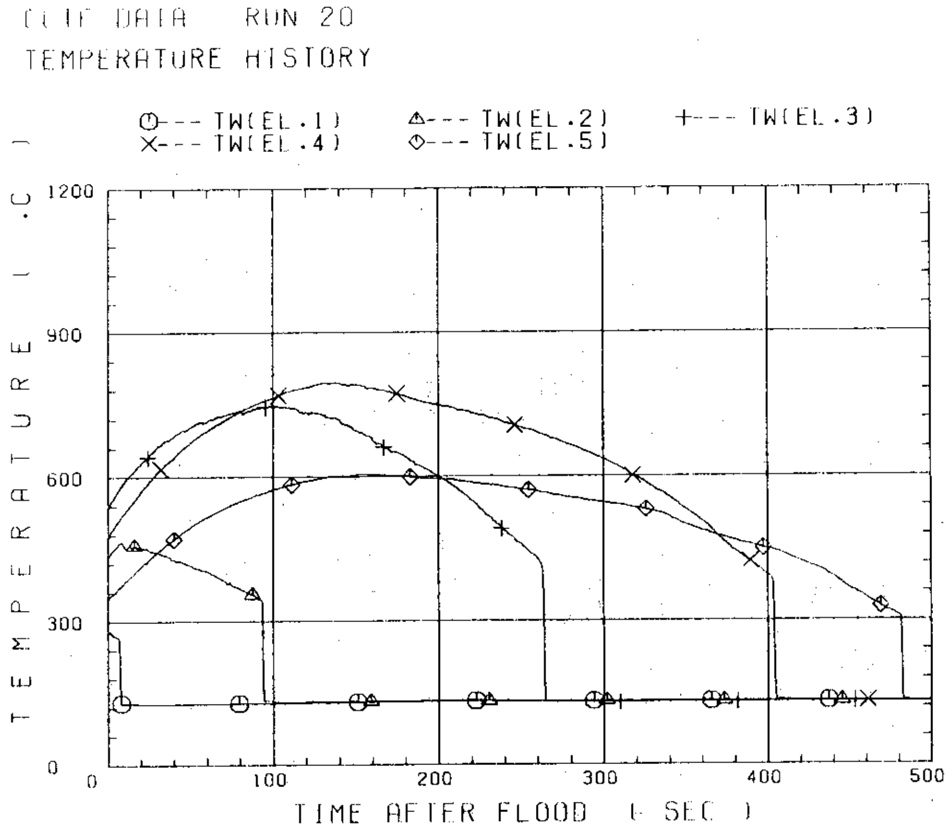

Fig. B.7.2 Rod surface temperatures (Experimental value)

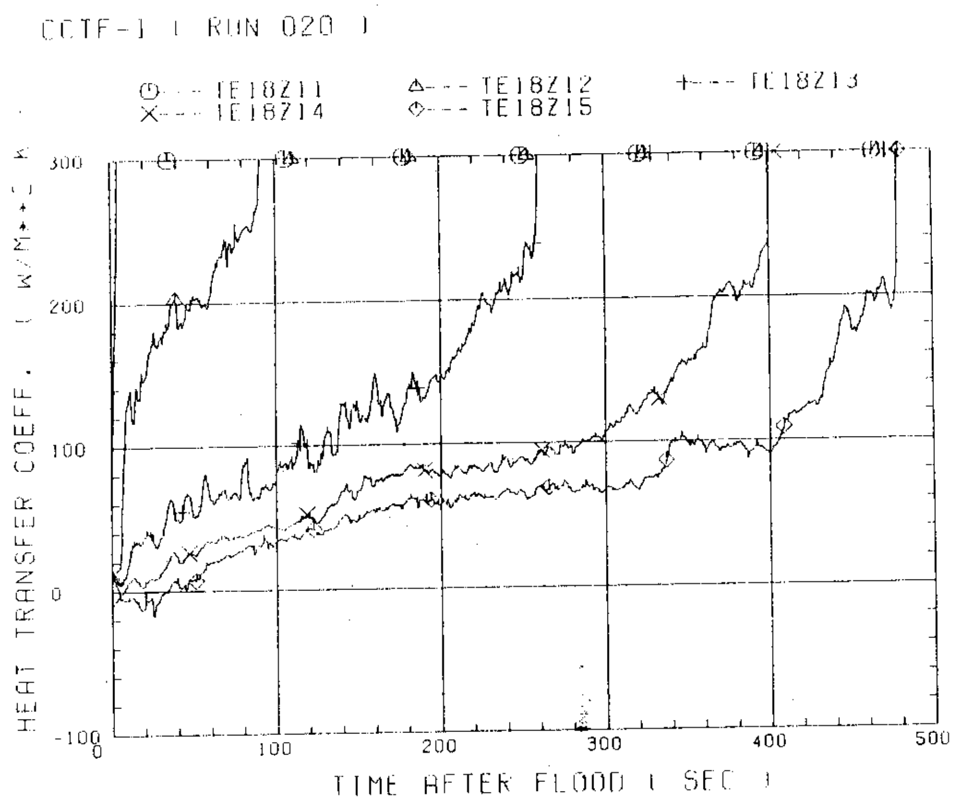

Fig. B.7.3 Heat transfer coefficients (Experimental values)

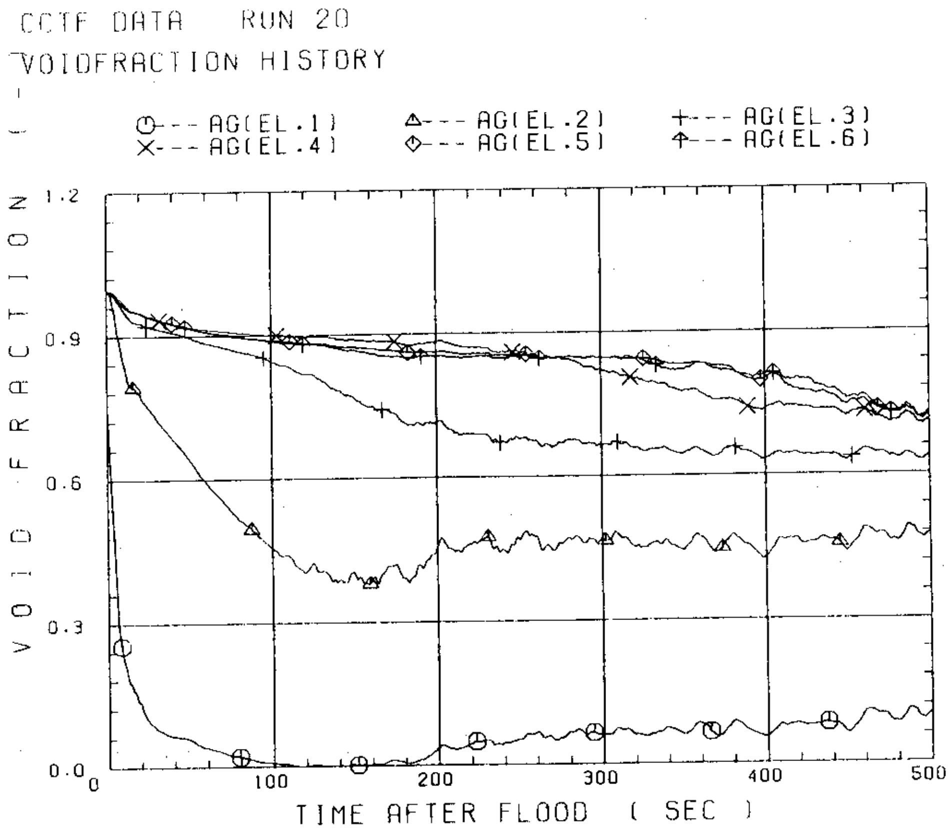

Fig. B.7.4 Void fractions (Experimental values)

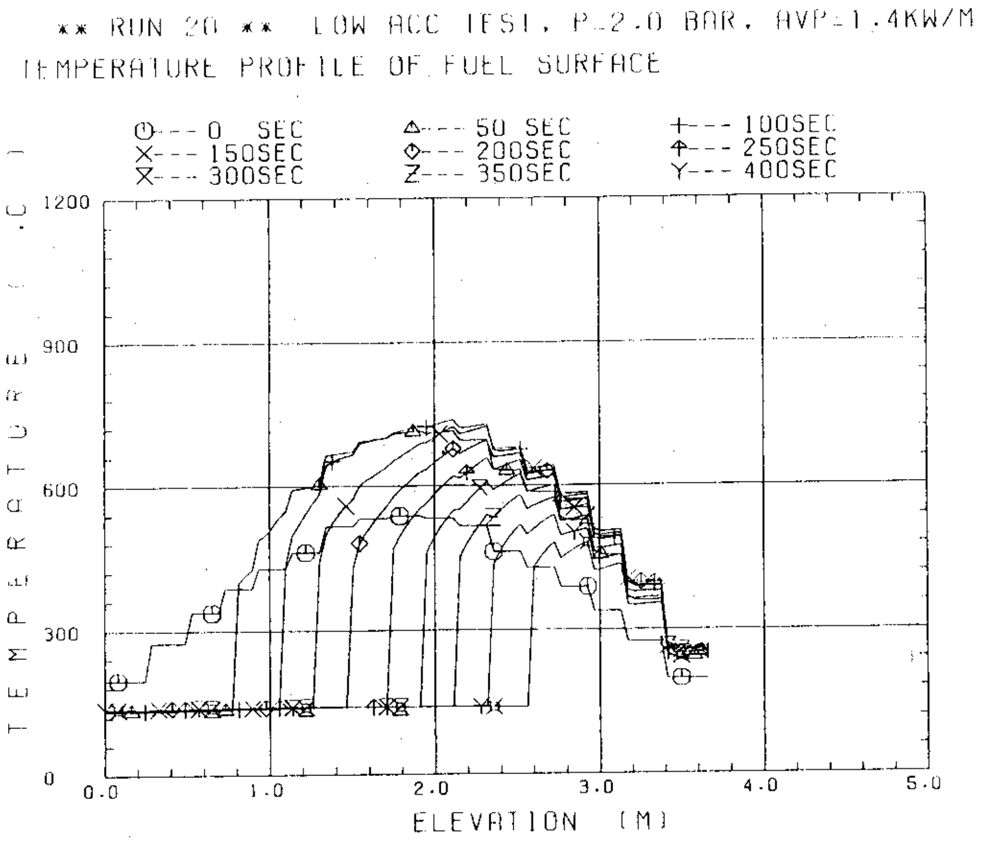

Fig. B.7.5 Rod surface temperature distributions

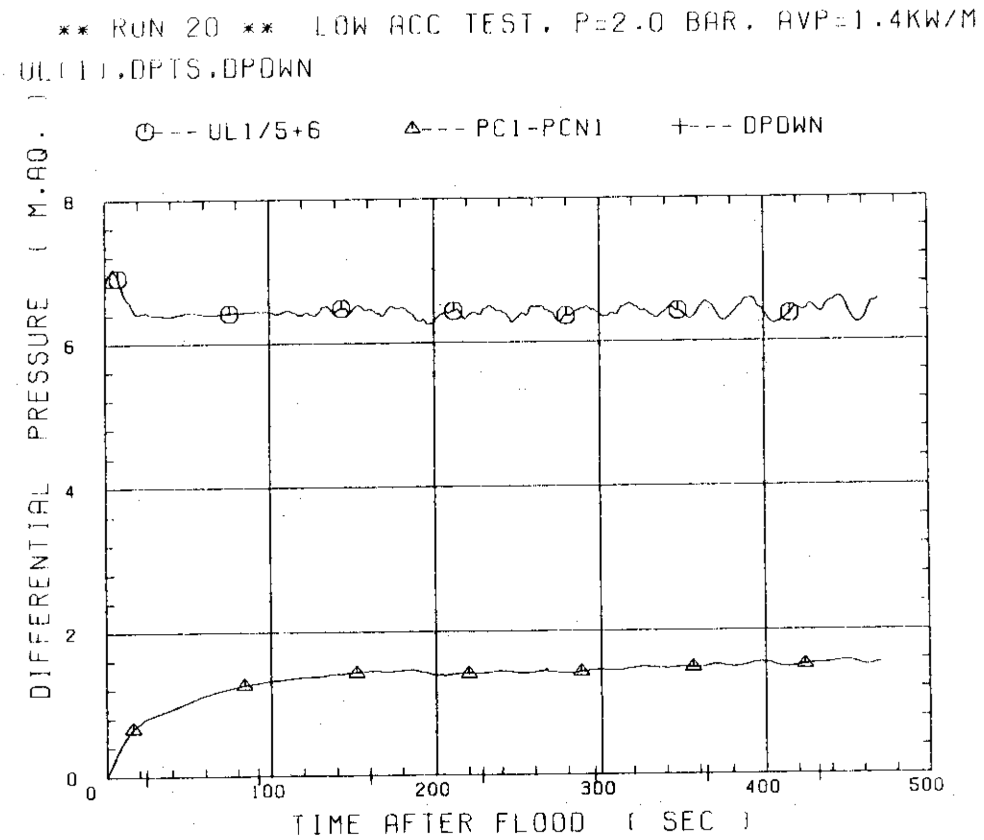

Fig. B.7.6 Core flooding rate (UL1) and core differential pressure (PC1-PCN1)

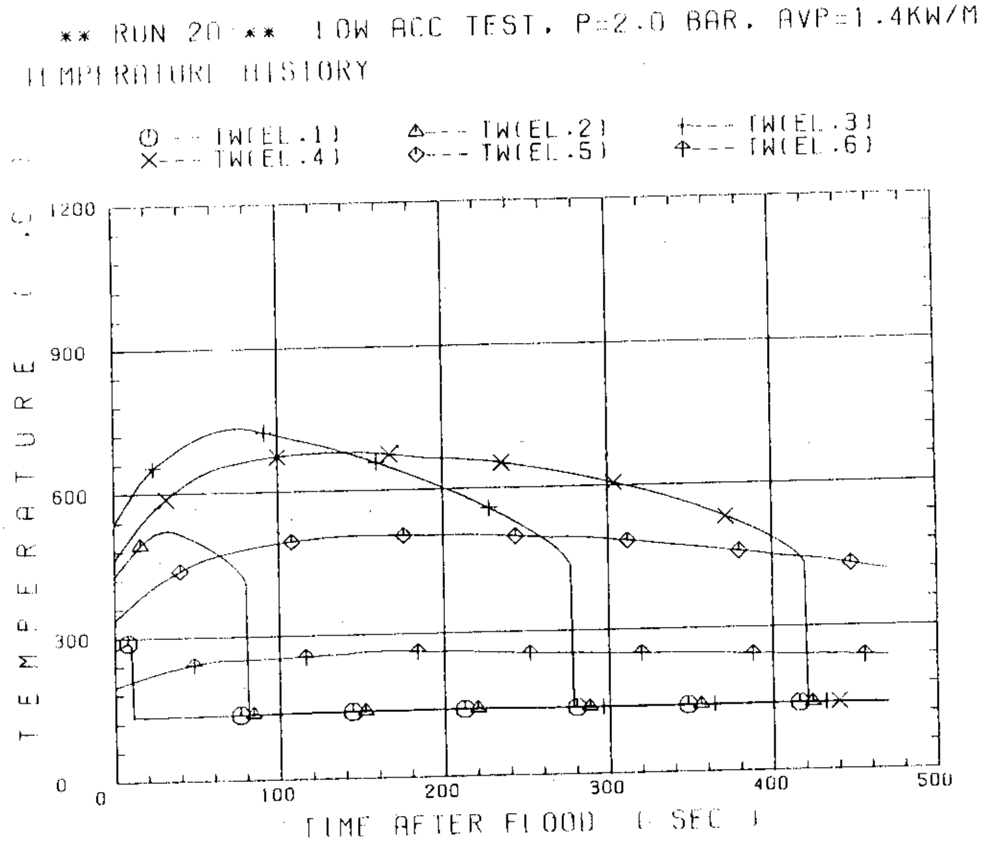

Fig. B.7.7 Rod surface temperatures

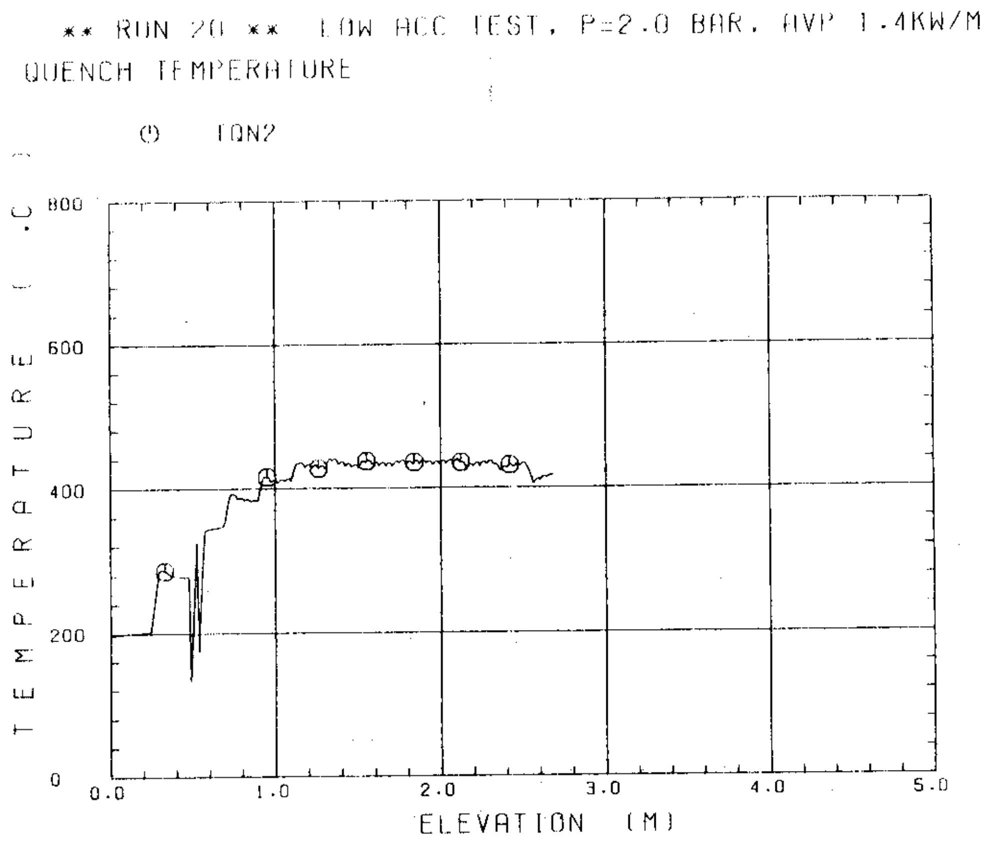

Fig. B.7.8 Quench temperatures

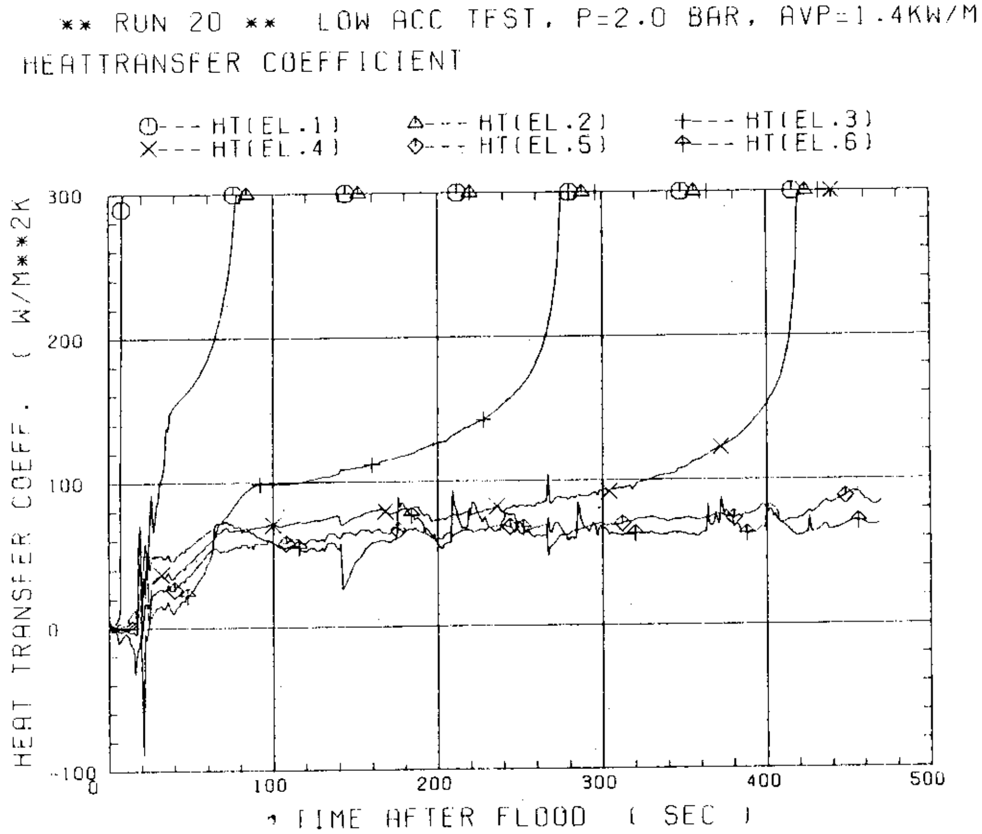

Fig. B.7.9 Heat transfer coefficients

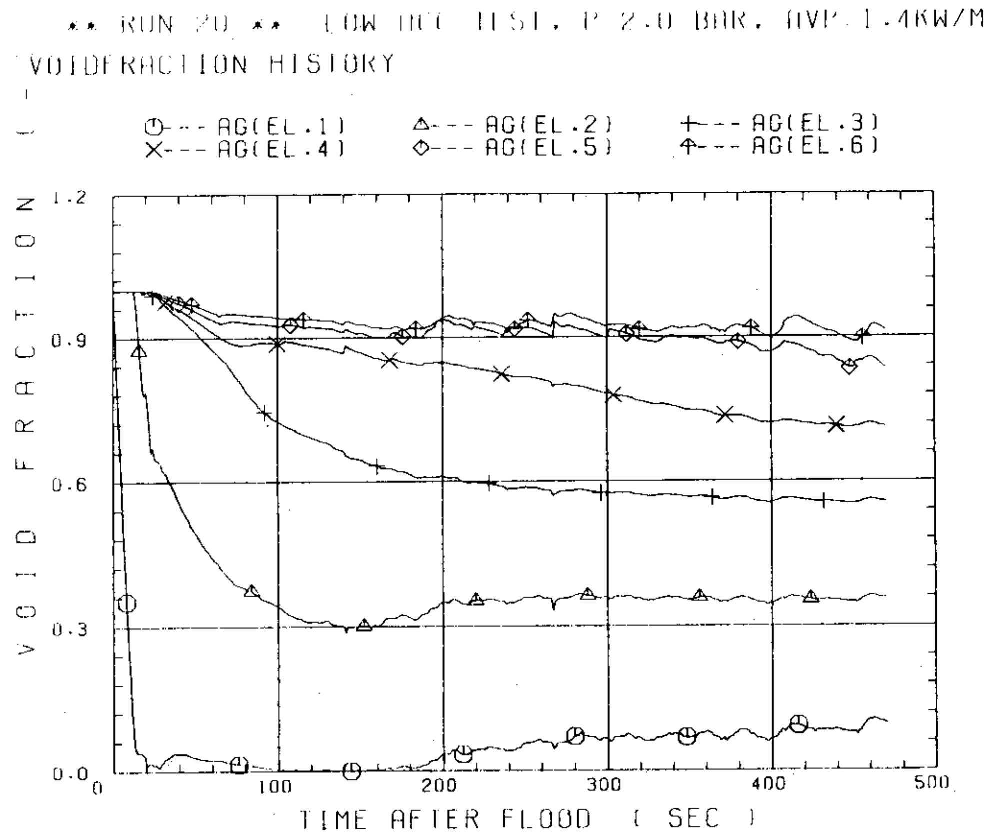

Fig. B.7.10 Void fractions

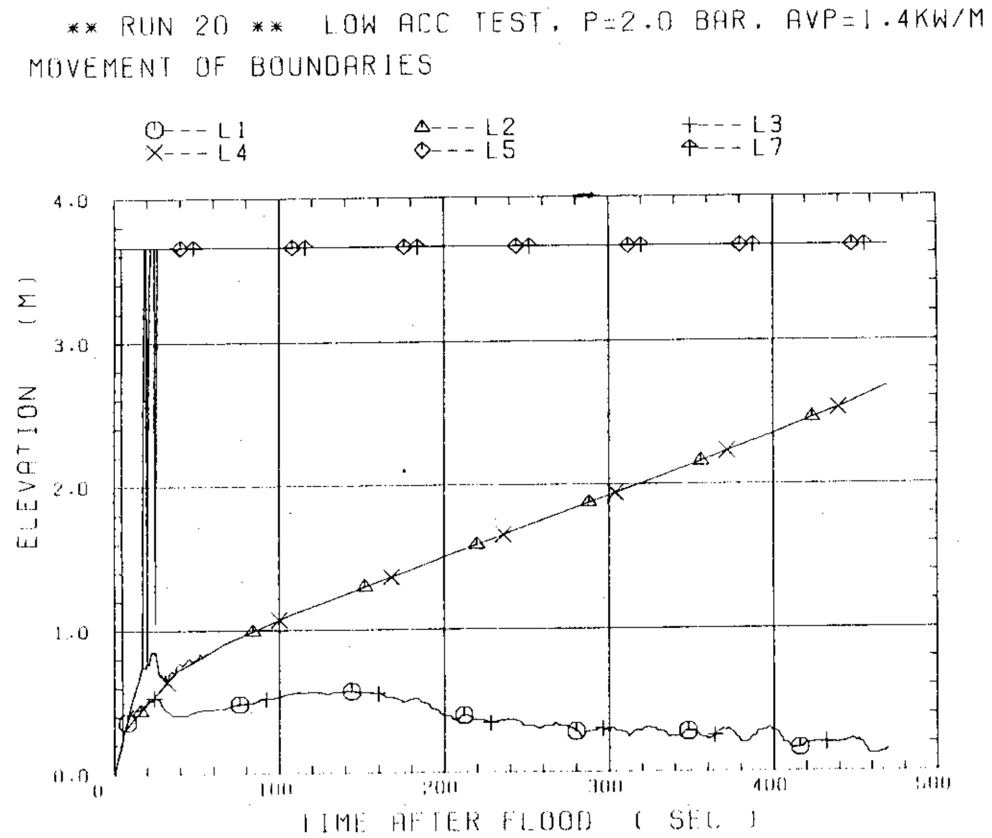

Fig. B.7.11 Movement of flow regime boundaries (L1: Boiling point, L2: Quench front)

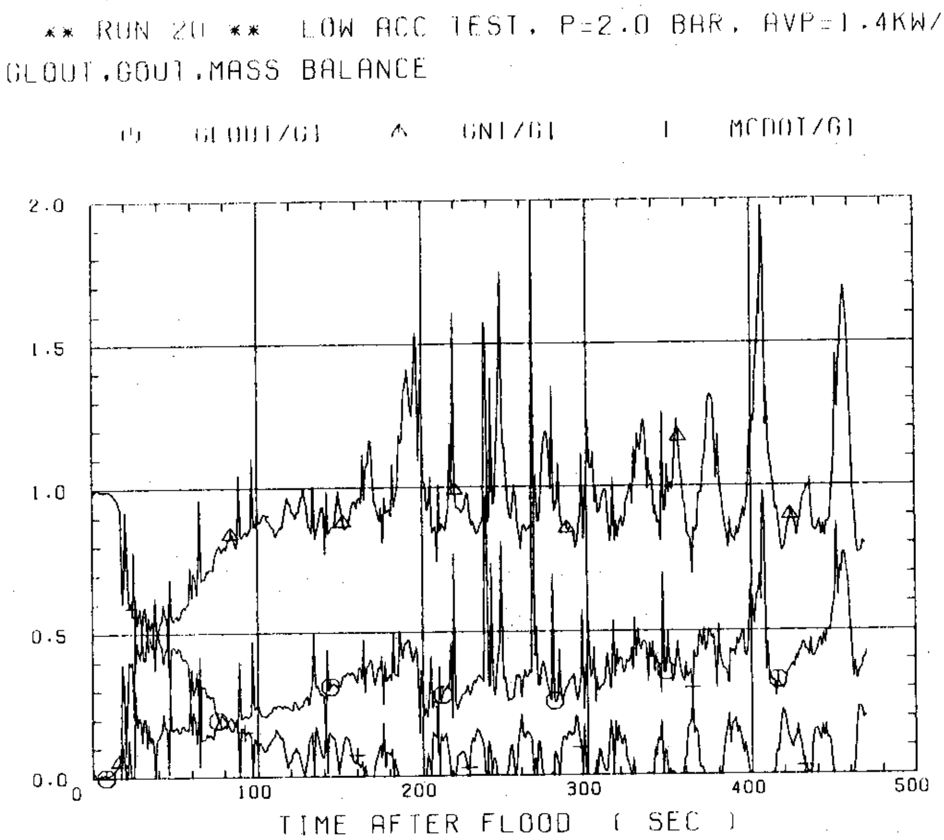

Fig. B.7.12 Liquid carryover rate fraction (GLOUT/G1), carryover rate fraction (GN1/G1) and water accumulation rate fraction (MCDOT/G1)

B.8 Test C1-6 (High LPCI injection rate)

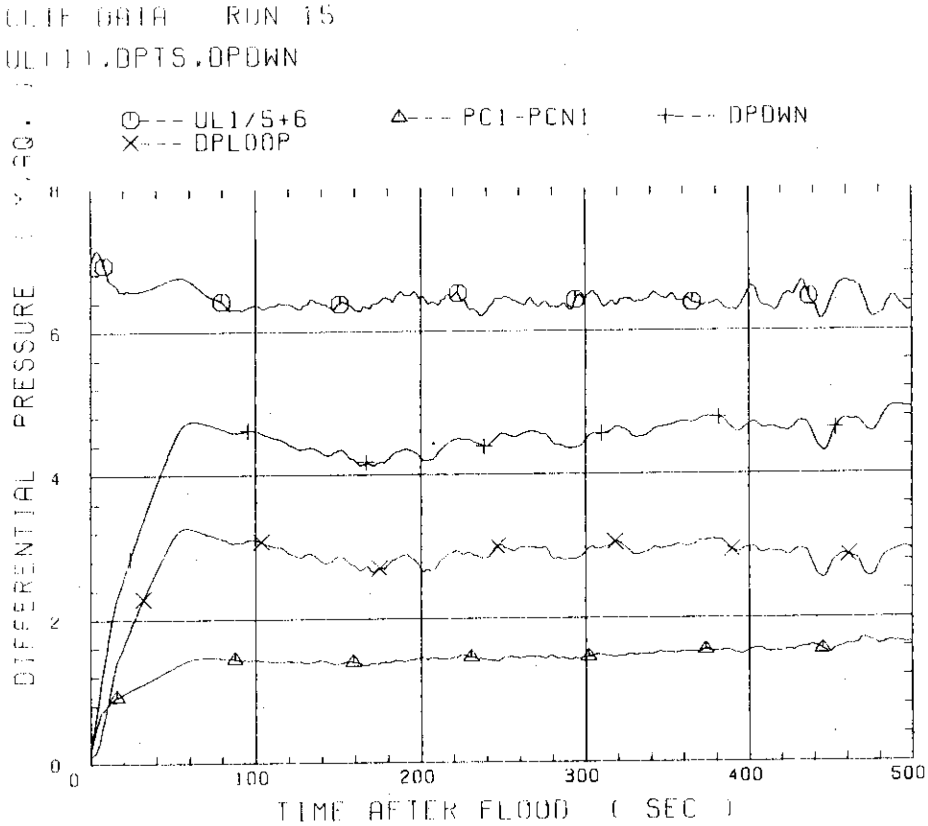

Fig. B.8.1 Core flooding rate (UL1), core differential pressure (PC1-PCN1), downcomer differential pressure (DPDWN) and loop differential pressure (DPLOOP) (Experimental value)

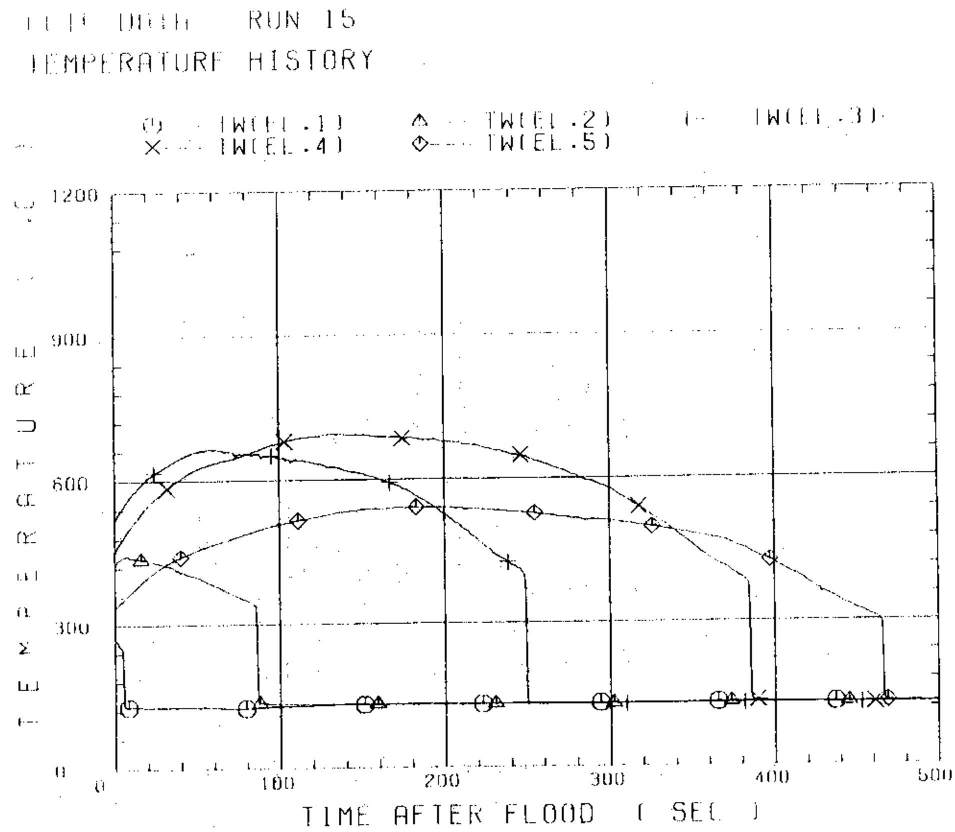

Fig. B.8.2 Rod surface temperatures (Experimental value)

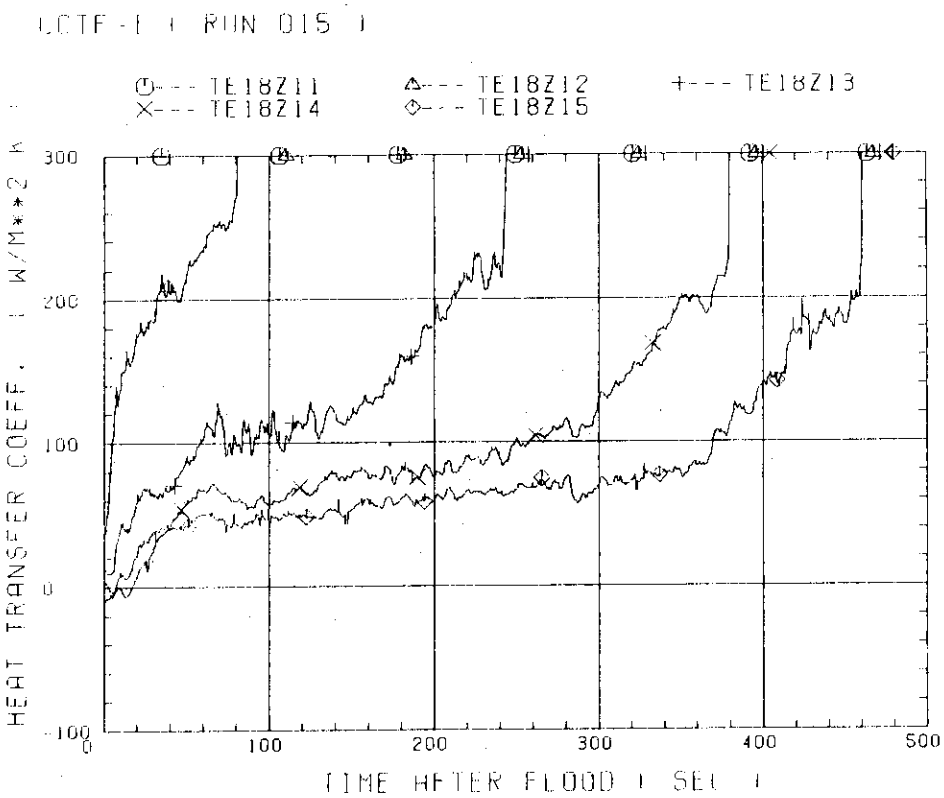

Fig. B.8.3 Heat transfer coefficients (Experimental values)

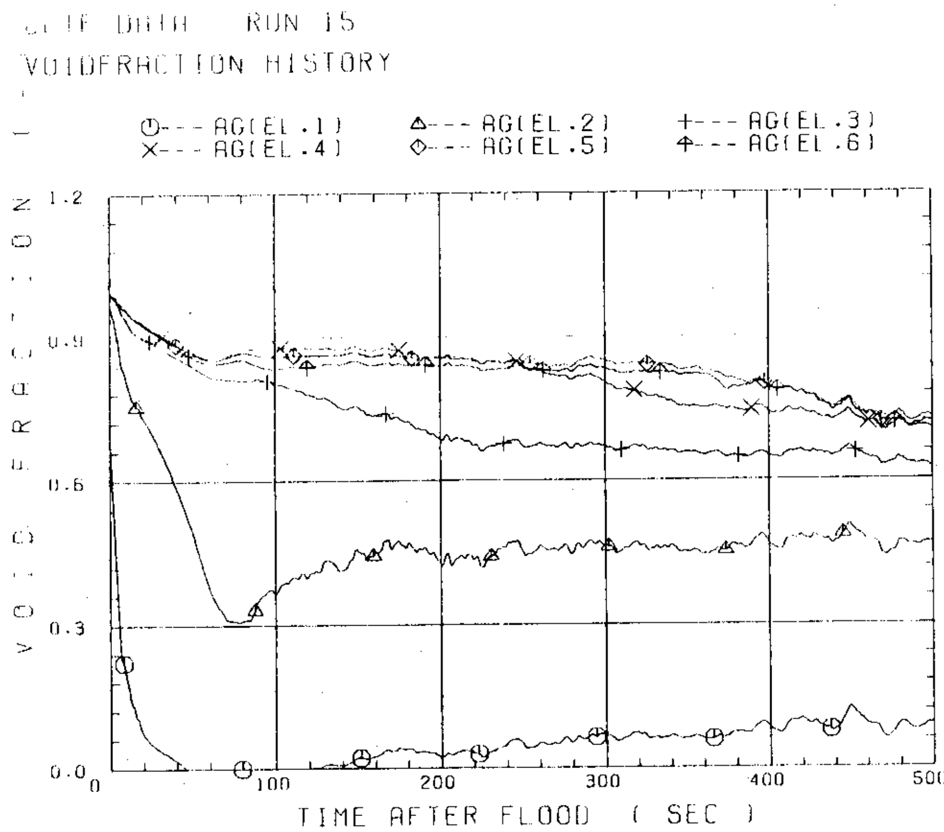

Fig. B.8.4 Void fractions (Experimental values)

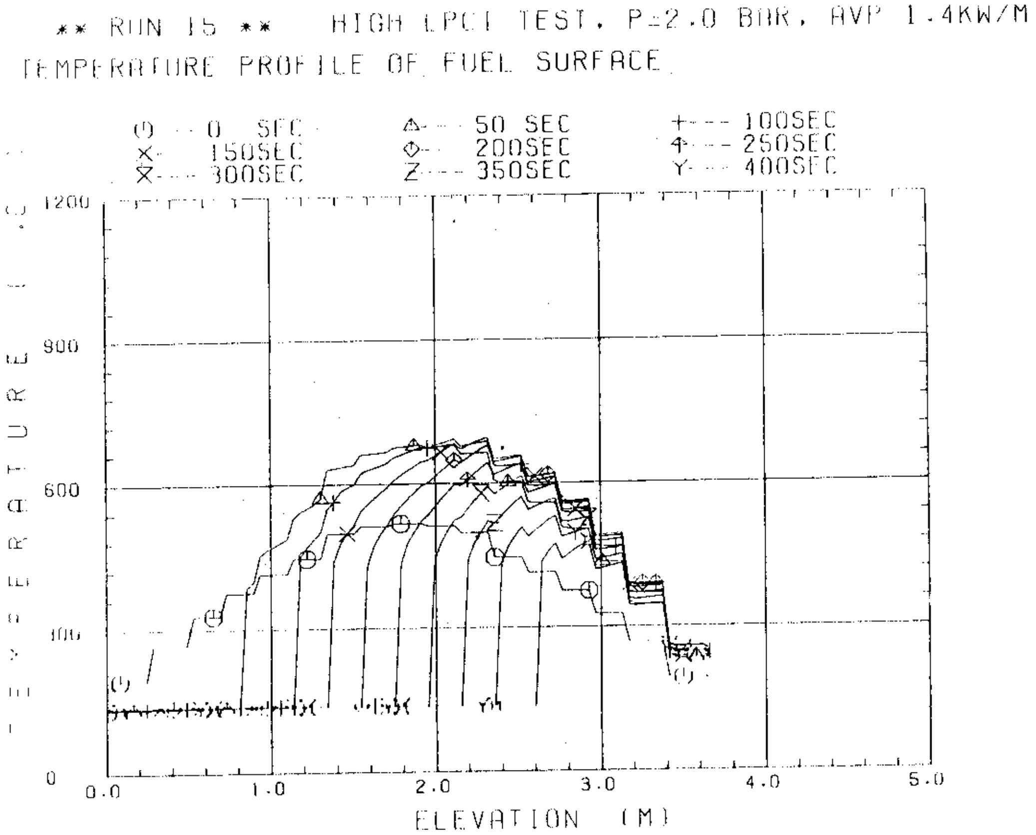

Fig. B.8.5 Rod surface temperature distributions

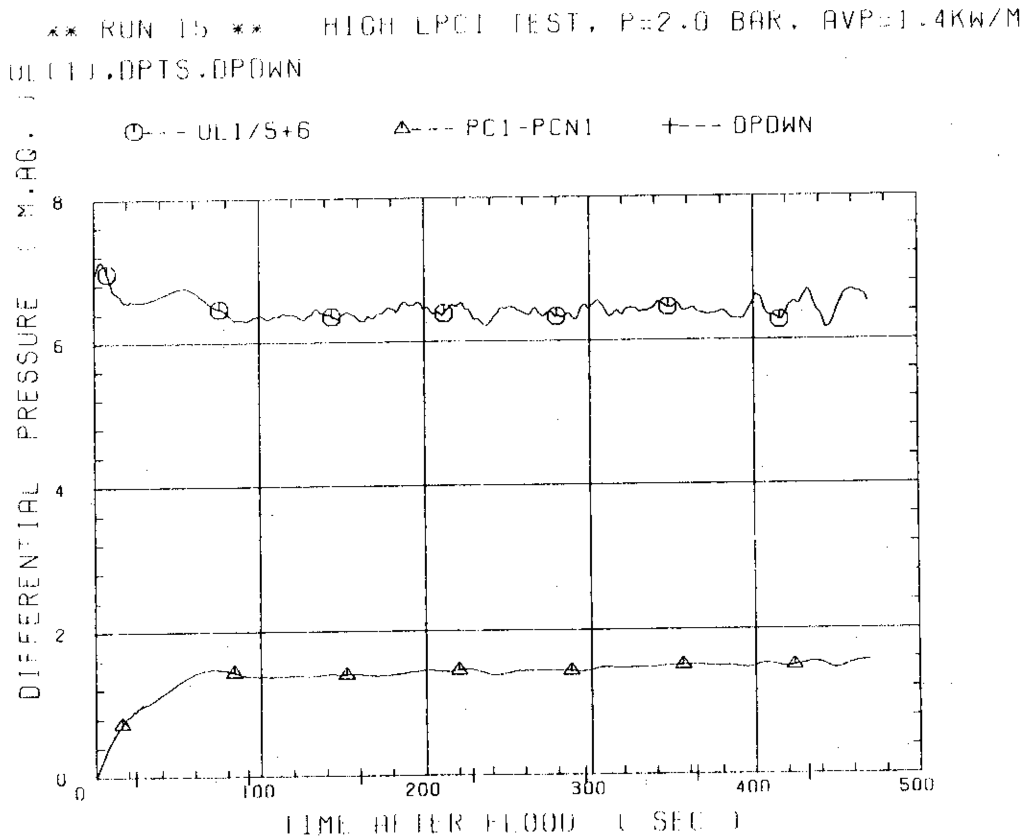

Fig. B.8.6 Core flooding rate (UL1) and core differential pressure (PC1-PCN1)

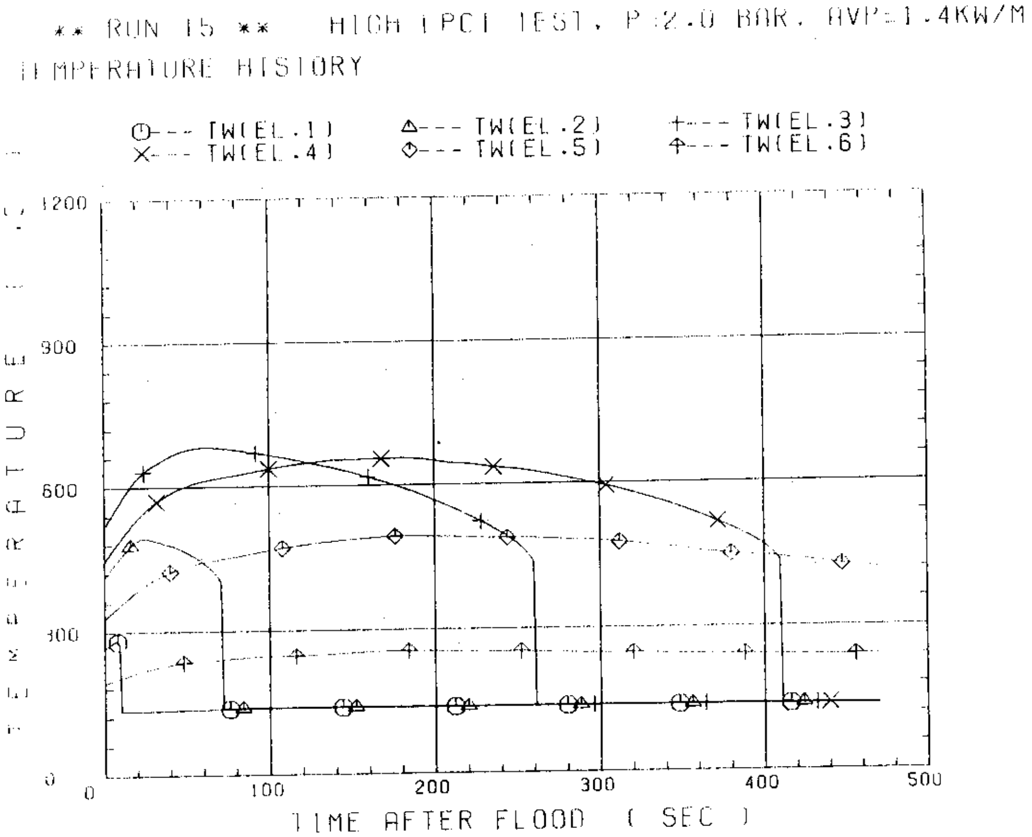

Fig. B.8.7 Rod surface temperatures

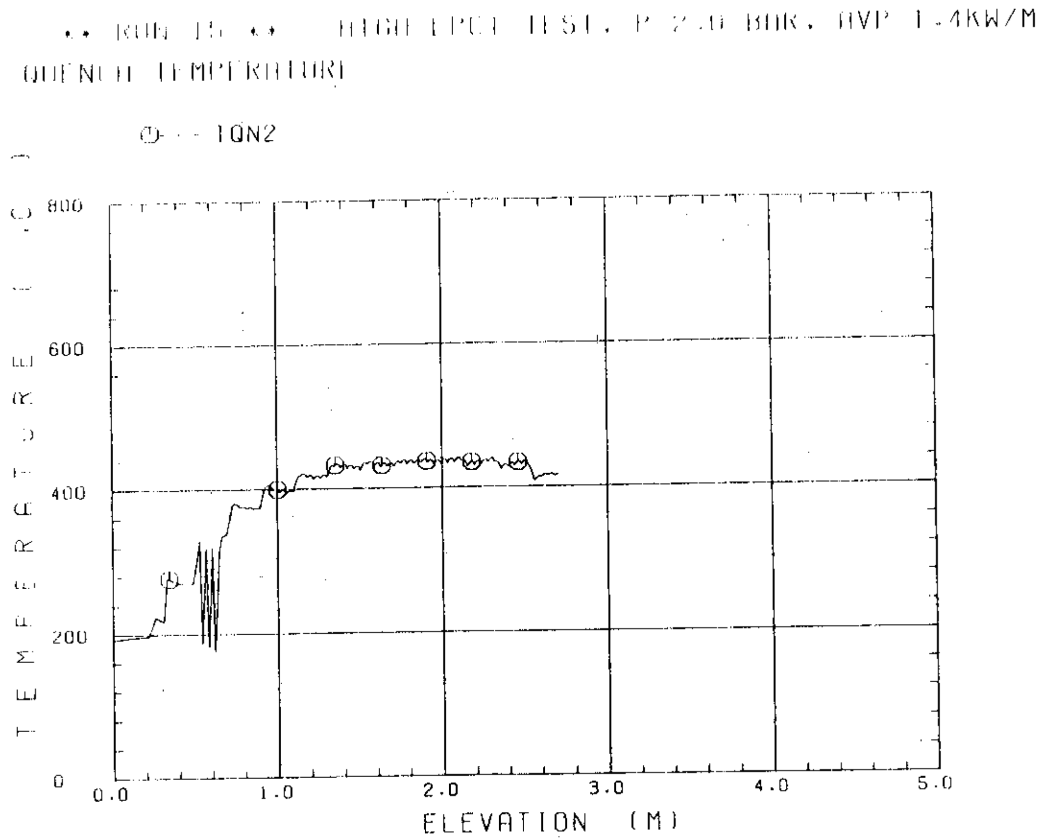

Fig. B.8.8 Quench temperatures

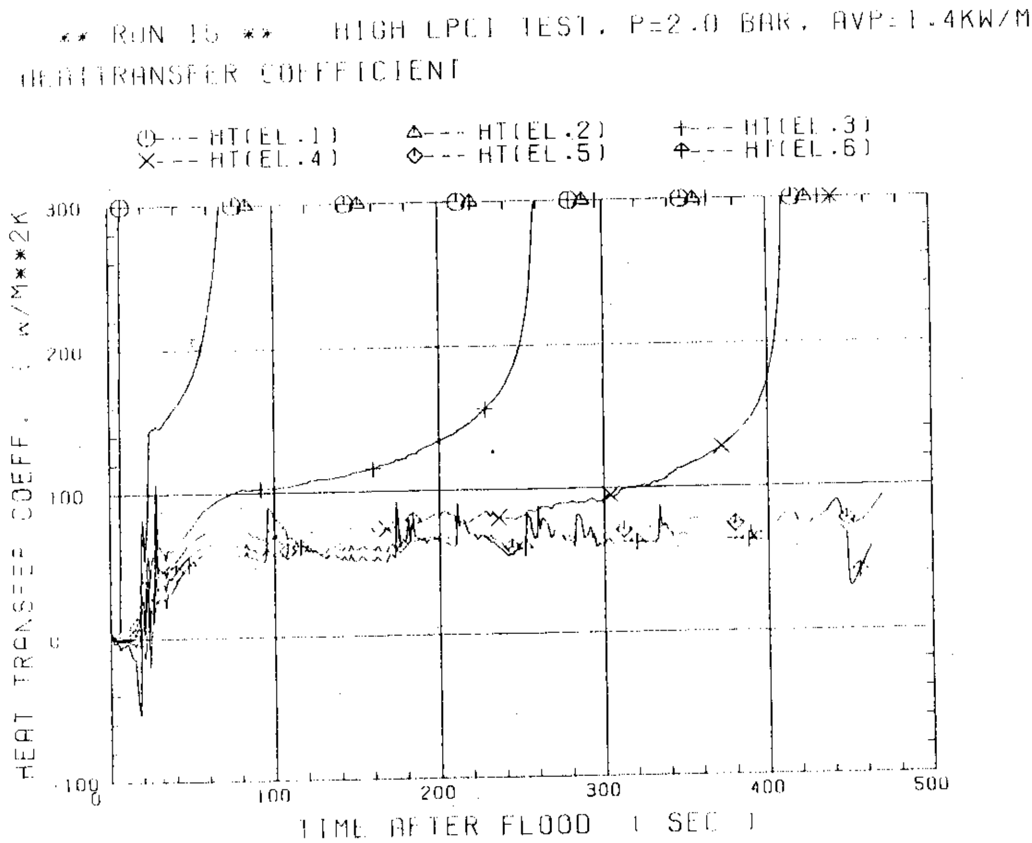

Fig. B.8.9 Heat transfer coefficients

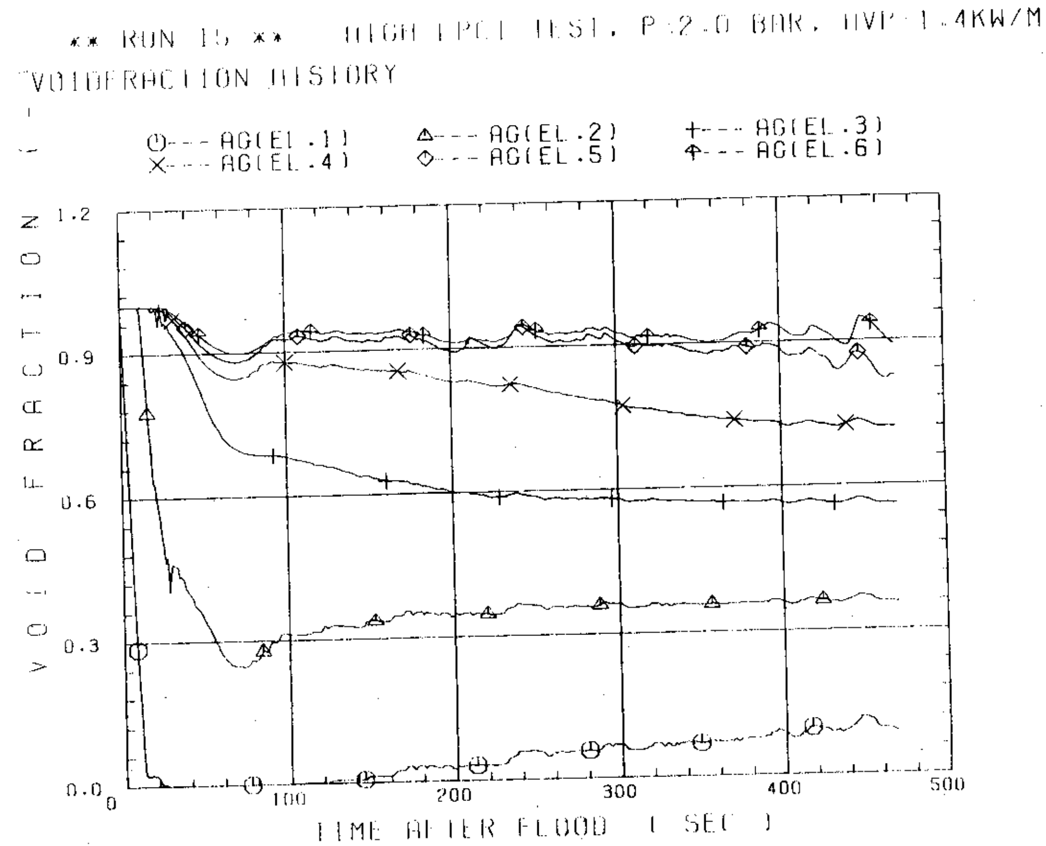

Fig. B.8.10 Void fractions

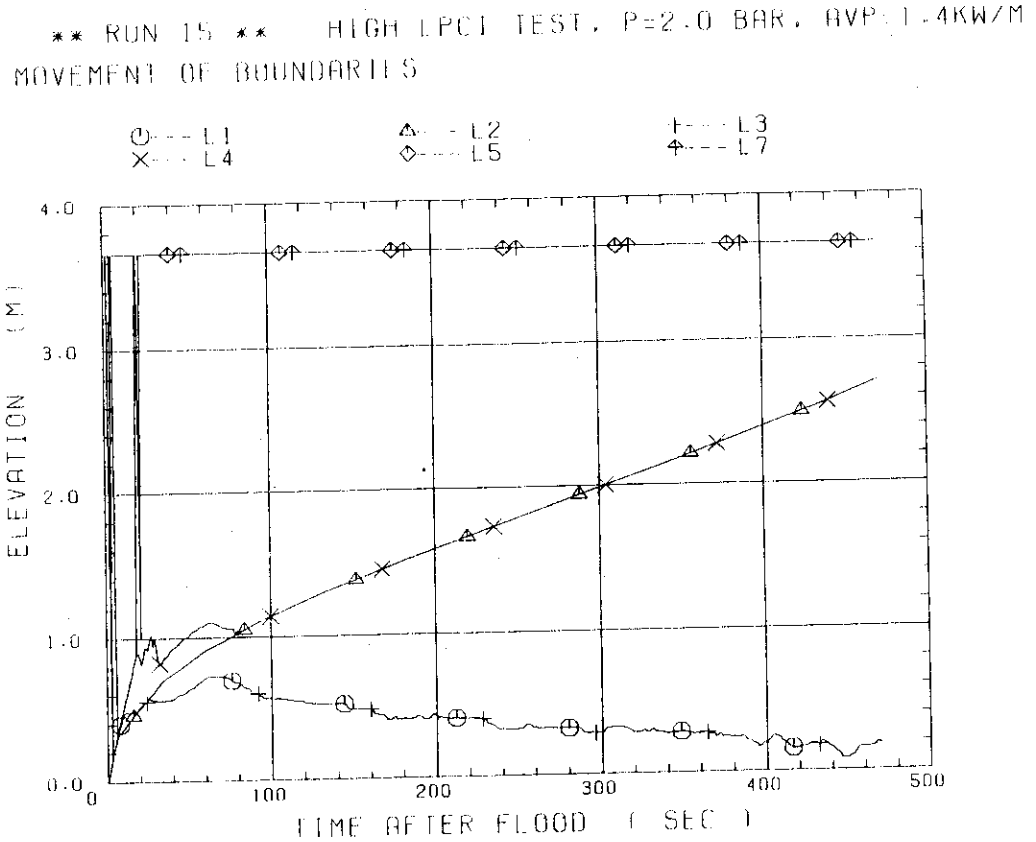

Fig. B.8.11 Movement of flow regime boundaries (L1: Boiling point, L2: Quench front)

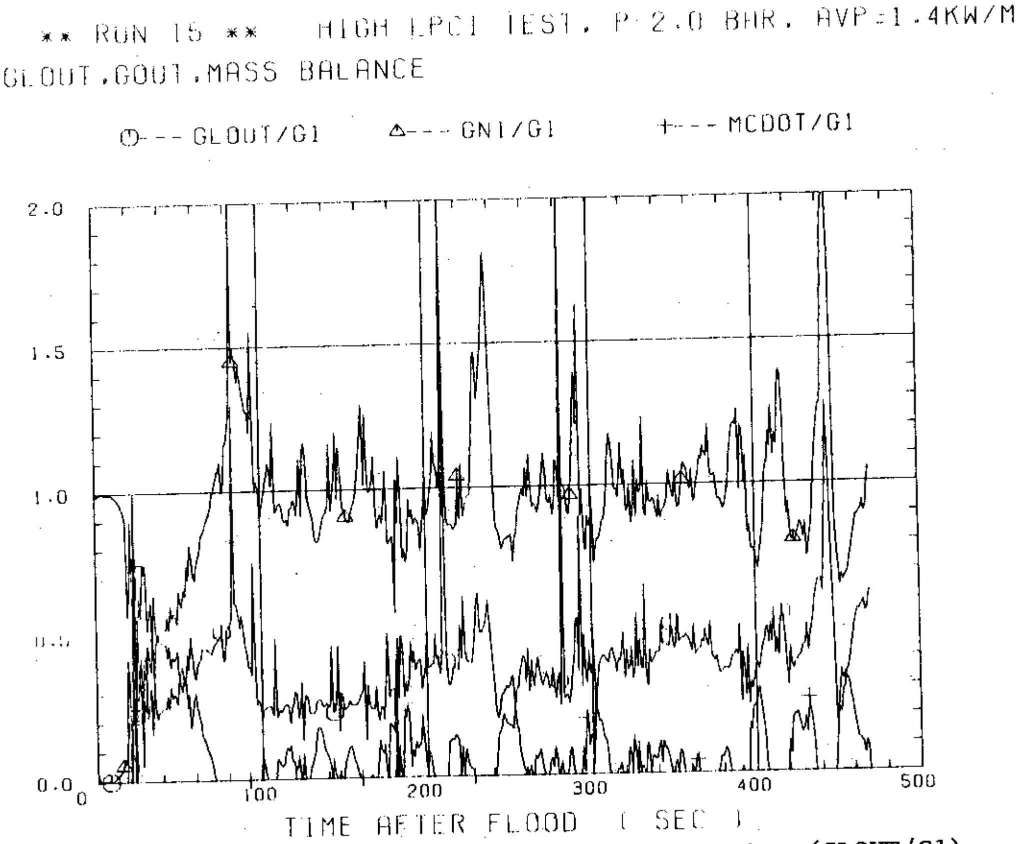

Fig. B.8.12 Liquid carryover rate fraction (GLOUT/G1), carryover rate fraction (GN1/G1) and water accumulation rate fraction (MCDOT/G1)

B.9 Test C1-9 (Low LPCI injection rate)

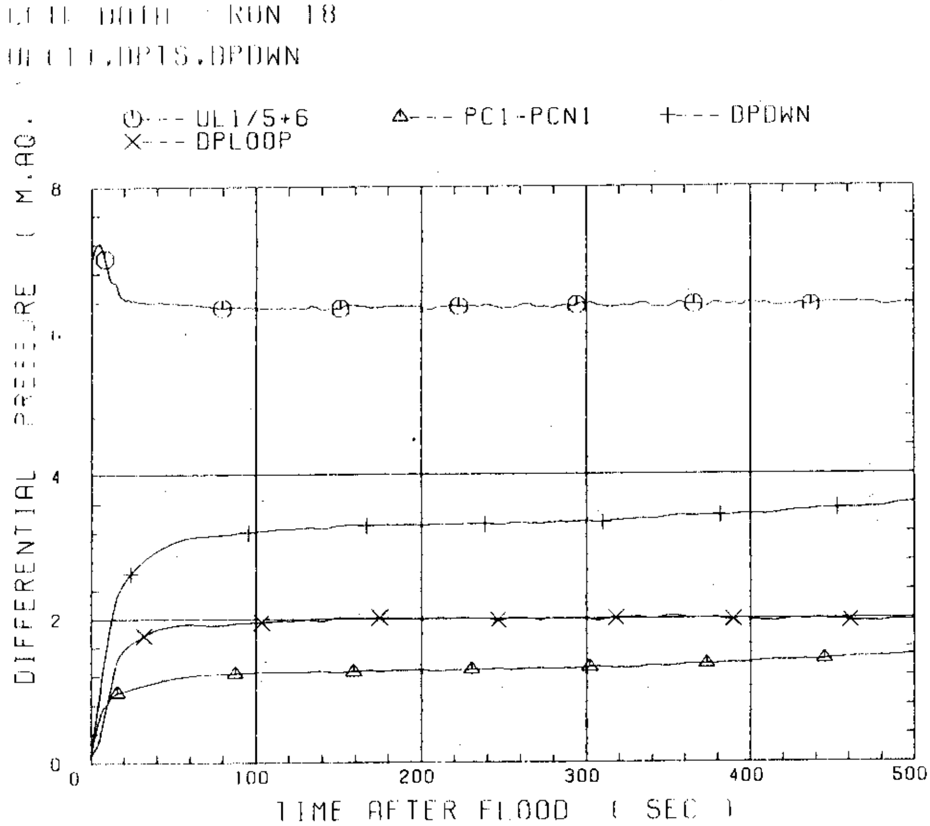

Fig. B.9.1 Core flooding rate (UL1), core differential pressure (PC1-PCN1), downcomer differential pressure (DPDWN) and loop differential pressure (DPLOOP) (Experimental value)

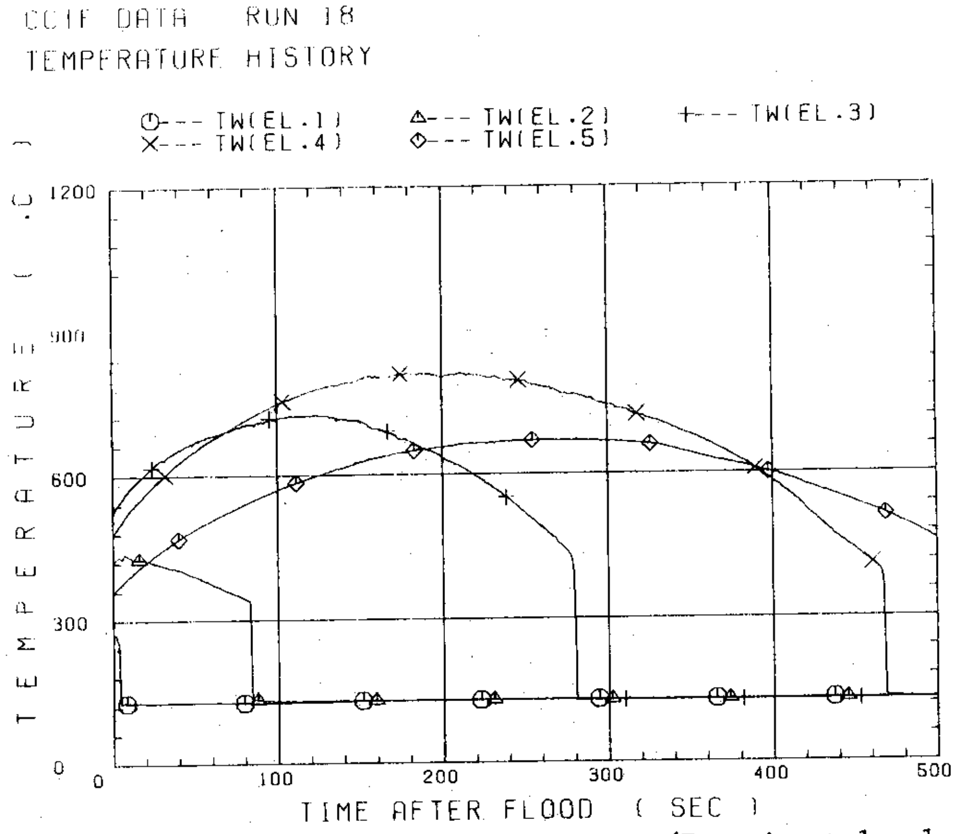

Fig. B.9.2 Rod surface temperatures (Experimental value)

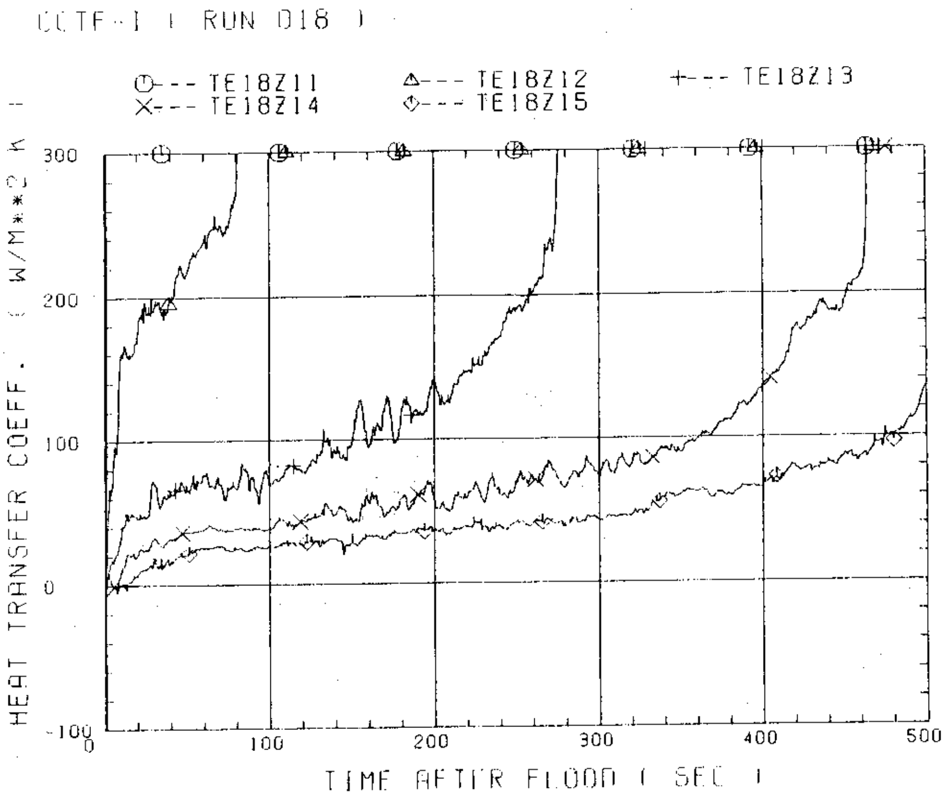

Fig. B.9.3 Heat transfer coefficients (Experimental values)

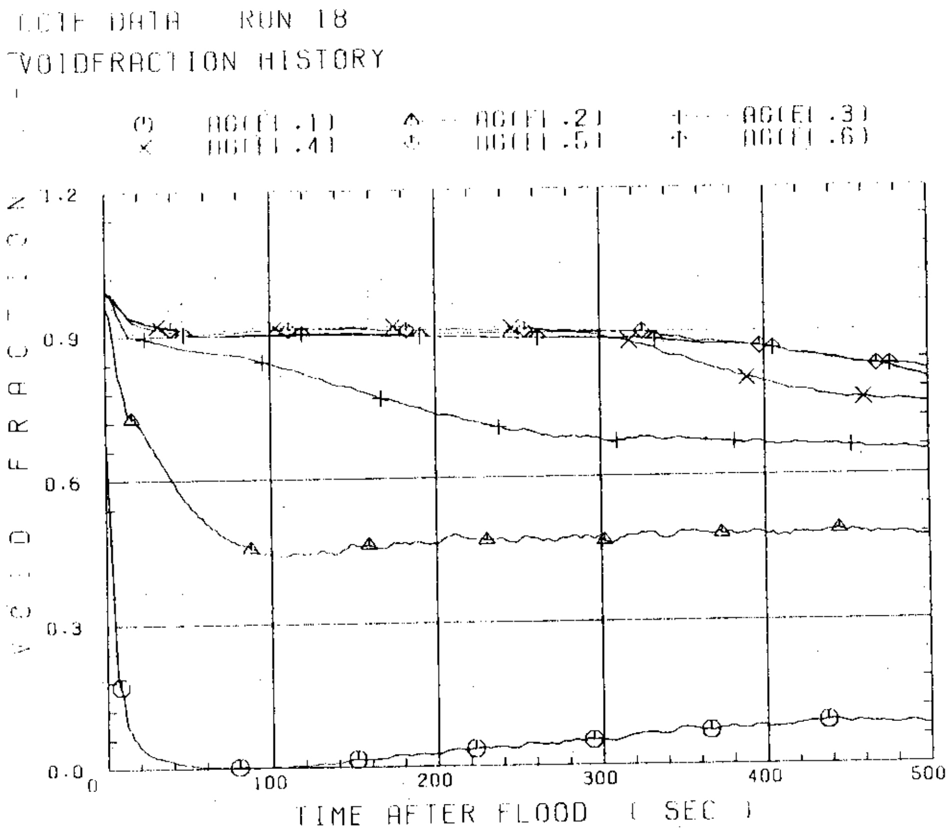

Fig. B.9.4 Void fractions (Experimental values)

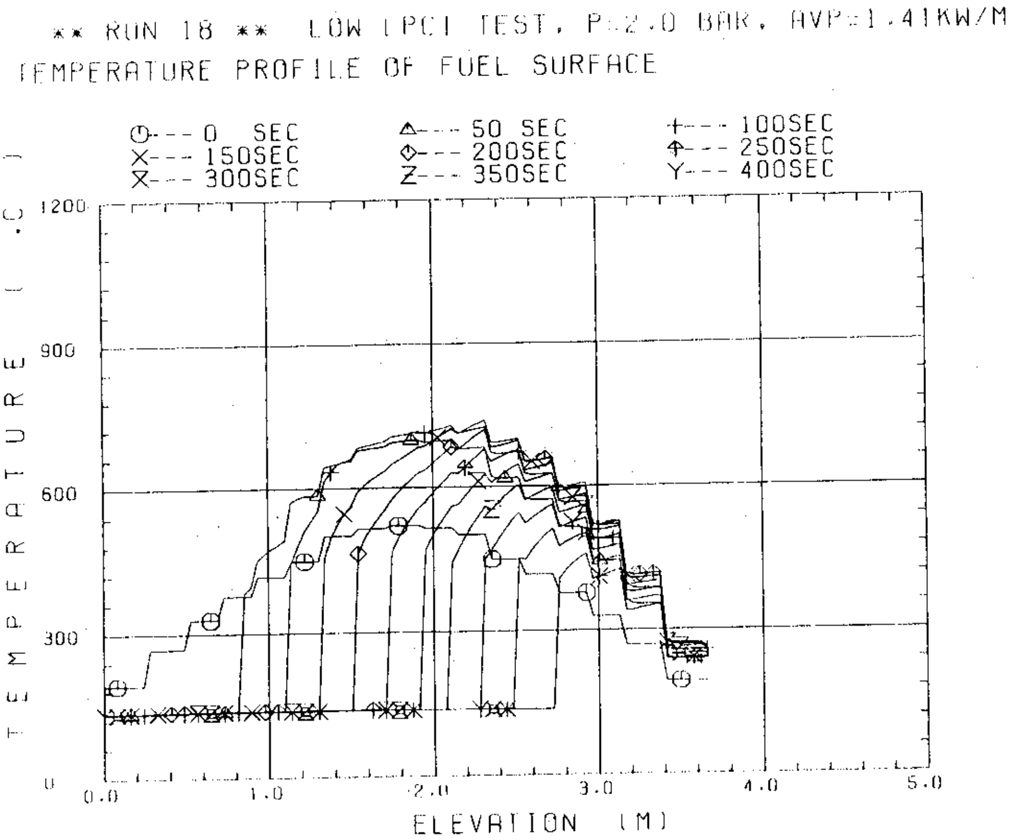

Fig. B.9.5 Rod surface temperature distributions

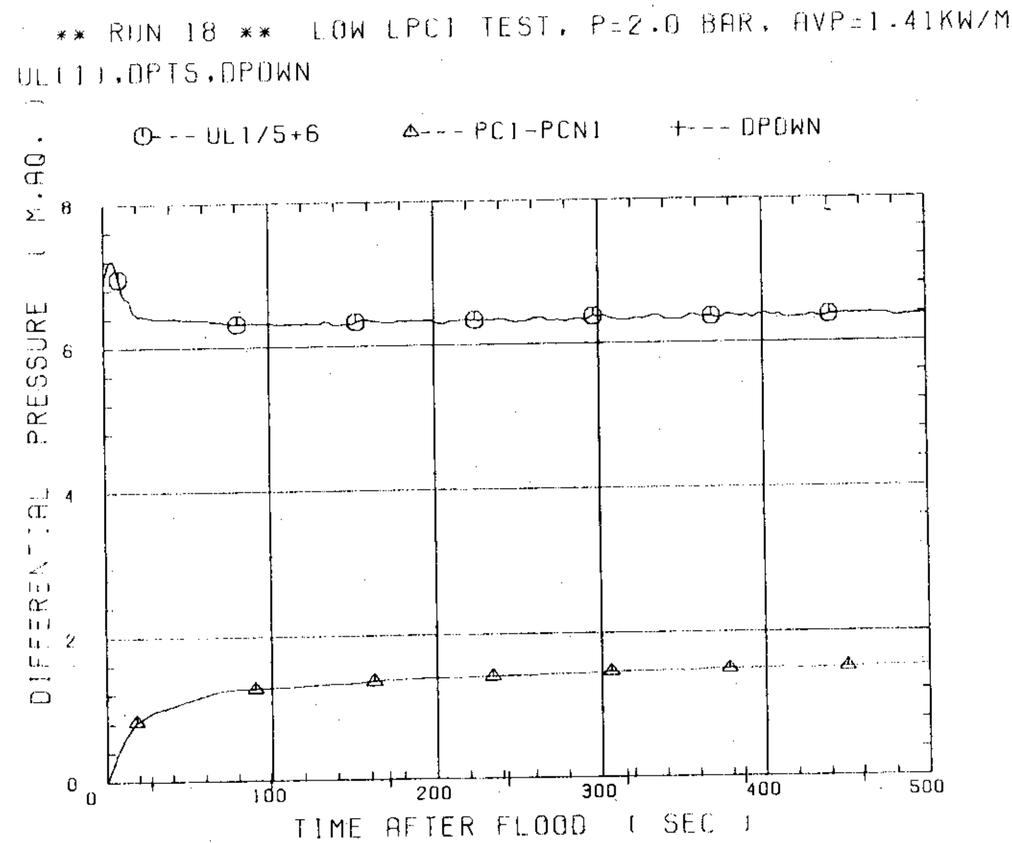

Fig. B.9.6 Core flooding rate (UL1) and core differential pressure (PC1-PCN1)

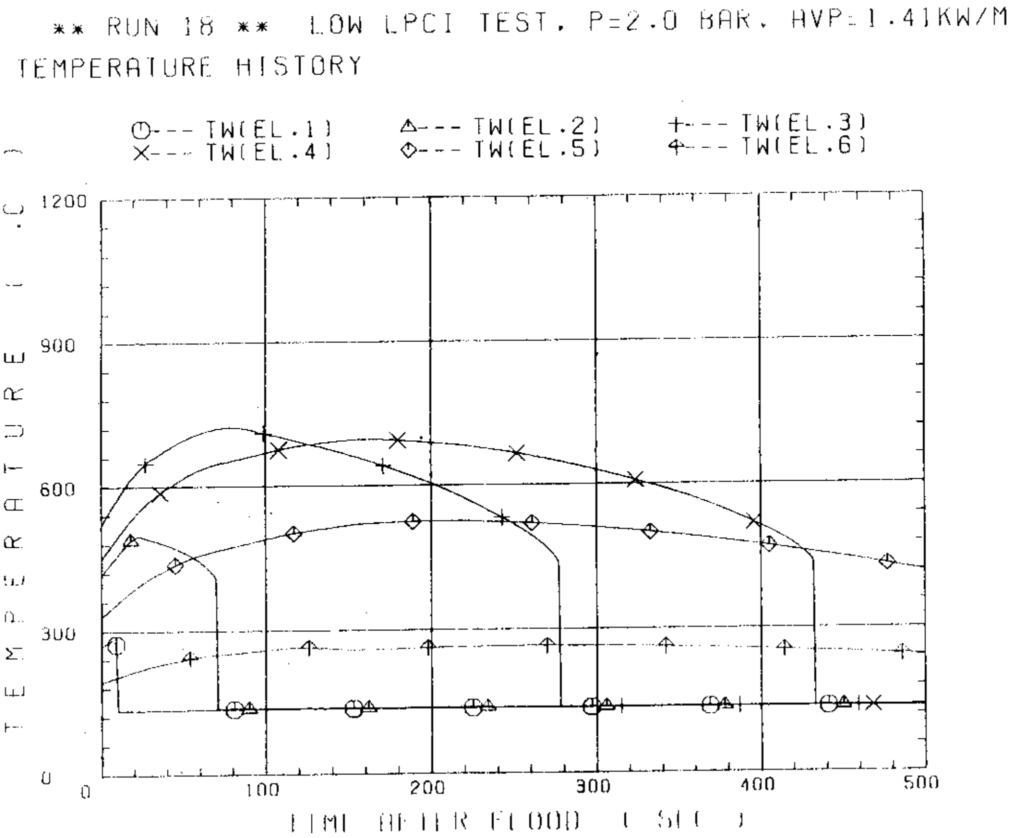

Fig. B.9.7 Rod surface temperatures

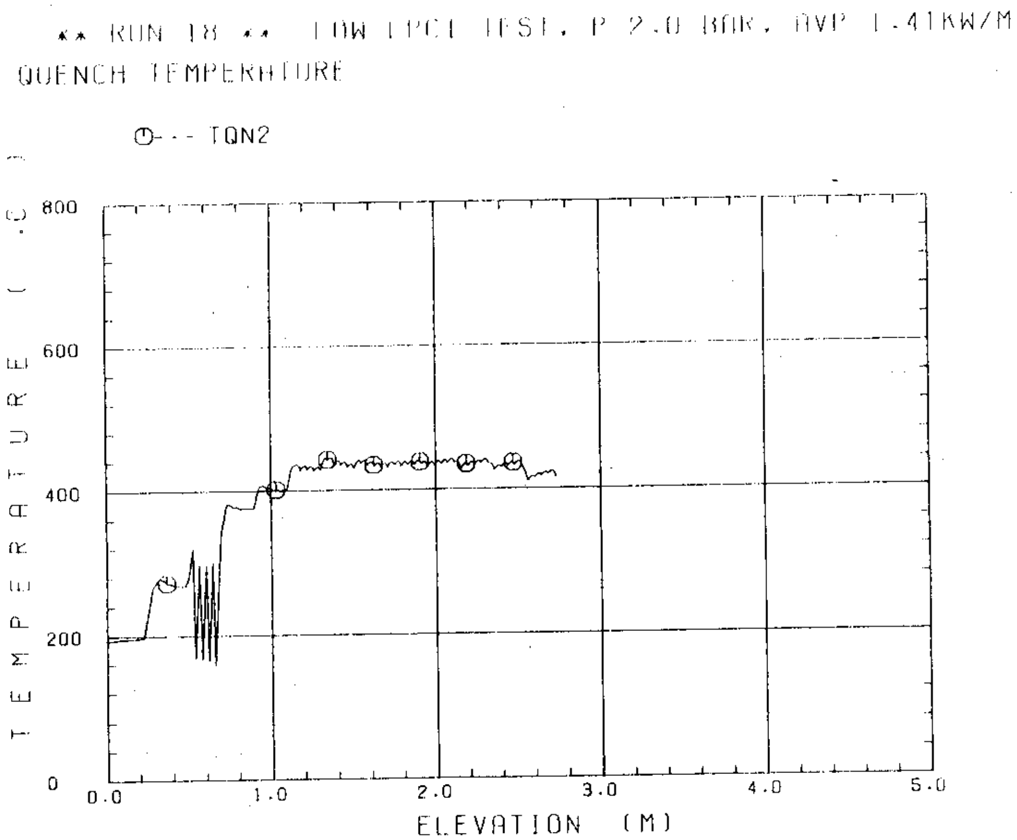

Fig. B.9.8 Quench temperatures

** RUN 18 ** LOW LPCI TEST, P=2.0 BAR, AVP=1.41KW/M
HEATTRANSFER COEFFICIENT

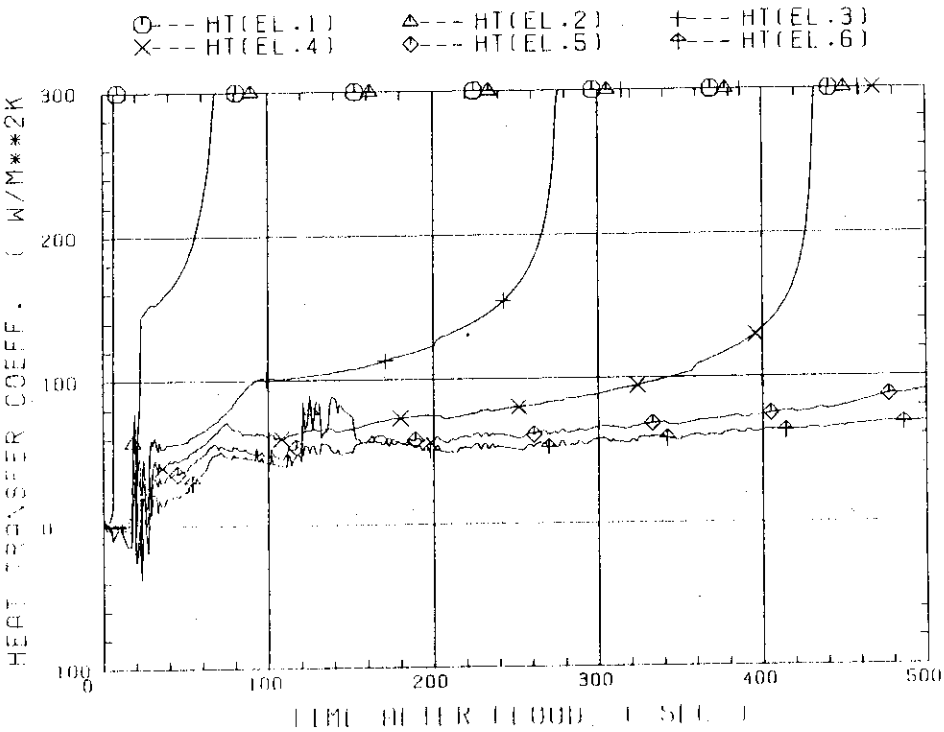

Fig. B.9.9 Heat transfer coefficients

** RUN 18 ** LOW LPCI TEST, P=2.0 BAR, AVP=1.41KW/M
VOIDFRACTION HISTORY

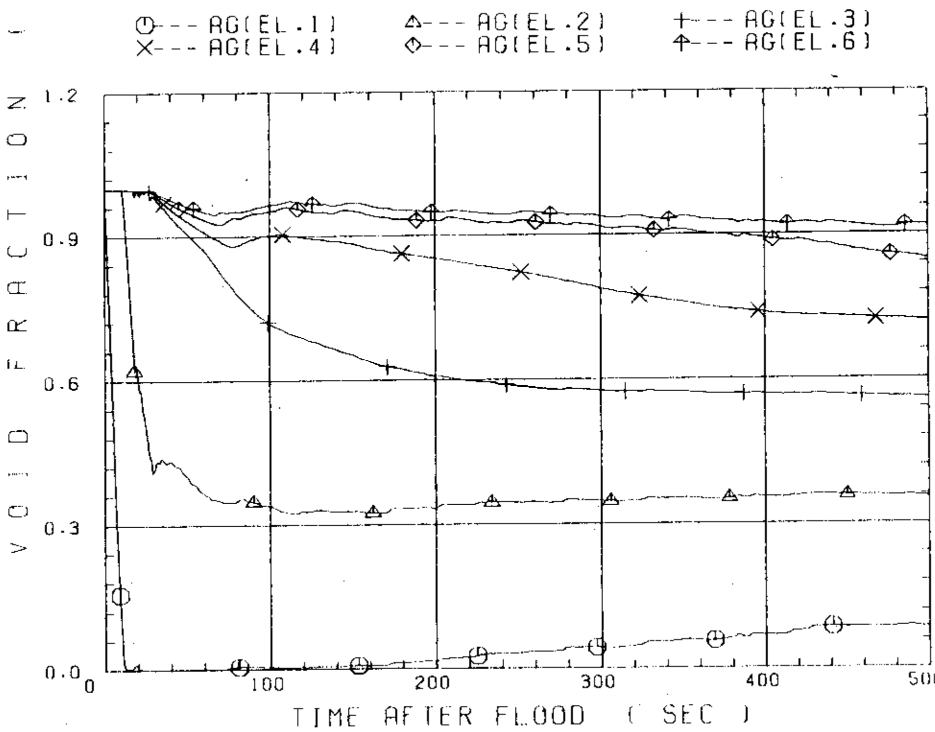

Fig. B.9.10 Void fractions

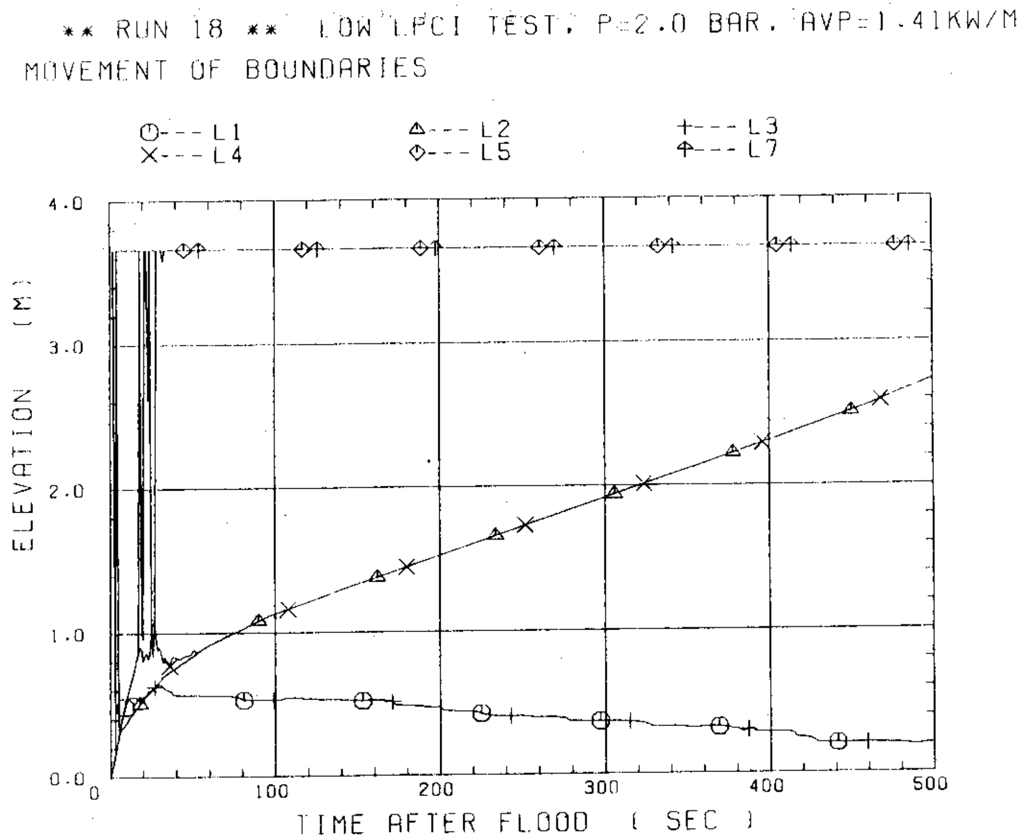

Fig. B.9.11 Movement of flow regime boundaries (L1: Boiling point, L2: Quench front)

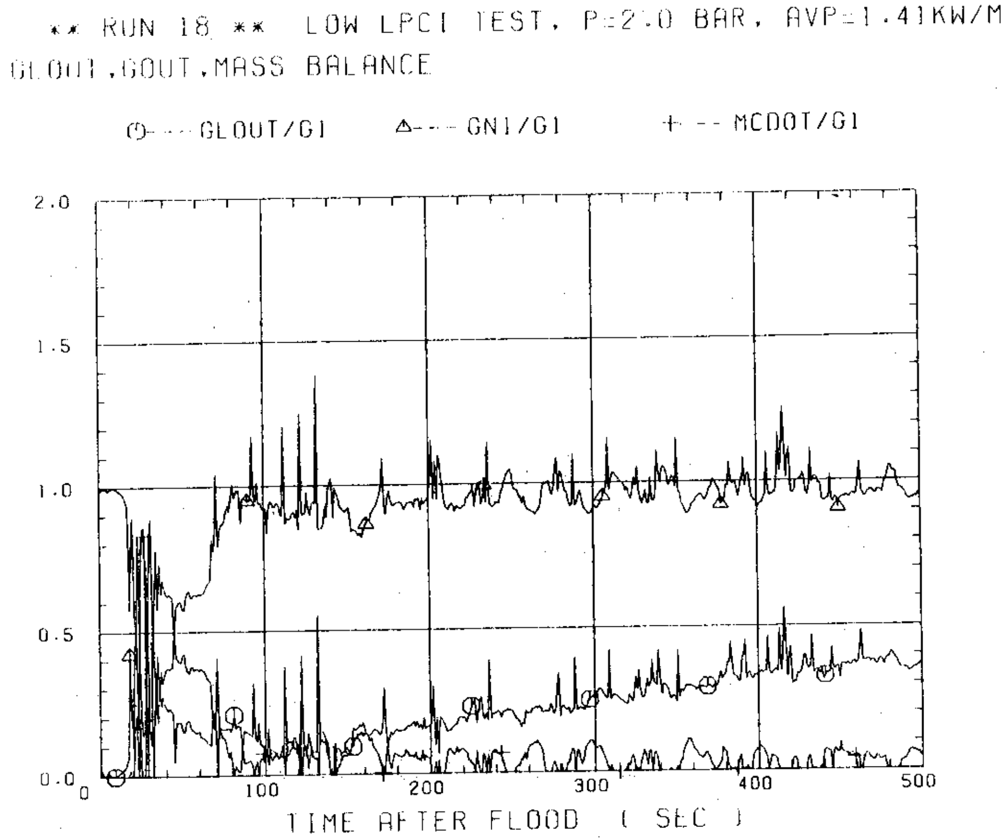

Fig. B.9.12 Liquid carryover rate fraction (GLOUT/G1), carryover rate fraction (GN1/G1) and water accumulation rate fraction (MCDOT/G1)

B.10 Test C1-2 (Superheated initial downcomer temperature)

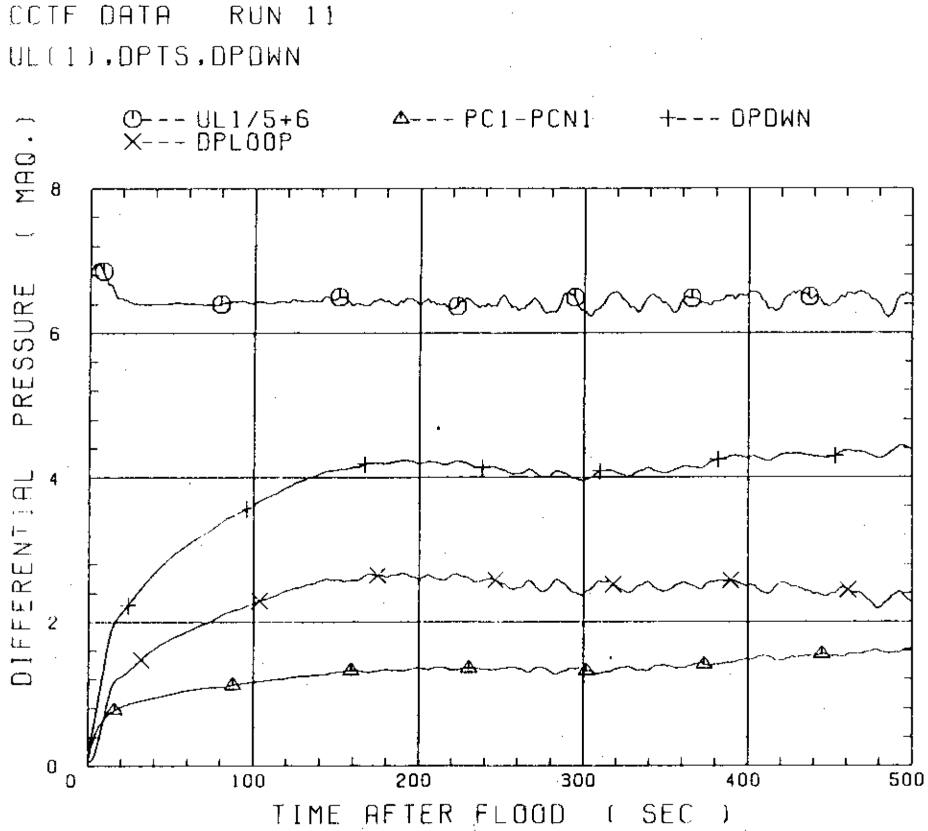

Fig. B.10.1 Core flooding rate (UL1), core differential pressure (PC1-PCN1), downcomer differential pressure (DPDWN) and loop differential pressure (DPLOOP) (Experimental value)

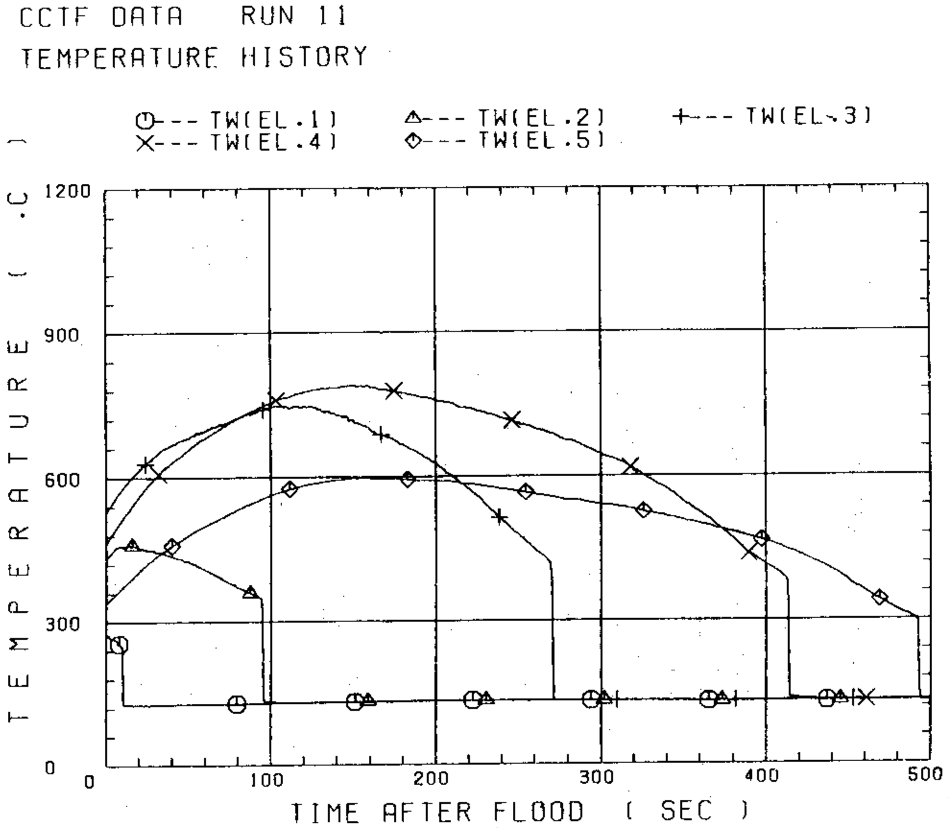

Fig. B.10.2 Rod surface temperatures (Experimental value)

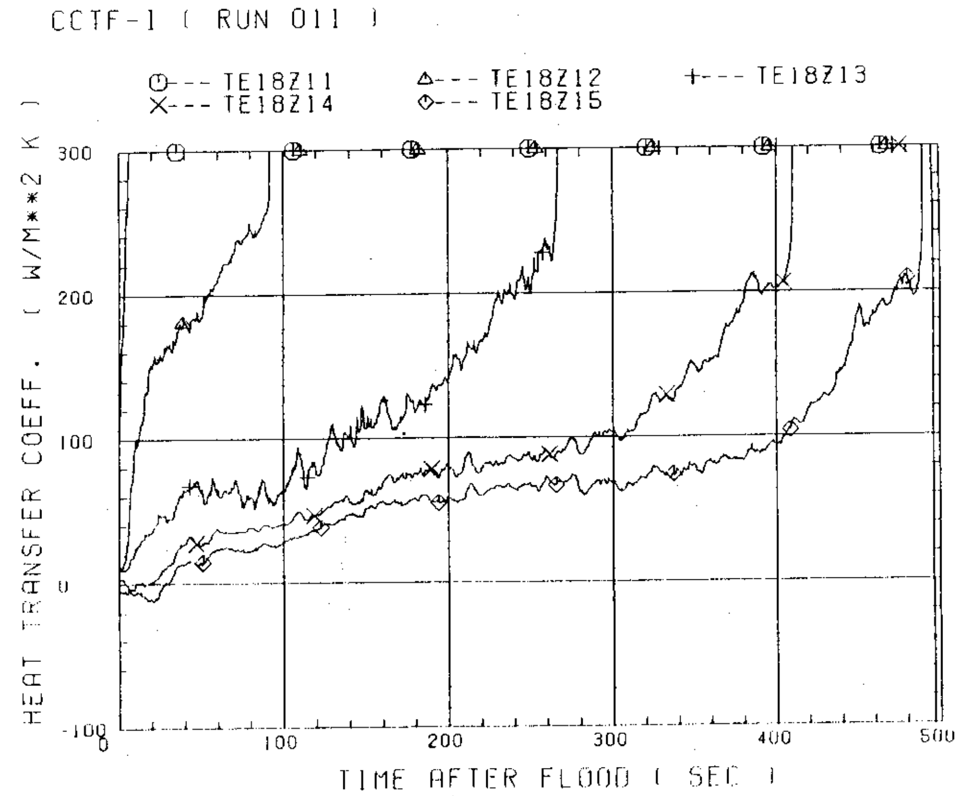

Fig. B.10.3 Heat transfer coefficients (Experimental values)

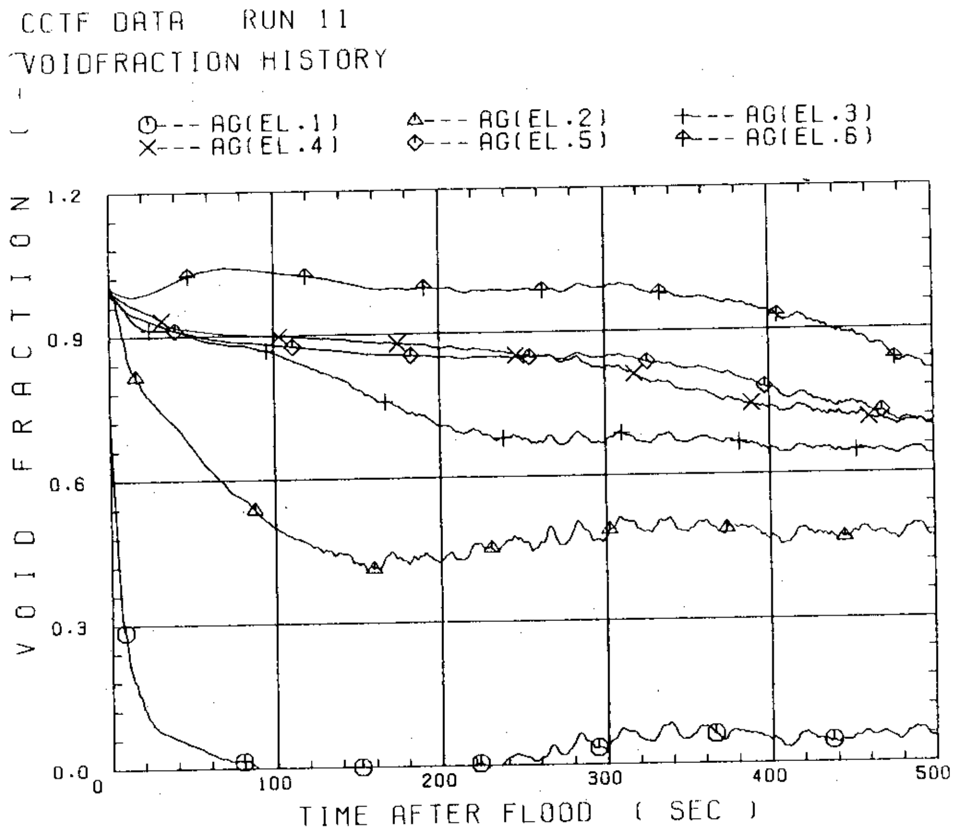

Fig. B.10.4 Void fractions (Experimental values)

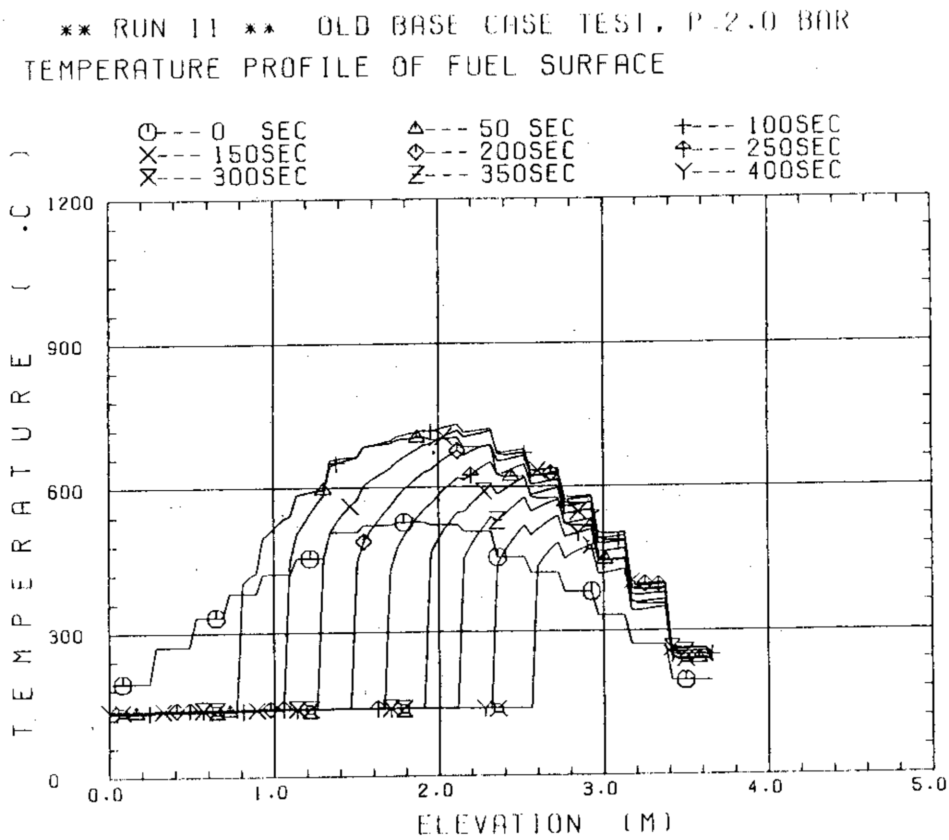

Fig. B.10.5 Rod surface temperature distributions

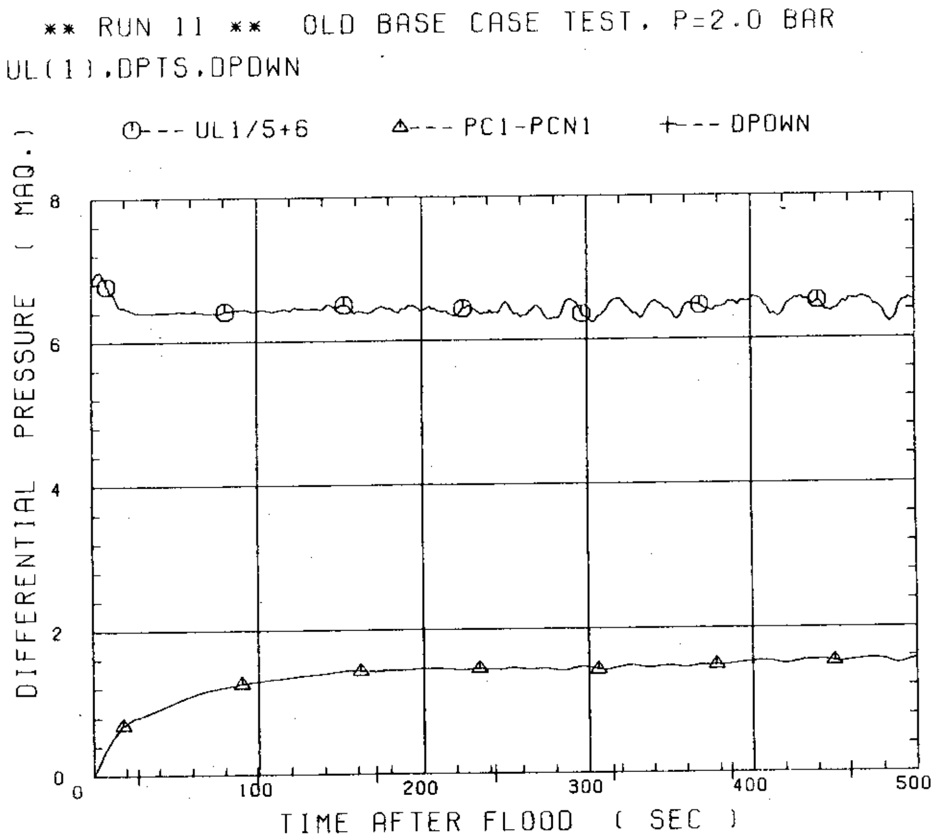

Fig. B.10.6 Core flooding rate (UL1) and core differential pressure (PC1-PCN1)

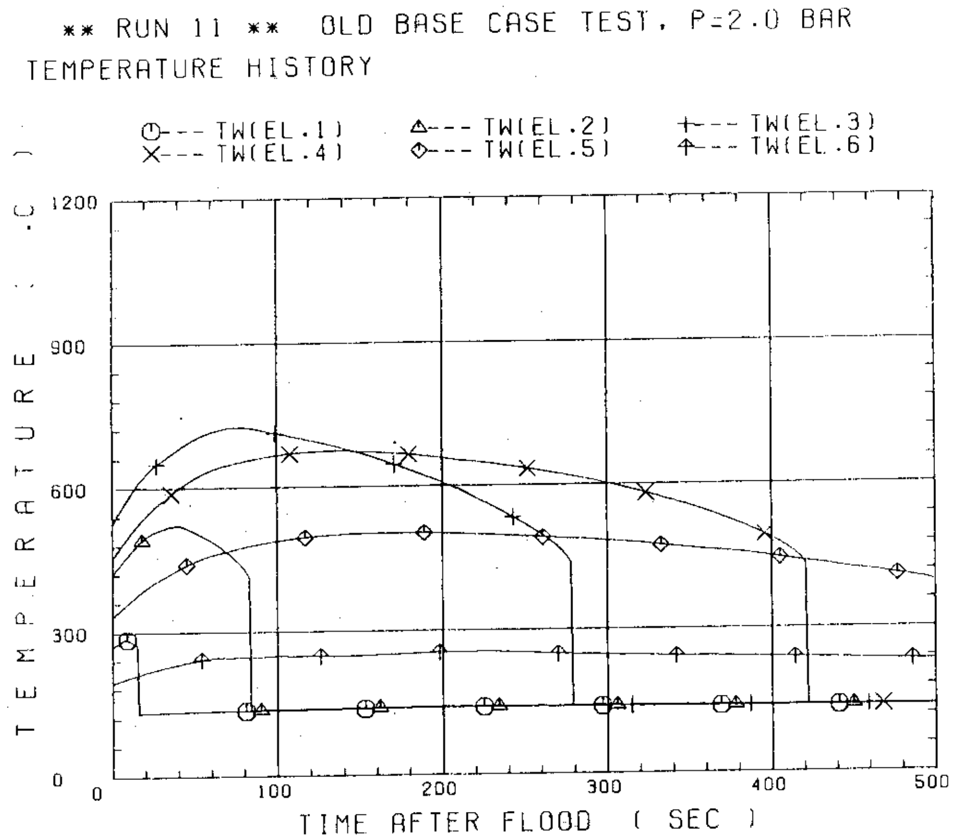

Fig. B.10.7 Rod surface temperatures

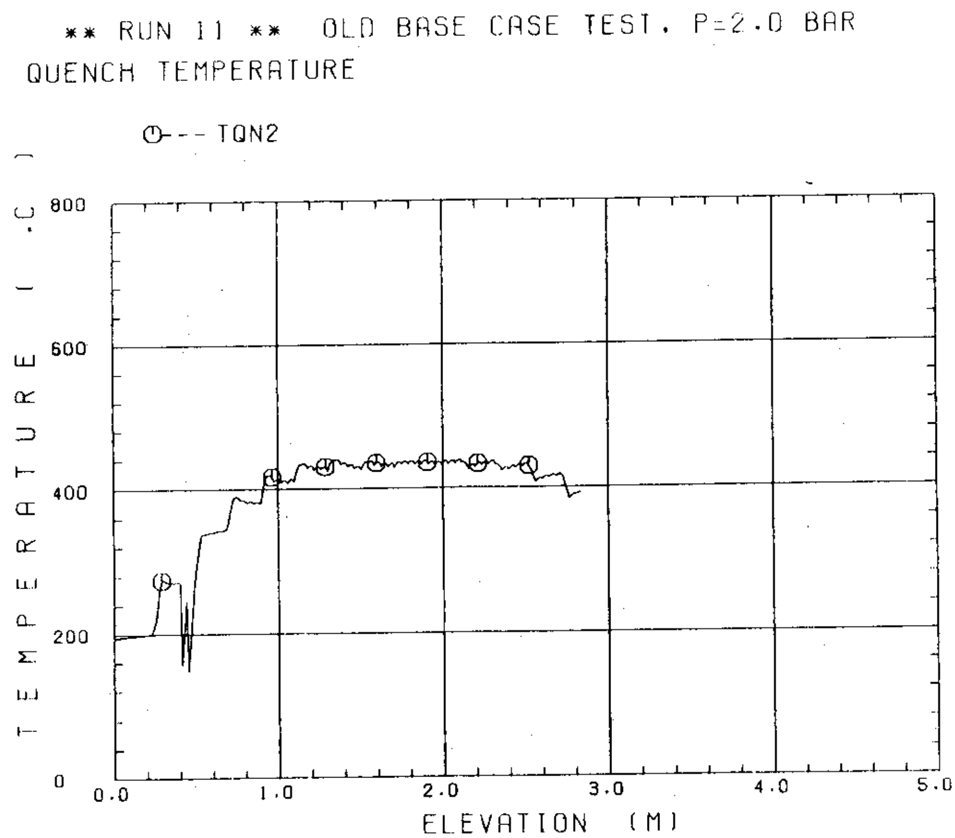

Fig. B.10.8 Quench temperatures

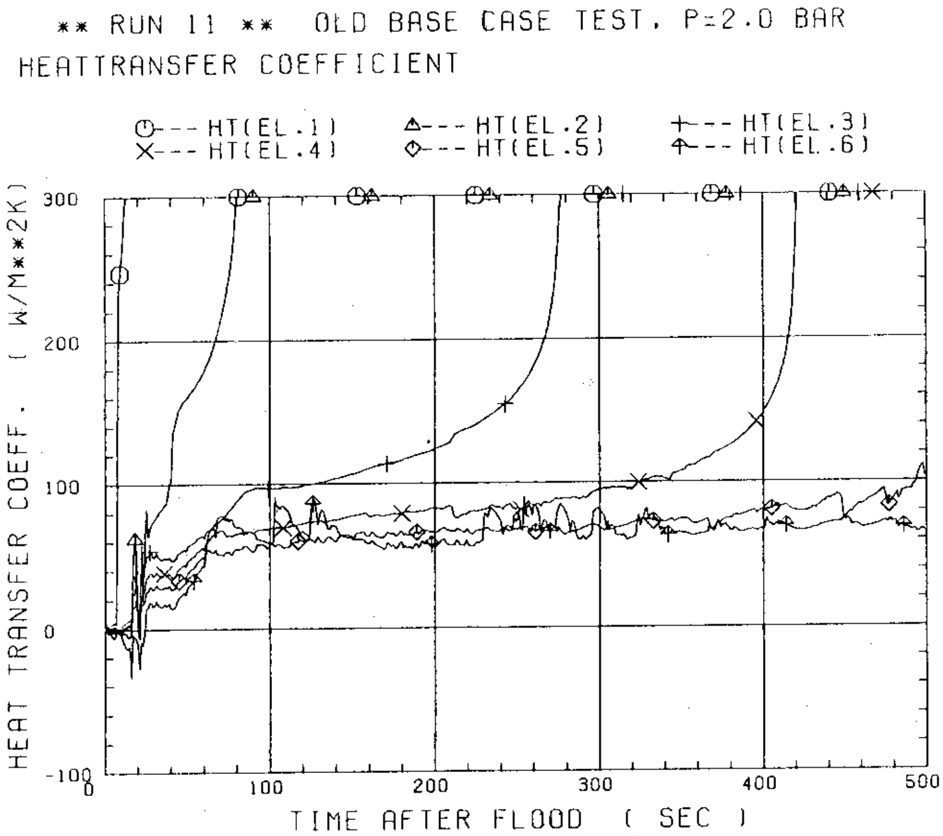

Fig. B.10.9 Heat transfer coefficients

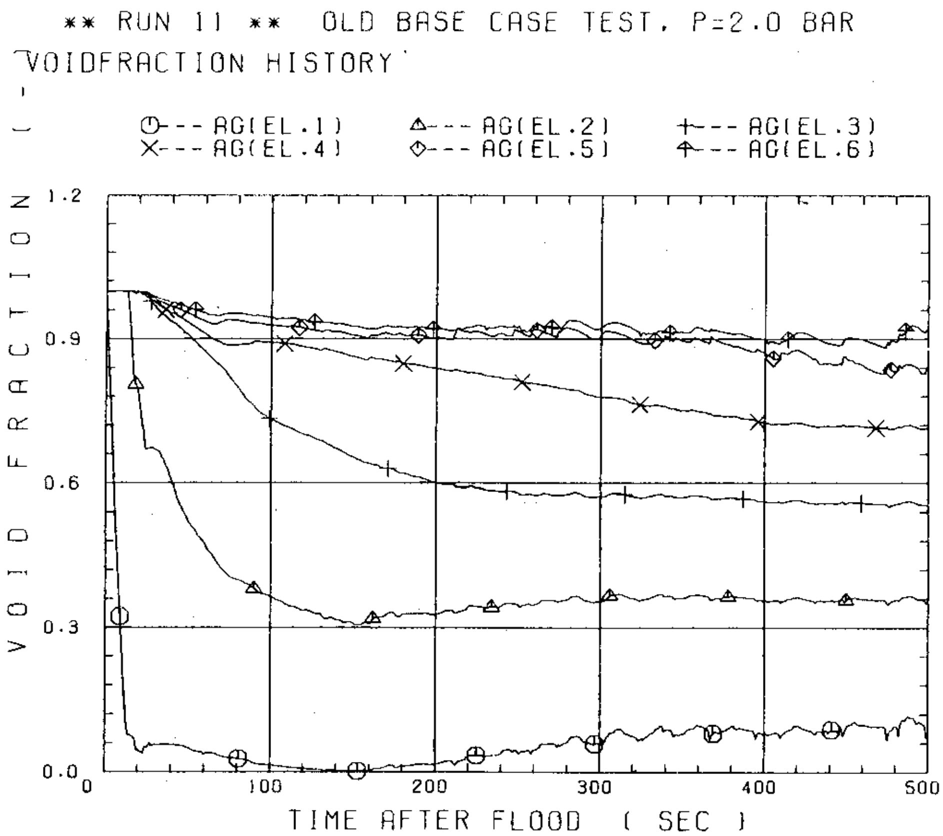

Fig. B.10.10 Void fractions

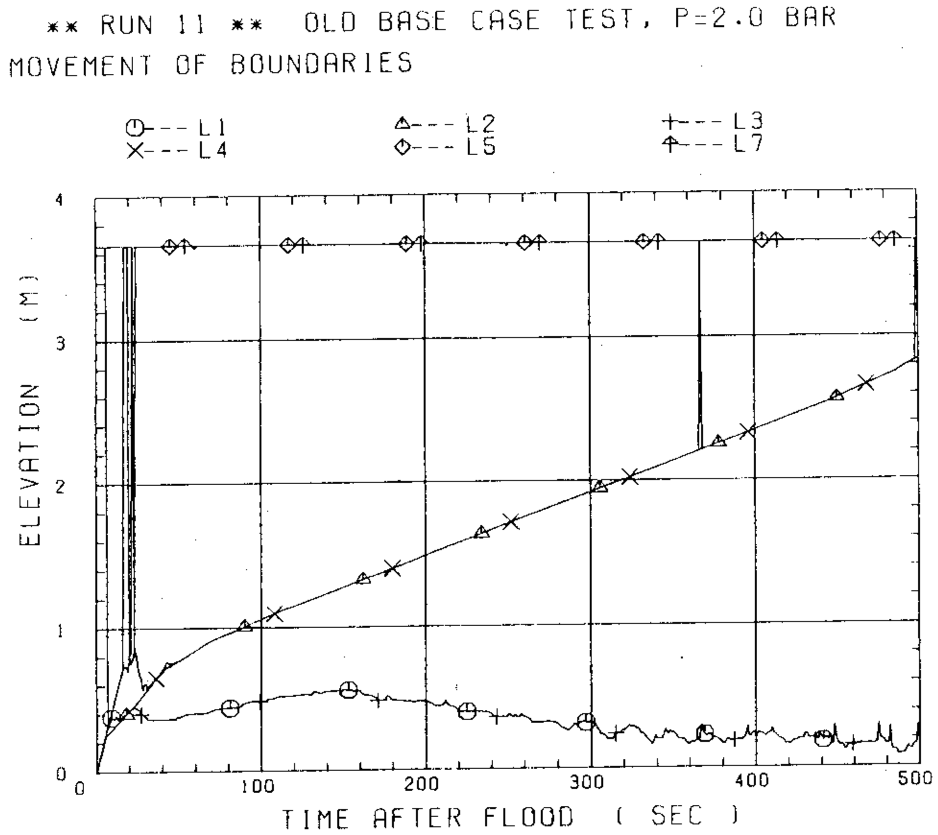

Fig. B.10.11 Movement of flow regime boundaries (L1: Boiling point, L2: Quench front)

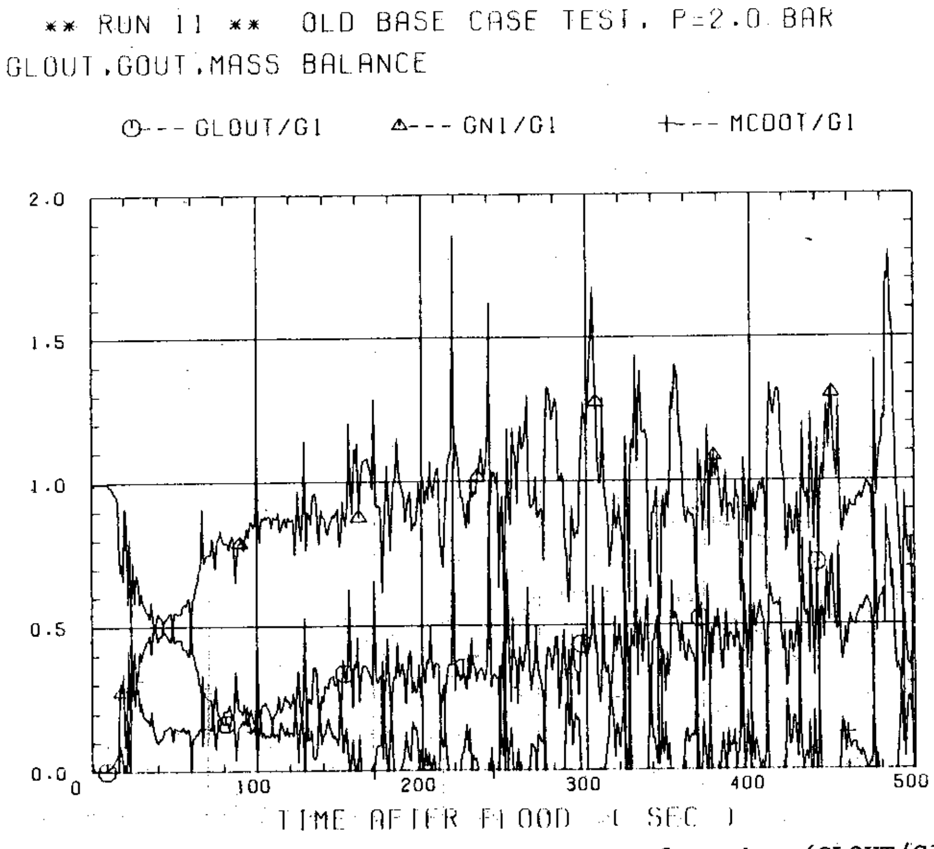

Fig. B.10.12 Liquid carryover rate fraction (GLOUT/G1), carryover rate fraction (GN1/G1) and water accumulation rate fraction (MCDOT/G1)

B.11 Test C1-3 (Saturated initial downcomer temperature)

CCTF DATA RUN 12

UL(1),DPTS,DPDWN

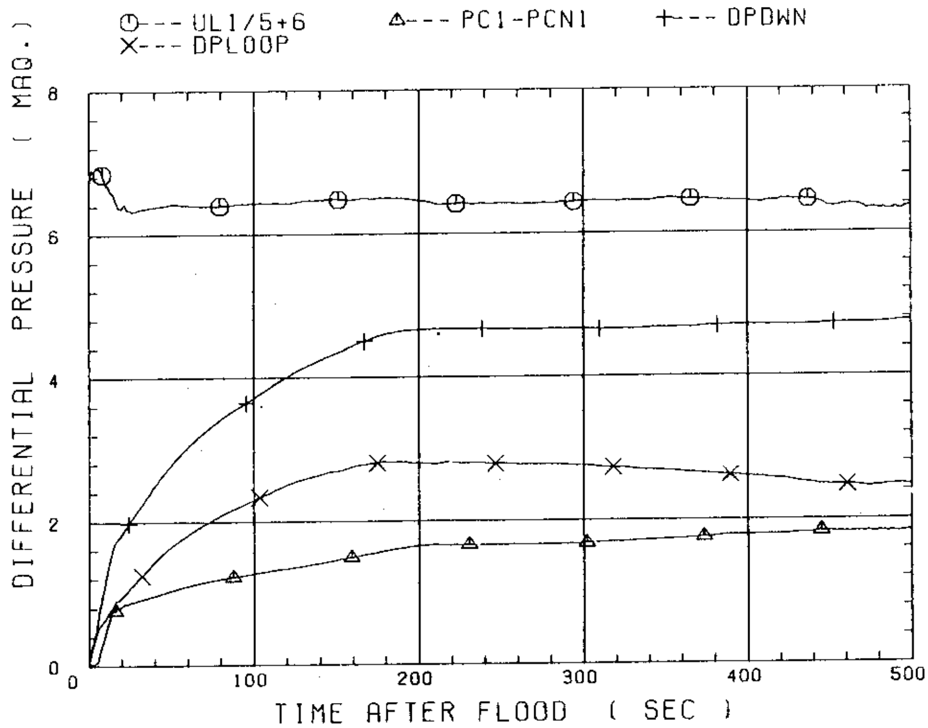

Fig. B.11.1 Core flooding rate (UL1), core differential pressure (PC1-PCN1), downcomer differential pressure (DPDWN) and loop differential pressure (DPLOOP) (Experimental value)

CCTF DATA RUN 12

TEMPERATURE HISTORY

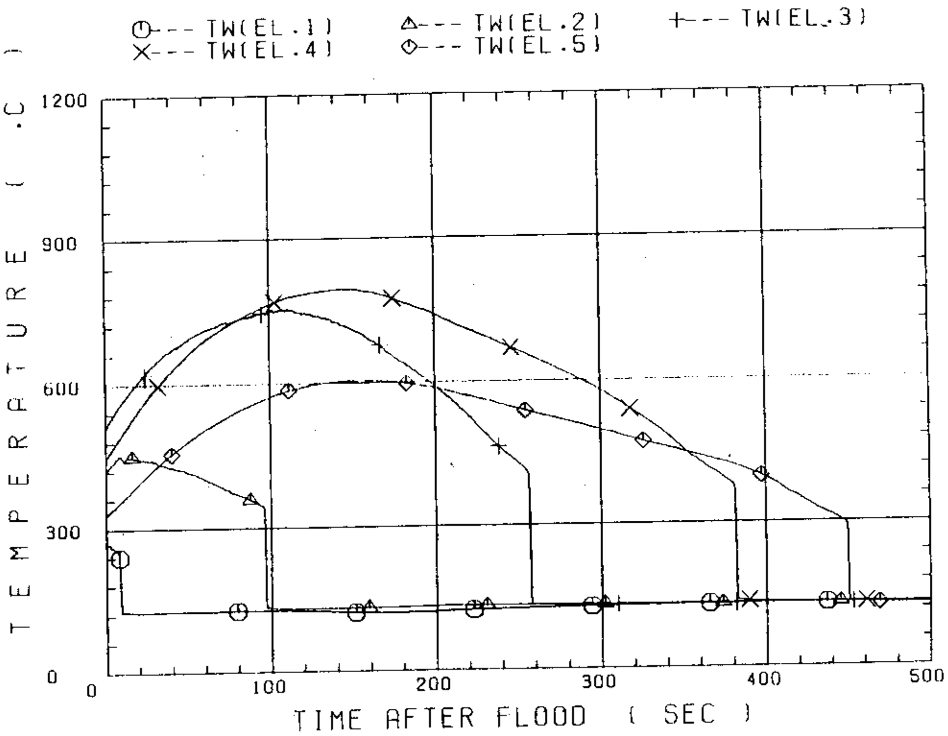

Fig. B.11.2 Rod surface temperatures (Experimental value)

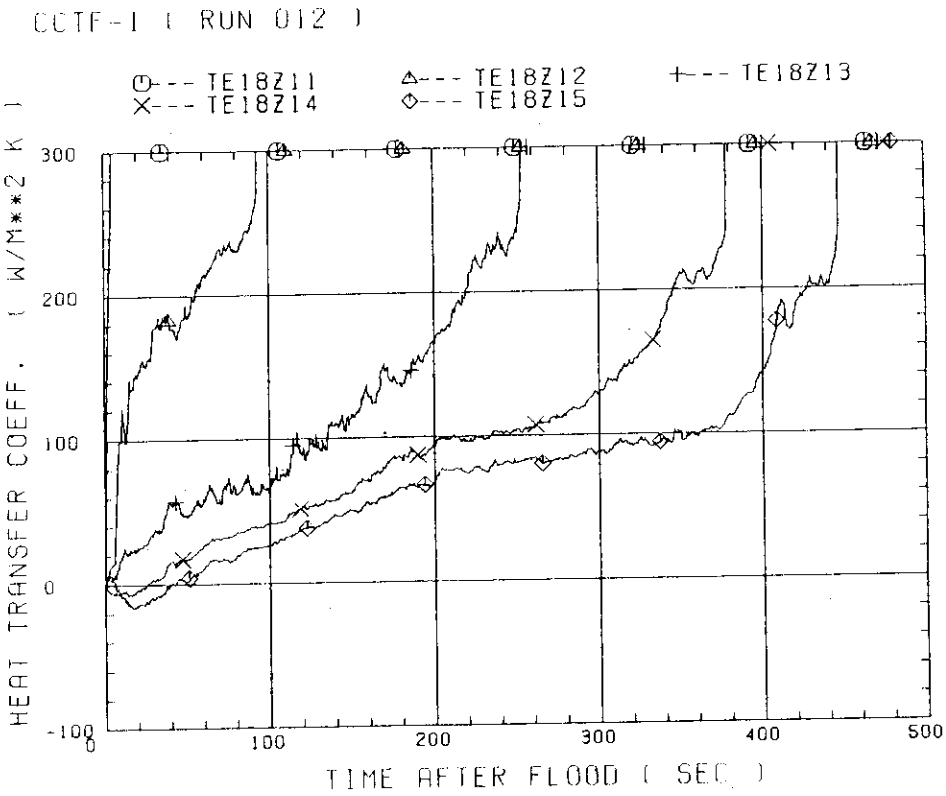

Fig. B.11.3 Heat transfer coefficients (Experimental values)

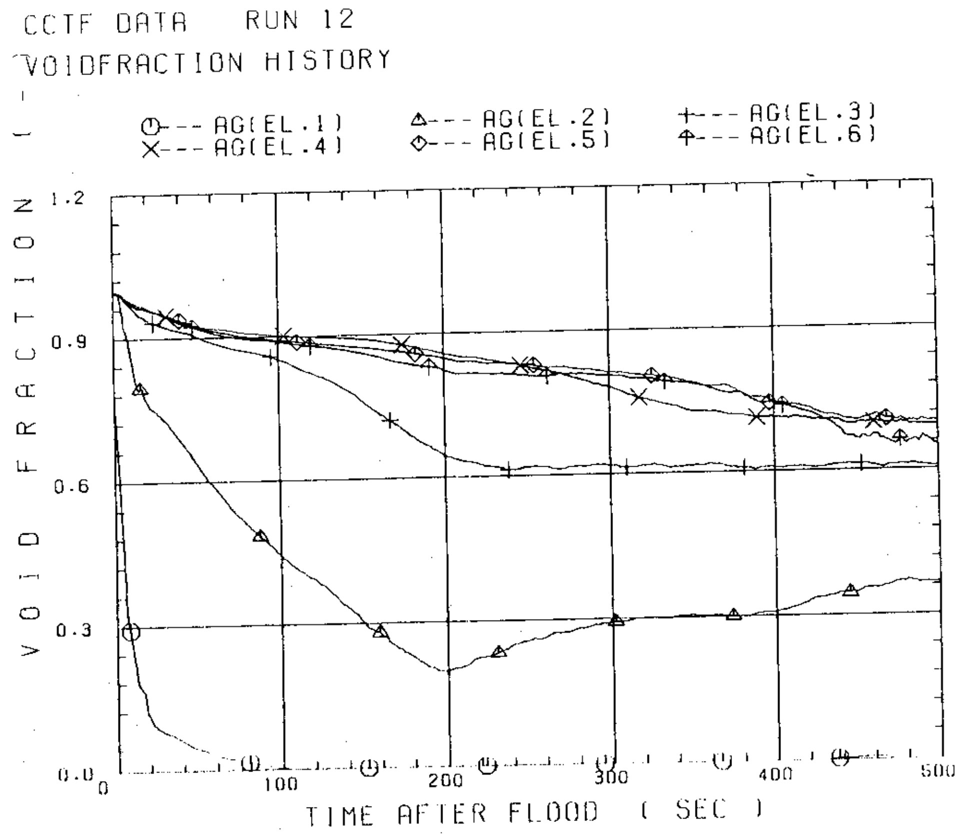

Fig. B.11.4 Void fractions (Experimental values)

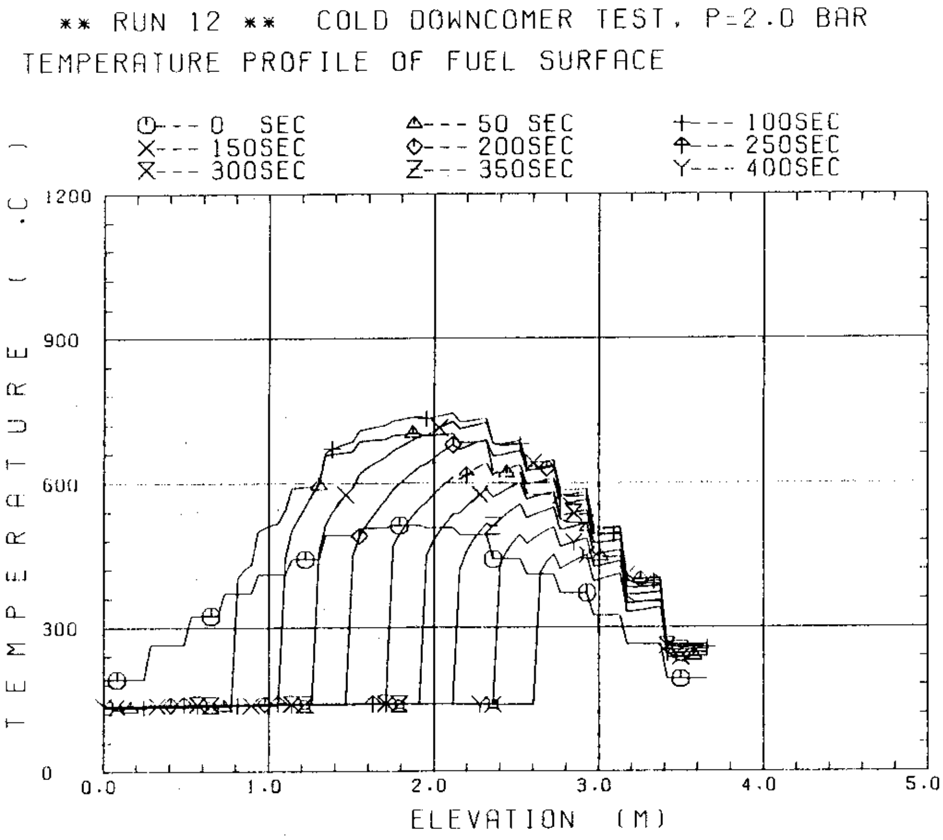

Fig. B.11.5 Rod surface temperature distributions

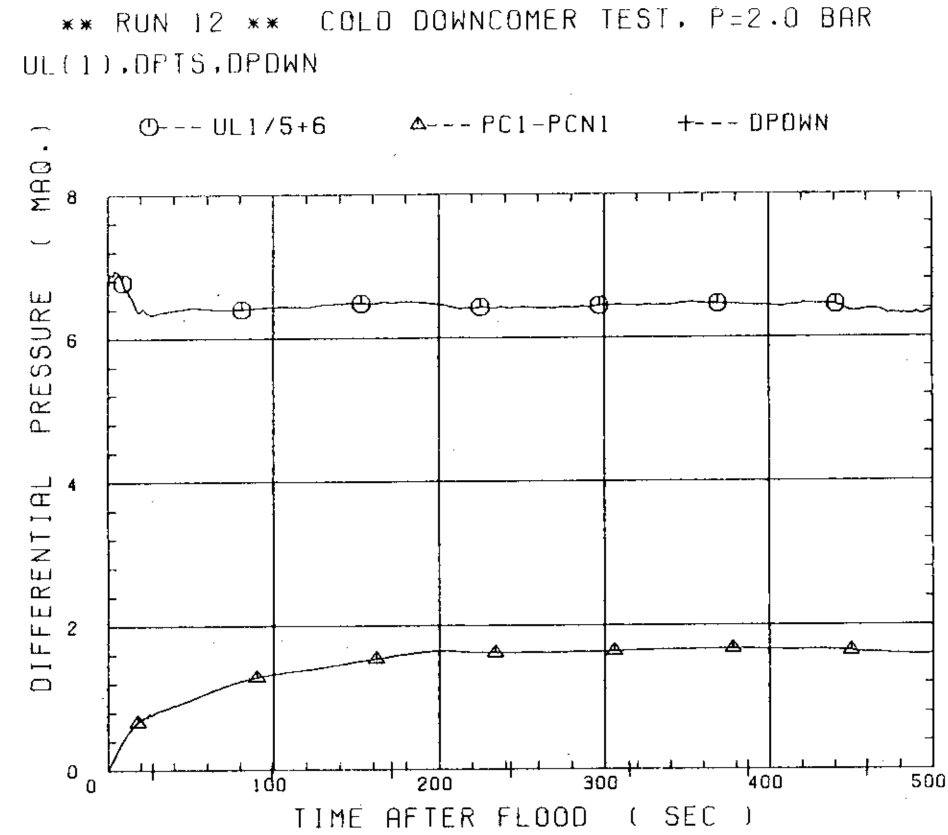

Fig. B.11.6 Core flooding rate (UL1) and core differential pressure (PC1-PCN1)

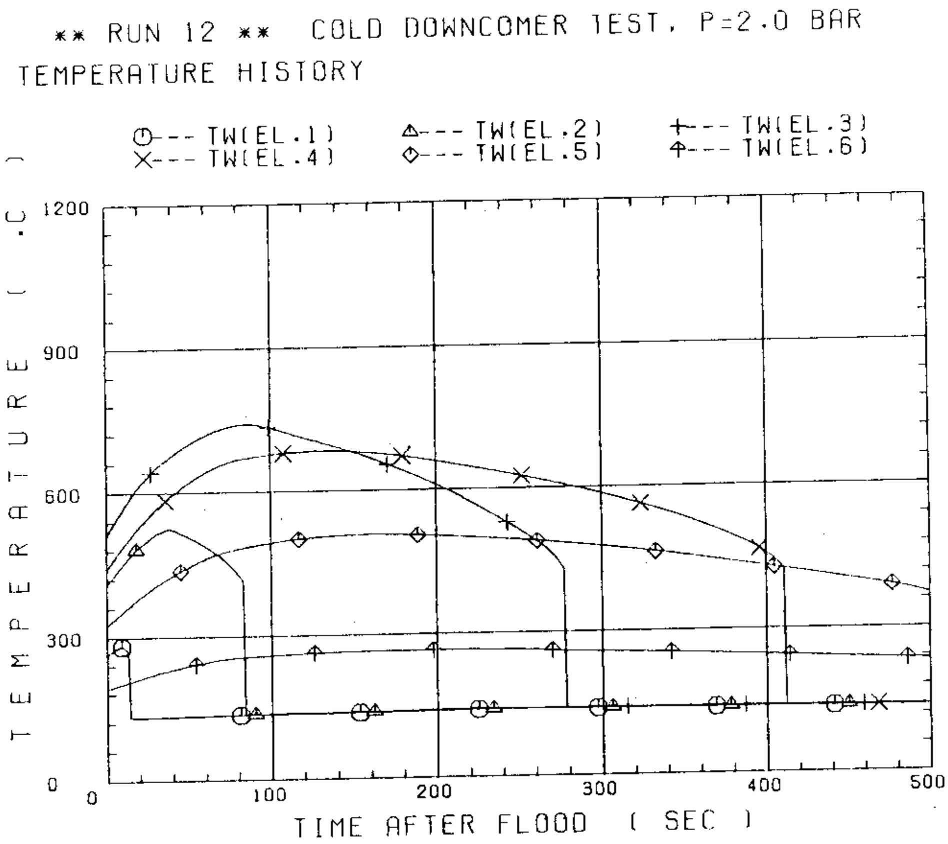

Fig. B.11.7 Rod surface temperatures

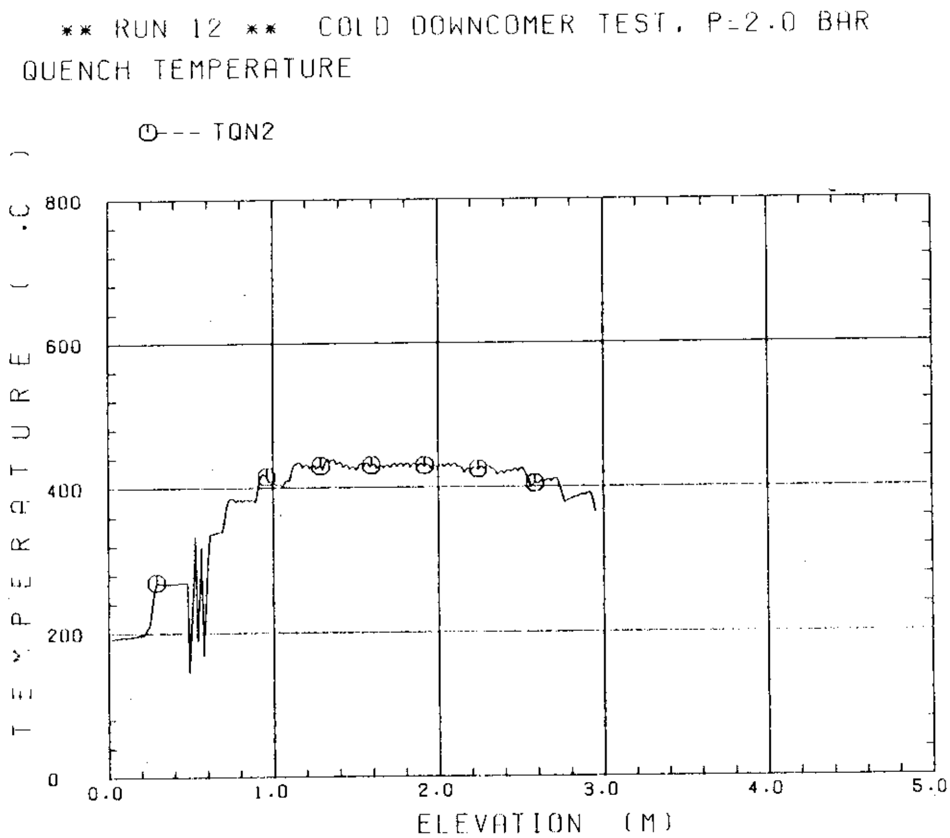

Fig. B.11.8 Quench temperatures

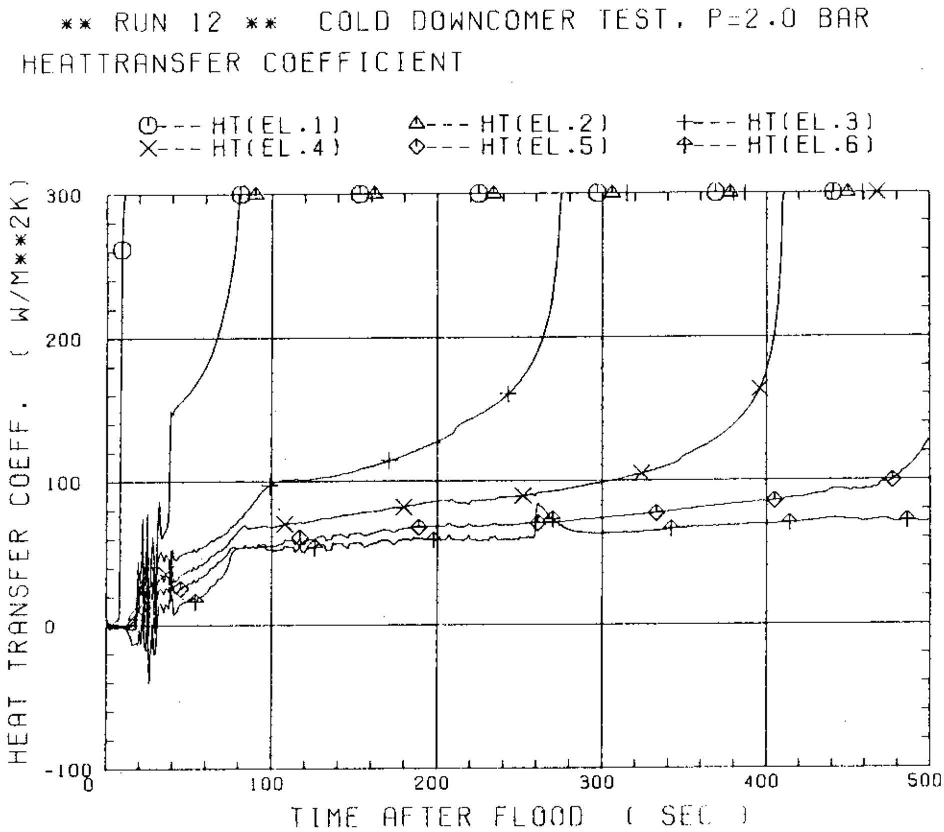

Fig. B.11.9 Heat transfer coefficients

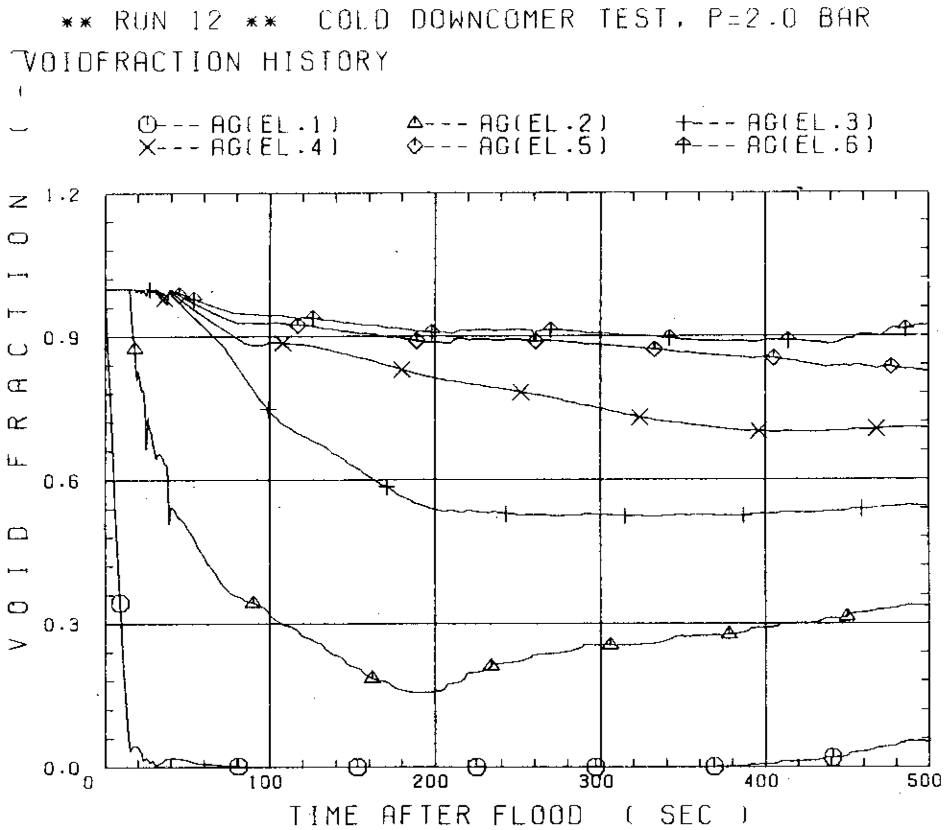

Fig. B.11.10 Void fractions

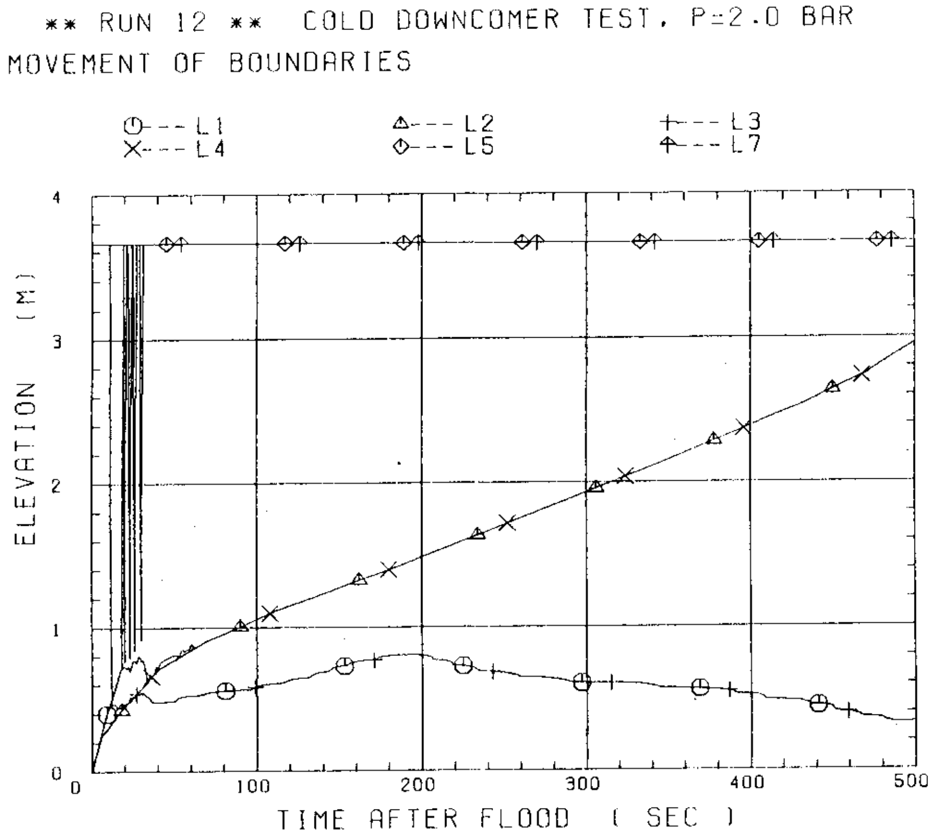

Fig. B.11.11 Movement of flow regime boundaries (L1: Boiling point, L2: Quench front)

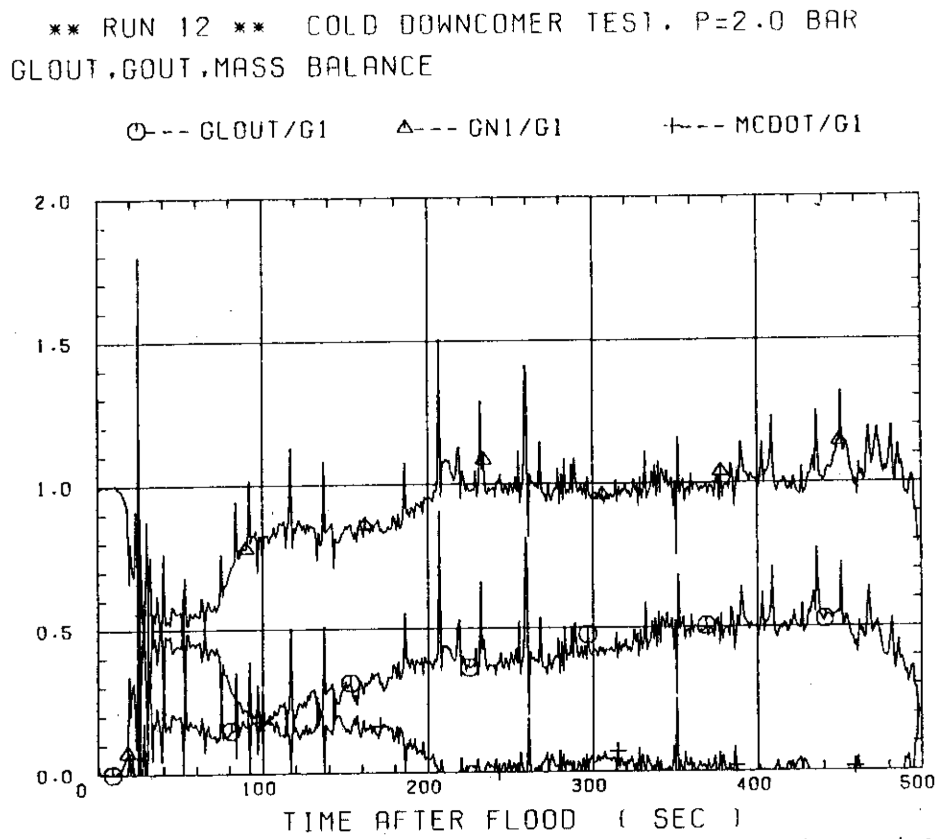

Fig. B.11.12 Liquid carryover rate fraction (GLOUT/G1), carryover rate fraction (GN1/G1) and water accumulation rate fraction (MCDOT/G1)

B.12 Test C1-19 (EM)

CCTF DATA RUN 38

UL(1).DPTS.DPDWN

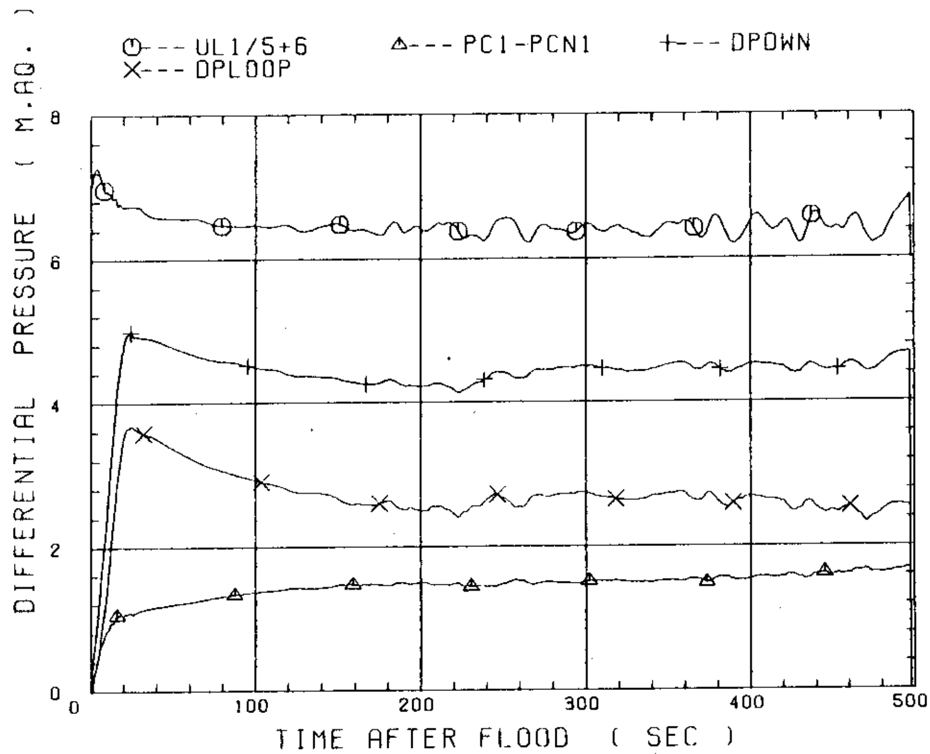

Fig. B.12.1 Core flooding rate (UL1), core differential pressure (PC1-PCN1), downcomer differential pressure (DPDWN) and loop differential pressure (DPLOOP) (Experimental value)

CCTF DATA RUN 38

TEMPERATURE HISTORY

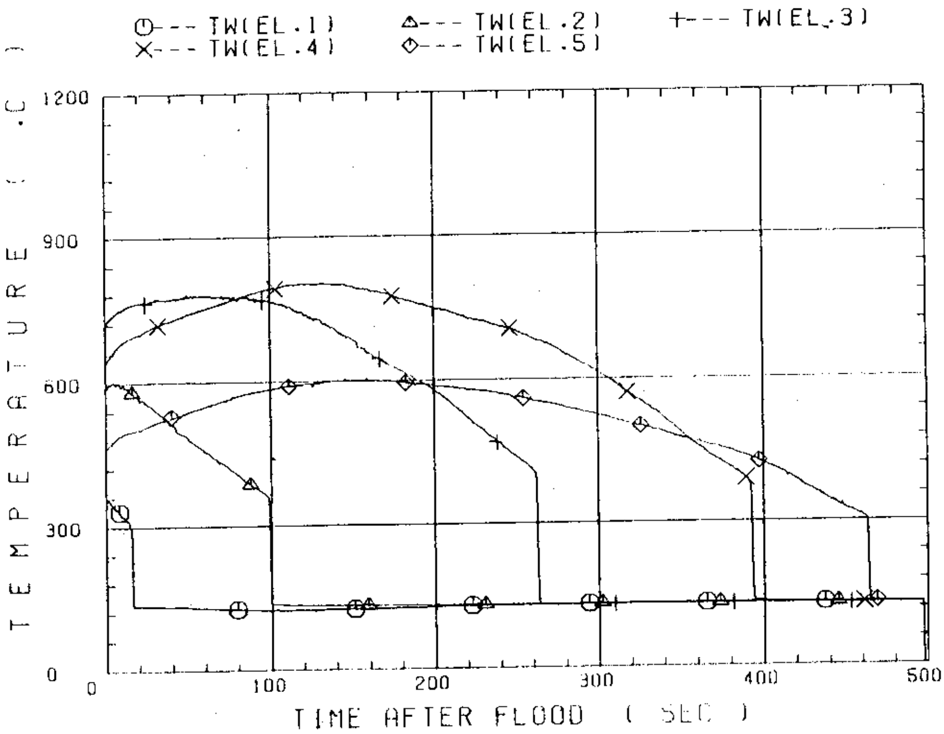

Fig. B.12.2 Rod surface temperatures (Experimental value)

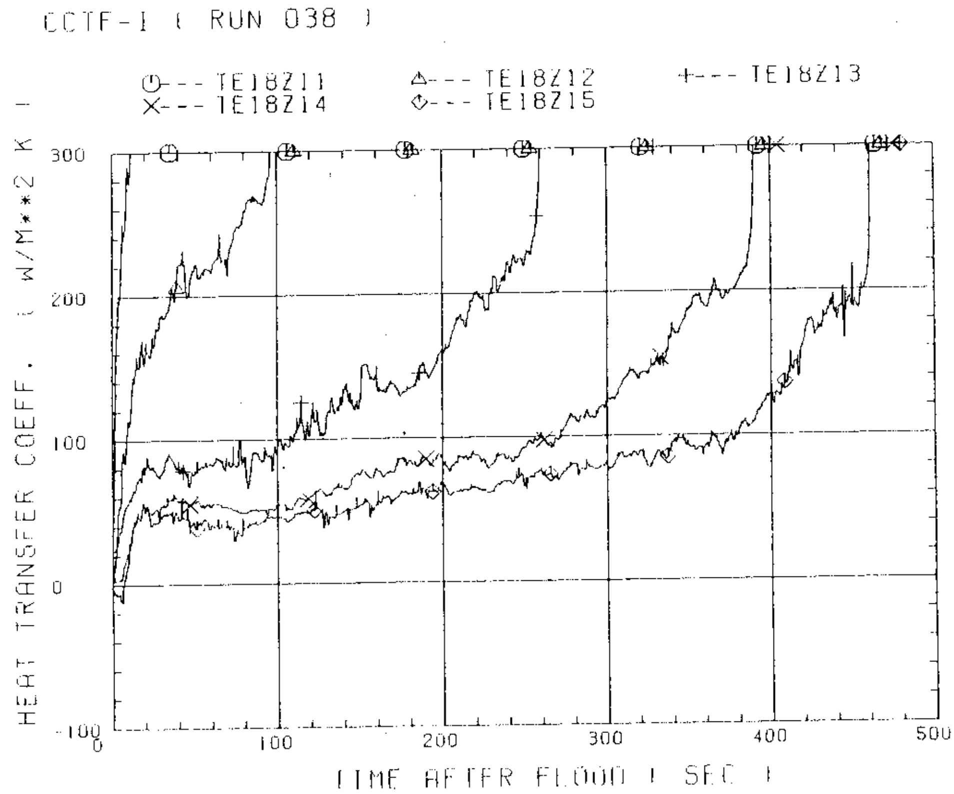

Fig. B.12.3 Heat transfer coefficients (Experimental values)

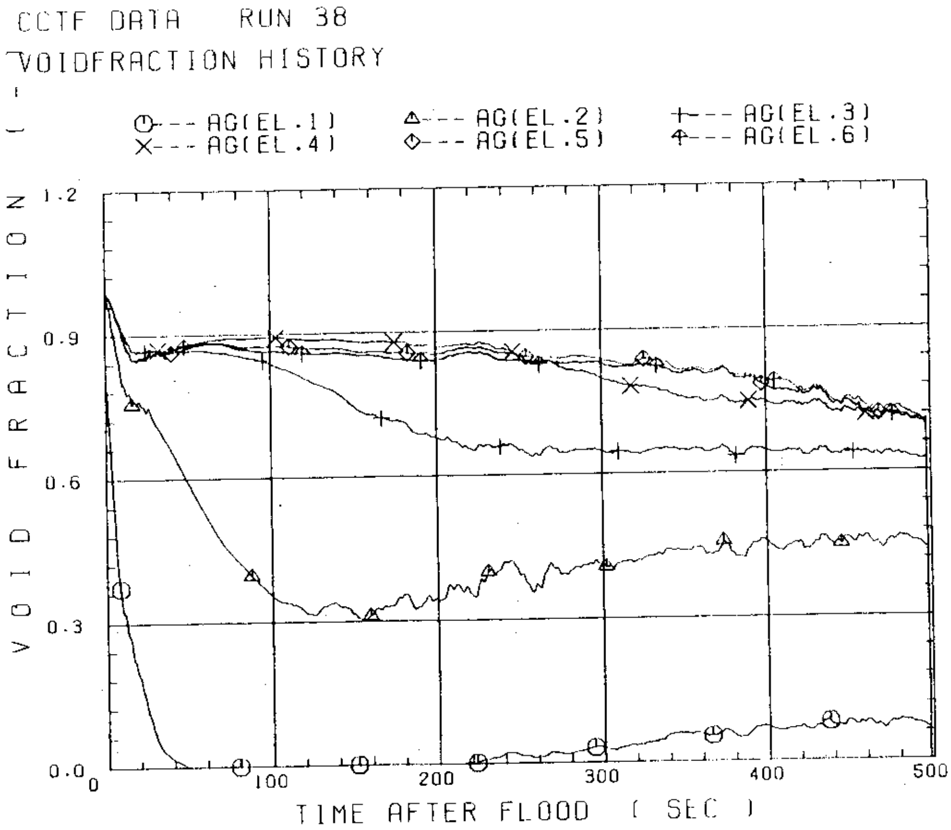

Fig. B.12.4 Void fractions (Experimental values)

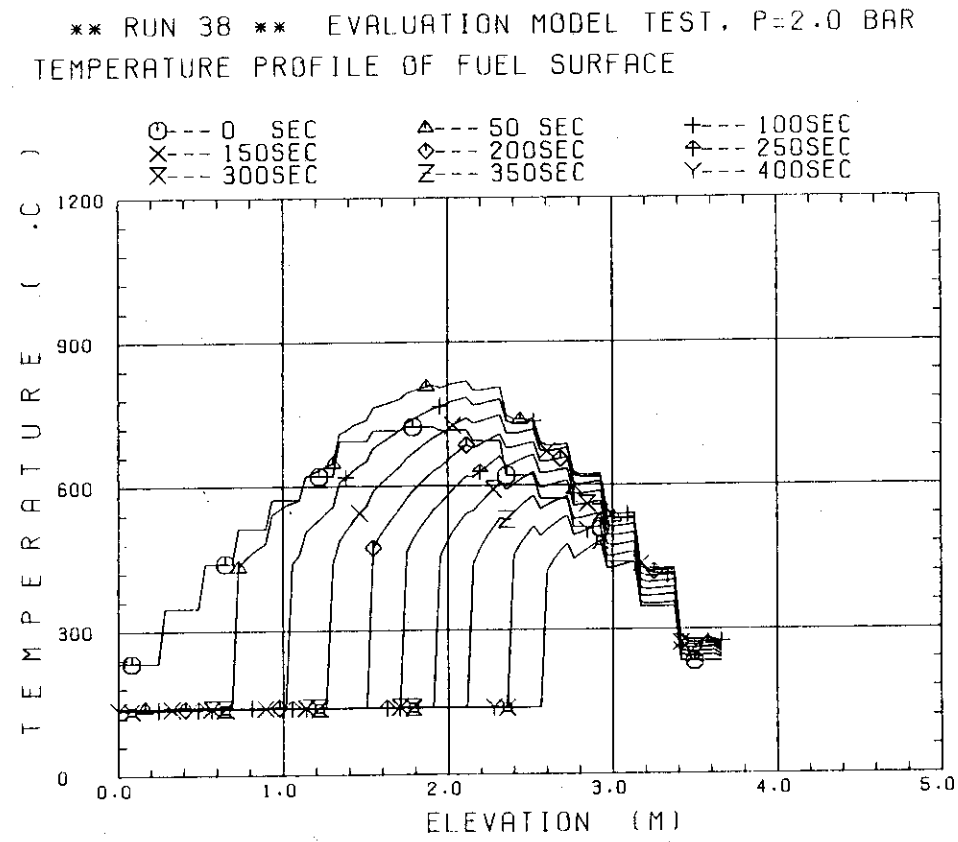

Fig. B.12.5 Rod surface temperature distributions

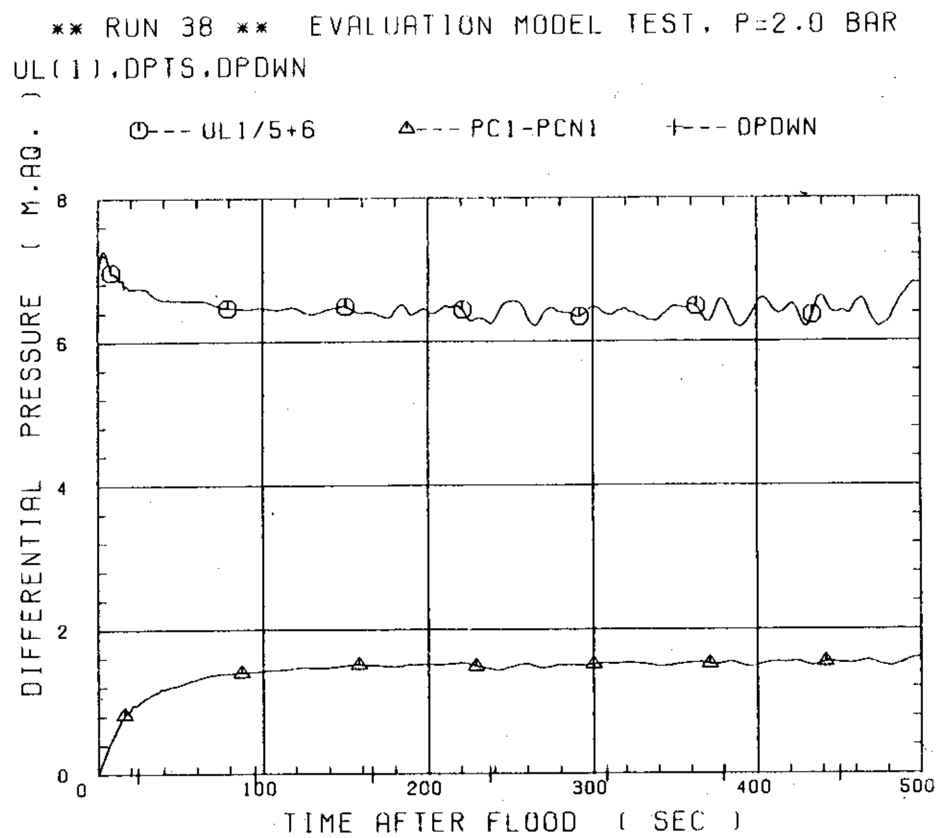

Fig. B.12.6 Core flooding rate (UL1) and core differential pressure (PC1-PCN1)

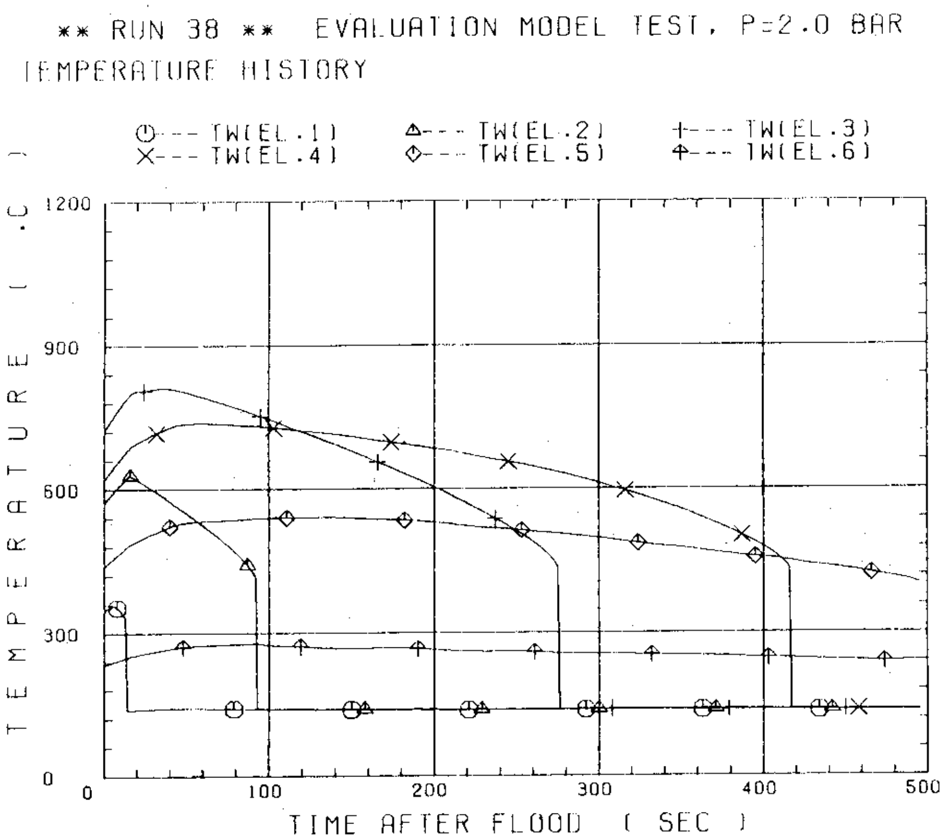

Fig. B.12.7 Rod surface temperatures

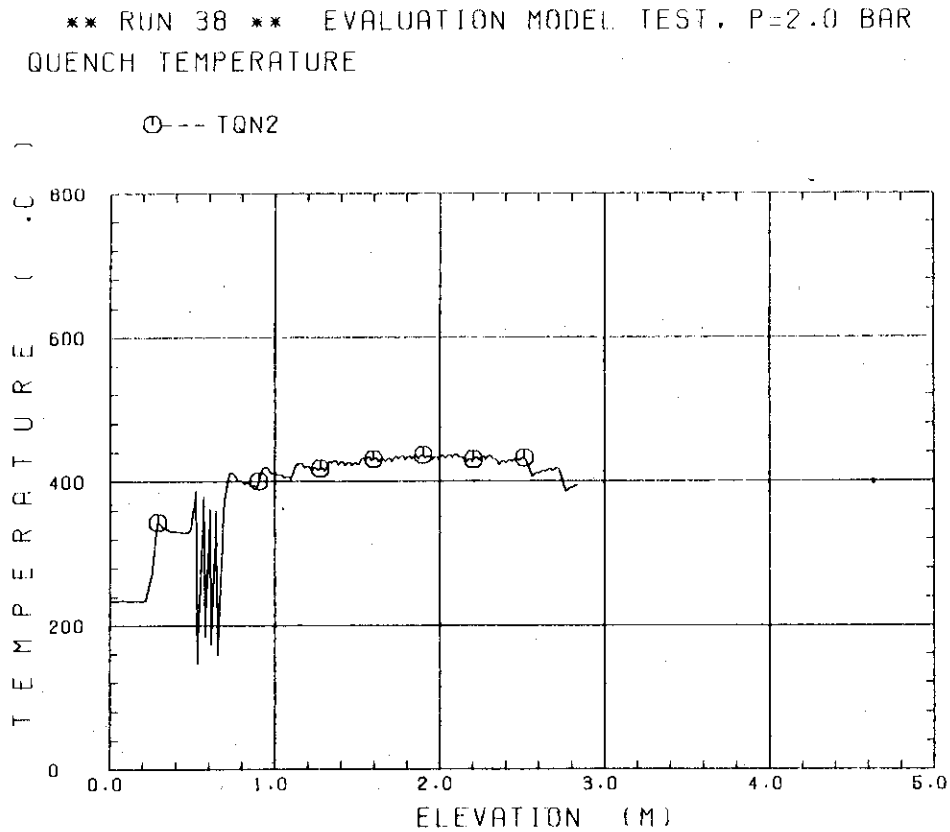

Fig. B.12.8 Quench temperatures

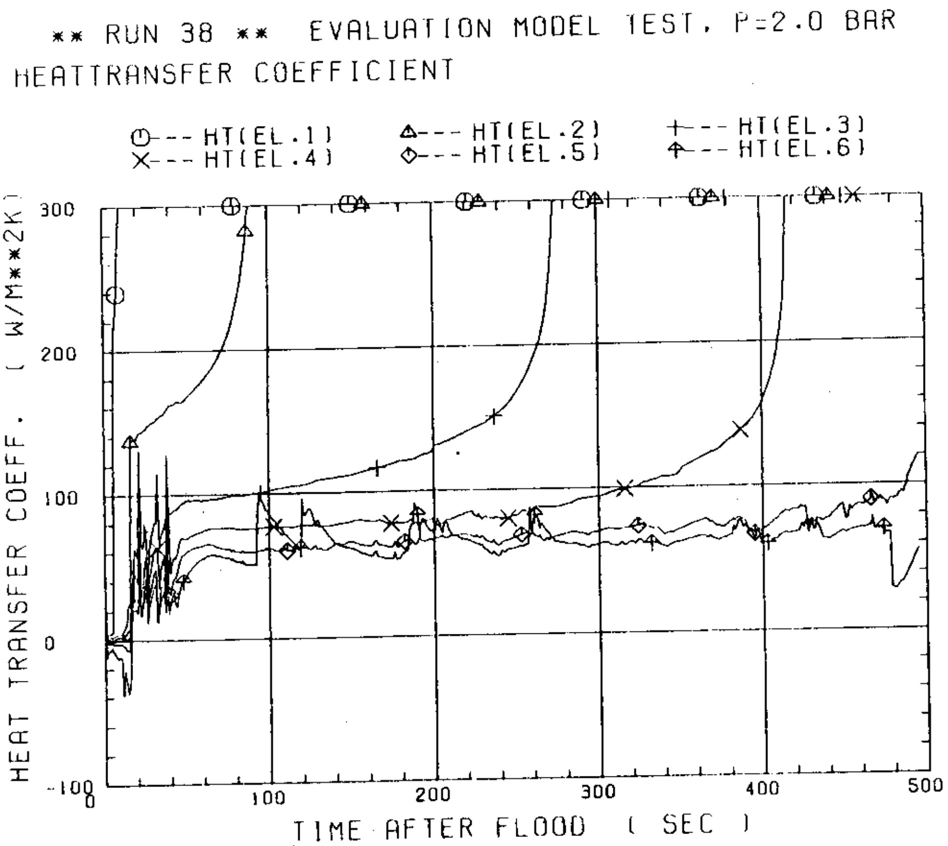

Fig. B.12.9 Heat transfer coefficients

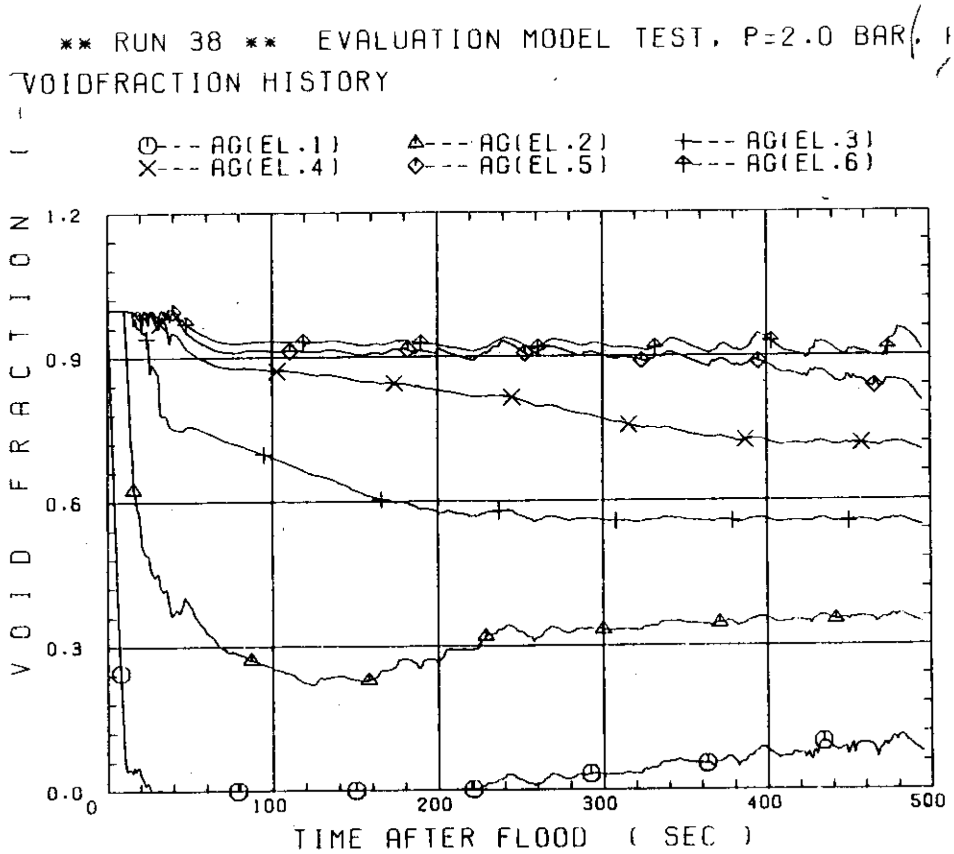

Fig. B.12.10 Void fractions

** RUN 38 ** EVALUATION MODEL TEST, P=2.0 BAR
MOVEMENT OF BOUNDARIES

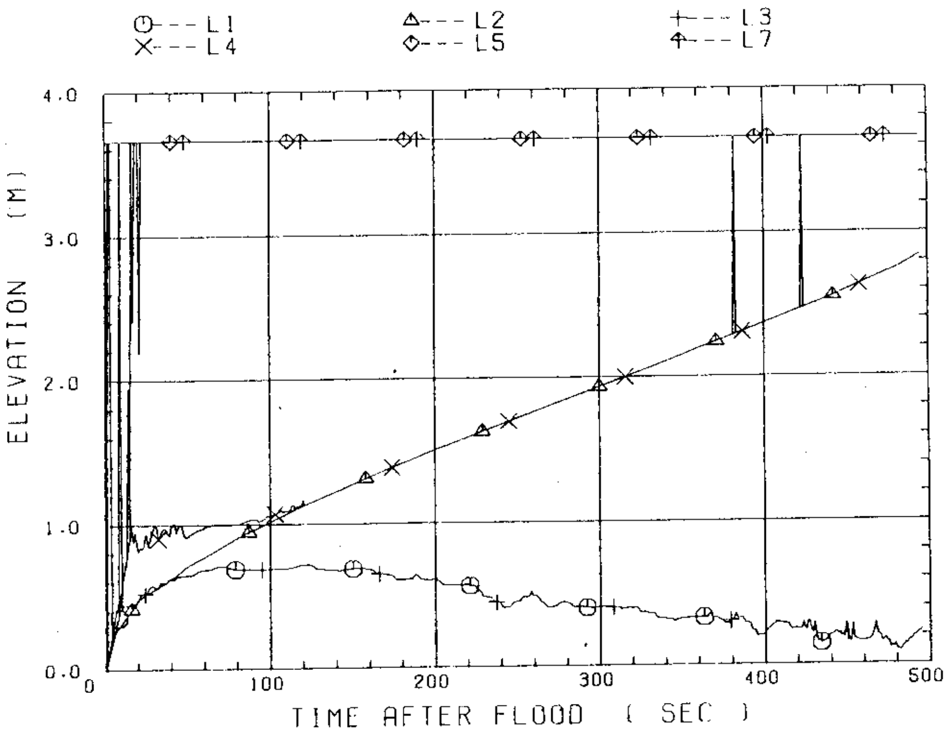

Fig. B.12.11 Movement of flow regime boundaries (L1: Boiling point, L2: Quench front)

** RUN 38 ** EVALUATION MODEL TEST, P=2.0 BAR,
GLOUT,GOUT,MASS BALANCE

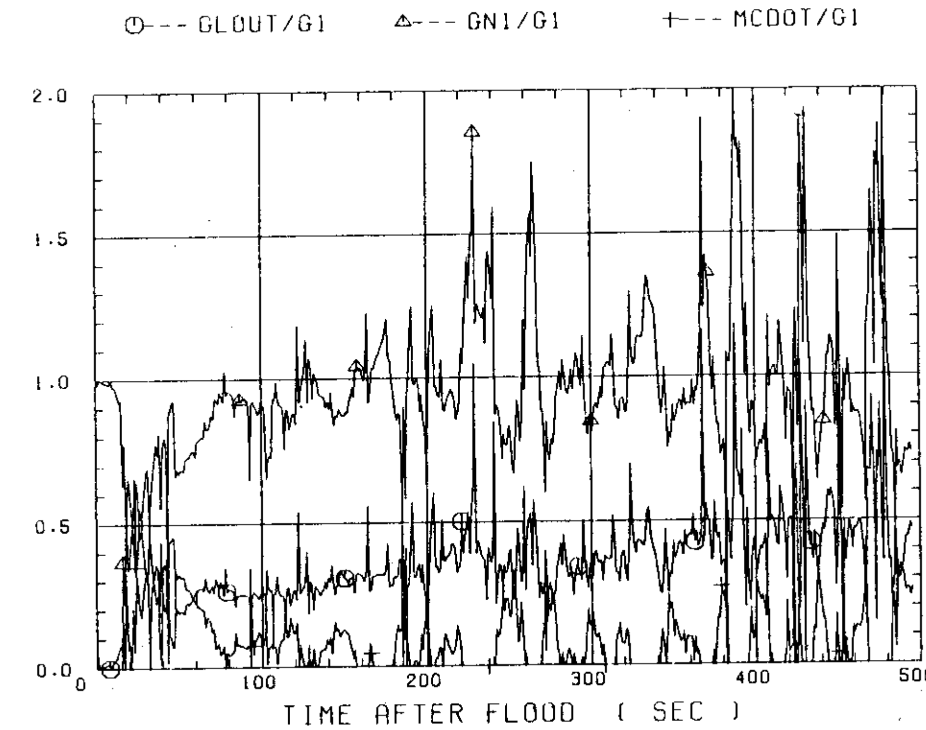

Fig. B.12.12 Liquid carryover rate fraction (GLOUT/G1), carryover rate fraction (GN1/G1) and water accumulation rate fraction (MCDOT/G1)